Investigating sensorimotor representations, processing and inhibition in Tourette Syndrome: Insights from fMRI, MRS and TMS

Caitlin Mairi Smith, BSc.

Thesis submitted to the University of Nottingham for the degree of

Doctor of Philosophy

September 2024

Acknowledgements

I would like to thank my supervisors, Stephen Jackson and Sue Francis, for their guidance and support throughout my studies – I am forever grateful for the opportunity to do this PhD.

There are many others I could not have done this PhD without. Firstly, without those that have taken the time to come in and participate in this research, this thesis would not have been possible. Mairi Houlgreave, thank you for all the guidance with this thesis, and help during scanning, data collection and analysis. Kat Dyke, thank you for all of the proof reading, encouragement and for introducing me to the world of TMS. Thank you to those in SPMIC – Michael Asghar, for all the 7T scanner-related help and digit map analysis, and Adam Berrington, for your guidance in everything MRS. A massive thank you also to lab members, Izzy Farr and Kat Gialopsou, for the laughs and the encouragement.

To my family, Mum, Dad, Ryan and Molly, for your endless support and inspiration throughout this PhD, especially during the trying times. The research gene has been well and truly passed on! To Aaron, thank you for keeping me grounded and forcing me to take breaks. I could not have done any of this without you all.

Contents

List of Tables

List of Figures

Abbreviations

ADHD	Attention-deficit hyperactivity disorder
ADM	Abductor digiti minimi
APB	Abductor pollicis brevis
ASD	Autism spectrum disorders
ATP	Adenosine triphosphate
BA	Broadmann area
BF	Bayes Factor
BOLD	Blood oxygenation level dependent
CBF	Cerebral blood flow
CBV	Cerebral blood volume
CMRO2	Cerebral metabolic rate of oxygen
CNS	Central nervous system
COG	Centre of gravity
CRLB	Cramér–Rao lower bounds
CS	Conditioned stimulus
CSF	Cerebrospinal fluid
CSTC	Cortico-striato-thalamo-cortical
cTBS	Continuous theta burst stimulation
cTOJ	Temporal order judgement with carrier
EEG	Electroencephalography
EMG	Electromyography
EPI	Echo-planar imaging
EV	Explanatory variable
FD	Framewise Displacement
FDI	First dorsal interosseous
FHD	Focal Hand Dystonia
FLIRT	FMRIB's linear image registration tool
fMRI	Functional magnetic resonance imaging
FOV	Field of view

FSL	FMRIB's Software Library
FWHM	Full width at half-maximum
GABA	y-aminobutyric acid
GE-EPI	Gradient-echo echo-planar imaging
GLM	General linear model
Glu	Glutamate
HRF	Haemodynamic response function
IAS	Interoceptive Accuracy Scale
IO curve	Input-output curve
IQ	Intelligence quotient
IQR	Inter-quartile range
ISI	Inter-stimulus interval
iTBS	Intermittent theta-burst stimulation
LFP	Local field potential
LTD	Long-term depression
LTP	Long-term potentiation
LW	Linewidth
M1	Primary motor cortex
MEG	Magnetoencephalography
MEP	Motor-evoked potential
MNI	Montreal Neurological Institute
MPRAGE	Magnetisation Prepared-Rapid Gradient Echo
MRI	Magnetic resonance imaging
MRS	Magnetic resonance spectroscopy
MSO	Mean stimulator output
NMDA	N-methyl-D-aspartate
NORDIC PCA	Noise Reduction with Distribution Corrected (NORDIC) principal component analysis (PCA)
OCD	Obsessive-compulsive disorder
OVS	Outer volume saturation
PSIR	Phase-sensitive inversion-recovery

PU	Premonitory urge
PUTS-R	Premonitory Urge for Tic Disorders Scale – Revised
RF	Radiofrequency
RMT	Resting motor threshold
ROI	Region of interest
rTMS	Repetitive transcranial magnetic stimulation
S1	Primary somatosensory cortex
SE-EPI	Spin-echo echo-planar imaging
seqAD	Sequential amplitude discrimination
SI1mV	1mV threshold
SICI	Short-interval intracortical inhibition
simAD	Simultaneous amplitude discrimination
SMA	Supplementary motor area
SPSQ	Sensory Processing Sensitivity Questionnaire
SSA	Single-site adaptation
TD	Typically developing
TE	Echo time
TFE	Two turbo field echo
TMS	Transcranial magnetic stimulation
TOJ	Temporal order judgement
TR	Repetition time
TS	Tourette syndrome
tSNR	Temporal signal to noise ratio
VAPOR	Variable pulse power and optimised relaxation decay
VOI	Voxel of interest
YGTSS	Yale Global Tic Severity Scale

Abstract

Tourette Syndrome (TS) is a hyperkinetic neurodevelopmental movement disorder, characterised by motor and phonic tics, and has been associated with disruptions to cortical inhibition. γ-aminobutyric acid (GABA) is the most abundant inhibitory neurotransmitter in the cortex. GABA has been linked to both the integrity of cortical representations and performance in the discrimination of tactile stimuli. In populations with disruptions to cortical inhibitory functioning, such as Focal Hand Dystonia (FHD) which involves involuntary repetitive movements of the hand, abnormalities are evidenced in cortical sensorimotor representations of the fingers and hand muscles. Additionally, individuals with FHD display abnormalities in the processing of sensory stimuli. Many individuals with TS also report experiences of abnormalities in sensory processing, such as premonitory urges (PU) prior to tics and hypersensitivity to external stimuli such as light, sound and touch. However, sensitivity to external stimuli has not been widely investigated in TS, despite being a source of discomfort. Moreover, there is mixed evidence regarding inhibitory abnormalities within the sensorimotor cortices, and a lack of insight into cortical representations of movements relating to tics.

This thesis first aimed to examine quantitative tactile sensory thresholds and magnetic resonance spectroscopy (MRS) measures of GABA and glutamate in individuals with TS. Chapter 3 demonstrated that quantitative sensory thresholds show abnormalities in adults with TS in comparison to typically developing (TD) controls. Moreover, a trend for reduced sensorimotor MRS-GABA was evident in the TS group. However, MRS-GABA and quantitative sensory thresholds were not correlated in both TS and TD groups.

In addition to quantitative sensory detection performance and MRS-GABA in TS, cortical representations were investigated. In Chapter 4 and 5, functional magnetic resonance imaging (fMRI) was utilised to determine if there are differences between adults with TS and TD controls in sensorimotor representations of the digits

(unrelated to tics) and facial movements of common tics (blinking, grimacing and jaw clenching). Moreover, fMRI responses of vibrotactile stimulation to the three sites of the face were compared across groups. While digit and vibrotactile facial maps showed some differences between groups, no differences were apparent between sensorimotor representations of facial movements. However, a conjunction analysis revealed the SMA activation was not consistently active across all facial movements in the TS group, whereas the SMA was consistently activated in the TD control group. This is in line with previous evidence of individuals with TS showing abnormalities in SMA activation when performing volitional movements.

Finally, Chapter 6 aimed to assess if manipulating GABAergic inhibition with intermittent theta-burst stimulation (iTBS) would result in changes to cortical motor representations of the digits measured with transcranial magnetic stimulation (TMS) and fMRI. While TMS measures revealed reductions in inhibition in individuals receiving active iTBS, inconsistent differences were evident in digit maps in both active and control groups. Coupled with a low number of participants, it was unclear if any differences in digit maps between groups were a direct result of the stimulation, or instead due to variability in iTBS after-effects and variability within the data.

Publications

Smith, C. M., Sigurdsson, H. P., Dyke, K., Panchuelo, R. S., Francis, S. T., Jackson, G. M., & Jackson, S. R. (2022). Somatomotor cortical mapping in Tourette syndrome using neuro-navigated transcranial magnetic stimulation. In *International Review of Movement Disorders* (Vol. 3, pp. 321-341). Academic Press. Chicago

Maiquez, B. M., Smith, C., Dyke, K., Chou, C. P., Kasbia, B., McCready, C., Wright, H., Jackson, J. K., Farr, I., Badinger, E., Jackson, G. M., & Jackson, S. R. (2023). A double-blind, sham-controlled, trial of home-administered rhythmic 10-Hz median nerve stimulation for the reduction of tics, and suppression of the urge-to-tic, in individuals with Tourette syndrome and chronic tic disorder. *Journal of neuropsychology*, *17*(3), 540–563. https://doi.org/10.1111/jnp.12313

1. Chapter 1 - Tourette Syndrome, somatosensation and functional representations

Key words: Tourette Syndrome (TS), cortico-striatal-thalamic-cortical (CTSC), primary motor cortex (M1), primary sensory cortex (S1), γ-aminobutyric acid (GABA), sensorimotor representations

This chapter contains sections from Smith et al. (2023).

1.1 Introduction to Tourette Syndrome

1.1.1 Clinical Presentation

Tourette Syndrome (TS) is a hyperkinetic movement disorder characterised by the repeated occurrence of both chronic motor and one or more phonic tics. Tics are involuntary, repetitive and stereotyped motor movements or vocalisations (American Psychiatric Association, 2013). Although tics are common among up to 20% of school-aged children, and tic-like movements and stereotypies are prevalent in a range of conditions, TS is a distinct diagnosis based on the chronic nature of tics, their characterisation and symptom duration (American Psychiatric Association, 2013; Martino & Hedderly, 2019; Scahill et al., 2014). Some characteristics that differentiate TS from other tic disorders are that individual's tic severity, frequency and characteristics of movements and vocalisations can vary day-to-day, yet still persist for over a year (American Psychiatric Association, 2013). This differs from provisional tic disorder, involving transient tics lasting less than a year, and persistent/chronic motor or vocal tic disorder, which involves long-term motor or phonic tics, but not both (Plessen, 2013; Scahill et al., 2014). Additionally, temporarily suppressing or controlling tics is common in TS but the ability to do this varies within and between individuals and is sometimes possible in other tic disorders (Greene et al., 2015; Kim et al., 2019; Martino & Hedderly, 2019). However, suppression of movements is uncommon and more difficult in other movement disorders, such as those involving tremor (Koller & Biary, 1989). Moreover, some have reported that their tics are

accompanied by sensory phenomena, such as premonitory urges (PU), which can also cause discomfort (American Psychiatric Association, 2013; Cohen et al., 2013; Leckman et al., 1993).

Tics can be simple or complex. Simple tics can be distinguished by their short durations – examples may include brief movements, such as shrugging or blinking, and vocalisations of a simple sound, such as grunting or sniffing (Cohen et al., 2013; Jackson et al., 2015). On the other hand, complex motor tics are typically of longer durations and can involve combinations of multiple simple motor tics that are performed in a stereotyped and coordinated manner. Complex phonic tics can also involve combinations of multiple simple phonic tics, words or syllables. Both complex motor and phonic tics may involve the repetition of other individual's movements/phrases (echopraxia/echolalia) or inappropriate gestures or vocalisations such as swearing (copropraxia/coprolalia) (American Psychiatric Association, 2013; Cohen et al., 2013). The frequency, severity, duration and location of tics will also vary across and within individuals, as can the interference of tics on voluntary and planned movements/vocalisations (Martino & Hedderly, 2019). For instance, certain contextual situations and emotional states such as stress and anxiety can exacerbate and increase tics, whereas concentrating on a pleasant or engaging task can reduce them (Cohen et al., 2013; Conelea & Woods, 2008).

The onset of this neurodevelopmental condition typically occurs in childhood between the ages of 4-6 and is present in ~1% of children between 5-18 years of age (Bloch & Leckman, 2009; Robertson, 2008). As a result, a diagnostic requirement for TS is that tic onset occurs before the age of 18. However, tics can suddenly present in adulthood, albeit rarely, and are more commonly due to different pathology to TS, such as infection or trauma (American Psychiatric Association, 2013; Chouinard & Ford, 2000). TS is more prevalent in males with an estimated male to female ratio of ~5.2 to 1 in child populations. However, this gender disparity is less pronounced in adulthood, with lower estimated male to female ratios of ~2-3 to 1 (Freeman et al., 2000; Levine et al., 2019). Upon onset, TS usually presents as simple motor tics in the

face and eyes, with phonic tics appearing 1-2 years later. With increasing age, these motor and phonic tics develop into more complex behaviours until ages 10-12, when tic severity typically peaks (American Psychiatric Association, 2013; Bloch & Leckman, 2009; Leckman et al., 1998). During adolescence, the severity of tics gradually declines and is evidenced to diminish in many of individuals by early adulthood (Bloch & Leckman, 2009; James F Leckman et al., 1998). However, in a minority of cases, TS persists into adulthood and is associated with higher tic severities in childhood and in females (Ricketts et al., 2022). These adult TS cases are generally more severe and consist of more extreme tic behaviours, such as self-injurious behaviour and coprolalia (Leckman, 2002). Moreover, although TS prevalence is higher in males, females are more likely to experience persistent symptoms and worsening tic severity into adulthood (Levine et al., 2019; Lichter & Finnegan, 2015).

TS is very rarely present in isolation. It is estimated that around 90% of children with TS also have comorbid conditions such as Obsessive-Compulsive Disorder (OCD) and Attention Deficit Hyperactivity Disorder (ADHD) which are generally more common during adolescence and early adulthood (Bloch & Leckman, 2009; Cavanna et al., 2009; Cohen et al., 2013). Moreover, the presence of OCD and/or ADHD in TS populations is associated with an increased prevalence of exhibiting comorbid symptoms such as rage, conduct disorders, anxiety, sleep disturbances and depressive symptoms compared to TS alone (Mol Debes, 2013). Tics already have a significantly negative impact on social, familial, academic and psychological wellbeing and these comorbid conditions can cause greater impairment and are associated with greater tic severity (Bloch & Leckman, 2009; Conelea et al., 2011; Sambrani et al., 2016). For instance, quality of life scores (QoL) are negatively correlated with tic severity and presence of comorbidities, suggesting that these can have a further significant impact on wellbeing in TS (Conelea et al., 2011). Furthermore, lower psychosocial functioning and QoL have been widely associated with depression, ADHD and OCD comorbidities in mild-moderate TS populations, with QoL scores being lower than the general population (Bernard et al., 2009; Conelea et al., 2013; Eapen et al., 2016; Evans et al., 2016; Jalenques et al., 2012). Higher rates of anxiety and depression are also

prevalent in TS, regardless of comorbidities, resulting in a lower quality of life and may be linked to the increased incidences of mortality and suicide in TS compared to the general population (Conelea et al., 2011, 2013; de la Cruz & Mataix-Cols, 2020; de la Cruz et al., 2017; Robertson et al., 1993; Robertson, 2006). Together, this demonstrates that a large number of individual's with TS exhibit greatly impaired QoL and wellbeing, both due to tics alone and in combination with comorbidities.

The volitional nature of tics is a topic of debate (Cavanna et al., 2017). While many refer to tics as involuntary movements (e.g., Ganos, Asmuss, et al., 2015), others have argued that tics are instead voluntary responses to urges prior to a tic, or 'premonitory urges' (PU) (Leckman et al., 2006). Many individuals with TS report that their tics are often preceded by PU, which are described as uncomfortable cognitive or bodily sensations that occur prior to a tic and are experienced as a strong urge for motor discharge (Cohen et al., 2013; Jackson et al., 2020; Patel et al., 2014). PU are commonly felt in the shoulders, neck and face and are described by many as like an inner urge, increased tension and impulse to move, but locations and the characterisation/feeling evoked by PU generally vary between individuals (Schunke et al., 2016). For this reason, it has been proposed that PU should be considered as the driving force behind the occurrence of tics, and that tics are a learnt response to the experience of PU (Cavanna et al., 2017; Leckman et al., 2006). As a result, there is mounting evidence that TS may be associated with the altered processing of somatosensory information, including altered interoception (Tinaz et al., 2015).

1.1.2 Pathophysiology of Tourette Syndrome

1.1.2.1 Cortico-striatal-thalamic-cortical (CSTC) circuitry

Tic generation is theorised to stem from dysfunction within the cortico-striato-thalamo-cortical (CSTC) circuitry. This neural circuit consists of connections between subcortical structures, such as the basal ganglia and the thalamus, and cortical structures. Specifically, impairment is thought to stem from neurons within the striatum, the main afferent structure within the basal ganglia (Albin et al., 1989). The specific pathways of the CSTC circuit can be separated into three parallel loops: the

motor circuit, associative circuit and the limbic circuit (Obeso et al., 2008; see Figure 1.1). Dysfunction in the motor loop is associated with movement disorders, where in TS, increased gain in CSTC circuits is thought to result in increased motor noise leading to tics (Ganos, Bongert, et al., 2015). This is supported by animal models, where disinhibition of sensorimotor functional subdivision of the striatum resulted in tic-like movements or myoclonic jerks (Bronfeld, Yael, et al., 2013; Worbe et al., 2009, 2013). Moreover, disinhibition in associative and limbic subdivisions are linked with hyperactivity and stereotyped behaviours (Bronfeld, Yael, et al., 2013; McCairn et al., 2009; Worbe et al., 2013). This may account for the high prevalence of co-morbid ADHD and OCD symptoms present within TS.

Figure 1.1

Illustration of the basal ganglia loops from Obeso et al. (2008)

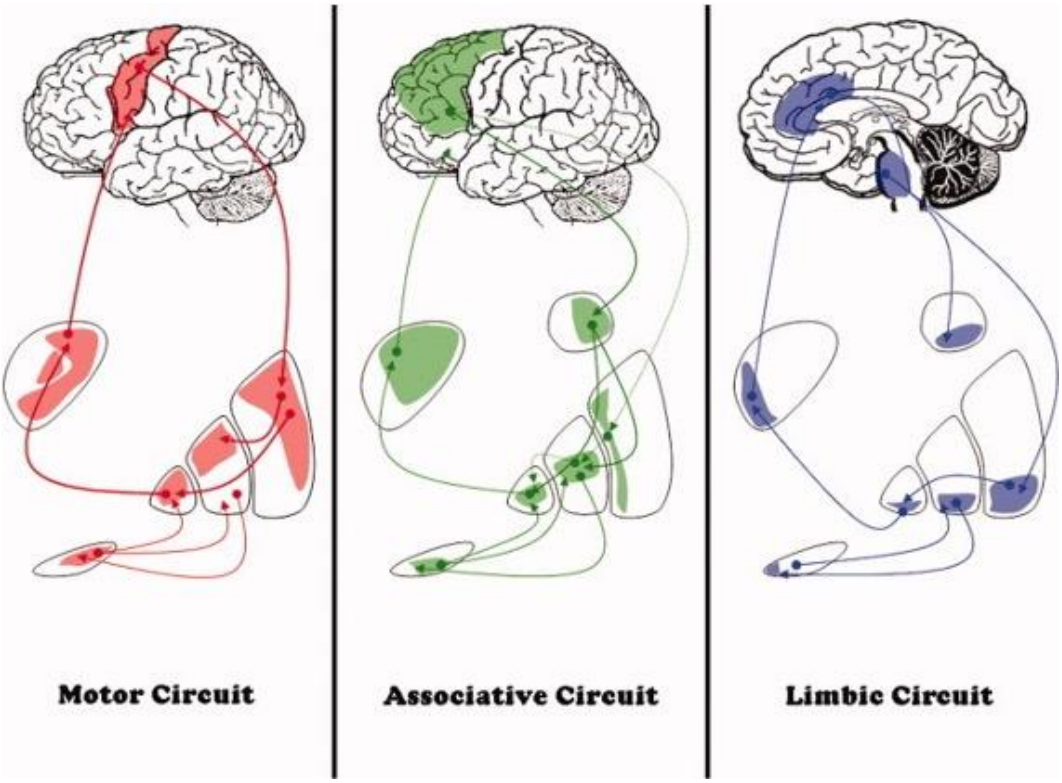

Note. Figure from Functional organization of the basal ganglia: Therapeutic implications for Parkinson's disease, Rodriguez, M. et al., 2008, Copyright 2008 Movement Disorder Society, John Wiley and Sons, Ltd. Figure reproduced with permissions

To produce a voluntary movement (determined by a specific motor pattern generator within the cortex), there is focal activation of striatal spiny projection neurons (SPNs), which inhibit basal ganglia output neurons, the global pallidus pars interna and substantia nigra pars reticulata (Albin & Mink, 2006). These structures project back via the thalamus to cortical motor pattern generators. Removal of inhibition from the basal ganglia output neurons facilitate the motor pattern, and therefore voluntary movement (Albin & Mink, 2006). Simultaneously, the subthalamic nucleus excites surrounding basal ganglia output neurons, projecting via the thalamus to competing motor patterns. This increases their inhibitory output and therefore inhibits competing motor patterns and unwanted movements (Albin & Mink, 2006).

However, in TS, there is dysfunction stemming from aberrant focal activation of striatal SPNs, cause unwanted inhibition of the basal ganglia output neurons and disinhibition of cortical motor pattern generators (Mink, 2001, 2003). While this mechanism causes facilitation of voluntary movements, this aberrant activity triggers competing, unwanted motor sequences (Mink, 2003). Repetition of this focal activation over time produces repeated, stereotyped and unwanted movements (i.e. tics), with abnormal activation of discrete sets of striatal SPNs corresponding to each stereotyped motor output (Mink, 2001, 2003). These behaviours may be facilitated due to the basal ganglia's role in habit formation and the input of reward signals from dopamine, resulting in reinforced altered action selection of the basal ganglia (Graybiel, 2008), and consequently, tics becoming habits which are difficult to unlearn.

Specific tic presentation has previously been theorised to be due to aberrant activity within discrete regions of the topographically organised motor areas of the cortex (see Section 1.2.1.1) and basal ganglia nuclei, which show dorsal-ventral organisation of the leg, arm and face (Alexander et al., 1986; Obeso et al., 2008). This is supported by rat models of TS, where discrete striatal injections of y-aminobutyric acid A receptor ($GABA_A$) antagonists result in tic-like movements relating to the striatum's topographical organisation (Bronfeld, Yael, et al., 2013). However, this is not reliably found across species such as in non-human primates, despite well documented dorsal-ventral organisation of the hindlimb, forelimb and face (Bronfeld et al., 2011; Bronfeld, Israelashvili, et al., 2013; Worbe et al., 2009). Instead, tics are mainly isolated to orofacial muscles, regardless of the topographical site of injection (Bronfeld et al., 2011; Bronfeld, Israelashvili, et al., 2013; McCairn et al., 2009; Worbe et al., 2009, 2013), aligning with human evidence of orofacial tics being the first and most common to appear (Baizabal-Carvallo et al., 2023; Cohen et al., 2013; Martino et al., 2012). This is proposed to be due to cortical magnification; whereby facial regions are more strongly represented in the striatum and therefore, preferentially recruited (Ganos, Bongert, et al., 2015; Miyachi et al., 2006).

However, there is increasing evidence that alterations in the balance of inhibition/excitation within the CSTC pathway constitutes a core feature of TS (Jackson et al., 2015). Specifically, several lines of converging evidence have implicated dysfunctional signalling within circuits involving GABA (Clarke et al., 2012; Gittis & Kreitzer, 2012; Ramamoorthi & Lin, 2011). Before discussing GABA in relation to TS and disordered inhibition, GABA's role in somatosensory processing and in the maintenance of cortical representations will be discussed.

1.2 Inhibition in the sensorimotor system

1.2.1 GABA

GABA is the primary inhibitory neurotransmitter within the human brain, acting through $GABA_A$ and $GABA_B$ receptors (Schmidt-Wilcke et al., 2018; Zhu et al., 2018) – $GABA_A$ receptors are present in approximately 20-50% of all synapses (Nutt & Malizia, 2001). GABA is synthesised from glutamate, which in turn is derived from glutamine; all three form part of a metabolic cycle which can be drawn upon for neurotransmission (Rae, 2014). At any one time only, a proportion of GABA within the brain will exist as neurotransmitter (Rae, 2014), the rest exists as metabolic pools which are most likely located within cell bodies and astrocytes (Liu et al., 2022; Rae et al., 2009). Overall, GABA plays a critical role in maintaining neural excitability within a functional range and is implicated in the majority of brain functions.

GABA within humans can be measured with magnetic resonance spectroscopy (MRS) and by using transcranial magnetic stimulation (TMS) to measure the inhibition of a motor-evoked potential (MEP) after applying a paired-pulse TMS method called short-interval intracortical inhibition (SICI; see Section 2.3.2.2). It is this SICI effect that thought to be dependent on $GABA_A$ interneurons (Di Lazzaro et al., 2006). However, when considering the evidence of alterations in GABA function in TS, it is important to be mindful of the limitations of these different approaches and the complexities involved in GABA synthesis and transport. Namely, while both approaches provide insight into cortical GABA, they have repeatedly found to be uncorrelated (Dyke et al., 2017; Stagg et al., 2011; Tremblay et al., 2013). The general consensus is that while

SICI largely reflects the synaptic activity of $GABA_A$ receptors (phasic inhibition), MRS reflects the non-synaptic wider pool of GABA as a neuro-metabolite (tonic inhibition).

1.2.1.1 Functional sensorimotor cortical representations

Topographical mapping of the body in the primary motor (M1) and somatosensory (S1) cortices was first described by Penfield and Boldrey (1937). They observed that movements and sensations could be evoked across the contralateral side of the body with electrical stimulation to discrete locations of the human pre (M1) and postcentral (S1) gyrus. This led to the creation of a topographic map, pinpointing motor and sensory representations across the body to specific cortical regions (Schott, 1993). A visual representation of this, the homunculus (Figure 1.2), was created to reflect the size and sequence of this cortical topography, showing that the human body is mapped upside-down in the cortex (Penfield & Boldrey, 1937; Schott, 1993). Furthermore, the size of each body part representation differs and is dependent on cortical magnification. This is whereby representations are reflective of the degree of communication between that discrete cortical region and subsequent body part. Therefore, this cortical magnification mirrors the extent of innervation that the M1 or S1 region sends or receives from this body region (Catani, 2017). For example, functional cortical areas relating to body parts are typically larger if they send/receive more information to the cortex, such as the tongue and hands (Catani, 2017; Schott, 1993).

Figure 1.2.

Illustration of the sensory (left) and motor (right) homunculus

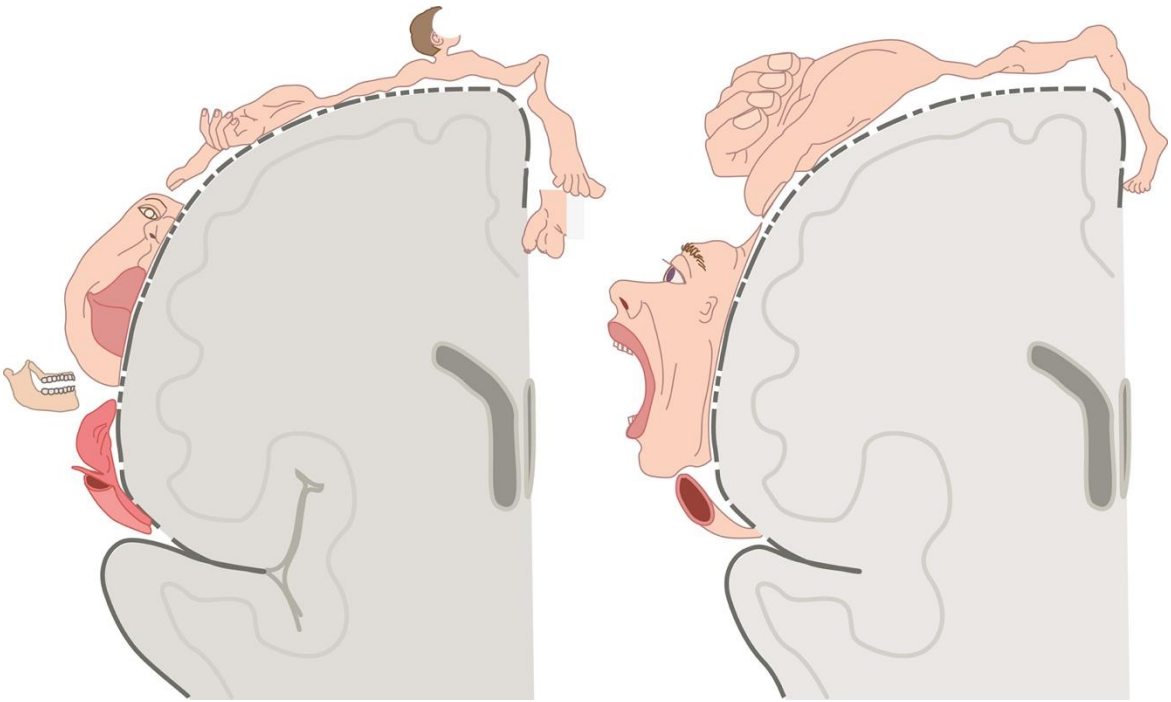

Note. Image from Slagter, R., https://anatomytool.org/content/slagter-drawing-cortical-motor-and-sensory-homunculus-dutch-labels, https://creativecommons.org/licenses/by-nc-sa/4.0/

The mechanisms that give rise to the stability and dynamic properties of sensorimotor representations are currently unclear. However, one key mechanism implicated in the mediation of sensorimotor representations is the inhibitory neurotransmitter GABA and its role in implementing surround inhibition (Beck & Hallett, 2011; Jacobs & Donoghue, 1991; Jones, 1993; Kolasinski et al., 2017; Sigurdsson, Molloy, et al., 2020). Surround inhibition, mediated through $GABA_A$ signalling, is a physiological mechanism that is thought to focus neuronal activity by exciting the receptive field centre of activation and inhibiting the surrounding areas to create a greater contrast between the signals (Beck & Hallett, 2011; Sillito, 1975; Sohn & Hallett, 2004). This concentric organisation is thought to improve the

discrimination of somatosensory events and aid the efficient selection of movements (Beck & Hallett, 2011). For instance, upon movement of a digit, the corresponding motor cortical area is activated while the adjacent muscles are inhibited (Sohn & Hallett, 2004). Moreover, sensorimotor surround inhibition is evidenced by the reduced stimulation-induced MEP on the second digit after simultaneous application of sensory stimulus to the first and third digits (Tamburin et al., 2005). Together, this supports the involvement of surround inhibition and centre-surround organisation within the sensorimotor systems, where the centre area of activation is activated and surround area inhibited.

However, there are questions surrounding the relationship between surround inhibition and human measures of GABA. As previously stated, MRS measures of GABA are likely to be reflective of extracellular tonic inhibition, rather than synaptic-level intracortical inhibition, therefore are unlikely to reflect mechanisms of surround inhibition (Dyke et al., 2017; Stagg et al., 2011; Tremblay et al., 2013). Moreover, while evidence suggests that SICI is reflective of $GABA_A$ activity (Di Lazzaro et al., 2006), there is mixed evidence to whether SICI is related to surround inhibition. For instance, previous TMS research has demonstrated increased SICI in the surrounding muscle during muscle movement onset, suggesting centre-surround organisation of cortical neurons within M1 (Stinear & Byblow, 2003). Moreover, recent TMS-electroencephalography (TMS-EEG) work has revealed that SICI and TMS-measured surround inhibition both modulate cortical mechanisms related to early TMS-evoked cortical potentials, associated with $GABA_A$ activity (Leodori et al., 2019; Premoli et al., 2014). However, this relationship has not yet been replicated (Sohn & Hallett, 2004) and may only play a role in impaired surround inhibition during movement initiation (Beck et al., 2008; Molloy et al., 2003). This suggests that there may be some underlying mechanisms linking SICI and surround inhibition together, however the specific means are not currently clear.

Although the mechanisms of surround inhibition are not clear, there is clear support for the role of $GABA_A$ in the integrity of sensorimotor representations. For

instance, in animal research it has been shown that injections of $GABA_A$-antagonist, bicuculline, within the motor cortex results in the fusion of motor representations between adjacent muscles and weakens sensory map plasticity and receptive field tuning (Foeller et al., 2005; Jacobs & Donoghue, 1991; Schneider et al., 2002). Disturbance of intracortical inhibitory mechanisms in the cat visual cortex using repetitive TMS (rTMS) has also resulted in disrupted visual cortical maps which are primed for plasticity (Kozyrev et al., 2014, 2018). Moreover, in human research using TMS mapping and TMS-SICI, Sigurdsson, Jackson, et al. (2020) demonstrated that SICI was a significant predictor of the first dorsal interosseous (FDI) muscle somatomotor representation area, with the full model (including age and RMT) accounting for 61% of the total variance. Specifically, this suggests that greater $GABA_A$ interneuron activation is predictive of greater excitability of the FDI somatomotor representation. Additional evidence has also demonstrated that the size of cortical hand representations are reduced in older adults and is thought to be due to reduced intracortical inhibition (Kalisch et al., 2008). Together, this strongly supports the role of $GABA_A$ synaptic inhibition in the maintenance of cortical sensorimotor representations.

Additionally, fMRI activity of cortical sensorimotor representations has recently been proposed to mediate the relationship between MRS-GABA and sensory processing. Recent evidence has identified a relationship between digit somatosensory processing and sensorimotor MRS-GABA, mediated by cortical activity in digit representations (Kolasinski et al., 2017). Specifically, greater S1 GABA levels are associated with more selective tuning of S1 cortical activity of digit representations which in turn, are linked to greater perceptual acuity of the digits (Kolasinski et al., 2017). Network integration may also have a role, with individuals with less segregated sensorimotor resting state networks showing reduced sensorimotor GABA levels and worse sensorimotor performance (Cassady et al., 2019). Together, this suggests that tonic GABA is implicated in the tuning of cortical activity within the sensorimotor system and also has a role in the processing of sensory information.

1.2.1.2 Somatosensory processing

MRS-GABA and its relationship to perceptual processing have been greatly researched across visual, auditory and tactile modailities (Li et al., 2022). In the sensorimotor system, relationships have been reported between MRS-GABA and tactile amplitude discrimination, frequency discrimination thresholds and temporal order judgement task performance (Li et al., 2022). Specifically, the threshold to detect which tactile stimuli had a greater amplitude, a greater vibration frequency, and was presented first in time, was lower in individuals with greater sensorimotor GABA levels (Li et al., 2022). Moreover, there is evidence suggesting that conditions with disordered GABA show abnormal somatosensory processing, such as Focal Hand Dystonia (FHD; Antelmi et al., 2017; Molloy, 2003) and Autism Spectrum Disorders (ASD; Puts et al., 2017).

The mechanism by which greater GABA is thought to contribute to the enhanced detection of sensory information in the sensorimotor cortices by enhancing surround inhibitory mechanisms by shaping the responses of cortical neurons, such as receptive field size and activation thresholds in response to peripheral stimulation (Hicks & Dykes, 1983; Kaneko & Hicks, 1990). This is evidenced by the malleability of cortical receptive fields after injections of GABA agonists and antagonists (Chowdhury & Rasmusson, 2002; Oka et al., 1986). This suggests GABA drives greater acuity of receptive fields, or enhancing surround inhibition, resulting in greater acuity to peripheral sensory information. However, as this is driven by synaptic GABA, it is unlikely to be captured by extracellular MRS-GABA and somatosensory processing relationships above (Dyke et al., 2017; Stagg et al., 2011; Tremblay et al., 2013). Instead, as discussed in 1.3.1.1, tonic MRS-GABA levels may be related to enhanced sensory detection thresholds due to the associated fine-tuning of cortical activity and efficient integration of networks (Cassady et al., 2019; Kolasinski et al., 2017).

1.2.2 Disordered GABAergic inhibition

The role of GABA in somatosensation and functional mapping has been supported by evidence of disordered sensory processing and cortical mapping in conditions displaying cortical GABAergic dysfunction, such as Focal Hand Dystonia (FHD).

1.2.2.1 Focal Hand Dystonia (FHD)

Focal Hand Dystonia (FHD) is a neurological condition characterised by the inappropriate co-contraction of muscles resulting in uncoordinated movements and abnormal hand postures (Meunier et al., 2003; Schabrun et al., 2009). This is a movement disorder associated with abnormal cortical inhibition in the sensorimotor system. For instance, GABA binding, as indexed by the binding potential of [11C] Flumazenil (a benzodiazepine antagonist that binds to $GABA_A$ receptors), was reduced in the sensorimotor cortex of individuals with FHD contralateral to their affected hand, compared to healthy controls (Gallea et al., 2018). Previous evidence has also demonstrated reduced $GABA_A$-mediated SICI and disordered surround inhibition in individuals with FHD (Beck et al., 2008; Beck & Hallett, 2011; Sohn & Hallett, 2004; Stinear & Byblow, 2004). Moreover, there is evidence suggesting that GABA inhibition is associated with somatosensory processing within FHD (Antelmi et al., 2017). Specifically, reduced GABAergic inhibition is linked with worse performance in somatosensory acuity tasks.

Further to this, individuals with FHD may present with abnormal cortical sensorimotor representations of the affected hand. Using TMS techniques to measure the size and extent of individual cortical muscle representations (see Section 2.3.2.3), studies have demonstrated that the TMS motor (muscle) maps obtained from FHD patients differ from those of healthy controls. Specifically, the maps of FHD patients exhibit larger areas and reduced inter-map distances between hand muscle representations (Byrnes et al., 1998; Schabrun et al., 2009; Schabrun & Ridding, 2007). Other evidence also indicates altered somatosensory and motor

representations in individuals with FHD (Bara-Jimenez et al., 1998; Butterworth et al., 2003; Byl et al., 2000; Byrnes et al., 1998; Elbert et al., 1998; Meunier et al., 2001, 2003).

Taken together the above evidence suggests that cortical sensorimotor maps are significantly altered in individuals with FHD, and these alterations may be associated with behavioural impairments in hand sensorimotor function and alterations in behavioural measures of hand function, which are likely linked to dysfunction in GABA signalling.

1.3 Inhibition and sensory processing in Tourette Syndrome

1.3.1 Disordered GABAergic inhibition in TS

Evidence of abnormal GABAergic inhibition in TS comes from post-mortem investigations of the brains of a small number of individuals with TS which demonstrated a substantial decrease (~50%) in the number of GABAergic interneurons within the striatum (Kalanithi et al., 2005). A later study also reported converging evidence for this using positron emission tomography, by demonstrating widespread alterations in $GABA_A$ receptor binding in the brains of individuals with TS, including decreases in $GABA_A$ receptor binding within the ventral striatum, globus pallidus and the thalamus (Lerner et al., 2012). This is supported by studies that have investigated the effects of striatal disinhibition in rodents and non-human primates, which consistently demonstrate that the localised administration of a micro-injection of $GABA_A$-antagonist can produce tic-like movements (Bronfeld, Israelashvili, et al., 2013; Bronfeld, Yael, et al., 2013; Matsumura et al., 1991; McCairn et al., 2013; McCairn & Isoda, 2013). Moreover, the site of these micro-injections determines the nature of behaviour/tic exhibited. For instance, injection of a $GABA_A$ antagonist into focal somatotopic areas of the striatum is demonstrated to produced tic-like movements in specific body parts within minutes, lasting for up to 2 hours (Bronfeld, Yael, et al., 2013).

Importantly, investigations into striatal disinhibition using $GABA_A$ antagonists has demonstrated the involvement of other neural regions for the generation of tic-like behaviours. Specifically, after micro-injections of striatal $GABA_A$ antagonist were administered to non-human primates, electrophysiological recordings - local field potential (LFP) spikes - were recorded at multiple sites including the striatum, pallidum, cerebellum, and M1 (McCairn et al., 2013). LFP spikes within the striatum were observed prior to tic-like behaviours but also in the intervals between tics (these it was suggested might be linked to the experience of PU, McCairn & Isoda, 2013). Conversely, LFP spikes in the cerebellum and motor cortex were always and only present immediately prior to tic execution, suggesting these sites may gate the occurrence of tic execution (McCairn et al., 2013). Together, this evidence strongly illustrates that GABA abnormalities within the CSTC circuit, resulting from striatal disinhibition, are inherent in TS.

1.3.1.1 MRS-GABA

Alterations of GABAergic inhibition in TS also do not appear to be limited to subcortical regions. Studies using measuring MRS-GABA concentrations of cortical regions in individuals with TS compared to healthy controls have yielded mixed results across the lifespan. Cortical MRS-GABA in TD individuals show rapid increases during childhood, followed by stability across early adulthood and a gradual decrease with ageing in later adulthood (Porges et al., 2021). However, MRS-GABA measured within the sensorimotor cortex of young children with TS is reportedly reduced compared to typically developing (TD) controls, suggesting it does not follow this trajectory (Puts et al., 2015)**.** Moreover, lower MRS-GABA levels were correlated with greater motor tic severity (Puts et al., 2015). Moreover, premotor cortex MRS-GABA concentrations were no different between TD children and children with TS. However, using a larger sample, this group failed to replicate these findings and concluded that MRS-GABA concentrations in the primary sensorimotor cortex, supplementary motor area (SMA), and insula were in fact comparable between children with TS and controls (He et al., 2022). This aligns with evidence suggesting MRS-GABA within the premotor cortex is no different between children with TS and controls (Mahone et al., 2018).

Nonetheless, they did report that reduced MRS-GABA levels within the SMA were associated with more severe and more frequent PU (He et al., 2022). This suggests that although sensorimotor cortical MRS-GABA concentrations may not differ between children with/without TS, reduced MRS-GABA may contribute to sensory experiences of TS, such as PU.

Furthermore, an ultra-high-field (7 Tesla) MRS study had previously reported that MRS-GABA levels within the SMA region were increased in adolescents with TS relative to matched controls, and that MRS-GABA levels within the SMA in TS were associated with alterations in both motor gain function (i.e., the increase in motor excitability ahead of a voluntary movement) and motor tic severity (Draper et al., 2014). As there may be increased MRS-GABA levels in adolescents with TS compared to controls, this could suggest that enhanced tonic inhibition in the motor system may therefore be an adaptive response to reduce the increased excitability found in the M1 in TS (Draper et al., 2014). This may reflect a heightened response to the proposed developmental increase of GABA between childhood to adolescence demonstrated in TD populations (Porges et al., 2020). However, no differences have been found within the sensorimotor cortices of adults with TS (Tinaz et al., 2014). Further research evaluating factors such as tonic inhibition and tic severity longitudinally is needed to better determine if MRS-GABA concentrations deviate from the typical trajectory and whether this is an adaptive response and consequence of TS.

1.3.1.2 TMS-SICI

Finally, TMS studies of physiological inhibition within M1 have demonstrated reduced $GABA_A$ receptor dependent physiological inhibition in TS, for both SICI (Orth, 2009) and interhemispheric inhibition protocols (Bäumer et al., 2010). While SICI may not necessarily be reduced in children with TS (Batschelett et al., 2023; Moll et al., 1999), a reduction in SICI has been consistently demonstrated in adults with TS (Heise et al., 2010; Orth, 2009; Orth et al., 2005, 2008; Ziemann et al., 1997). Moreover, SICI measurements are correlated with both motor tics and ADHD symptoms in children and adults with TS, with lower levels of SICI associated with greater tic severity and

more severe ADHD symptoms (Batschelett et al., 2023; Gilbert et al., 2004, 2005). Again, this suggests that although motor GABA may not differ between groups, SICI may contribute to tic severity of TS.

As evidenced above, lower SMA and M1 cortical inhibition may contribute to increased tic and PU severity, however there is a double dissociation between regions associated with each (Batschelett et al., 2023; Gilbert et al., 2004, 2005; He et al., 2022). While tic severity and PU severity are positively correlated (Batschelett et al., 2023), SMA disinhibition is associated with greater urge severity only and GABAergic inhibition of M1 is associated with more severe tics. Batschelett et al. (2023) offer a model of tic generation to explain this. Specifically, increased tic severity may be driven by GABA disinhibition within the SMA (He et al., 2022) which leads to an increased downstream tic severity. Moreover, reduced TMS inhibition from SMA to M1 (Bruce et al., 2021) and reduced TMS-SICI (greater cortical excitability) within M1 is associated with increased tic severity (Batschelett et al., 2023), leading to increased upstream of urges. This infers that greater tic and urge severity are associated with top-down reductions in SMA inhibition and reduced modulation of M1 activity due to this and reduced inhibition within the M1.

1.3.2 Abnormal sensory processing in TS

1.3.2.1 Premonitory sensory phenomena and urges

As noted above, the majority (~90%) of individuals with TS report that their tics are often preceded by PU, which are of particular clinical importance because they form the core component of behavioural therapies that are currently used in the treatment of tic disorders (Cohen et al., 2013). Importantly, it has been suggested that PU arise in part from increased sensitivity to somatic stimulation (Belluscio et al., 2011; Jackson et al., 2011). However, our understanding of sensory abnormalities in TS and their relationship to tic phenomenology, such as suppression and tic severity, is currently limited.

Reports of urge in cross-sectional and longitudinal suggest that PU experiences increase with age and are experienced by over 80-90% of those with TS in adolescence/adulthood (Banaschewski et al., 2003; Cohen & Leckman, 1992; Draper et al., 2016; Gulisano et al., 2015; Kwak et al., 2003; Leckman et al., 1993; Sutherland Owens et al., 2011). However, it is unlikely that urges are due to TS symptom progression, and instead reflect language, cognitive and introspective development. For instance, when evaluating the global PU measure, Premonitory Urge for Tic Scale (PUTS), it is evident that PUTS demonstrates lower temporal stability and internal consistency in children under 10 years old, whereas PUTS in older individuals show stable and consistent properties (Steinberg et al., 2010; Woods, Piacentini, et al., 2005). Therefore, this reported increase in PU from the age of 10 is instead likely to be reflective of cognitive development and the enhanced awareness of urges (Banaschewski et al., 2003; Li et al., 2019). For instance, PU are associated with higher intelligence quotient (IQ) scores and therefore may reflect a greater verbal and expressive ability (Reese et al., 2014; Sambrani et al., 2016). As a result, the increased reporting of urges may be due to a developmental shift in introspective, cognitive and linguistic development, which are necessary to recognise and accurately describe emotional states and behaviours (Lane & Schwartz, 1987; Sutherland Owens et al., 2011). This development may allow children to recognise their urges and as a result, can allow for accurate differentiation between types of behaviours. For example, tic behaviours may become more recognised as compulsive behaviours as a result of urge awareness, rather than as involuntary behaviours (Kane, 1994). This increase of urges over ages is therefore likely to reflect cognitive development for the awareness and expression of urges and their characteristics.

One argument for tics being voluntary responses to PU is that during suppression of tics, real-time measures of urge intensity demonstrate similarities during free-ticcing and suppression, namely that urges increase prior to a tic and decrease after a tic is executed (Brandt et al., 2016; Houlgreave, 2023). However, the urge increase during suppression increases over a longer period of time and peaks earlier until a tic is executed – this could suggest that urge intensity accumulates during suppression

until relieved by tic discharge (Brandt et al., 2016). Moreover, tics are more likely to be executed when urge intensity is rated as medium or high, compared to low (Specht et al., 2014). Together, this indicates that urges may act as cues to execute a tic and that tics may persist in order to provide relief from uncomfortable PU experiences, underlying the negative reinforcement model of TS (Leckman & Riddle, 2000; Specht et al., 2013). This evidence corroborates many patient reports describing tics as voluntary responses to involuntary uncontrollable sensations, which can often feel more disruptive than the tics themselves (Cohen & Leckman, 1992; Cohen et al., 2013; Jackson et al., 2020; Kwak et al., 2003; Leckman et al., 1993).

However, the PU and tic suppression relationship is likely far more complex than simply tic suppression increasing urge. For instance, as previously mentioned, there are similarities in the pattern of PU sensations preceding and after a tic in both free-ticcing and suppression conditions (Brandt et al., 2016). Moreover, it has been demonstrated that although some participants with tic disorders experienced higher urge ratings during periods of reinforced suppression, other participants show no clear pattern or even reduced urge ratings (Brabson et al., 2016). Moreover, others have found little evidence linking PU intensity and tic suppression (Ganos et al., 2012; Matsuda et al., 2020; Sambrani et al., 2016; Specht et al., 2013). This mixture of evidence is also evident when examining the relationship between PU and tic severity measures (Literature showing some support: Ganos, Garrido, et al., 2015; Gu et al., 2020; Langelage et al., 2022; Li et al., 2019; Matsuda et al., 2020; Reese et al., 2014; Sambrani et al., 2016. Literature showing no support: Ganos et al., 2012; Gulisano et al., 2015; Jackson et al., 2020; Müller-Vahl et al., 2014; Steinberg et al., 2010; Sutherland Owens et al., 2011). This strongly suggests that there may be great individual differences when assessing the relationships between PU, suppression and tic severity, especially when using multidimensional measures (e.g. PUTS and Yale Global Tic Severity Scale, YGTSS; (Leckman et al., 1989) as averaged scores assume uniformity across individuals and will mask individual differences present in each dimension of the questionnaire. As a result, we cannot conclusively confirm that suppression and tic severity are linked to PU through the use of instruments such as

PUTS and YGTSS. However, real-time urge measures and the acknowledgement of individual differences may give more insight into this complex interaction. As a result, these relationships are far more complex than greater urges being associated with greater tic severities and tics simply being the relief of urges, i.e. negative reinforcement.

However, some neuroimaging evidence has supported the notion of urges as involuntary cues to voluntary tic execution. For example, using magnetoencephalography (MEG), increases in beta power over the motor cortex, followed by a decrease, have been demonstrated prior to a tic (Niccolai et al., 2019). This initial increase in beta power is suggested to be reflective of compensatory inhibitory mechanisms and was found to be linked to motor PU intensity, inferring a role of PU in inhibitory mechanisms. Furthermore, the decrease in beta power preceding a tic is a pattern typically evident before voluntary movement, suggesting there may be a voluntary mechanism behind tics. Moreover, hyperconnectivity in neural networks linked to voluntary movement have been demonstrated in TS, and this hyperconnectivity is associated with greater severity of PU, also suggesting a role for PU in tic generation (Rae et al., 2020). Additionally, enhanced engagement of the prefrontal cortex was found to be necessary in TS in order to inhibit movements arising from hyperactivity in the M1 (Rae et al., 2020). Again, this could suggest a voluntary component to tics due to hyperconnectivity and involvement of networks underpinning volitional movement, along with a greater need for input from neural inhibitory mechanisms to control tics.

Further to this, there may be some separation of PU and tic phenomena, as not all individuals with TS experience PU and children may have tics without awareness of their urges (Banaschewski et al., 2003; Cohen et al., 2013; Leckman et al., 1993). For instance, it has been demonstrated that tics can persist during sleep, further supporting that tics can occur independently of urges (Cohrs et al., 2001; Jiménez-Jiménez et al., 2020; Kostanecka-Endress et al., 2003). Moreover, neuroimaging evidence investigating PU and tics in TS have also supported the idea that these are

independent phenomena. Specifically, the insula and cingulate cortex have been heavily associated with TS and PU experiences – these areas also align with the functional regions involved in urges, such as swallowing and yawning, in typically developing populations (Jackson et al., 2011; O'Neill et al., 2019). Functional imaging studies have, in fact, demonstrated that the insular and cingulate cortex show significant increases in activity directly prior to a tic and thus is likely reflective of PU, whereas at tic onset, different regions (e.g. sensorimotor cortex) show increases in activity, suggesting separate mechanisms behind PU and tic generation (Bohlhalter et al., 2006; Neuner et al., 2014). Furthermore, separation is seen discretely within the insula and cingulate cortices, with anatomical data demonstrating that motor tic severity and PU scores are separately associated with different anatomical regions in both of these structures (Jackson et al.; Jackson et al., 2020). As a result, there may be some separation of urge and tic phenomenology, however this seems to be a highly complex relationship suggestive of significant individual differences. Overall, causes of urges are still relatively unknown and despite being a largely reported source of discomfort in those with TS, research into PU is generally lacking.

1.3.2.2 Interoceptive awareness

Although there is a complex interaction between urges and tic generation, the detection of urges may be a result of altered interoceptive awareness or interoception. Interoception reflects an individual's awareness of their internal bodily processes, and is reportedly increased in TS, as evidenced by self-reported measures (Eddy et al., 2014; Ganos, Garrido, et al., 2015; Rae, Larsson, et al., 2019). This may indicate those with TS are more aware of their internal bodily sensations and thus have a greater capacity to experience PU as a consequence. Consistent with this proposal, interoceptive awareness scores have been demonstrated to predict of PU severity (Ganos et al., 2015; Rae et al., 2019 – although see Eddy et al., 2014; Pile et al., 2018 for alternative findings). However, although self-reported measures suggest heightened interoceptive awareness in TS, objective interoceptive detection tasks, such as heartbeat tracking, have demonstrated, paradoxically, lower detection accuracy to interoceptive signals compared to controls (Ganos et al., 2015; Rae et al.,

2019). This discrepancy, or interoceptive prediction error, might suggest that there is an increased higher-order sensitivity to bodily signals, but noisier detection of peripheral afferent signals. In other words, those with TS may be both oversensitive and yet less precise to internal bodily signals (Rae et al., 2019). Alternatively, reduced interoceptive detection ability may reflect a compensatory interoception down-regulation in order to suppress PU, and may be an alternative explanation for why interoceptive awareness is related to PU (Ganos et al., 2015). Further investigation into the role of interoceptive prediction error in TS and its relationship with PU is essential. However, due to the mismatch between self-reported and objective measures of interoception, it is most likely that this discrepancy arises from abnormal central processing mechanisms.

1.3.2.3 Exteroceptive awareness

As with detection of internal stimuli, it has been proposed that individuals with TS may also be hypersensitive to external somatosensory stimuli, i.e., exteroception (e.g., Belluscio et al., 2011). For instance, hypersensitivity to sensory stimuli, such as clothing materials, lights, and sounds, has been self-reported in ~70% of individuals with TS and can cause considerable discomfort (Belluscio et al., 2011; Cohen & Leckman, 1992; Cohen et al., 2013; Isaacs & Riordan, 2020). Moreover, individuals with TS are more likely to report over-inclusion/hyper-awareness of, and feeling 'flooded' and easily distracted by, external stimuli, all of which are enhanced under stress and anxiety (Sutherland Owens et al., 2011). This is especially the case with faint, non-salient and repetitive stimuli which are perceived as more disruptive and bothersome than intense stimuli in individuals with TS compared to TD individuals (Belluscio et al., 2011). This suggests sensory gating abnormalities where individuals cannot filter or suppress redundant sensory input. This is consistent with other neurodevelopmental disorders thought to show impaired sensorimotor gating (e.g. ASD and ADHD, although is variable; Schulz et al., 2023), and therefore, those with comorbidities such as OCD, ADHD and ASD who show more severe alterations in sensory perception (see Isaacs & Riordan, 2020 for a review).

To quantitively measure sensory processing, quantitative sensory thresholds can be measured by applying tactile vibrating stimuli to the fingertips and asking participants to distinguish between varying parameters such as the frequency, amplitude and temporal sequence of vibration. However, objective quantitative somatosensory testing has demonstrated that afferent detection thresholds to thermal, tactile and pain stimuli are not significantly different between individuals with TS and TD controls (Schunke et al., 2016). However, alternative evidence suggests static tactile detection thresholds are significantly worse in children with TS (Puts et al., 2015). This indicates that those with TS may detect weak stimuli less efficiently than TD children. Moreover, while baseline the ability to detect the higher amplitude of two stimuli (amplitude discrimination) shows no difference between TS and TD control groups, if one stimulus is preceded by a long ('adapting') stimulus, TD controls amplitude discrimination thresholds become significantly worse, whereas TS groups show comparable performance (Puts et al., 2015). This supports abnormalities in quantitative sensory performance, perhaps reflecting abnormalities in sensory gating and lateral inhibition in TS (Isaacs & Riordan, 2020; Puts et al., 2015).

Overall, this infers that any hypersensitivity to external somatosensory stimuli is unlikely to reflect an underlying deficit in basic afferent somatosensory processing mechanisms. Instead, somatosensory abnormalities in TS, whether interoception or exteroception, may reflect abnormal higher-order sensorimotor processing mechanisms and sensory gating. Nonetheless, studies involving quantitative testing of sensory function in TS are lacking and considerable further investigation is required.

1.4 Functional representations in Tourette Syndrome

As previously shown, TMS motor maps differ in individuals with disordered inhibitory mechanisms and somatosensation compared to TD populations (Section 1.2.2.1). As a result, it can be hypothesised that individuals with TS, shown to have altered GABA functioning (Section 1.3.1), would show altered sensorimotor mapping compared to TD individuals. Cortical thinning is seen in face and hand areas

(commonly affected by tics) of pre- and post-central gyrus of children with TS and these are inversely related to tic severity (Sowell et al., 2008). However, it is unclear whether this cortical thinning is a pathophysiological feature of TS or whether these features are a result of compensatory adaptation.

Using neuronavigated TMS, preliminary evidence has shown that some motor representations are altered in TS compared to typically developing populations (Sigurdsson, Jackson, et al., 2020). The targeted muscles for cortical maps were all related to tic occurrence and the experience of PU, specifically the FDI (hand), deltoid (shoulder), orbicularis oris (lips) and massteter (jaw), (Ganos et al., 2012; Kwak et al., 2003; Schunke et al., 2016). Statistically significant differences were identified between the spatial location of the COG for the FDI muscle, which was shifted more medially in the TS group. The area of the FDI representation was significantly reduced in TS, although no significant differences were seen between Euclidean Distances and Dice coefficients, nor were characteristics of other muscle representations between each group. However, although some motor reorganisation is shown in TS, muscle representations may be more similar to healthy populations than first thought and not show alterations that are evident in FHD despite physiological similarities in inhibitory mechanisms. For instance, where FHD has shown abnormal homuncular organisation of finger representations (Bara-Jimenez et al., 1998; Byl et al., 2000; McKenzie et al., 2003; Meunier et al., 2001), the topographical organisation of the cortical muscle representations in the TS group were comparable to that of the control group, as both groups' maps reflected the topography of the sensorimotor cortex, as described by (Penfield & Boldrey, 1937).

Nevertheless, although few differences were found between groups, features of muscle maps within the TS group were linked to PU severity in TS (Sigurdsson, Jackson, et al., 2020). For instance, reduced distances between hand and facial muscle representations were associated with an increase in PU severity. PU severity was also significantly negatively related to Euclidean distances between cortical hand and facial representations in TS. Moreover, although an increase in the FDI area in the TS

group was associated with greater PU severity, a decrease in the facial muscle cortical area was associated with greater PU severity. This is consistent with tic presentation in TS as facial tics are one of the most prevalent motor tics (Baizabal-Carvallo et al., 2023). However, GABA and SICI's link to TS sensorimotor representations, PU and other sensory phenomena evident in TS is unclear, as this was not investigated. As a result, the extent of PU and heightened sensitivity to internal and external stimuli may be linked with alterations of sensorimotor representations in the cortex, but the role of GABA inhibition in this requires further investigation. Moreover, further quantitative sensory testing evidence in TS is required to determine the extent, or lack thereof, of external sensory processing in TS (Belluscio et al., 2011; Puts et al., 2015; Schunke et al., 2016).

1.5 Research aims

Together, this suggests that abnormalities in sensory processing may be related to a dysfunction in GABAergic inhibition in TS. The relationship to abnormal inhibitory functions and altered sensory processing of internal and external stimuli would provide potential targets and great insight into the causes of discomfort and distress caused by abnormal sensory processing. Moreover, the sensorimotor mapping of sensory and motor function in TS warrants further investigation.

As a result, the following aims this thesis are:

- Do measures of cortical inhibition and sensory processing differ between TS and TD controls? Are these measures correlated in both groups? Do tic and urge severity correlate with these measures?
- Do fine-grained sensorimotor representations of non-tic-related movements (finger tapping) differ between TS and TD controls?
- Do sensorimotor functional representations of tic-related facial movements and responses to low-frequency vibration of facial areas differ between TS and TD controls?
- Can functional representations be manipulated with rTMS?

2. Chapter 2 - Methodology: Investigation and modulation of the sensorimotor cortices

Key words: Magnetic resonance imaging (MRI), functional magnetic resonance imaging (fMRI), magnetic resonance spectroscopy (MRS), γ-aminobutyric acid (GABA), transcranial magnetic stimulation (TMS), short-interval intracortical inhibition (SICI)

2.1 Functional magnetic resonance imaging

2.1.1 MRI physics

Magnetic resonance imaging (MRI) is a non-invasive method of imaging human tissue. Water molecules, which make up between 70-90% of human tissue contain hydrogen nuclei which exhibit nuclear magnetic resonance (MR) (McRobbie et al., 2017). The hydrogen nucleus is a single, positively charged proton that precesses around an axis, producing intrinsic magnetisation, or 'spin' and possesses a magnetic moment, as shown in Figure 2.1a. In the absence of a strong magnetic field, the ensemble of protons in the body point in random orientations resulting in no net magnetisation (McRobbie et al., 2017).

Figure 2.1

Images of (a) a hydrogen hydrogen nucleus with intrinsic spin, and (b) the precession of a hydrogen nucleus about the axis of the B_0 magnetic field at the Larmor frequency with magnetisation M_z.

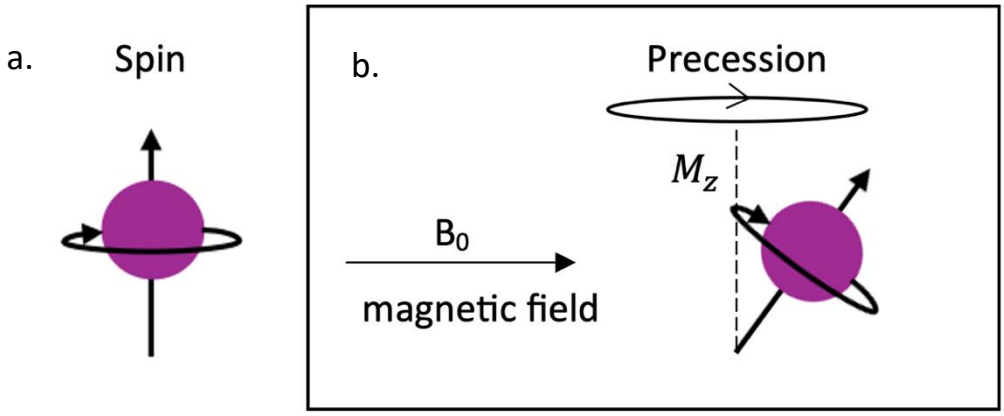

Note. B_0 = magnetic field strength, M_z = net magnetisation in the longitudinal plane

In MRI, a range of static magnetic field strengths are used, ranging from 1.5 to 3 to 7 Tesla (*T*) (Chappell et al., 2020). When placed in an external static magnetic field, the proton will have a magnetic moment that is either in near alignment (parallel) or opposed alignment (antiparallel) with the B_0 field. The parallel state of protons is slightly favoured, as it has the lowest energy level (McRobbie et al., 2017), with the difference in the distribution of protons between the two directions given by the Boltzmann distribution (McRobbie et al., 2017). The larger proportion of proton spins in the parallel state results in a net magnetisation (M) parallel to the B_0 field (see Figure 2.1a). The magnitude of M is field strength-dependent, underlying the push for higher magnetic fields for MRI to provide higher signal-to-noise.

When protons are placed in a magnetic field, they will undergo precession about the axis of the B_0 field at a frequency proportional to its strength (Sharma, 2009), Figure 2.1b. This precession frequency is called the Larmor (or resonant) frequency

which falls within the radiofrequency (RF) range, and is given by the Larmor Equation 2.1:

$$\omega_0 = \gamma B_0 \quad (2.1)$$

where the Larmor frequency (ω_0; MHz) is determined by multiplying the main field strength (B_0; *T*) with the gyromagnetic ratio (γ; 42.58 MHz/*T* for hydrogen nuclei) (Chappell et al., 2020; McRobbie et al., 2017). This precessing net magnetisation in the longitudinal direction (M_z) can then be measured by applying a time-varying current to generate a RF pulse (B_1 field) using a RF coil to knock the magnetisation into the transverse plane (M_{xy}) (Chappell et al., 2020). For instance, delivering a 90° RF pulse centred at the resonant frequency ω_0 tips the alignment of net magnetisation away from the M_z into the M_{xy} plane which then induces a current in the RF detector coil through electromagnetic induction.

Once the RF pulse is turned off, the protons then relax back to M_z (Buxton, 2013; Chappell et al., 2020; McRobbie et al., 2017). T_1 (longitudinal) relaxation describes the time constant of the exponential return of net the longitudinal magnetisation (M_z) to align along B_0 (return to M_0) whereas the T_2 or T_2* (transverse) relaxation refers to the rapid exponential decay of transverse magnetisation due to dephasing of the spins (Chappell et al., 2020). As different tissues take different times to relax back to M_z after excitation, this mechanism can be used to create contrast between different tissues on MRI images.

After applying a 90^0 RF pulse and knocking the spins into the transverse plane, the signal can be spatially encoded to produce an image. Spatial information is encoded using gradient coils within the scanner in the three orthogonal directions G_x, G_y and G_z. The resultant gradient causes the precession frequency of the spins to vary linearly in a spatially dependent manner in each of these planes. These gradient coils can be turned on and off by applying different currents through the coils to create controlled magnetic fields, called gradient fields, and thus a precession frequency can

be attributed to a known spatial location (Chappell et al., 2020; McRobbie et al., 2017).

To restrict the measurement of MR signals to a specific slice, a slice-selective gradient is applied at the same time as an RF excitation pulse such that a narrow range of frequencies is excited (McRobbie et al., 2017). The gradient changes the resonant frequency with spatial location, and this means that a narrow bandwidth RF pulse will then excite regions of tissue with a matching bandwidth only, thus restricting the measurement of the MR signal to a 2D plane (McRobbie et al., 2017). The other gradient directions are then used to encode in-plane and define MR signals in the coordinate system k-space (Song et al., 2006; see Figure 2.2a). From this, a Fourier transform is implemented to convert signals encoded at spatial frequencies into image components (Figure 2.2b) (Chappell et al., 2020; McRobbie et al., 2017).

Figure 2.2

Images depicting (a) k-space reconstruction of a slice from (b) Magnetisation Prepared-Rapid Gradient Echo (MPRAGE) structural image

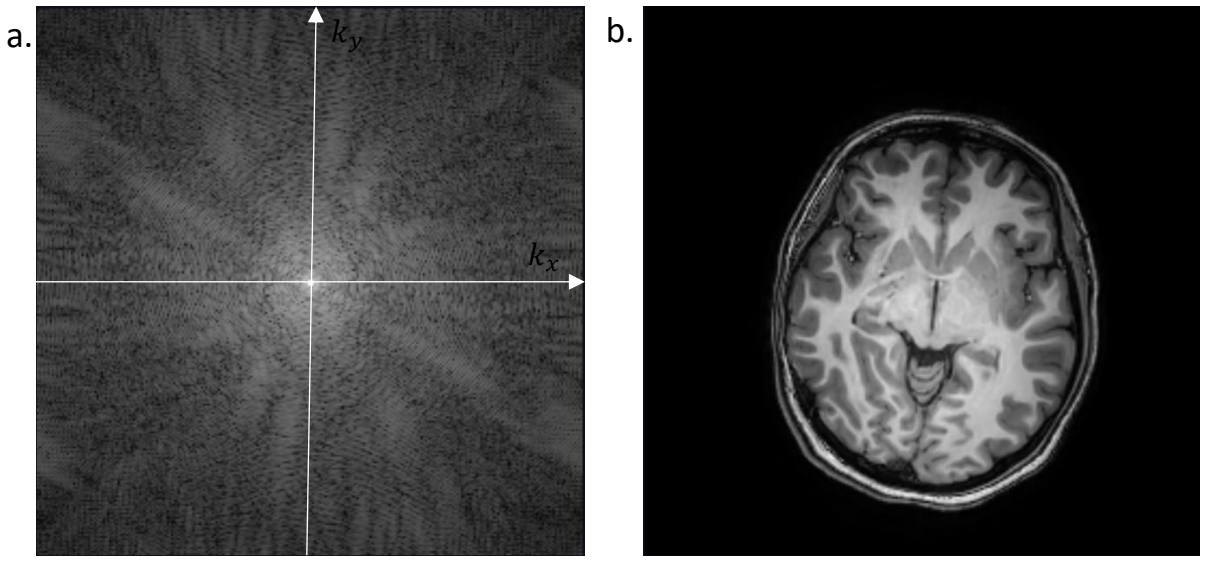

Note. k_x = x-axis of k-space coordinate system, k_y = y-axis of k-space coordinate system. Structural image from Chapter 5 Study 1 Map03 (slice 102). k-space reconstructed using https://k-space.app

In this thesis, two main MR image types are collected: (1) structural images, which provide high quality detail of the brain, and (2) functional images to study at a coarser resolution the haemodynamic changes which dynamically occur in the brain. These will be described below.

2.1.1.1 Structural Images

The structural images used in this thesis are T_1-weighted images, with contrast created from T_1 longitudinal relaxation (Chappell et al., 2020). For example, in Chapter 5 (Study 2), structural images are collected using an inversion recovery sequence, where protons are inverted with an 180^0 RF pulse to flip the net magnetisation into negative $\mathrm{M_z}$. The longitudinal magnetisation is allowed to recover, and after a given time, the inversion time T_I, another RF pulse is applied to knock the $\mathrm{M_z}$ magnetisation at T_I into the transverse plane. This generates contrast between tissue types which have differing T_1 relaxation times within a T_1-weighted image (see Figure 2.2b for an example of a T_1-weighted structural scan). T_1 relaxation times are also field strength-dependent with longer T_1 values at higher field strengths. At 7T for example, fluids such as cerebrospinal fluid (CSF) have long T_1 values (~3000-5000 ms), whilst tissues such as grey and white matter are shorter at ~ 2000 ms and 1200 ms, respectively (Rooney et al., 2007).

2.1.1.2 Functional Images

2.1.1.2.1 Blood Oxygenation Level Dependent (BOLD) response

One method of measuring activity in the brain is to use functional MRI (fMRI) to dynamically measure the Blood Oxygenation Level Dependent (BOLD) contrast over time. BOLD is an indirect measure of neuronal activity based on the notion that more active areas of the cortex with increased neuronal signalling require more oxygenated blood due to greater metabolic demand (Buxton, 2013)**.** Action potentials to trigger this neuronal signalling require energy from adenosine triphosphate (ATP) generated through aerobic respiration (Buxton, 2013)**.** Therefore, in areas with increased

neuronal activity, there is a localised requirement for ATP and oxygenated blood. This results in a localised haemodynamic response of increased cerebral blood flow (CBF), cerebral blood volume (CBV) and cerebral metabolic rate of oxygen ($CMRO_2$) (Arthurs & Boniface, 2002; Buxton, 2013; Chappell et al., 2020; Glover, 2011). The BOLD signal is generated by the ratio of oxyhaemoglobin (Hb) and deoxyhaemoglobin (dHb), due to paramagnetic properties of dHb which causes dephasing and signal loss (Logothetis & Wandell, 2004). In active brain regions the brain overcompensates to increase the delivery of CBF and CBV to the area. This, counterintuitively, results in increased blood oxygenation in active brain regions, and the ratio of Hb to dHB decreases leading to an enhanced BOLD signal, which is of the order of 3% at 3T and increases to of order of 7% at 7T in response to a finger tap (van der Zwaag et al., 2009).

2.1.1.2.2 T2* Relaxation

Specifically, the BOLD signal relies on T_2* relaxation or transverse magnetisation decay. As previously noted, T_2* relaxation refers to the rapid decay of transverse magnetisation (Chappell et al., 2020). This involves dephasing of the net magnetisation in the transverse plane. T_2* relaxation is dependent on changes in localised magnetic field inhomogeneity within tissue which means that protons will precess at different frequencies in different locations depending on the magnetic field they experience (Plewes & Kucharczyk, 2012). This results in a loss of phase coherence of protons, causes dephasing and a reduction in the net magnetisation (Chappell et al., 2020; Logothetis & Wandell, 2004).

Magnetic field inhomogeneities arise from tissues with paramagnetic properties, meaning T_2* relaxation is sensitive to haemodynamic oxygenation variations (Chavhan et al., 2009). Consequently, T_2* relaxation can indirectly measure neural activity from the change in venous blood oxygenation depending on the ratio of paramagnetic dHb to diamagnetic Hb within each voxel. Specifically, in regions with a greater level of dHb to Hb, dephasing occurs due to T_2*relaxation being shorter for deoxygenated blood and a more rapid MR signal decay (Chappell et al., 2020; McRobbie et al., 2017). Conversely, in areas with greater neuronal activity and

oxygenated blood flow, the ratio of dHb to Hb is reduced. This leads to a slower rate of dephasing and longer T_2* relaxation, thereby increasing the recorded MR signal (Chappell et al., 2020; Chavhan et al., 2009; McRobbie et al., 2017). Consequently, voxels in regions with enhanced activity, and a higher proportion of oxygenated blood, will exhibit a higher BOLD signal. As a result, T_2*-weighted gradient echo images are used to detect the BOLD signal with high spatial resolution and produce a time-series of this signal for each voxel in response to a task or stimulus (Chappell et al., 2020; Chen & Glover, 2015). To rapidly sample the T^2*changes which occur in brain activity a gradient echo echo-planar imaging (GE-EPI) sequence is used. A GE-EPI sequence can collect images rapidly as it samples all of k-space in a single shot, with GE-EPI slice and k-space recontruction shown in Figure 2.3 (Stehling et al., 1991). Multiband (or simultaneous multislice) RF pulses can also be used to reduce acquisition time and provide more spatial coverage. These sequences allow multiple slices to be excited simulatenously using a shaped RF pulse (Moeller et al., 2010).

Figure 2.3

Images of (a) GE-EPI slice and (b) k-space reconstruction with single-shot trajectory

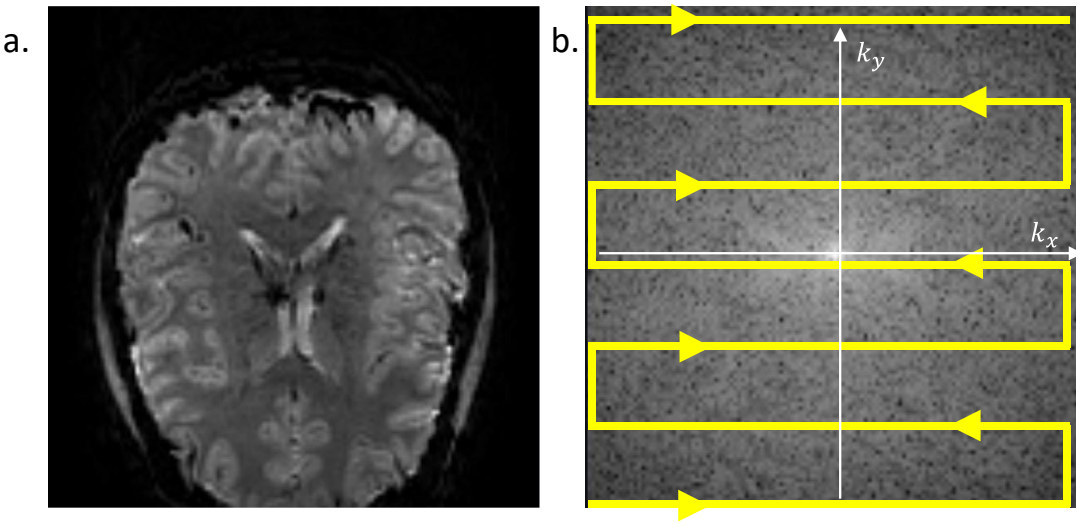

Note. k_x = x-axis of k-space coordinate system, k_y = y-axis of k-space coordinate system. GE-EPI slice from Map03 (Chapter 4 Study 1). k-space reconstructed using https://k-space.app

However, there is a possibility of misinterpreted attribution of neuronal activity to the BOLD signal. For example, the physiological basis behind the localised haemodynamic response and the specific neural mechanisms underlying this (neurovascular coupling) are relatively unknown. Although the BOLD signal is well correlated with neuronal activity, the causal neuronal mechanisms and contributions to the BOLD signal are unclear (Song et al., 2006). For instance, BOLD signal increases in response to a stimulus are more likely to reflect extracellular membrane potentials (e.g. LFP), rather than spiking activity of individual neurons as these are very variably correlated with both the BOLD signal and LFPs (Buzsáki et al., 2012; Logothetis, 2003; Logothetis et al., 2001; Logothetis & Wandell, 2004). Moreover, individual factors impacting cardiovascular functioning, such as ageing and disease can impact the haemodynamic BOLD signal (D'Esposito et al., 2003; Pineiro et al., 2002; Röther et al., 2002; Tsvetanov et al., 2021). This means that differences in BOLD signal activations attributed to differences in neuronal activity may in fact result from abnormal neurovascular coupling (Hillman, 2014). As a result, attributions of the BOLD signal to specific neuronal bases should be made with caution.

2.1.1.3 fMRI experimental design

In this thesis, fMRI studies are conducted using block designs involving sensory stimulation and simple movement tasks, and a digit tapping travelling wave design. With these tasks, we can gain insight into sensorimotor cortical representations of the body at high resolution. These maps can successfully be created for different areas of the body including the foot, lip and digits with high precision, and can even reflect complexities of movements (Lotze et al., 2000). Moreover, fine-grained maps of specific anatomy, such as the digits and facial regions, which are more difficult to achieve using electrical or magnetic stimulation, can be explored using ultra-high field fMRI. For instance, fMRI alongside vibrotactile stimulation to the digits can be used to map the topography of the digits at high resolutions, even achieving visualisation of multiple parts of a single digit (Besle et al., 2013; Da Rocha Amaral et al., 2020; Kolasinski et al., 2016; O'Neill et al., 2020; Sánchez-Panchuelo et al., 2014; Sanchez-Panchuelo et al., 2010; Rosa M. Sanchez-Panchuelo et al., 2012; Stringer et al., 2011).

The location, size and distances between these maps can therefore be investigated within and between subjects.

In a block design, a sensory stimulus is presented or motor task performed in a repeated fashion for a short period before a longer rest period. This period of rest allows for the BOLD signal timeseries (Figure 2.4a) to return to baseline before the task is performed again. This task and rest block pattern is repeated for several cycles to create an fMRI timeseries as shown in Figure 2.4a**.** The task blocks and rest blocks can be separately averaged across cycles and compared to determine significant areas of task-related activation.

For a travelling wave design there is no rest period; instead, a modulated task is presented. For each digit, tapping is performed for a few seconds sequentially in a forward direction (thumb-little finger) for several cycles and then repeated in reverse (little finger-thumb). Forward and reverse travelling wave scans are then combined and averaged for each digit to isolate task-related activation for each digit. By creating a travelling wave of activity across adjacent parts of the sensorimotor cortices, there is a temporal distribution of the haemodynamic response function (HRF). Consequently, each voxel that responds to a particular location will evoke a sinusoidal response within a given phase, which allows for direct association between the phase and the location. (Figure 2.4b; Besle et al., 2013).

Figure 2.4

Example fMRI task paradigms and predicted fMRI BOLD timeseries in response to (a) a block design and (b) a travelling wave design

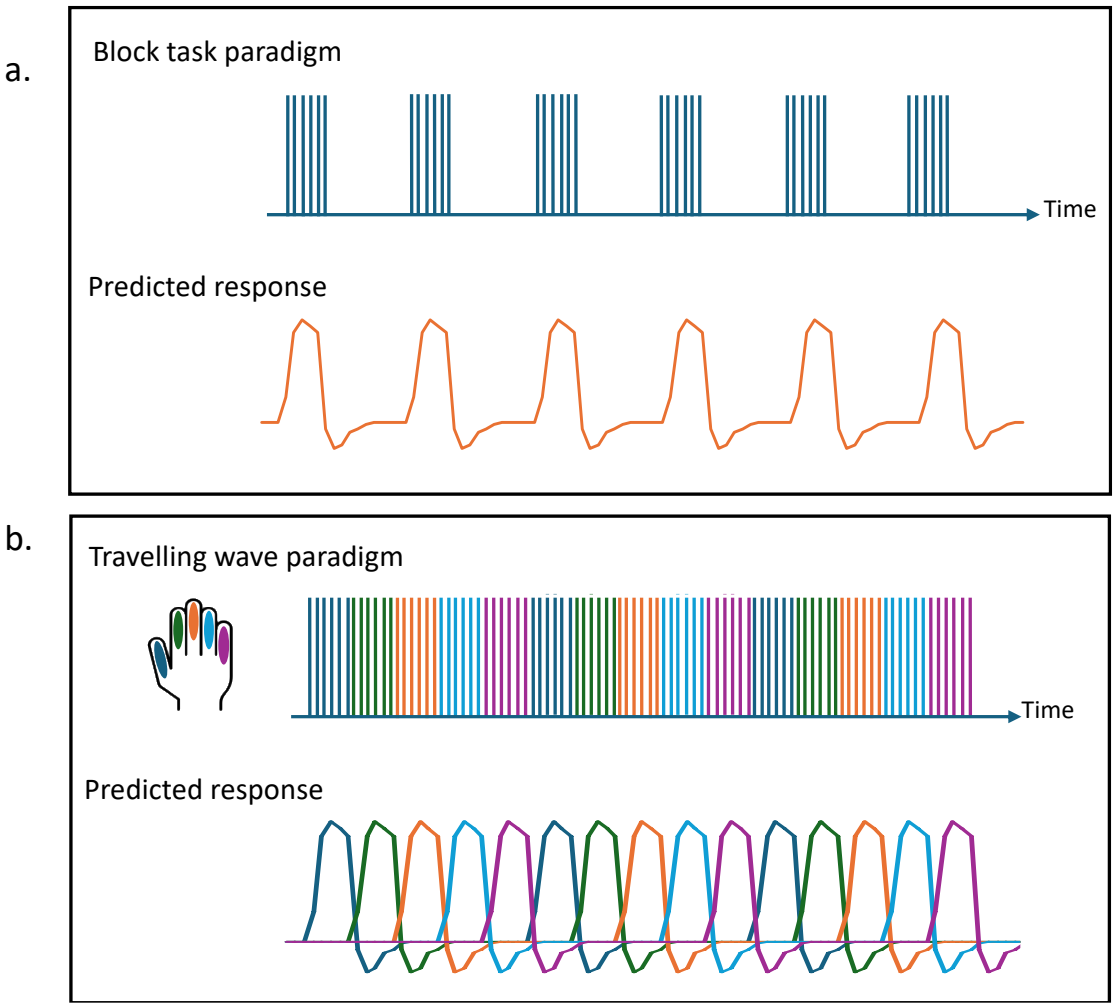

2.1.2 Conventional fMRI analysis

As shown in Figure 2.5, the measured fMRI time-series contains signals from BOLD and from variability in the data unrelated to the BOLD signal (noise). Noise can originate from many sources, for example, structured non-white noise (e.g. physiological fluctuations, motion, low-frequency drift) and random white noise (e.g. thermal current fluctuations or scanner instabilities) (Dowdle et al., 2023; Edelstein et al., 1986; Friston et al., 1995; Poldrack et al., 2011). Before analysis of the fMRI

signal, the raw data must be pre-processed. Minimising the impact of these unrelated signals increases the signal-to-noise ratio (SNR) of data, improving the detection of expected stimulus-induced MR signal changes in statistical analyses (Friston et al., 1995; Poldrack et al., 2011).

Figure 2.5

Example measured fMRI timeseries with signals from the expected BOLD response and noise

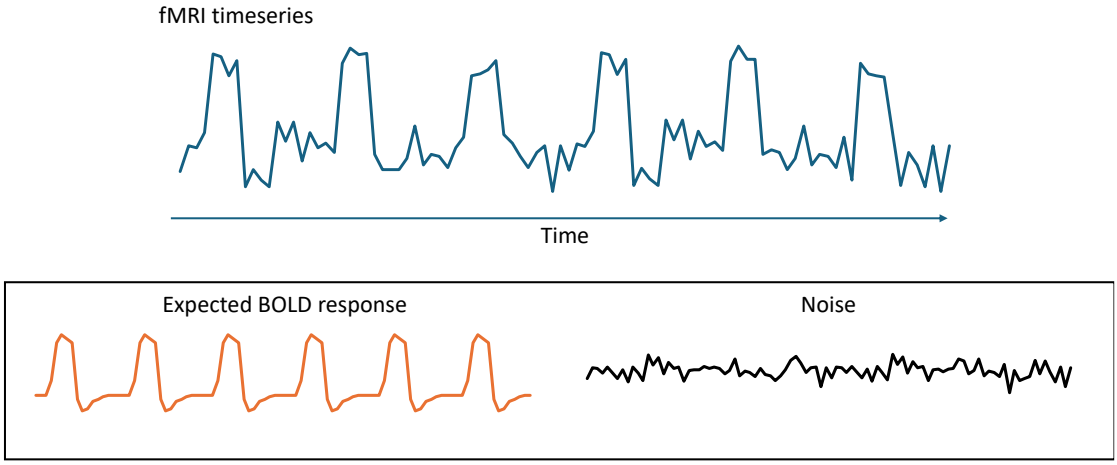

2.1.2.1 Pre-processing

2.1.2.1.1 Noise correction

2.1.2.1.1.1 Thermal noise correction

One source of white noise introduced into the measured fMRI signal is thermal noise. This is an unavoidable source of random noise generated from randomly fluctuating currents in electronics and human tissue (Edelstein et al., 1986; Vizioli et al., 2021). In pre-processing, we can selectively suppress this noise from the fMRI signal through methods such as Noise Reduction with Distribution Corrected (NORDIC) principal component analysis (PCA) (Moeller et al., 2021; Vizioli et al., 2021). NORDIC denoises fMRI data by removing signal components that cannot be

distinguished from zero-mean Gaussian thermal noise. This leaves white noise within the fMRI time-series, including the fMRI signal of interest.

2.1.2.1.1.2 Susceptibility-induced distortion correction

Geometric distortions can occur near tissue boundaries during the acquisition of echo-planar imaging (EPI) sequences used in fMRI. Geometric distortions arise due to the different magnetic susceptibilities between different tissue types and the low bandwidth in the direction of phase-encoding in an EPI acquisition (Andersson et al., 2003). As a result, fMRI images will not spatially align with structural images, which do not suffer from geometric distortions and the true spatial location of BOLD signal may not be accurate (Jezzard, 2012). This geometric distortion can be reduced by acquiring two spin-echo EPIs (SE-EPI) with the same fMRI acquisition parameters but opposite phase-encoding directions, resulting in opposite directions of distortion with equal magnitude. The displacement field (B_0 field) can be estimated from these blip-up and blip-down images (phase-encode reverse pairs). This displacement field is then applied using a least-squares method to reconstruct the distorted image (Andersson et al., 2003). This method results in improved spatial selectivity of fMRI activation due to the enhanced alignment between functional and structural images.

2.1.2.1.1.3 High-pass filtering and pre-whitening

Low-frequency drift is another type of structured noise introduced in fMRI data, which may arise due to physiological properties and scanner hardware (Poldrack et al., 2011). To remove this low-frequency signal from the data, high-pass filtering is applied. However, the resulting fMRI timeseries are temporally autocorrelated, where correlations increase as the temporal proximity of data points increases. This violates assumptions of the general linear model (GLM) used to model the fMRI BOLD response (see Section 2.1.2.2), in which data must not be correlated and variance should be constant over time (Poldrack et al., 2011). Violating these assumptions can introduce bias and increases the rate of false positives in the model. An approach to remove temporal autocorrelation is to pre-whiten the fMRI data prior to the GLM

analysis. Pre-whitening removes temporal autocorrelation related only to noise rather than the fMRI signal of interest (Poldrack et al., 2011). This involves estimating the structure of the correlated noise before running pre-whitening to remove this from the GLM (Poldrack et al., 2011).

2.1.2.1.1.4 Spatial smoothing

High-frequency signals are also introduced within fMRI data which impacts the SNR. To improve SNR, spatial smoothing is applied which removes high-frequency information and blurs the fMRI images (Friston et al., 1995; Poldrack et al., 2011). Smoothing also reduces the impact of individual variability of spatial locations across participants at group-level analyses (Poldrack et al., 2011). A common method of spatial smoothing involves convolution of the three-dimensional (3D) dataset with a 3D Gaussian filter. The amount of smoothing imposed by the filter is determined by the width of the distribution at half of its maximum (full width at half-maximum; FWHM). Too much spatial smoothing can lead to decreased detection of small clusters of activation in analysis and therefore, it is recommended that a smaller level of spatial smoothing (usually FWHM of twice the voxel dimensions) is applied (Poldrack et al., 2011).

2.1.2.1.2 Motion correction

Motion correction removes the impact of participant head movement during fMRI scans. Head movement can be problematic as it can result in a mismatch between a voxel timeseries and the true voxel location in the brain. Stimulus-correlated motion is particularly problematic as this may result in artefactual false-positive activations (Hajnal et al., 1994).

Motion correction reduces the misalignment of voxel timeseries and location by aligning each dynamic in a fMRI timeseries with a common reference image (usually the middle time-point) using image registration. To compare the reference and target image alignment, an affine rigid-body spatial transformation model is required to

create parameter estimates for each timepoint. The displacement between target and reference images is calculated using a cost function which measures the linear relationship between target and reference images. Using this cost function, motion parameters are estimated based on three translational axes (X, Y, Z), three rotational axes (yaw, pitch, roll) and the similarity of intensities across images (Poldrack et al., 2011). These transformations and interpolation are then applied to each voxel of the original fMRI image to create a realigned timeseries (Poldrack et al., 2011). These estimates can also be transformed to a temporal derivative of motion parameters, which infer head displacement from time-point to time-point (Poldrack et al., 2011). The sum of these results in an estimate of overall motion across time, denoted Framewise Displacement (FD) (Power et al., 2012).

If there is excessive motion across an fMRI dataset, removal of the data should be considered due to the impact on SNR and data quality. However, some strategies may reduce the impact of this motion. For instance, FD can be input into a subsequent GLM analyses to account for motion-related variance and model motion-related noise within the data. However, careful assessment of motion regressors is also required as the presence stimulus-correlated motion may result in the removal of task-related signals as the model cannot distinguish between experimental and motion sources (see Figure 2.6) (Poldrack et al., 2011). Finally, specific timepoints of FD over a certain threshold can be identified and input into the GLM as a nuisance variable. This will exclude timepoints associated with excessive movements, reducing the impact of motion confounds in the model and the impact on data quality (Poldrack et al., 2011).

Figure 2.6

(a) Motion plot with task-related motion peaks and (a) BOLD timeseries after motion correction with task-related motion

a.

b.

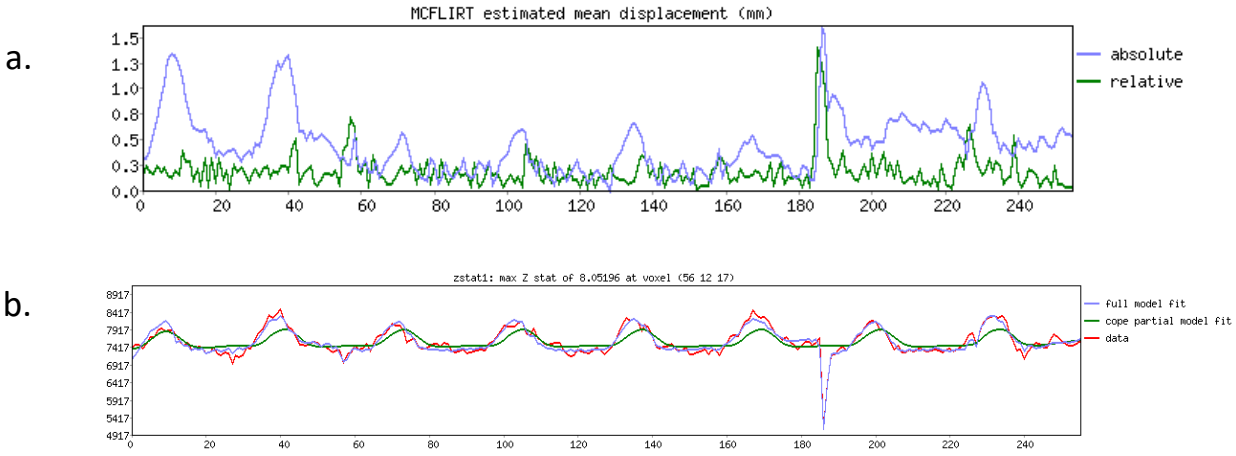

Note. FSL FEAT (Jenkinson et al., 2012) output for TS07 blink (Chapter 5, Study 1). Figure 2.6a shows framewise displacement at specific intervals across the scanning session (purple line), aligning with the full model fit, based on task timings (green line), and the BOLD timeseries (red line) in Figure 2.6b

2.1.2.1.3 Registration and spatial normalisation

For comparison or generalisation of fMRI data across subjects, individual fMRI datasets can be spatially transformed from their native space into the same standard space, such as the Montreal Neurological Institute (MNI) space. This involves co-registration of a subject's fMRI data to their skull-stripped anatomical image (e.g. MPRAGE) using an affine transformation, which applies four linear transformations across x-, y- and z-axes (transformations, rotations, zooms and shears) (Poldrack et al., 2011). Following this, spatial normalisation and volume-based registration is conducted using an affine linear registration to spatially align each fMRI dataset with a standard space image (Poldrack et al., 2011). The registration of images to standard space can then be visually examined to assess the success of the normalisation process (see Figure 2.7).

Figure 2.7

Example of an individual subject registration from (a) functional image to structural image, (b) structural image to standard image, and (c) functional image to standard image

a.

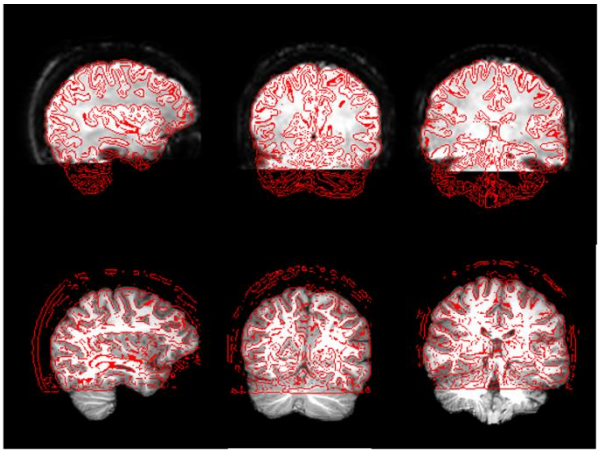

b.

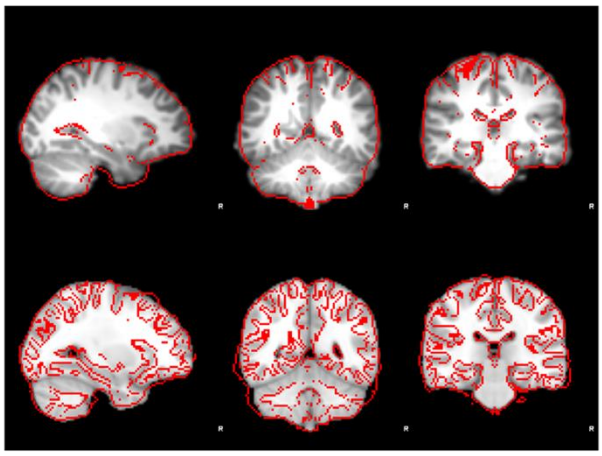

c.

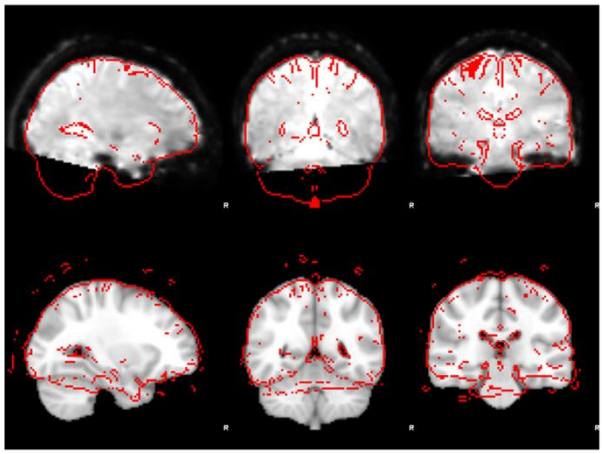

Note. This output is taken from the registration output of Map03 (Chapter 5, Study 1), analysed with the FMRIB's Software Library (FSL) FEAT programme (Jenkinson et al., 2012)

2.1.2.2 General Linear Model (GLM)

Once pre-processed, individual denoised fMRI datasets are statistically analysed to determine the voxels activated in response to the experimental stimuli. To do this, the expected BOLD response can be modelled based on stimuli timings and compared to BOLD time-series data (Smith, 2004). For this, a General Linear Model (GLM) is commonly used; this models the BOLD signal time-series for a given voxel based on one or more explanatory variables (Jenkinson et al., 2020; Poldrack et al., 2011) using Equation 2.2.

$$\Upsilon = X\beta + \epsilon \tag{2.2}$$

where Υ is the measured BOLD signal from one voxel, X is a regressor (e.g. stimulus timing), β is the beta coefficient (scaling parameter for the regressor), and ϵ is the residual error variance (noise). For each voxel, the predicted response is scaled by β to match the data until it results in minimal residual variance, i.e. the best fit (Jenkinson et al., 2020).

2.1.2.2.1 Haemodynamic response function (HRF)

When modelling the expected BOLD response to a stimulus, the temporal nature of the BOLD response must be considered (Glover, 2011). Although there is a localised haemodynamic response, this is a relatively slow haemodynamic process that limits the temporal resolution of fMRI (Poldrack et al., 2011). Where the neuronal response to a stimulus lasts milliseconds, the BOLD signal is detected after a ~6-second lag with an initial dip (due to initial oxygen consumption before increase in CBF and CBV), followed by a peak after approximately 6 seconds due to an increase in CBF and CBV which is greater than the $CMRO_2$ consumption (the stimulus response) (McRobbie et al., 2017; Poldrack et al., 2011). This is followed by an undershoot of 15-20 seconds before returning to baseline (Poldrack et al., 2011). This expected BOLD signal response to stimulation is the HRF (see Figure 2.8).

Figure 2.8

Haemodynamic response function

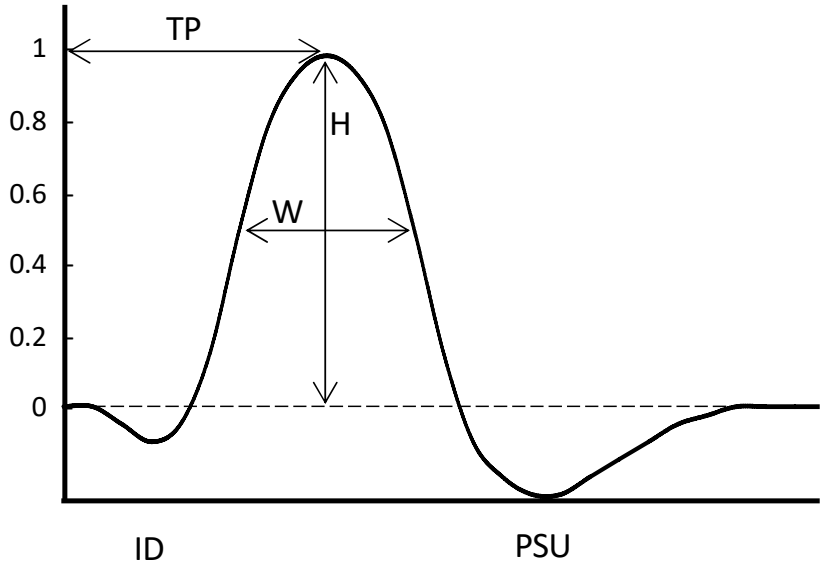

Note. TP = time to peak, H = response height, W = full width at half maximum, ID = initial dip, PSU = post-stimulus undershoot. Image based on Poldrack et al. (2011)

To accurately model the HRF, regressors are included in the GLM to reduce error and improve the goodness-of-fit with the BOLD signal. For instance, the canonical HRF is modelled with two gamma functions (double-gamma HRF) to more accurately model characteristics of the BOLD signal: namely, the stimulus response and the undershoot (Poldrack et al., 2011). Moreover, there are linear time-invariant properties between the neural response and the BOLD signal. This means that neural responses and BOLD signals are scaled by the same factor (or additive if stimuli occur close in time) and are shifted in time by the same factor (Poldrack et al., 2011). Therefore, the HRF can be convolved depending on stimulus strength, timings of stimulus onset and duration to improve the fit of the model with the observed BOLD data (Poldrack et al., 2011; Smith, 2004). This is illustrated in Figure 2.9, where stimulus timings are used to convolve the HRF. However, there may be some incidences where there are non-linear properties between the neuronal response and the BOLD signal, which can be problematic for GLM assumptions of linearity (Poldrack

et al., 2011). For instance, previous work has shown that a visual stimulus presented for 1000 ms evokes only twice the BOLD response of a 5 ms stimulus, despite being 200x longer in duration (Yeşilyurt et al., 2008). This nonlinearity also differs between cortical regions (Soltysik et al., 2004). However, this can be controlled with careful experimental design, for instance, ensuring tasks are at least 7 seconds long to produce linear BOLD responses within the motor cortex (Soltysik et al., 2004). Moreover, nuisance variables such as motion regressors can also be input into the GLM to avoid error variance and artefacts introduced due to head movement (described in Section 2.1.2.1.2 on motion correction) (Poldrack et al., 2011). These allow for more accurate modelling of the HRF signal, therefore improving signal detection.

Figure 2.9

Example estimation of the BOLD signal

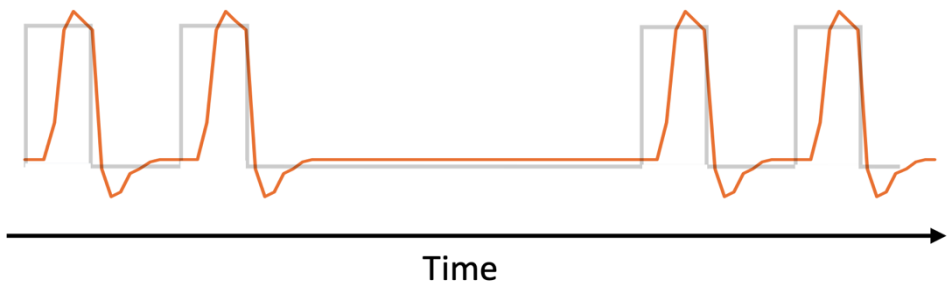

Note. Orange line depicts the haemodynamic response function convolved based on stimulus strength, timings and duration (grey line)

2.1.2.3 Cluster-level inference

After pre-processing, first-level analyses are conducted using the GLM and modelling each fMRI dataset's BOLD signal change in response to a stimulus. If there are multiple within-subject fMRI runs, these are averaged during second-level analyses. From this, individual averaged datasets are assessed at the group level

during a third-level analysis to assess the average BOLD response to a stimulus across individuals and between groups. This is completed using a mixed-effects analysis.

Cluster-level inferences allow the identification of activated voxels which co-occur together within a cluster. While voxel-level inferences are more spatially selective, they are less sensitive than cluster-level inferences and cannot identify the spatial extent of activations as brain regions activated during a task are larger than a single voxel (Friston et al., 1994, 1996; Poldrack et al., 2011; Woo et al., 2014). Moreover, fMRI data are spatially smoothed and oversampled during spatial normalization which results in a spread of signal across several voxels. During cluster-level analysis, clusters are created by first implementing an arbitrary cluster-forming threshold to identify groups of contiguous voxels within statistical maps created after first-/second-level analyses. Secondly, the significance of the cluster is determined by measuring its size and comparing this to a critical cluster-size threshold (Friston et al., 1994; Poldrack et al., 2011; Woo et al., 2014; Worsley et al., 1996). Familywise error rates of the thresholded maps are also controlled (Poldrack et al., 2011). This analysis results in group-level contrast images of significant cluster activation maps.

2.2 Magnetic Resonance Spectroscopy

MRI can also be used to detect concentrations of chemical compounds in human tissue. *In vivo* proton (^{1}H)-MRS utilises NMR properties of protons to non-invasively quantify levels of neuro-metabolites within a single voxel.

As discussed in Section 2.1.1, when a magnetic field is applied, protons precess about the B_0 axis at the same Larmor frequency depending on the gyromagnetic ratio and magnetic field strength. However, there are discrete variations in the precession frequency which are determined by the environment surrounding the proton nucleus (Juchem & Rothman, 2014; Puts & Edden, 2012). An example of this is chemical shift. This refers to the change in precession frequency of proton nuclei part of a chemical compounds due to shielding of the B_0 field by electrons in the surrounding molecular structure (Juchem & Rothman, 2014). This causes differences in the magnetic field experienced by a proton and the resultant Lamour frequency (Juchem & Rothman, 2014). This forms the basis of the MRS spectra, as chemical shifts result in an MR frequency spectrum which relates to different neuro-metabolites, in the order of parts per million (ppm). The amplitude of spectral peaks corresponding to each chemical shift are proportional to the number of resonating protons (Juchem & Rothman, 2014), allowing quantification of neuro-metabolites within a voxel.

Another factor influencing precession frequency is J-coupling. This describes the influence of adjacent proton spins within the same molecule on the magnetic field experienced by protons (Puts & Edden, 2012; Tognarelli et al., 2015). This coupling causes measured signals to split into multiple sub-peaks (multiplets) with a lower peak intensity and a dispersed profile along the spectrum (Puts & Edden, 2012)**.** This is the case for glutamate and GABA, which makes them more difficult to detect and measure (Puts & Edden, 2012). However, this can be mitigated by using higher field strengths, as the relative width of multiplets scales inversely with field strength, causing tightening of the peaks (Puts & Edden, 2012). Furthermore, using MRS at 7T has shown two-fold increases in SNR compared to 4T, with more precise neuro-metabolite quantification (Tkáč et al., 2009). Therefore, MRS at higher field strengths

have the advantage of more precisely identifying and quantifying metabolites with lower concentrations/J-coupling, such as GABA.

During an MRS sequence, after exciting protons with a brief RF pulse, relaxation emits RF signals (Tognarelli et al., 2015). The measured signal (free induction decay) undergoes Fourier transformation to create an MR spectrum (Figure 2.10), with neuro-metabolites within a voxel separated according to their chemical shift and plotted against their signal intensity (spectral peak) (Puts & Edden, 2012; Tognarelli et al., 2015). Water suppression is also applied, as its presence in 70-85% of brain tissue means that it holds the greatest signal the spectra and leads to distortions in the baseline spectra (Tkáč et al., 2021). Therefore, suppressing this water peak allows for more accurate detection and reliable quantification of neuro-metabolites of interest. The resulting spectra is used for quantification neuro-metabolite levels within the voxel of interest, which can be normalised using a stable internal reference metabolite, such as total creatine (Stagg, 2014).

Figure 2.10

Example (a) ^{1}H MRS spectra, and (b) individual peaks

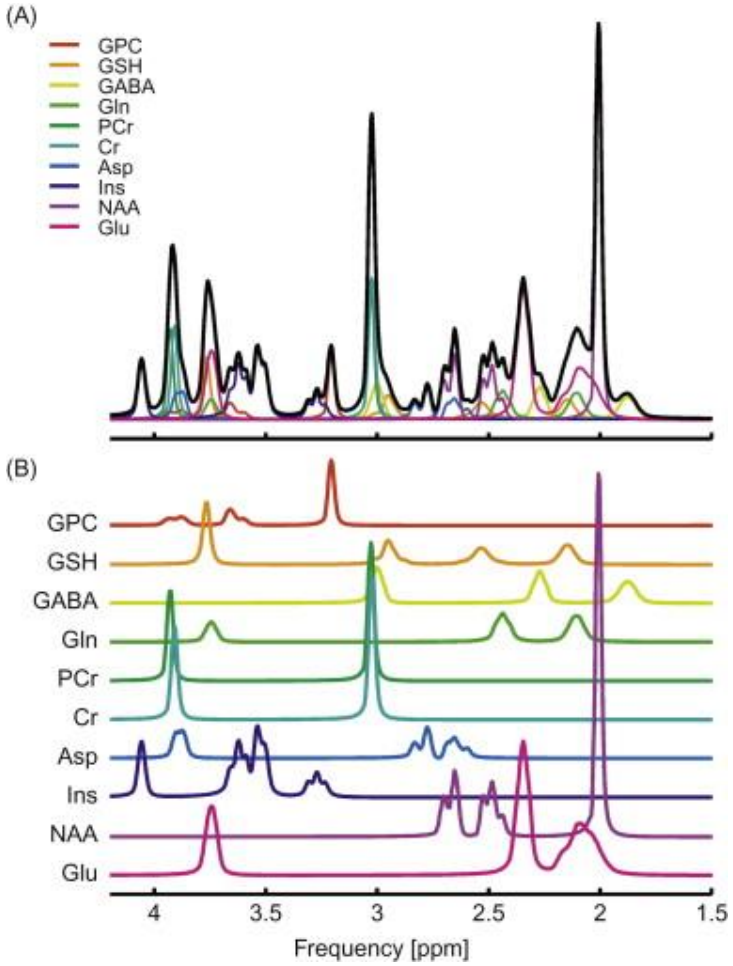

Note. Figure from Chapter 1.1 - Basis of Magnetic Resonance, by C. Juchem and D. L. Rothman, 2014, Copyright 2014 Elsevier, Inc. Figure reproduced with permissions

2.3 Transcranial Magnetic Stimulation

Transcranial Magnetic Stimulation (TMS) is a method of non-invasive brain stimulation with the capacity to modulate and measure neural processing and activity (Pascual-Leone et al., 2000). TMS acts through Faraday's principle of electromagnetic induction (Maeda & Pascual-Leone, 2003), where passing an electrical current through a coil of wire generates a magnetic field and can induce a secondary current in a nearby conductor if this magnetic field is time-varying (Pascual-Leone et al., 2000). TMS involves using a coil, within which are loops of copper wire. The discharge of a large current through this copper wire induces a brief, but strong, time-varying magnetic field perpendicular to the plane of the coil (Figure 2.11a), with a rise time of ~0.1ms and field strength of ~2T (Maeda & Pascual-Leone, 2003; Rotenberg et al., 2014). Upon placing this coil tangentially to the scalp and discharging an electrical current, the resultant magnetic field passes through the scalp and skull to induce a brief current parallel to the coil in the brain (Maeda & Pascual-Leone, 2003; Rotenberg et al., 2014). This secondary current results in activation of neurons by depolarising neuronal membranes to generate action potentials, activating the direct site of stimulation or spreading to projection neurons which signal to the spinal cord or other brain regions (Maeda & Pascual-Leone, 2003; Spampinato et al., 2023).

The depth of the TMS-induced current is limited to the first ~1.5-2cm of the cortex due to an inverse exponential relationship between magnetic field power and the distance from the original current (Daniela et al., 2018; Rotenberg et al., 2014). As a result, TMS is used to stimulate cortical targets. Moreover, the strength and specific localisation of the generated magnetic field, and therefore the focal point of neuronal activation, is impacted by many characteristics such as coil shape. This can be mitigated by using figure-eight coils, which combine two circular coils with current flows in opposite directions (Miniussi & Rossini, 2011), creating two vortices which merge at centre of the coil (Ueno & Sekino, 2021) (Figure 2.11b). These coils allow for a stronger, more focal magnetic field than a circular coil alone, with a small figure-eight coil thought to achieve spatial specificities of around 1-2 cm^2 (Rotenberg et al., 2014).

Figure 2.11

Illustration of (a) TMS coil with opposing current flow directions which cause (b) two vortices of which merge at the centre of the coil

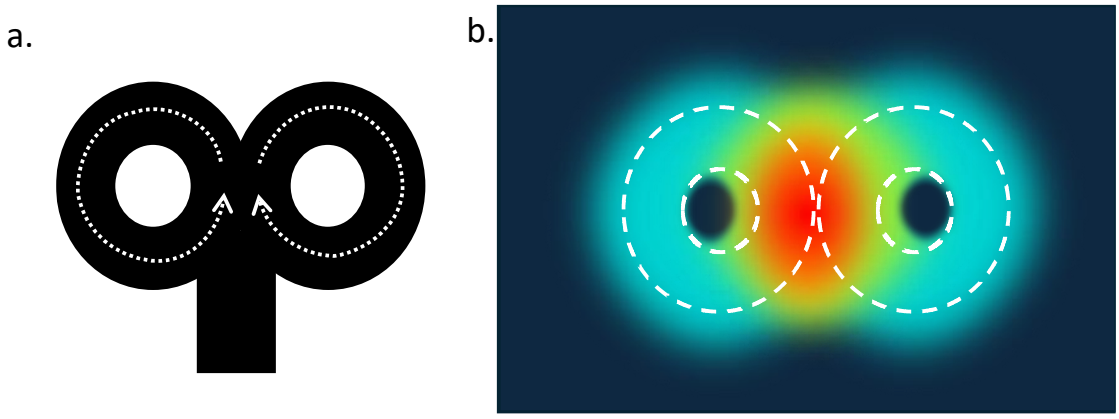

Note. Red area in 2.11b denotes the location of the peak magnetic field

However, the precise depth and focality of TMS are dependent on the TMS-generated cortical electrical field (E-field) and influenced by numerous factors such as coil orientation, pulse intensity, cortical target and individual anatomy, such as cortical folding (Konakanchi et al., 2020; Numssen et al., 2023; Opitz et al., 2013). Although this variability may be problematic for TMS targets within deeper regions and cortical folds, TMS to the M1 is believed to exhibit more reliable specificity. For instance, E-field modelling indicates that M1 TMS primarily focuses targets on the crown-lip of the precentral gyrus, where muscle representations are located, at an optimal angle of 45-degrees to the midline of the head (Janssen et al., 2015; Numssen et al., 2021; Siebner et al., 2022). This is in line with previous evidence which has shown TMS mapping can isolate single finger muscle representations (Numssen et al., 2021, 2023; Ueno et al., 1990). However, E-field estimations are susceptible to orientation of current, as cortical neurons stimulated in M1 are preferentially activated when the induced current flows in the posterior-anterior direction (an orientation of 45 degrees to the medial-sagittal plane of the head) (Di Lazzaro & Rothwell, 2014). As a result,

M1 TMS to target specific muscle representations can be conducted with a relatively high degree of spatial selectivity,

2.3.1 Primary motor cortex TMS

TMS to the M1 activates cortical interneurons and induces descending volleys in pyramidal neurons. These project to the spinal cord and activate spinal motoneurons (Figure 2.12a). If this activation is strong enough, these corticospinal volleys cause motoneurons to fire, evoking involuntary muscle contractions (Di Lazzaro & Ziemann, 2013; Klomjai et al., 2015; Spampinato et al., 2023). TMS can induce these muscle contractions throughout the contralateral side of the body depending on the discrete cortical site stimulated, relating to the motor homunculus (see Figure 1.2). The induced muscle contractions can be assessed by measuring the ensuing electrical potentials called motor-evoked potentials (MEP; shown in Figure 2.12b). MEPs are recorded with electromyography (EMG) using surface electrodes on the muscle in, for example, a belly-tendon formation (see set up on hand in Figure 2.12a). Figure 2.12b displayes the EMG trace of a TMS pulse discharging with a latency period before an MEP, reflecting the conduction time between the TMS pulse to muscle response (Spampinato et al., 2023). MEPs amplitudes are commonly measured from peak-to-peak and are indicative of M1 broad corticospinal excitability encompassing circuitry within the cortex, brainstem and spinal cord, with greater MEP amplitudes indicative of greater corticospinal excitability (Polanía et al., 2018; Spampinato et al., 2023).

Figure 2.12

Illustration of (a) example TMS set up and (b) motor-evoked potential

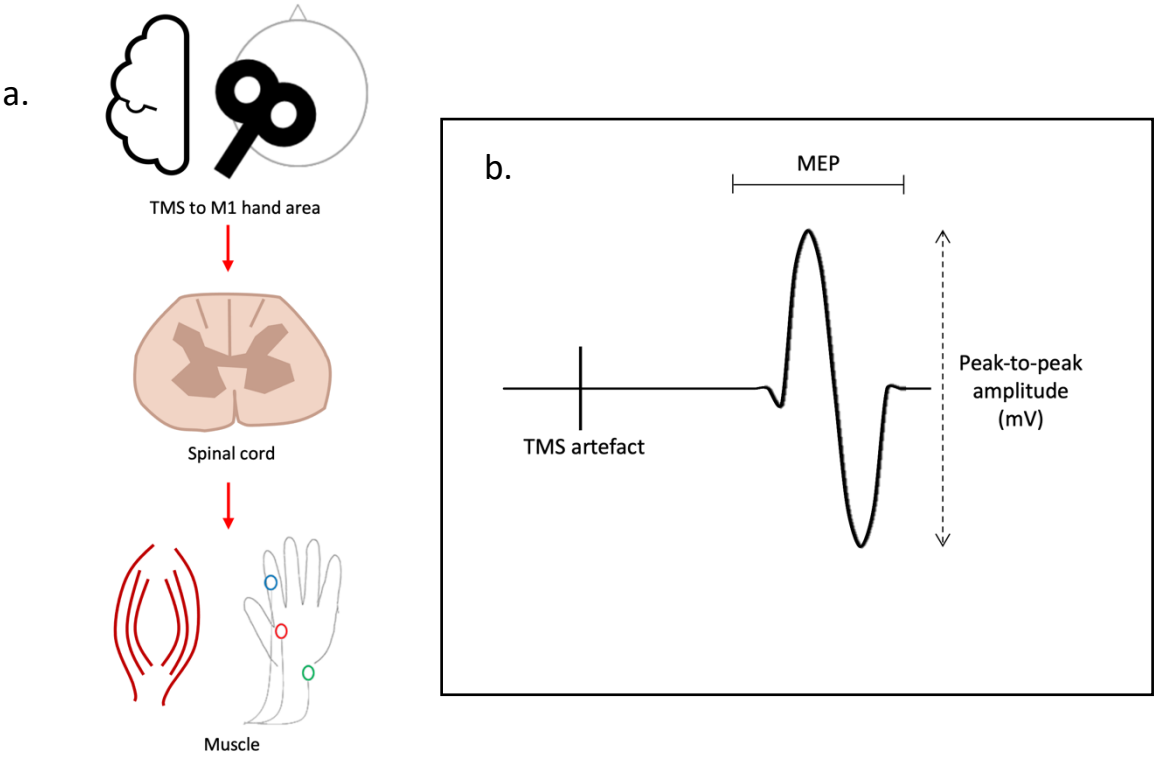

Note. The TMS coil is positioned over the left hemisphere motor cortex 'hand area' and EMG electrodes (circles) are placed in a belly-tendon montage to target the right hand first dorsal interosseous muscle (FDI). Active electrode = red, reference electrode = blue, ground electrode = green. MEP = motor-evoked potential

2.3.2 TMS measures

2.3.2.1 Single-pulse TMS

Single-pulse TMS measures refer to protocols in which TMS pulses are triggered in isolation and are separated by intervals of a few seconds. These measures are typically used to measure corticospinal excitability at rest, however it must be noted that these measures are also impacted by individual variability in neuroanatomical structure and function, such as grey matter volume, functional connectivity between premotor and motor cortices, coil to cortex distance and age (Rosso et al., 2017). This section overviews the single-pulse TMS methods used in this thesis.

2.3.2.1.1 Resting motor threshold

The resting motor threshold (RMT) is a single-pulse TMS measure used to determine individual levels of corticospinal excitability. The RMT is described as the lowest TMS intensity (the percentage of the maximum stimulator output; %MSO) required to evoke an MEP response in the target muscle at rest, with a minimum peak-to-peak amplitude of 50μv in ~5 out of 10 stimulation trials – lower RMT values are indicative of greater excitability (Rossini et al., 2015). The RMT is thought to reflect the excitability of a central pool of neurons under the focal point of the TMS coil and their membrane excitability. This is because previous research has evidenced that thresholds can be altered with administration of drugs that act upon sodium and calcium channels which are present on cell membranes and regulate axon excitability (Hallett, 2000; Hodgkin & Huxley, 1952; Ziemann, 2013).

2.3.2.1.2 1mV threshold

An additional marker of corticospinal excitability is the 1mV threshold (SI1mV). This is the TMS intensity (%MSO) necessary to generate MEPs in the target muscle at an amplitude of 1mV. This therefore requires a suprathreshold TMS intensity to evoke. The SI1mV is also used to indicate the intensity needed to generate 50% of the maximum MEP response in an individual, or the midpoint of the input-output (IO) curve, discussed in Section 2.3.2.1.3 and shown in Figure 2.13 (Pitcher et al., 2015). As higher stimulus intensities are required, SI1mV is believed to reflect wider cortical excitability within a larger pool of neurons, which have greater activation thresholds (Hallett, 2007; Siebner et al., 2009).

2.3.2.1.3 Input-output curve

The IO-curve is a measure of corticospinal excitability, using TMS intensities adjusted in percentages surrounding the RMT (usually 100-150%RMT). By adjusting stimulus intensities and measuring MEP responses for each intensity from the target muscle, this results in a sigmoid-shaped curve between stimulus intensity and MEP amplitude, illustrated in Figure 2.13 (Kemlin et al., 2019). The slope of this curve is

used as an indication of wider corticospinal excitability of neurons further from the centre of maximum activation, with steeper slopes reflecting greater levels of excitability (Stagg et al., 2011). However, the specific mechanisms behind this measure of corticospinal excitability are unclear (Hallett, 2000).

Figure 2.13

Input-output curve

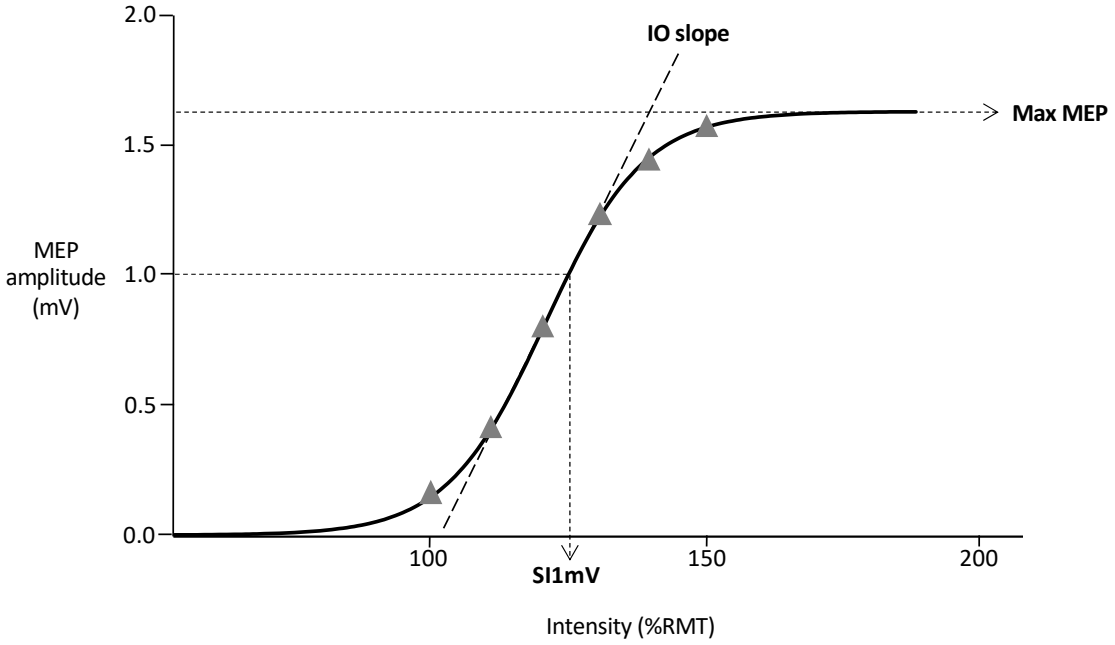

Note. MEP = motor-evoked potential, IO slope = input-output curve slope, Max MEP = maximum amplitude of the motor-evoked potential, SI1mV = 1 mV stimulus intensity, %RMT = percentage of resting motor threshold

Evidence has suggested that IO curve slopes are reflective of M1 glutamatergic activity and widespread glutamate concentration (Di Lazzaro et al., 2003). For example, Di Lazzaro et al. (2003) demonstrated that with increasing ketamine dosage, a drug that influences glutamatergic activity, individuals displayed increasing MEP amplitudes. Moreover, a positive relationship has been exhibited between M1 glutamate concentration (measured with MRS) and IO curve slopes, with individuals displaying higher concentrations of glutamate demonstrating steeper IO curves (Stagg et al., 2011). This indicates that in regions of greater excitability, there are larger stores

of pre-synaptic glutamate. In response to increasing TMS intensities, this pre-synaptic glutamate is released and results in steeper IO curve slopes. However, this has not been replicated in recent research investigating associations between MRS and TMS measurements, which failed to find an association between MRS-glutamate and IO curve slopes with a greater number of participants (12 vs 27) (Dyke et al., 2017). Despite this outcome, authors acknowledge the physiological complexities that IO curves must consider; although steeper IO curve slopes and amplitudes may reflect greater corticospinal excitability, this does not necessarily signify increased outputs of glutamate. Instead, it is speculated that IO curve slopes may reflect the balance of excitation and inhibition in M1 (Dyke et al., 2017).

2.3.2.2 Paired-pulse TMS

Paired-pulse TMS are used to measure aspects of cortical excitability. These involve delivering two successive TMS pulses (a conditioning pulse followed by a test pulse) which either inhibit or facilitate MEPs depending on the interstimulus intervals (ISI) and intensity of the conditioning pulse (Klomjai et al., 2015). Although there are many paired-pulse TMS protocols that can give insight into inhibitory or faciliatory cortical mechanisms, this thesis only used a SICI protocol in Chapter 6 (Study 1), due to its ability to provide insight into GABAergic cortical inhibitory mechanisms (Kujirai et al., 1993).

2.3.2.2.1 Short-interval intracortical inhibition

SICI is assessed using a subthreshold conditioning pulse 1-6 ms prior to a suprathreshold (SI1mV or 120% RMT) pulse. This causes a reduction in the size of MEPs and is thought to be induced by the inhibition of excitability in the motor cortex (see Figure 2.14) (Kujirai et al., 1993; Nakamura et al., 1997). By comparing unconditioned MEP amplitudes to conditioned MEP amplitudes, we can assess levels of inhibition which are strongly suggested to reflect $GABA_A$ receptor-mediated post-synaptic inhibition (Kujirai et al., 1993). This is supported with studies evidencing that after administration of benzodiazepines that enhance $GABA_A$ receptor activity, SICI is

significantly increased (Di Lazzaro et al., 2007; Di Lazzaro, Oliviero, et al., 2005; Di Lazzaro, Pilato, et al., 2005; Di Lazzaro et al., 2006). However, SICI as a measure of GABAergic activity is understood to be localized to phasic inhibition and the synaptic level of neurotransmission, as no relationship has been demonstrated between SICI and MRS-GABA (Dyke et al., 2017). While SICI is indicative of M1 phasic inhibition, and MRS-GABA reflects extracellular pools of GABA and the overall inhibitory tone of a region (Dyke et al., 2017; Stagg et al., 2011).

Figure 2.14

Short-interval intracortical inhibition

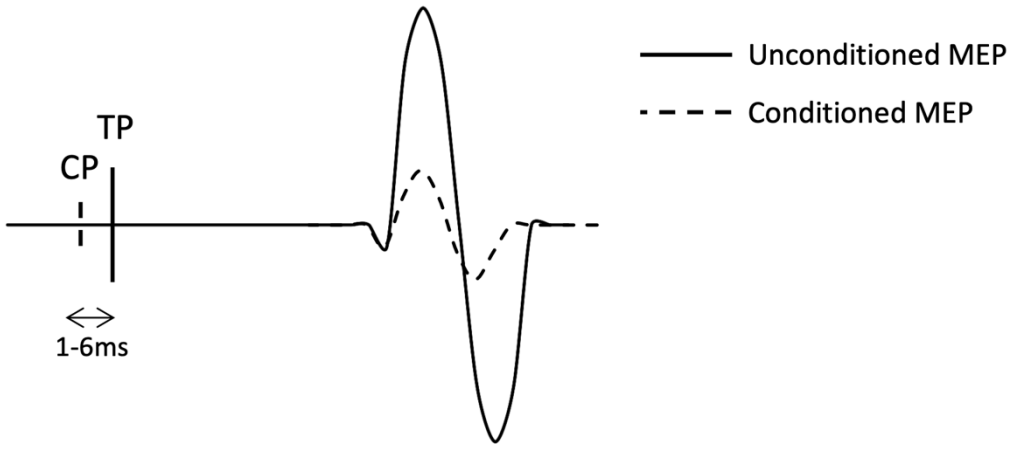

Note. TP = test pulse, CP = conditioning pulse, MEP = motor-evoked potential

2.3.2.3 TMS motor mapping

As discussed in Section 2.3.1, TMS over the M1 can evoke muscle movement throughout the contralateral side of the body depending on the specific motor cortical area stimulated corresponding to the M1 homunculus. Representations of muscles can be outlined and located using neuronavigated TMS and measuring muscle responses with EMG (van De Ruit et al., 2015; van de Ruit & Grey, 2016;

Wassermann et al., 1992; Wilson et al., 1993). By measuring the spread of corticospinal excitability of a muscle we can create a cortical 'map' of activation.

TMS motor maps are thought to reflect the spatial distribution of pyramidal tract neurons and represent the corticospinal excitability of the target muscle (Di Lazzaro et al., 2008). Motor maps are created by evoking single pulses of TMS (above-threshold) to pseudorandom coordinates of a pre-defined cortical region to induce MEPs in the target muscle (Hamdy et al., 1998; van De Ruit et al., 2015). When stimulating the cortex at the target muscle representation site, the target muscle will show an MEP response, but the distribution of cortical activity will vary dependent on the spatial location of the stimulation. For instance, MEP amplitudes will be larger the closer they are to the 'hotspot' of muscle representation and are smaller the further they are from this peak (Wassermann et al., 1992). Therefore, when multiple sites within the cortical region for the target muscle are stimulated, with their spatial coordinates and MEP responses recorded, a map of corticospinal excitability for the muscle can be created (see schematic example in Figure 2.15) (Borghetti et al., 2008).

Figure 2.15

Schematic example of a TMS map of corticospinal excitability

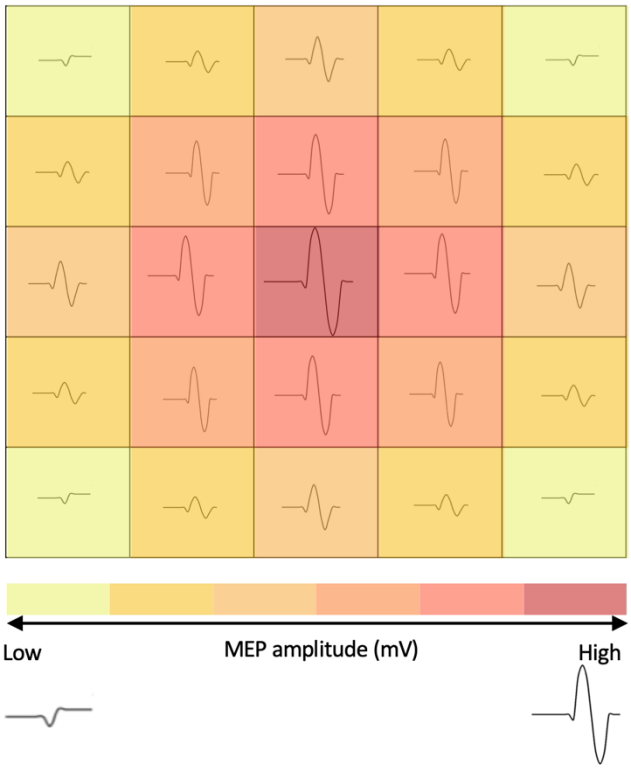

Note. MEP = motor-evoked potential, mV = millivolt

Certain aspects of these TMS maps can be quantified for statistical comparison and visualised on a map to illustrate the area of the muscle representation by showing the spatial distribution of MEP responses, the 'hotspot' of activity and the centre of gravity (COG) coordinates (Hamdy et al., 1998; Julkunen, 2014). The 'hotspot' is the spatial site evoking the largest MEP response and is therefore likely the optimal location of the target muscle in the cortex, whereas the COG is the average optimal area of the muscle representation (Julkunen, 2014; Rossini et al., 2015). When multiple muscles are evaluated, the Euclidean distances between hotspots or COG coordinates of different muscles can additionally be calculated to determine the degree of separation between representations and any spatial overlaps can be determined using the Dice similarity coefficient (Dice, 1945). This provides a non-invasive method of mapping motor representations in the M1.

2.3.3 TMS neuromodulation

2.3.3.1 Repetitive TMS

While single- and paired-pulse TMS methods can evoke brief muscle responses, repetitive-TMS (rTMS) is a method of neuromodulation with the potential to produce relatively long-term responses by discharging repetitive TMS pulses at particular frequencies (Hallett, 2000; Ridding & Rothwell, 2007). rTMS may induce enduring effects by triggering excitatory or inhibitory-like mechanisms in neural synaptic transmission; specifically, long-term potentiation (LTP) and long-term depression (LTD) (Huang et al., 2005, 2011). LTP and LTD influence long-term plasticity through different means; where LTP enhances, LTD weakens synaptic transmission/strength (Bliss & Cooke, 2011; Kolb & Whishaw, 1998). It is proposed that these processes operate through postsynaptic calcium ions (Ca^{2+}). Where LTP is triggered by a patterned influx of Ca^{2+}, sustained levels of Ca^{2+} slowly induce LTD (Huang et al., 2011; Yang et al., 1999). While evidence of overall excitatory or inhibitory effects of rTMS are highly variable (Fitzgerald et al., 2006; Huang et al., 2017), it is generally suggested that low-frequency rTMS (< 1 Hz) diminishes cortical excitability, whereas high-frequency rTMS (> 5 Hz) enhances cortical excitability (Klomjai et al., 2015).

2.3.3.2 Theta-burst stimulation

Theta-burst stimulation (TBS) is a patterned type of rTMS where 3-pulse bursts, at a frequency of 50Hz, are delivered every 200ms. Intermittent TBS (iTBS) involves delivering 20 cycles of 10 bursts (lasting 2 seconds) every 10 seconds and increases M1 excitability (Suppa et al., 2016). iTBS is theorised to induce LTP-like facilitation of excitability due to short bursts of stimulation and its intermittent nature, mimicking the LTP temporal pattern of postsynaptic Ca^{2+} influx and allowing for a rapid build-up of excitation (Huang et al., 2011). Conversely, continuous TBS (cTBS) involves 100-200 bursts continuously for 20 seconds or more and decreases M1 excitability (Di Lazzaro et al., 2008; Huang et al., 2005; Suppa et al., 2016). cTBS is thought to induce LTD-like inhibition due to its continuous nature, allowing for a slow build-up of inhibition (Huang et al., 2005). Consequently, iTBS may enhance M1 excitability by increasing

the effectiveness of excitatory and inhibitory neurotransmission, whereas cTBS reduces this effectiveness.

GABA and glutamate are proposed to be the main physiological drivers implicated in the after-effects of TBS. Glutamatergic synaptic neurotransmission is mediated by N-methyl-D-aspartate (NMDA) receptors and NMDA receptor antagonists have been evidenced to block TBS after-effects, indicating that TBS acts through NMDA receptors to enhance or hinder cortical excitability (Huang et al., 2007; Labedi et al., 2014). Further supporting their role in TBS, NMDA receptors are also greatly implicated in LTP and LTD processes due to their ability to initiate influxes of Ca^{2+} (Huang et al., 2007). Additionally, $GABA_A$ antagonists are demonstrated to enhance LTP in response to excitatory stimulation in rat cortical tissue, supporting the notion that GABAergic mechanisms are involved in TBS after-effects (Grover & Yan, 1999; Hess et al., 1996). However, the precise physiological mechanisms that TBS acts upon are still unclear, as after-effects are highly variable between individuals (Hamada et al., 2013; Suppa et al., 2016).

2.3.3.2.1 iTBS-induced changes in MEP amplitudes

Many studies investigating M1 iTBS have demonstrated MEP amplitude and IO curve slope increases in response to iTBS compared to sham stimulation, strongly supporting its excitatory effect in M1 (Brownjohn et al., 2014; Hsieh et al., 2015; Huang et al., 2005, 2007; Murakami et al., 2012; Nettekoven et al., 2014). Further support has come from systematic reviews investigating the efficacy and temporal nature of iTBS after-effects. Reviews have demonstrated that iTBS increases MEP amplitudes for between 30-60 minutes post-stimulation (Chung et al., 2016; Wischnewski & Schutter, 2015). Moreover, M1 iTBS has been evidenced to improve recovery post-stroke and enhance motor learning mechanisms, giving it therapeutic promise (Chen et al., 2019; Platz et al., 2018; Talelli et al., 2007). However, the extent to which these therapetuic improvements are exclusively attributable to enhanced iTBS-induced excitation is not clear, as this was not causally assessed. Although more clarity is required on iTBS after-effects, this strongly indicates that iTBS can induce

somewhat lasting, albeit short-term, excitation in the M1 and that it may have therapeutic potential in motor recovery.

However, there is uncertainty about iTBS's influence on wider cortical areas and the notion of variability in response across individuals. For example, iTBS after-effects are not localized to the stimulated region, with one study demonstrating significantly facilitated MEP amplitudes in an adjacent cortical region relating to an adjacent muscle after iTBS, with this muscle demonstrating significantly greater increases in excitation compared to the targeted muscle (Morris et al., 2019). This suggests that iTBS induces facilitation beyond the target site of stimulation. Moreover, great variability is commonly observed in the response to iTBS, with many individuals displaying unchanged, or even diminished, excitability (Hamada et al., 2013; López-Alonso et al., 2014). However, the influence of iTBS is generally stable within individuals, with one study demonstrating consistency in iTBS after-effects across two separate iTBS sessions in ~ 73% participants (Hinder et al., 2014). This indicates that individual differences may be responsible for the high irregularity in response to iTBS, however, it is unclear what these individual differences may be. Overall, this evidence provides some support that iTBS produces a facilitatory effect on M1 cortical excitability. However, it must be noted that activation is variable between individuals and may induce changes in corticospinal excitability beyond the site of stimulation.

2.3.3.2.2 iTBS-induced changes in SICI

As discussed in Section 2.3.3.2, $GABA_A$ receptors are understood to have a role in LTP, as GABA antagonists are evidenced to enhance after-effects of excitatory stimulation (Grover & Yan, 1999; Hess et al., 1996). This could indicate that GABAergic mechanisms are diminished or disrupted to allow for increases in cortical excitability and has been supported by animal research (Kozyrev et al., 2014, 2018). In human research, this has also been evidenced by significantly reduced SICI inhibition after excitatory rTMS (Peinemann et al., 2000; Quartarone et al., 2005; Wu et al., 2000). Moreover, preliminary evidence has also indicated that excitatory rTMS can induce reductions in MRS-GABA, suggesting tonic inhibition may also be reduced by

excitatory stimulation (Gröhn et al., 2019). However, others have demonstrated that SICI remains stable following iTBS (Chung et al., 2016; Murakami et al., 2012; Tse et al., 2018). This indicates that the influence of iTBS on M1 inhibitory circuits and neurotransmission warrants further investigation.

3. Chapter 3 - Investigating sensory phenomena and neurometabolites in Tourette Syndrome

Key words: Tourette Syndrome (TS), typically developing (TD), temporal order judgement (TOJ), amplitude discrimination (AD), magnetic resonance spectroscopy (MRS), γ-aminobutyric acid (GABA), glutamate (Glu)

3.1 Introduction

As discussed in Section 1.3.2, TS is a disorder associated with alterations in sensory phenomena, some of which can cause great discomfort (Belluscio et al., 2011; Cohen & Leckman, 1992; Cohen et al., 2013). These sensory abnormalities are evident in interoceptive domains, such as urges preceding tics, and the self-reported enhanced detection of internal stimuli, yet poor interoceptive accuracy in quantitative testing (Eddy et al., 2014; Ganos, Garrido, et al., 2015; Rae, Larsson, et al., 2019). This altered central processing and interoceptive awareness has been proposed to underly the reported hypersensitivity to external stimuli (Schunke et al., 2016). However, exteroceptive sensitivity evidence is limited to self-reported hypersensitivity to external stimuli without great investigation into quantitative sensory thresholds. For example, at the time of writing, only three studies have published quantitative tactile sensory testing in 19, 14 and 23 participants with TS and have yielded mixed results. Specifically, while one study has evidenced poorer tactile detection thresholds and less susceptibility to 'adapting' amplitude discrimination stimuli compared to TD controls (Puts et al., 2015), others have found no evidence of altered quantitative tactile sensory thresholds in TS (Belluscio et al., 2011; Schunke et al., 2016). As a result, further investigation is necessary to determine if this reported hypersensitivity is inherent in TS due to central processing deficits.

As proposed in Section 1.2.1.2, sensorimotor inhibition (specifically, GABA) is thought to play a role in fine-tuning activity and enhancing acuity of cortical neurons and is associated with greater detection of somatosensory stimuli and their features (Cassady et al., 2019; Hicks & Dykes, 1983; Kaneko & Hicks, 1990; Kolasinski et al., 2017). This is supported by evidence in TD populations, as greater levels of S1 and sensorimotor GABA are associated with greater sensorimotor performance. Specifically, lower thresholds are evidenced for frequency discrimination (Mikkelsen et al., 2018; Puts et al., 2011, 2015; Puts, Wodka, et al., 2017), static temporal order judgement (TOJ; Kolasinski et al., 2017) and amplitude discrimination tasks (Mikkelsen et al., 2018), with less susceptibility to adaptation effects (Puts et al., 2015). Moreover, this pattern is seen in disorders associated with abnormal sensorimotor GABA, such as FHD and ASD, with evidence of increased temporal and spatial detection and discrimination thresholds compared to TD controls (Antelmi et al., 2017; Bara-Jimenez et al., 2000; Bara–Jimenez et al., 2000; Puts, Wodka, et al., 2017). Moreover, in ASD, there is also evidence of impairments in amplitude discrimination and reduced susceptibility to adapting stimuli (Puts et al., 2014). There is also some evidence to suggest that individuals with ASD seem to be immune from the detrimental effect of persistent background (carrier) stimuli on TOJ thresholds (cTOJ). It was demonstrated that while individuals performed significantly worse in TOJ and cTOJ tasks compared to the TD group, the ASD group showed comparable thresholds across conditions while TD group had significantly worse thresholds from TOJ to cTOJ tasks (Tommerdahl et al., 2008). A similar pattern has been demonstrated in ADHD, a common comorbidity in TS, where TOJ performance is poorer in comparison with a TD control group, yet cTOJ performance is comparable across groups, suggesting that the carrier effect may be stronger in TD populations (Puts, Harris, et al., 2017). This provides strong support for the notion that GABAergic inhibitory mechanisms have a role in sensory processing of sensory stimuli.

As TS is associated with abnormal inhibitory processes (see Section 1.3.1), it is proposed that somatosensation will be less efficient, due to reduced fine-tuning of cortical activity, surround inhibition, receptive field acuity of cortical neurons, and less

integration across sensorimotor networks (Kolasinski et al., 2017; Cassady et al., 2019; Kaneko & Hicks, 1990; Hicks & Dykes, 1983). This means that detection of sensory stimuli and their features will be less precise. However, the notion that abnormalities in cortical inhibition is an inherent feature of TS is still widely debated. As discussed in Section 1.3.1.2, while SICI is consistently shown to be reduced in adults with TS (Heise et al., 2010; Orth, 2009; Orth et al., 2005, 2008; Ziemann et al., 1997), there has been mixed evidence when assessing MRS-GABA across the SMA, sensorimotor and premotor cortices (He et al., 2022; Mahone et al., 2018; Puts et al., 2015; Tinaz et al., 2014). Despite questions into the inherent nature of GABA in TS, lower MRS-GABA levels in the SMA and sensorimotor cortices of children and adolescents with TS have shown significant associations with more severe experiences of sensory phenomena such as premonitory urges and motor tic severity (Draper et al., 2014; He et al., 2022; Puts et al., 2015). This relationship is also evident with reduced SICI in adults and adolescents with TS, who demonstrate more severe motor tics and symptoms of ADHD (Batschelett et al., 2023; Gilbert et al., 2004, 2005). This suggests that, while quantitative measures of GABA and inhibition within cortical motor regions are greatly variable and may not differ between TS and TD populations, these may be related to individual tic phenomenology and sensory experiences in TS.

However, although GABAergic inhibition may be related to symptomology of TS such as tic severity and premonitory urge severity, its relationship to quantitative sensory processing in TS are unclear. Despite previous investigations showing that TS participants exhibit poorer tactile detection thresholds and reduced susceptibility to adaptation effects compared to TD controls, in tasks associated with GABAergic inhibition, frequency discrimination and adaptation effects were only significantly related to TD control group MRS-GABA levels (Puts et al., 2015). However, this may instead reflect the inability of MRS to reveal the complexities of GABAergic mechanisms. While these sensory tasks are likely to reflect inhibitory features of cortical neurons, such as surround inhibition and feedforward inhibition, MRS as a measurement tool cannot capture these discrete processes, only the ‘bulk’ within a region (Puts et al., 2015; Tommerdahl et al., 2019). An alternative view is that instead,

both excitation and inhibition within TS have roles in sensory processing and symptom phenomenology. For example, glutamate measured with MRS (MRS-Glu) is increased in TS compared to TD population (Mahone et al., 2018). Moreover, greater MRS-Glu levels are associated with improved behavioural performance in TS, specifically motor selective inhibition (the ability to inhibit prepotent movements; Mahone et al., 2018). Additionally, TMS-measures of M1 cortical excitability (associated with motor tic severity) were inversely related with MRS-GABA concentrations in the SMA of adolescents with TS (Draper et al., 2014). As a result, both excitatory and inhibitory neurometabolites warrant further investigation into their potential role in tactile sensory functioning and symptomology in TS.

3.1.1 Aims

Study 1 aimed to conduct quantitative sensory testing to identify any significant differences in quantitative tactile sensory thresholds between TS and TD control groups. It was hypothesised that measured thresholds would be higher in TS groups due to the proposed disruption of GABAergic inhibition inherent in TS. Moreover, it was predicted that adaptation would worsen amplitude discrimination and TOJ thresholds in the TD group only, and the TS group would show reduced susceptibility to adaptation effects compared to TD controls, as shown in Puts et al. (2015). Moreover, it was hypothesised that TS participants would also show reduced susceptibility to the detrimental effect of a carrier stimulus on TOJ thresholds, as shown in ASD and ADHD populations (Puts, Harris, et al., 2017; Tommerdahl et al., 2008).

Finally, Study 2 used ^{1}H-MRS to investigate neurometabolite levels in a subset of adults with TS and TD controls with the aim of assessing levels of sensorimotor MRS-GABA and -Glu between groups. It was predicted that MRS-GABA would be significantly lower and MRS-Glu significantly higher in the TS group compared to TD controls. Moreover, self-reported interoceptive and exteroceptive awareness questionnaires were completed to identify any differences between groups, with the hypothesis that TS participants would show higher scores, reflecting hypersensitivity

to internal and external stimuli compared to TD controls. Quantitative sensory thresholds were also taken to allow for the assessment of any correlations between somatosensory processing and sensorimotor MRS-GABA and -Glu in each group, with the addition of tic phenomenology (urge and tic severity scales) in the TS group. Relationships were assessed between MRS-GABA and -Glu with interoceptive and exteroceptive sensitivity for each group to identify any relationships with self-reported measures of sensory processing. For quantitative sensory testing, it was predicted that, in each group, greater MRS-GABA concentrations would be associated with lower sensory thresholds (better performance). Additionally, TS participants were hypothesised to show significant relationships between MRS-GABA, -Glu and tic phenomenology, such as tic severity and urge severity.

3.2 Study 1: Quantitative Sensory Testing in TS and TD controls

3.2.1 Methods

3.2.1.1 Participants

Twenty-seven patients with TS and 29 TD control participants completed quantitative sensory testing. Participants were recruited through convenience sampling of those taking part in studies outlined in Chapter 3 (Study 2), Chapter 4 and Chapter 5. Demographics of this group are shown in Table 1. Two-tailed Mann-Whitney *U* tests showed no significant differences between age ($U = 381$, $p = 0.870$) and sex (X^2 (1, $N = 56$) = 0.351, $p = 0.554$) between groups (descriptives shown in Table 3.1).

Table 3.1

Demographics of TD and TS Groups in Study 1

Group	N	Age	Sex
TD	27	30.0 (±1.4)	10 male, 17 female
TS	29	30.5 (±1.4)	12 male, 17 female

Note. TD = Typically developing control group, TS = Tourette Syndrome group, *N* = number of participants, mean (±standard deviation)

Participants gave informed consent, and ethics were approved by the local ethics committee (School of Psychology, University of Nottingham: S1500). No participants in the TD group were taking CNS-active drugs and were free from any mood or neurological illness during the experimental timeline. All medications and clinical scores for the TS group are displayed in Appendix A.1. All TD and TS participants were screened prior to participation to assess MR safety and tic phenomenology, to ensure low tic severities, especially with head and facial tics, which may impact subsequent

MR quality. All participants were right-handed, as assessed by the Edinburgh handedness questionnaire (Oldfield, 1971).

3.2.1.2 Clinical measures in TS participants

3.2.1.2.1 Yale Global Tic Severity Scale

The Yale Global Tic Severity Scale (YGTSS) is a clinician-administered structured interview which measures tic severity across motor and vocal tics within the last week. Tic severity is evaluated across subscales which assess multiple domains of tic phenomenology, specifically the number, frequency, intensity, complexity and interference of motor and phonic tics separately (Leckman et al., 1989) Each subscale is scored on a 6-point Likert scale, from 0 (none) to 5 (severe). This is followed by a separate item assessing overall impairment (across both motor and phonic tics) and is scored out of 50. Validation of the YGTSS has shown good internal consistency, stability and discriminant validity (Haas et al., 2021; Leckman et al., 1989; Storch et al., 2005). All scores can be summed to create a global severity score, but separating scores into motor, phonic and impairment subscales show greater insight into tic symptomology (Haas et al., 2021).

3.2.1.2.2 Premonitory Urge for Tic Disorders Scale – Revised

The Premonitory Urge for Tic Disorders Scale – Revised (PUTS-R) is a 24-item self-report scale assessing the urge-like feelings that may be experienced by an individual prior to a tic (Baumung et al., 2021). Items include the statement 'Right before I do a tic…' and assess different urge severity and urge qualities that may be experienced, such as feeling pressure, energy, or sensations similar to an itch prior to a tic. Each item is marked on a 5-point Likert scale, from 0 (not at all) to 4 (very much) and summed to create a final score of up to 96 with higher scores reflecting greater severities of premonitory urge experience. The original PUTS scale has shown to have good reliability, convergent validity, internal consistency and temporal stability (Woods, Piacentini, et al., 2005). The revised PUTS-R scale also shows good

discriminate validity, with greater internal consistency in children than the original PUTS scale (Baumung et al., 2021). Moreover, PUTS scores may give insight into interoceptive awareness, as greater PUTS scores have shown significant associations with interoceptive awareness assessed by self-reported internal sensitivity and heartbeat counting tasks (Ganos, Garrido, et al., 2015; Rae, Larsson, et al., 2019).

3.2.1.3 Tactile quantitative sensory tests

Quantitative sensory testing was conducted using the Brain Gauge 2-point vibrotactile stimulator (Cortical Metrics, USA; Tommerdahl et al., 2019). The computer-mouse-shaped device contains two round probes (5mm diameter) positioned at the top of the device that deliver vibrotactile sinusoidal stimuli. Participants were instructed to place the tips of their left-hand (non-dominant) index (D2) and middle (D3) finger on the device. This device is controlled via USB interface connection to a MacBook Pro (13-inch screen), where instructions were displayed on the Brain Gauge app for participants to follow for each test battery. Participants were instructed to use a computer mouse with their right hand (dominant) to navigate the Brain Gauge interface and select items on the screen.

Each battery involved a practice task with feedback and participants were instructed to make a best guess if they were unsure of an answer throughout, with no time limits on responses. The Brain Gauge system is automated via a two-alternative forced-choice (2AFC) step-wise tracking system which calculates individual thresholds by varying the task variables (e.g. amplitude, interstimulus interval; ISI) depending on which task is being presented and the previous participant response. For instance, if an individual responded to a TOJ trial correctly, the ISI was reduced. This occurs until the participant can no longer distinguish between stimuli as their sensory threshold is reached.

3.2.1.3.1 Amplitude discrimination

Amplitude discrimination involves asking participants to compare two 25Hz stimuli based on their amplitude (intensity) starting at 400µm across 20 trials (adjusting by 20 µm depending on correct/incorrect answer). Stimuli were either presented sequentially, simultaneously or with a conditioning stimulus presented to one digit before simultaneous stimuli (single-site adaptation). Thresholds for each variation were calculated as the smallest difference detected between amplitudes (measured in µm) across trials, with an additional percentage calculated reflecting the percent change in threshold between simultaneous and SSA conditions. Amplitude discrimination paradigms are thought to reflect levels of surround inhibition (Puts et al., 2017).

3.2.1.3.2 Simultaneous amplitude discrimination

Simultaneous amplitude discrimination (simAD) was assessed by presenting two vibrating stimuli of different amplitudes to D2 and D3 for 500ms at the same time (Figure 3.1a). Participants were instructed to select which side had a larger/stronger amplitude. Due to technical problems, three TS participants did not complete the simAD task and one TD control participant's threshold was removed from analysis as these were 1.5x the inter-quartile range (IQR) above the third quartile (TD N = 28, TS N = 24).

3.2.1.3.3 Sequential amplitude discrimination

Sequential amplitude discrimination (seqAD) was assessed by presenting a vibrating stimulus to D2 for 500ms with a 500ms ISI, followed by a vibrating stimulus of a different amplitude to D3 for 500ms (Figure 3.1b). Participants were instructed to choose which side had a larger/stronger amplitude. Due to technical problems, two TS participants did not complete the seqAD task and one TS participant's data was removed from subsequent analysis as it was 1.5x the IQR above the third quartile (TD N = 29, TS N = 24).

3.2.1.3.4 Single-site adaptation amplitude discrimination

Single-side adaptation (SSA) involved presenting a conditioning stimulus to one digit for 1000ms, before immediately presenting two vibrating stimuli of different amplitudes to D2 and D3 for 500ms at the same time (Figure 3.1c). Participants were instructed to ignore the conditioning stimulus and to select which side had a larger/stronger amplitude. The adapting stimulus leads to a decrease in the ability of a participant to distinguish between the two stimuli, proposed to be due to the adapting stimulus causing reduced responsivity and tuning of cortical neurons to the subsequent test stimuli (Kohn & Whitsel, 2002; Tannan et al., 2007). Due to technical problems, six TS participants and four TD control participants did not complete the SSA task and one TS participant's data was removed from subsequent analysis as it was 1.5x the IQR above the third quartile (TD $N = 25$, TS $N = 20$).

Figure 3.1

Protocol for (a) simultaneous, (b) sequential, (c) single-site adaptation amplitude discrimination tasks

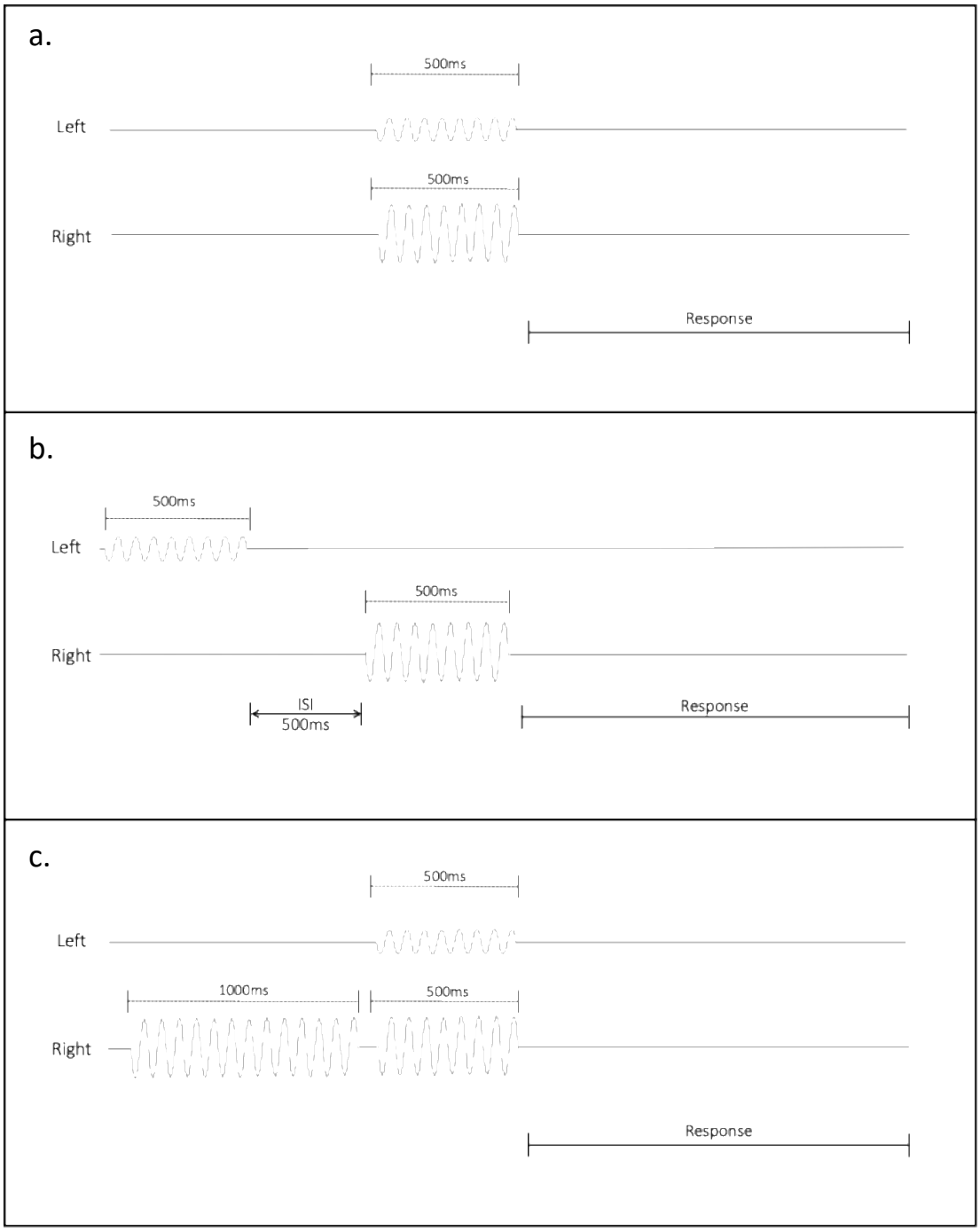

Note. ISI = inter-stimulus interval. Left and right refers to each probe – digit 2 of the left hand is placed over the left probe and digit 3 of the left hand is placed over the right probe. Figure adapted based on parameters from Brain Gauge User Manual (https://downloads.corticalmetrics.com/support/Brain_Gauge_MD_User_Manual.pdf)

3.2.1.3.5 Temporal order judgement

The static TOJ task assesses whether participants can correctly distinguish the temporal order of two stimuli. Two 'pulse' stimuli are delivered to each probe asynchronously with a varying ISIs (starting at 150ms and adjusted by 15% based on correct/incorrect responses for 20 trials; Figure 3.2a). Participants were instructed to select whether they felt the first stimulus on the left or the right digit. TOJ is calculated as the shortest ISI (in ms) needed for both stimuli to be distinguished as separate and is thought to reflect inhibitory interneuron functioning and their role in sharpening of temporal processing of stimuli in S1 (Antelmi et al., 2017; Rocchi et al., 2016). Due to technical problems, one TS participant did not complete the TOJ task and two TS and four TD control participant's data was removed from subsequent analysis as these were 1.5x the IQR above the third quartile (TD N = 25, TS N = 24).

3.2.1.3.6 Temporal order judgement with carrier

The cTOJ task is identical to the TOJ task, with the addition of a continuous vibrating stimulus delivered to both probes during the time that both stimuli are presented (Figure 3.2b). Like with TOJ, cTOJ is calculated as the shortest ISI (in ms) necessary for both stimuli to be distinguished as separate. Delivery of this carrier vibration has previously been shown to significantly increase TOJ thresholds in TD controls, as individuals find it more difficult to distinguish the temporal order of the test stimuli (Tommerdahl et al., 2007, 2008). This is thought to be a stimulus-driven synchronisation effect, where the synchronous conditioning stimulus entrains the cortical activity relating to D2 and D3, making it more difficult to temporally separate the input of each digit (Tommerdahl et al., 2008). As a result, stimuli input to each digit is perceptually harder to separate. For this task, two values are calculate; the cTOJ threshold and percent change when compared to TOJ thresholds. Due to technical problems, two TS participants and one TD control participant did not complete the TOJ task and four TS and three TD control participant's data was removed from subsequent analysis as these were 1.5x the IQR above the third quartile (TD N = 25, TS N = 21).

Figure 3.2

Protocol for (a) static, (b) carrier temporal order judgement task

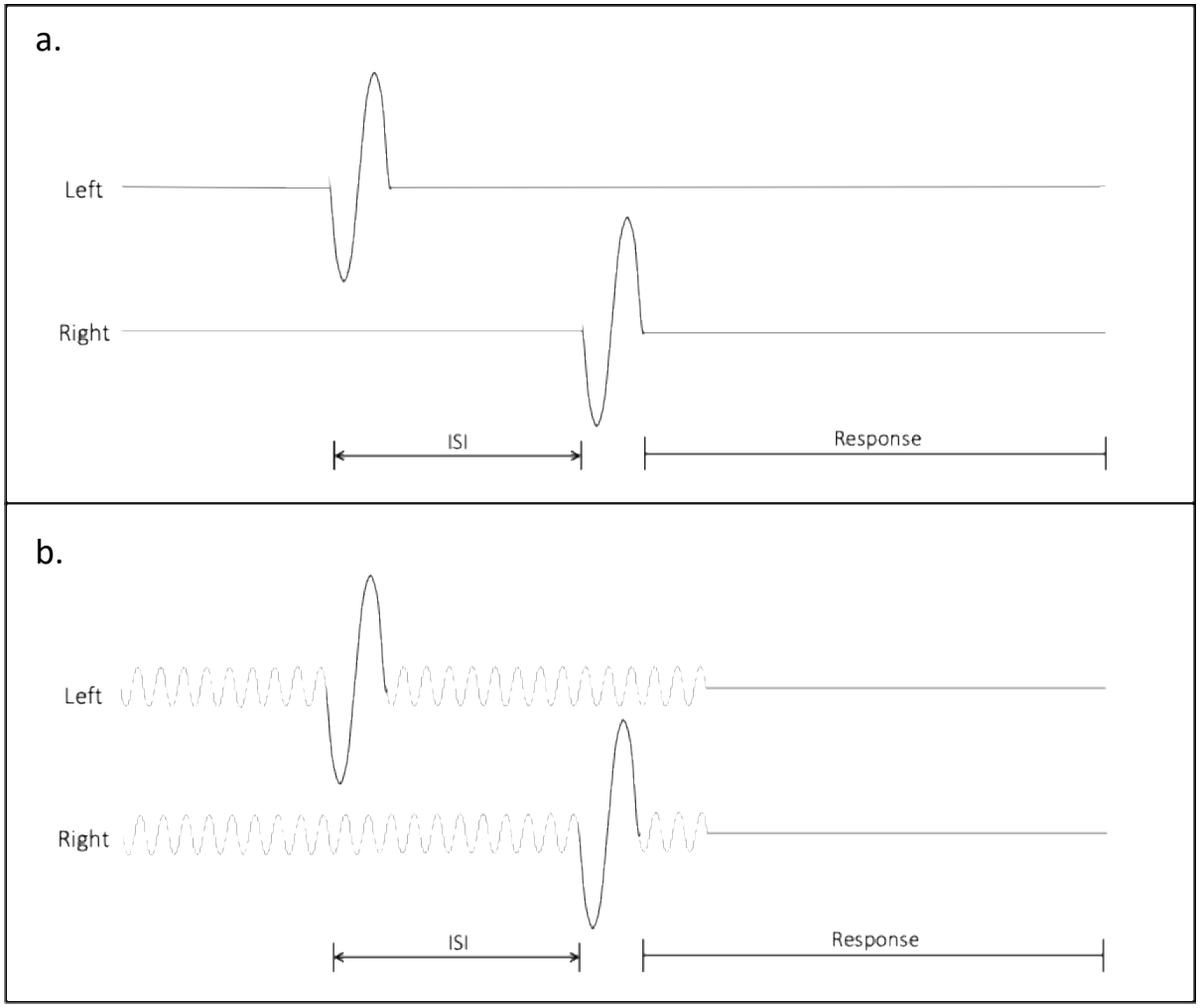

Note. ISI = inter-stimulus interval. Left and right refers to each probe – digit 2 of the left hand is placed over the left probe and digit 3 of the left hand is placed over the right probe. Figure adapted based on parameters from Brain Gauge User Manual (https://downloads.corticalmetrics.com/support/Brain_Gauge_MD_User_Manual.pdf)

3.2.1.3.7 Adaptation and carrier effects

Percentage change between simAD and SSA thresholds and TOJ and cTOJ thresholds were also calculated to assess adaptation and carrier effects. Any datasets that exceeded 1.5x the IQR above the third quartile were removed from subsequent analyses, including one TD participant for the adaptation effects (TD *N* = 20, TS *N* = 25) and three TD participants for carrier effects (TD *N* = 22, TS *N* = 28).

3.2.1.3.8 Statistical analysis

To assess TS and TD group differences in amplitude discrimination thresholds (simAD, seqAD, SSA) and temporal order judgement thresholds (TOJ, cTOJ), one-tailed independent *t*-tests were conducted. To assess within-group differences between simAD and SSA thresholds, and TOJ and cTOJ thresholds, one-tailed paired *t*-tests were conducted for the TD group and two-tailed paired *t*-tests were conducted for the TS group. One-tailed independent *t*-tests were also performed to identify between group differences in the percentage change between adaptation and carrier effects.

Where normality assumptions were not met, independent *t*-tests were replaced by Mann Whitney-*U* tests and paired *t*-tests were replaced by Wilcoxon signed-rank tests. Bayesian statistics were implemented alongside traditional inferential statistics in order to quantify the strength of support for the null hypothesis (H_0) or alternative hypothesis (H_1). A Bayes factor of 10 (BF_{10}) was used with a Cauchy distribution with a scale of γ = 0.707 used as the prior distribution (Rouder et al., 2009; Schönbrodt & Wagenmakers, 2018). Interpretation of BF_{10} values is shown in Table 3.2. All statistical analyses were conducted using jamovi (v 2.3.28; jamovi.org).

Table 3.2

Interpretation of BF_{10} values

BF_{10}	Interpretation
>100	Extreme evidence for H_1
30-100	Very strong evidence for H_1
10-30	Strong evidence for H_1
3-10	Moderate evidence for H_1
1-3	Anecdotal evidence for H_1
1	No evidence
0.33-1	Anecdotal evidence for H_0
0.1-0.33	Moderate evidence for H_0
0.03-0.1	Strong evidence for H_0
0.01-0.03	Very strong evidence for H_0
< 0.01	Extreme evidence for H_0

Note. BF_{10} = Bayes Factor 10, H_1 = alternative hypothesis, H_0 = null hypothesis. Figure based on values from Schönbrodt & Wagenmakers (2018)

3.2.2 Results

Means and standard deviations of thresholds for amplitude discrimination and TOJ tasks are shown in Table 3.3.

Table 3.3

Means and standard deviations for amplitude discrimination and temporal order judgement tasks for TD and TS groups in Study 1

	Amplitude discrimination thresholds (µm)				Temporal order judgement thresholds (ms)		
Group	**Sequential**	**Simultaneous** †	**Single-site adaptation** †	**Adaptation effect (%)**	**Static** * ††	**Carrier** *	**Carrier effect (%)**
TD	48 (±27.8)	48.9 (±23.9)	71.8 (±25.7)	75.5% (±101%)	22.7 (±6.22)	42.6 (±36.4)	117.2% (±215%)
TS	53.2 (±30)	57.5 (±23.2)	95 (±64.2)	87.9% (±146%)	28 (±10.9)	46.1 (±21.3)	92.2% (±123%)

Note. TD = Typically developing control group, TS = Tourette Syndrome group, mean (±standard deviation). * = $p < 0.05$, † = anecdotal evidence for the alternative hypothesis, †† = moderate evidence for the alternative hypothesis

3.2.2.1 Amplitude discrimination

Group means and standard deviations are shown in Table 3.3 and Figure 3.3. SeqAD thresholds were also not significantly different between groups (U = 323, p = 0.331), with Bayesian statistics suggesting anecdotal evidence for the null hypothesis (BF_{10} = 0.476). SimAD thresholds were also not significantly different between TS and TD groups (t(50) = -1.324, p = 0.096), with Bayesian statistics suggesting anecdotal evidence for the alternative hypothesis (BF_{10} = 1.01). SSA thresholds were not significantly different between groups (t(32.9) = -1.649, p = 0.054). However, Bayesian statistics suggest anecdotal evidence for the alternative hypothesis (BF_{10} = 1.36). Overall, this suggests that although mean amplitude discrimination thresholds were greater in TS group compared to TD controls, these differences were not significantly different, with only anecdotal evidence for the alternative hypothesis in simAD and SSA thresholds when assessed with Bayesian statistics.

Figure 3.3

Mean and standard deviations (error bars) of amplitude discrimination thresholds for sequential, simultaneous and single-site adaptation tasks in TD and TS groups

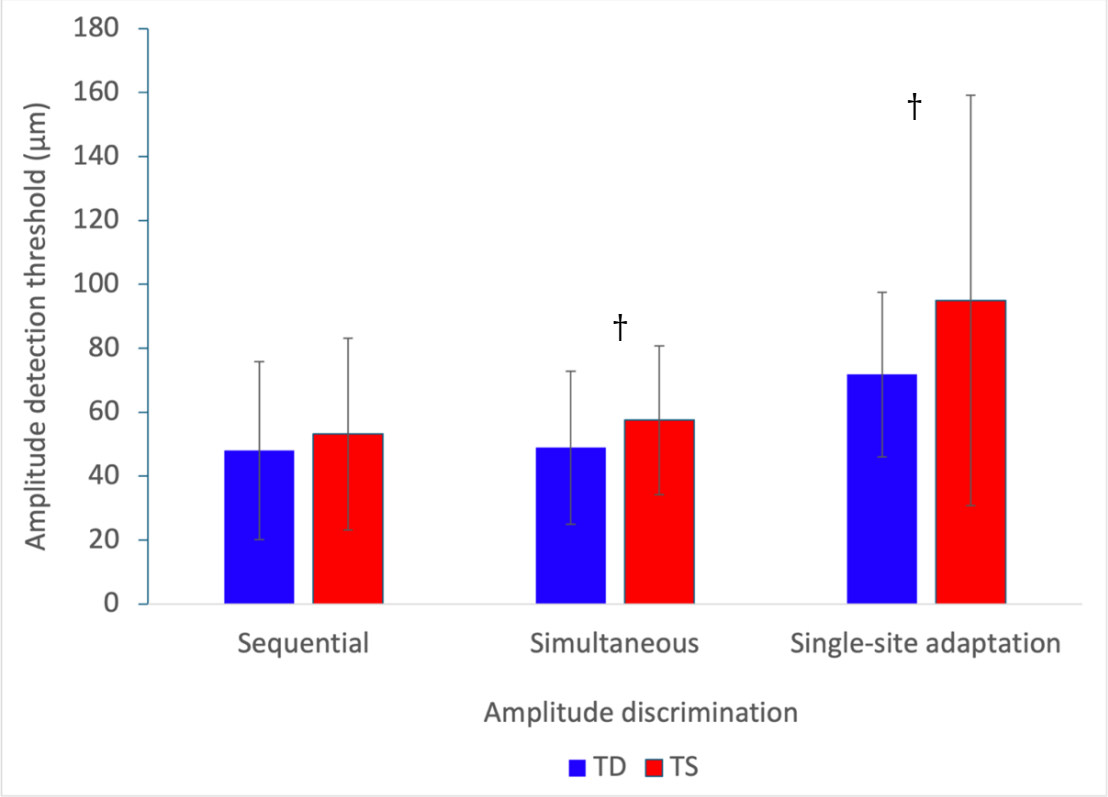

Note. µm = micrometres, TD = typically developing control group, TS = Tourette Syndrome group. † = anecdotal evidence for the alternative hypothesis. Group differences are non-significant ($p > 0.05$)

3.2.2.2 Temporal order judgement

TOJ thresholds were significantly greater in TS group compared to TD controls, meaning TD control participants were better at judging the temporal order of stimuli at smaller timings between stimuli presentation (U = 210, p = 0.036). Bayesian statistics show moderate evidence for alternative hypothesis (BF_{10} = 3.01). Moreover, cTOJ thresholds were significantly greater in TS group compared to TD controls (U = 187, p = 0.049), however Bayesian statistics suggest anecdotal evidence for the null hypothesis (BF_{10} = 0.401). As a result, TOJ thresholds are significantly different for

both TOJ and cTOJ tasks between TS and TD groups, with TS group showing significantly greater thresholds (worse performance) compared to TD controls. However, this is only supported by Bayesian statistics for TOJ alone. Group means and standard deviations are shown in Table 3.3 and Figure 3.4**.**

Figure 3.4

Mean and standard deviations (error bars) of temporal order judgement thresholds for static and carrier tasks in TD and TS groups

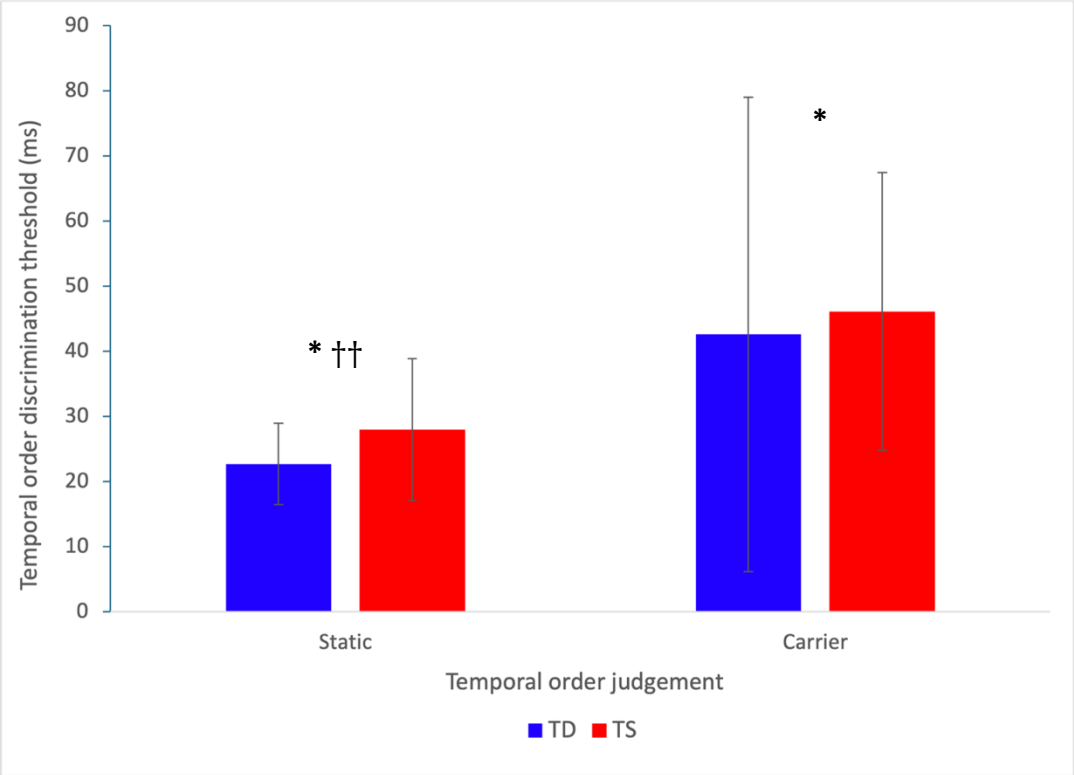

Note. ms = milliseconds, TD = Typically developing control group, TS = Tourette Syndrome group. * = $p < .05$ †† = moderate evidence for the alternative hypothesis

3.2.2.3 Adaptation and carrier effects

In the TD group, one tailed paired *t*-test identified a significant difference was found between mean simAD and SSA thresholds; $t(19) = -2.44$, $p = 0.012$. Bayesian statistics showed moderate evidence for the alternative hypothesis ($BF_{10} = 4.81$). For

the TS group, a two-tailed paired *t*-test also revealed a significant difference between mean simAD and SSA thresholds; $t(23) = -2.52$, $p = 0.019$. Bayesian statistics also provide moderate evidence for the alternative hypothesis ($BF_{10} = 5.58$). This demonstrates that thresholds were significantly increased after adaptation amplitude discrimination tasks for both TD and TS groups. Adaptation effects for each group were also assessed with a one-tailed Mann-Whitney *U* test. The difference between adaptation effects did not significantly differ between TS and TD control groups ($U = 246$, $p = 0.464$), suggesting comparable adaptation effects across groups. Bayesian statistics provide anecdotal evidence for the null hypothesis ($BF_{10} = 0.239$). Means and standard deviations shown in Table 3.3 and Figure 3.5.

In the TD group, a one-tailed paired Wilcoxon signed-ranks test demonstrated a significant difference between mean TOJ and cTOJ thresholds; $W = 45.5$, $p = 0.024$. Bayesian statistics show anecdotal evidence for the alternative hypothesis ($BF_{10} = 2.54$). For the TS group, a significant difference between TOJ and cTOJ thresholds was also identified after a two-tailed paired *t*-test; $t(20) = -3.70$, $p = 0.001$. Bayesian statistics provided very strong evidence for the alternative hypothesis ($BF_{10} = 53.18$). This demonstrates that temporal order thresholds were significantly worse in the carrier condition for both TD and TS groups. To assess any differences in carrier effects between groups, a one-tailed Mann Whitney-*U* test was conducted. Carrier effects did not significantly differ between TS and TD control groups ($U = 297$, $p = 0.588$), suggesting comparable carrier effects were present across groups. Bayesian statistics provide anecdotal evidence for the null hypothesis ($BF_{10} = 0.431$). Group means and standard deviations are shown in Table 3.3 and Figure 3.5.

Figure 3.5

Mean and standard deviations (error bars) of the (a) adaptation effect and (b) carrier effect in TD and TS groups

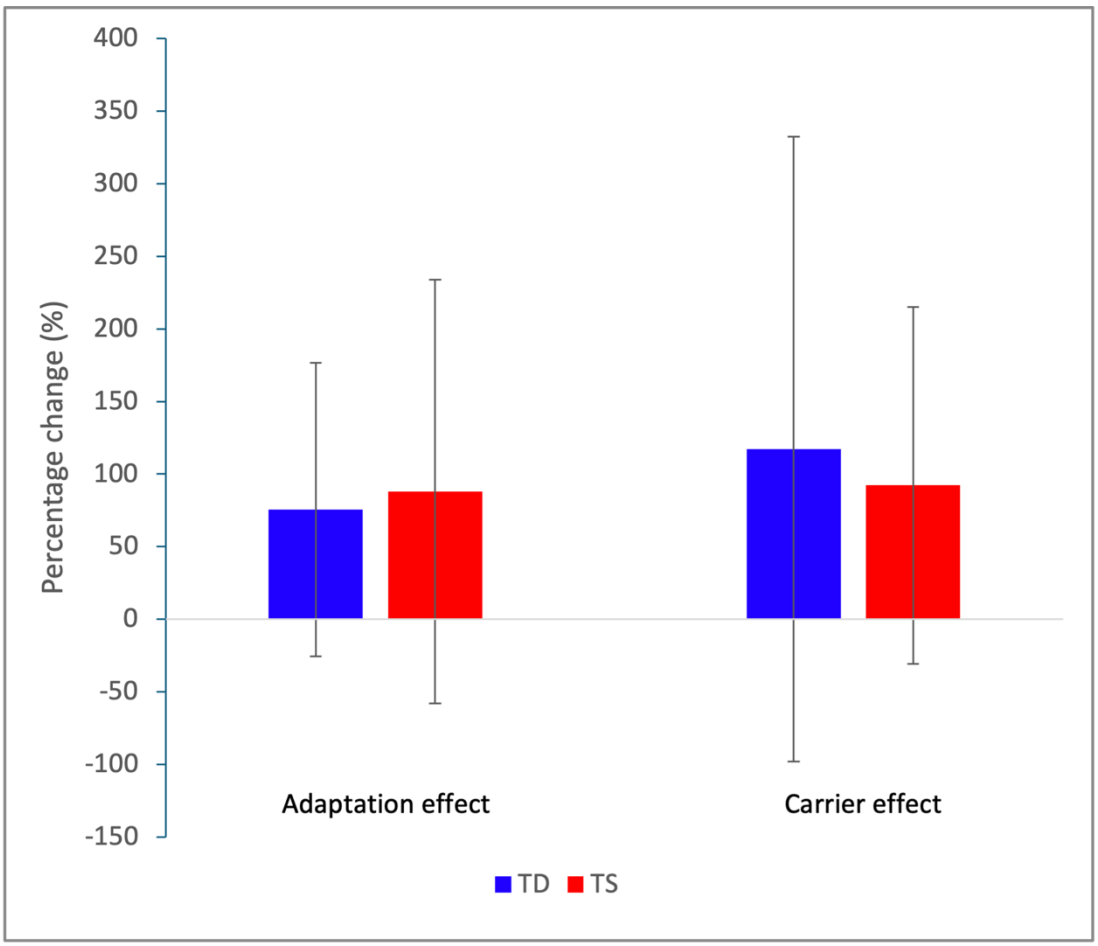

Note. TD = Typically developing control group, TS = Tourette Syndrome group. Group differences are non-significant ($p > 0.05$)

3.2.3 Discussion

Sensory processing abnormalities are thought to be inherent in TS. However, exteroceptive domains of sensation have not been widely investigated, despite many reports of abnormalities in the processing of external stimuli (see Section 1.3.2). As a result, Study 1 aimed to assess tactile quantitative sensory testing in a TD group and TS group in a larger cohort than previous research, which have provided mixed results (Puts et al., 2015; Schunke et al., 2016). It was predicted that individuals with TS would display greater amplitude discrimination and TOJ thresholds, indicating worse somatosensory performance and reduced ability to detect discrete amplitude/temporal differences in vibrotactile stimuli. Overall, it was demonstrated that although mean amplitude discrimination and TOJ thresholds were higher in the TS group compared to the TD group, only TOJ and cTOJ thresholds were significantly higher in the TS group compared to the TD group. However, Bayesian inference provided anecdotal evidence for higher simAD and SSA and TOJ thresholds in the TS group compared to the TD group, with cTOJ and seqAD showing no support for differences between groups. This provides some support that there are some abnormalities in the central processing of external tactile stimuli within TS, pointing toward abnormalities in inhibitory functioning in TS.

Moreover, it was hypothesised that effects of an adapting stimulus would increase amplitude discrimination thresholds in both groups, but that the adaptation effect would be greater in the TD group compared to the TS group. This pattern was also hypothesised for the TOJ task, where a carrier stimulus would increase TOJ thresholds in both groups, but the carrier effect would be greater in TD controls. While it was confirmed that both groups demonstrated significant increases in amplitude discrimination and TOJ thresholds with adaptation and carrier stimuli, supported by Bayesian inference, there was no significant difference between adaptation or carrier effects between groups. This infers that both groups showed comparable levels change in their thresholds, suggesting those with TS are not any less susceptible to adaptation and carrier effects.

Similarities between adaptation and carrier effects could indicate that the cortical mechanisms that provide the optimal conditions for the induction of adaptation and carrier effects in TD controls are no different in TS. For example, previous evidence has attributed abnormalities in adaptation effects to abnormalities in sensory gating, adaptive modulation of sensory signals and the tuning of cortical neurons (Isaacs & Riordan, 2020; Puts et al., 2015). Moreover, abnormalities in carrier effects have been attributed to the disrupted synchronisation of neurons and activity within the somatosensory system (Tommerdahl et al., 2008). However, as the synchronisation of cortical activity and tuning of cortical neurons are thought to reflect GABAergic inhibitory processes, this could suggest that intracortical GABAergic inhibition may not be disrupted in TS.

Alternatively, adaptation and carrier effects may not be related to inhibitory processes in TS. For example, previous findings of abnormalities in adaptation effects in children with TS also demonstrated that adaptation effects were not significantly related to MRS-GABA, whereas these were significantly correlated in the TD control group (Puts et al., 2015). Authors suggested that the TS group may instead use alternative strategies for tactile discrimination and synchronisation of cortical activity that are not reliant on inhibitory mechanisms. Moreover, while abnormalities in adaptation were significantly different between children with TS and healthy controls in Puts et al. (2015), this was not found in the current study in adults for adaptation of carrier effects. Therefore, this may reflect a compensatory strategy for tactile discrimination in TS, which becomes more efficient across the lifespan.

Additionally, the absence of adaptation and carrier effects may also be related to a specific of comorbidities in the TS sample used in this study. For example, sensory abnormalities have also been demonstrated in samples with ADHD and ASD (Puts et al., 2017; Tommerdahl et al., 2008), which are common comorbidities in TS. However, comorbidities were not controlled when assessing adaptation and carrier effects in this sample, so it is unclear if individuals with ADHD/ASD comorbidities show less susceptibility to these effects. However, Puts et al. (2015) assessed their sample of

individuals with TS without comorbidities and found no significant difference in adaptation scores between individuals with and without ADHD. This suggests that abnormalities in adaptation effects are similar across children with TS who are diagnosed with and without ADHD.

3.3 Study 2: MRS-GABA and MRS-Glu in TS and their relationships with sensory phenomena

3.3.1 Methods

3.3.1.1 Participants

To determine if there was sufficient power to identify correlations between MRS neurometabolite concentrations and sensory processing or tic/urge phenomenology, a power analysis was conducted (G*Power; Faul et al., 2007), using the resulting *r* values from correlation analyses conducted in Puts et al. (2015). This research identified significant relationships between sensorimotor MRS-GABA and tactile thresholds in a TD control group (sequential frequency discrimination: r = -0.58; adaptation effect: r = -0.44) and tic severity scores (r = -0.55) in a group of children with TS. As a result, to detect a large effect sizes (r = 0.5) with a bivariate correlation analysis, group sample sizes of 24 (one-tailed) or 30 (two-tailed) would be sufficient to yield statistical power of at least 0.80 with an alpha of 0.05. Ideally, to account for drop out and poor data quality, an even larger sample size would be required. However, due to the limited availability and timescale of funding, a target sample size of 20 participants per group was chosen.

In total, a subset of 20 TD control participants and 16 patients with TS underwent MRI and MRS, before completing quantitative sensory testing and self-report questionnaires assessing interoception and exteroception. Two participants from the TS group and five participants from the TD control group were removed from MRS analysis due to quality concerns detailed in Section 3.3.1.5. One TS participant was also removed from MRS analysis due to MRS data corruption. One TD control was removed from all analyses due to a diagnosis of OCD. Demographics of the final group are shown in Table 3.4. There were no significant differences between age (U = 108, p = 0.406) and sex (X^2 (1, N = 33) = 0.035, p = 0.085) between groups.

Table 3.4

Demographics of TD and TS Groups in Study 2

Group	N	Age	Sex
TD	19	27.63 (±6.4)	6 male, 13 female
TS	16	25.88 (±9.6)	3 male, 13 female

Note. TD = Typically developing control group, TS = Tourette Syndrome group, *N* = number of participants, mean (±standard deviation)

Participants gave informed consent and ethics were approved by the local ethics committee (School of Psychology, University of Nottingham: S1500). No participants in the TD group were taking CNS-active drugs and were free from any mood or neurological illness during the experimental timeline. All medications and clinical scores for the TS group are displayed in Appendix A2. All TS participants were screened prior to participation to assess tic phenomenology, to ensure low tic severities, especially with head and facial tics, which may impact subsequent MRS quality. All participants were free from any contraindications for MRI, as assessed by completion of an MRI safety screening form. All participants were right-handed as assessed by the Edinburgh handedness questionnaire (Oldfield, 1971).

3.3.1.2 Questionnaires

Clinical questionnaires used in Study 1 (Section 3.2.1.2), were implemented and both groups also completed questionnaires assessing self-reported interoceptive and exteroceptive sensitivity.

3.3.1.2.1 Interoceptive Accuracy Scale

The Interoceptive Accuracy Scale (IAS) is a 21-item questionnaire assessing self-reported accuracy in perceiving interoceptive signals (internal physical sensations or related to insula activation, associated with interoceptive processing) (Murphy et al., 2020). The IAS was administered to both TD and TS groups. Participants were

instructed to rate their interoceptive accuracy for each item on a scale of 1 (Strongly Disagree) to 5 (Strongly Agree) (See Appendix A.3). Scores range from 21-105, with higher scores indicating greater self-reported accuracy in the detection of interoceptive signals. Investigation into the IAS has demonstrated it holds good internal consistency and test re-test reliability and has shown a moderate relationship with objective measures of interoceptive accuracy (heartbeat tracing task) (Murphy et al., 2020). Questionnaires were sent online via Qualtrics (Provo, UT) and were completed by 12 TS participants and 15 TD controls. Outliers were identified and removed if they were 1.5x the IQR above the third quartile or below the first quartile. No dataset fell outside of these thresholds.

3.3.1.2.2 Sensory Processing Sensitivity Questionnaire

The Sensory Processing Sensitivity Questionnaire (SPSQ) is a 16-item questionnaire assessing self-reported awareness of sensitivity to external stimuli in two subscales. The 8-item Sensory Sensitivity Subscale involves sensitivity to external sensory stimuli such as light, sounds and tactile stimuli, whereas the 8-item Other Sensitivity Subscale involves sensitivity to external stimuli such as emotions, criticism and sudden changes. This questionnaire asks participants to indicate the extent to which they are sensitive to external stimuli compared to other people, where 0 is not sensitive at all compared to other people, 5 is the same sensitivity as other people and 10 is much more sensitive compared to other people (Appendix A.4). In this study, only the Sensory Sensitivity Subscale was used to assess to self-reported sources of hypersensitivity in TS (Malinakova et al., 2021). On the possible score range of 0-80 for this subscale, lower scores indicate perceived hyposensitivity to external stimuli compared to others and higher scores indicate perceived hypersensitivity to external stimuli compared to others (Malinakova et al., 2021). Psychometric investigation into the SPSQ shows high temporal stability and excellent internal consistency (Malinakova et al., 2021). Questionnaires were sent online via Qualtrics (Provo, UT) and were completed by 12 TS participants and 15 TD controls. Outliers were identified and removed if they were 1.5x the IQR above the third quartile or below the first

quartile; as a result, one TS and one TD participant's scores were removed from subsequent analysis.

3.3.1.3 Tactile quantitative sensory tests

Quantitative sensory testing in Study 2 included amplitude discrimination (seqAD, simAD and SSA), TOJ and cTOJ. These were identical to those described in Study 1 (Section 3.2.1.3) and were conducted after MRS to avoid the potential of neurometabolite modulation with sensory stimulation.

Due to technical errors, two TD participants did not complete the simAD, one TD and two TS participants did not complete the SSA task, one TD participant did not complete the TOJ and one TD and one TS participant did not complete the cTOJ task. Outliers were identified and removed if they were 1.5x the IQR above the third quartile or below the first quartile for each group. As a result, three TD participants were removed from the seqAD task (TD N = 16, TS N = 16), one TS participant was removed from simAD task (TD N = 17, TS N = 15), two TD and one TS participants were removed from SSA task (TD N = 16, TS N = 13). For the TOJ task, two TD and one TS participant's data was removed (TD N = 16, TS N = 15) and for the cTOJ task, three TD and two TS participant's thresholds were removed (TD N = 15, TS N = 13). For adaptation effects, one TD participant was removed (TD N = 16, TS N = 13) and for carrier effects, three TD participants were removed (TD N = 15, TS N = 14).

3.3.1.4 MRI

MRI and MRS data were acquired using a Philips 7T Achieva MRI scanner (Philips Healthcare, Best, The Netherlands) using a 32-channel head coil in the Sir Peter Mansfield Imaging Centre at the University of Nottingham, Nottingham, UK. The scanning that took place in this chapter was part of a wider scanning session, which used fMRI to investigate sensorimotor digit mapping (Chapter 4) and vibrotactile sensorimotor representations of the face (Chapter 5 Study 2).

3.3.1.4.1 T1-weighted MRI parameters

Prior to MRS, an anatomical T_1-weighted 3D gradient echo PSIR (phase-sensitive inversion-recovery) scan was acquired (matrix size = 320 x 320, FOV = 224 x 224 x 157 mm, 0.7mm isotropic, 224 slices, TR/TE = 6.3/2.8 ms, flip angle = 5°, acquisition time 6.25 minutes) with two turbo field echo (TFE) readouts after each inversion pulse at TI1 = 780 ms and TI2 = 2380 ms. The two PSIR readouts were converted into T_1-weighted images using an in-house Python (v.3.9.12) script (https://github.com/oliviermougin/PSIR). This was to allow identification of anatomical landmarks for MRS voxel placement.

3.3.1.4.2 MRS parameters

In vivo ^{1}H MRS data were acquired from a 20x20x20mm^3 voxel of interest (VOI) placed over the sensorimotor hand knob area of the left hemisphere (the hemisphere of the dominant right hand). See Figure 3.6 for average voxel placements for each group in MNI space, with example spectra of one participant from each group. A semi-LASER (sLASER) sequence was used (TR/TE = 5914/30ms, sample size = 2048, spectral bandwidth = 6000Hz, phase cycles = 8, number of signals averaged = 64, acquisition time 6.42 minute), with water suppression achieved using variable pulse power and optimised relaxation decay (VAPOR; Tkác et al., 1999). Outer volume saturation (OVS) was also applied to suppress signal components outside of the VOI (Tkáč & Gruetter, 2005), and Philips second-order projection-based method was used to increase B_0 homogeneity.

Figure 3.6

Average voxel placement with example spectra from one participant in the (a) TD control group and (b) TS group

a.

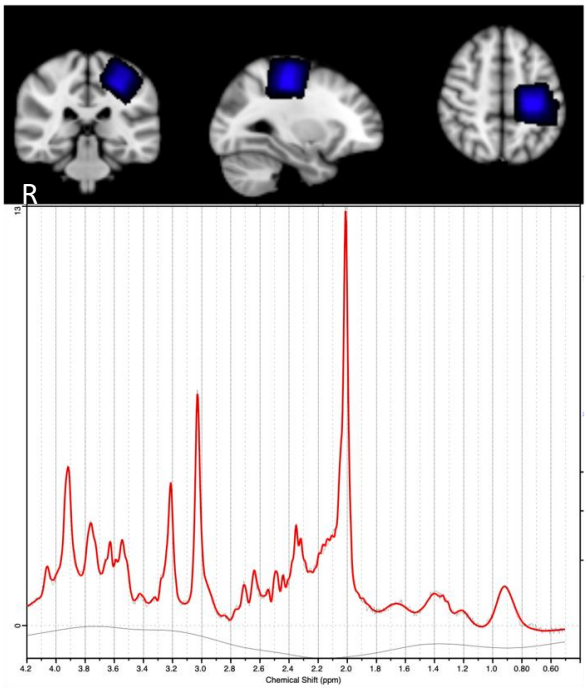

b.

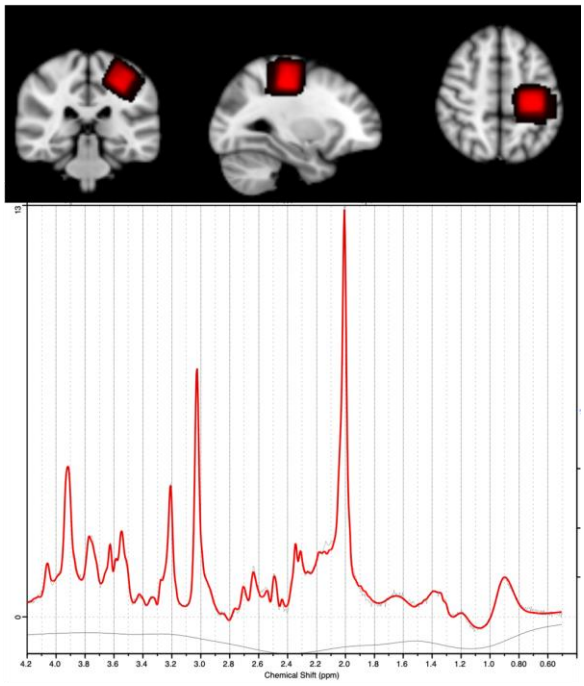

Note. R = right hemisphere. Brighter colours represent more overlap across participants. Individual spectra LCModel outputs from participants (a) Map07 and (b) TS23

3.3.1.5 MRS analysis

In vivo ^{1}H raw spectral data (.data/.list format) were processed using an in-house MATLAB script (MATLAB_R2019a, Mathworks, Natick, MA) to pre-process and fit spectra and output concentrations of neurometabolites (https://github.com/aberrington/specReg). First, raw data were visually inspected for any large water or lipid artefacts. Spectra were then coil-combined and eddy current corrected, with outliers automatically rejected if the mean square error around the Choline peak is larger than +/- 3 standard deviations from the mean.

Pre-processed spectra were then fit in the LCModel software package (Provencher, 1993). A 7T sLASER (TE = 30ms) model basis spectra were used to fit the pre-processed spectra with a spectral range of 0.5 – 4.2ppm. Total creatine (tCr; creatine + phosphocreatine), GABA and Glutamate (Glu) concentrations were quantified using the LCModel output, with tCR used as the internal reference for quantification. Final GABA and Glu concentrations are presented as a ratio relative to tCr.

The SNR and estimated linewidth of unsuppressed water were identified, with datasets rejected from subsequent analysis if the estimated linewidth was above 15Hz (0.05 ppm) and SNR deviated +/- 3 standard deviations from the mean. Three TD and two TS participants were removed from MRS analysis due to linewidths over 15Hz. Absolute Cramér–Rao lower bounds (CRLB) > 100% were also removed from subsequent analyses, meaning two GABA concentrations were removed from the TD control group. The resulting N, mean absolute CRLB, SNR and linewidths for GABA and Glu for each group are shown in Table 3.5.

Table 3.5

Mean and standard deviations of LW, SNR and CRLB for GABA and Glu in TD and TS groups

			GABA		Glu	
Group	LW	SNR	N	CRLB	N	CRLB
TD	10.99 (±1.62)	264.19 (±65.12)	14	32.14 (±13.666)	16	6.375 (±2.446)
TS	11.22 (±1.28)	264.88 (±41.97)	13	40.769 (±15.653)	13	6.923 (±1.935)

Note. LW = linewidth, SNR = signal to noise ratio, *N* = number of participants, CRLB = Absolute Cramér–Rao lower bounds, TD = Typically developing control group, TS = Tourette Syndrome group, mean(±standard deviation)

3.3.1.6 Statistical analysis

To assess for any differences between TS and TD groups in MRS-GABA and MRS-Glu concentrations, self-reported interoceptive/exteroceptive sensitivity scores (measured with the IAS and SPSQ) and quantitative sensory thresholds (simAD, seqAD, SSA, TOJ and cTOJ), one-tailed independent *T*-tests were conducted**.** To assess within-group differences between simAD and SSA thresholds, and TOJ and cTOJ thresholds, one-tailed paired *t*-tests were conducted for the TD group and two-tailed paired *t*-tests were conducted for the TS group. One-tailed independent *t*-tests were also performed to identify between group differences in the adaptation effects and carrier effects.

Finally, two-tailed Pearson correlations were conducted to identify any relationships between MRS-GABA or -Glu concentrations for each group with individual IAS and SPSQ scores. Moreover, TS and TD groups underwent one-tailed Pearson correlation analyses between MRS-GABA and amplitude discrimination, TOJ thresholds and amplitude/carrier effects. Two-tailed Pearson correlations were also conducted for each group between MRS-Glu with amplitude discrimination, TOJ thresholds and amplitude/carrier effects. Additionally, the TS group underwent two-

tailed correlation analyses between individual neurometabolites and PUTS, YGTSS-motor, YGTSS-phonic and YGTSS-impairment scores. Where variables showed non-Gaussian distributions, Spearman correlations were used.

Where normality assumptions were not met, Mann Whitney-*U* tests were used instead of independent *t*-tests and Wilcoxon signed-rank tests instead of paired *t*-tests. Bayesians statistics were also implemented with a BF_{10}, prior 0.707 (Table 3.2) (Rouder et al., 2009). All statistical analysis was conducted using jamovi (v 2.3.28; jamovi.org).

3.3.2 Results

3.3.2.1 *t*-tests

3.3.2.1.1 MRS

While TS showed a trend of lower MRS-GABA concentrations, independent one-tailed *t*-tests evidenced no significant differences between relative MRS-GABA concentrations between TS (M = 0.228, SD = 0.052) and TD controls (M = 0.288, SD = 0.135), $t(17) = 1.55$, $p = 0.07$. Bayesian statistics supported anecdotal evidence for alternative hypothesis ($BF_{10} = 1.47$). Means and standard deviations are shown in Figure 3.7.

MRS-Glu concentrations also showed no significant differences between TS (M = 1.12, SD = 0.215) and TD controls (M = 1.08, SD = 0.149); $U = 100$, $p = 0.440$. Bayesian statistics showed additional anecdotal evidence for the null hypothesis ($BF_{10} = 0.502$). Means and standard deviations are shown in Figure 3.7.

Figure 3.7

Mean and standard deviations (error bars) for MRS-GABA and MRS-Glu concentrations in TD and TS groups

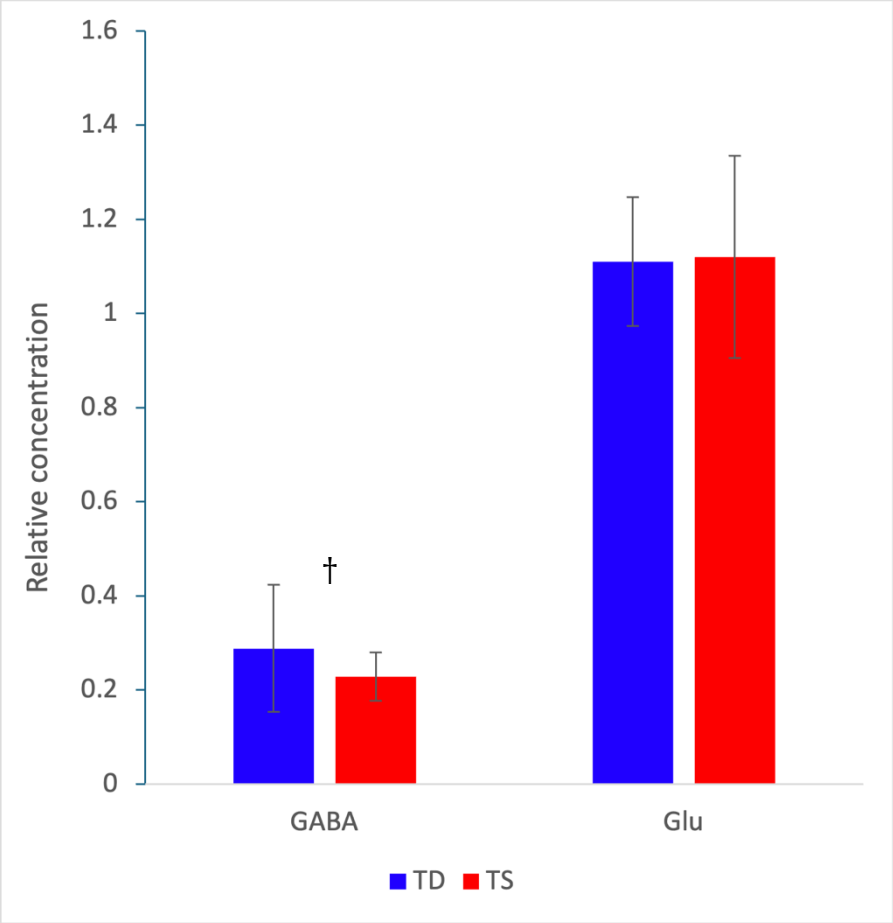

Note. TD = Typically developing control group, TS = Tourette Syndrome group. † = anecdotal evidence for the alternative hypothesis

3.3.2.1.2 Self-reported interoceptive and exteroceptive sensitivity

Means and standard deviations are shown in Table 3.6. SPSQ scores showed no significant differences between TS and TD controls; $t(23) = -.985$, $p = 0.167$. Bayesian statistics showed moderate evidence for the null hypothesis ($BF_{10} = 0.309$). IAS scores showed no significant differences between TS and TD controls; $t(25) = 0.235$, $p = 0.592$. Bayesian statistics revealed anecdotal evidence for the null hypothesis ($BF_{10} = 0.837$).

Table 3.6

Mean and standard deviations of TD and TS group scores for SPSQ and IAS

Group	SPSQ	IAS
TD	46.9 (±6.53)	82.7 (±14.7)
TS	49.5 (±6.14)	81.4 (±12.5)

Note. SPSQ = Sensory Processing Sensitivity Questionnaire, IAS = Interoceptive Accuracy Scale, TD = Typically developing control group, TS = Tourette Syndrome group, mean(±standard deviation)

3.3.2.1.3 Quantitative tactile sensory testing

All group means and standard deviations are shown in Table **3.7**.

Table 3.7

Means and standard deviations for amplitude discrimination and temporal order judgement tasks for TD and TS groups in Study 2.

	Amplitude discrimination thresholds (µm)				Temporal order judgement thresholds (ms)		
Group	**Sequential** †	**Simultaneous**	**Single-site adaptation**	**Adaptation effect (%)**	**Static**	**Carrier**	**Carrier effect (%)**
TD	42.6 (±16.9)	54.1 (±30.2)	63.9 (±30.4)	43.7% (±63.4%)	23.9 (±7.98)	44.2 (±40.5)	50.0% (±76%)
TS	53.9 (±31.1)	55 (±30.5)	77.2 (±46.6)	101% (±150%)	25 (±8.21)	47.5 (±26.9)	146% (±148%)

Note. TD = Typically developing control group, TS = Tourette Syndrome group, mean (±standard deviation). † = anecdotal evidence for the alternative hypothesis

3.3.2.1.3.1 Amplitude discrimination

In this cohort, SimAD thresholds were not significantly different between TS and TD groups ($t(30) = -0.0821$, $p = 0.468$), with Bayesian statistics showing anecdotal evidence for the null hypothesis ($BF_{10} = 0.357$). SeqAD thresholds were also not significantly different between groups ($t(23.2) = -1.2796$, $p = 0.107$), though Bayesian statistics provided anecdotal evidence for the alternative hypothesis ($BF_{10} = 1.081$). SSA thresholds were not significantly different between groups ($t(27) = -0.9251$, $p = 0.182$), with anecdotal support for the null hypothesis ($BF_{10} = 0.757$). Overall, this suggests that although mean amplitude discrimination thresholds were greater in TS group compared to TD controls, these differences were not statistically significant.

3.3.2.1.3.2 Temporal order judgement

TOJ thresholds were not significantly different between the TS group and TD controls; $t(29) = -0.3585$, $p = 0.361$. Bayesian statistics show anecdotal evidence for the null hypothesis ($BF_{10} = 0.444$). cTOJ thresholds were also not significantly different between groups; $U = 75.5$, $p = 0.161$), and Bayesian statics suggest anecdotal evidence for the null hypothesis ($BF_{10} = 0.423$). Therefore, in the Study 2 sample, there is no evidence to suggest significant differences between TOJ and cTOJ thresholds.

3.3.2.1.3.3 Adaptation and carrier effects

In the TD group, one-tailed paired *t*-test identified no significant difference between mean simAD and SSA thresholds; $t(14) = -1.02$, $p = 0.163$, with anecdotal evidence for the null hypothesis ($BF_{10} = 0.673$). For the TS group, a two-tailed paired *t*-test also revealed no significant difference between mean simAD and SSA thresholds; $t(12) = -1.41$, $p = 0.185$. Bayesian inference highlighted anecdotal evidence for the null hypothesis ($BF_{10} = 0.621$). This demonstrates that thresholds were comparable after adaptation in amplitude discrimination tasks for both TD and TS groups in this cohort. Differences between TD and TS groups in adaptation effects were then assessed, with group mean percentages and standard deviations shown in

Table 3.7. The difference between amplitude effects did not significantly differ between TS and TD control groups ($t(17) = -1.32$, $p = 0.898$). Bayesian statistics provide moderate evidence for the null hypothesis ($BF_{10} = 0.169$).

In the TD group, a one-tailed paired Wilcoxon signed-rank test demonstrated significant difference between mean TOJ and cTOJ thresholds; $W = 19.5$, $p = 0.037$. Bayesian statistics revealed anecdotal evidence for the alternative hypothesis ($BF_{10} = 1.757$). For the TS group, a significant difference was also identified after a two-tailed paired *t* test; $t(11) = -2.94$, $p = 0.014$. Bayesian statistics demonstrate moderate evidence for the alternative hypothesis ($BF_{10} = 4.625$). This demonstrates that cTOJ thresholds were significantly worse than TOJ thresholds for both TD and TS groups. Group means and standard deviations are shown in Table 3.7. The difference between carrier effects did not significantly differ between TS and TD control groups ($t(20.9) = -2.23$, $p = 0.981$). Bayesian statistics provide moderate evidence for the null hypothesis ($BF_{10} = 0.129$).

3.3.2.2 Correlation analyses

3.3.2.2.1 MRS-GABA, -Glu and quantitative sensory thresholds

In both groups, one-tailed correlation analyses were conducted to identify any significant correlations between MRS-GABA concentrations and quantitative sensory thresholds. No significant correlations were identified for either group between MRS-GABA and simAD, seqAD, SSA, TOJ, cTOJ, adaption and carrier effects ($p > 0.05$). Two-tailed correlation analyses were also conducted between MRS-Glu and quantitative sensory thresholds for each group. No significant correlations were identified between MRS-Glu and simAD, seqAD, SSA, TOJ, cTOJ, adaptation and carrier effects ($p > 0.05$). Correlation statistics are shown in Appendix A.5.

3.3.2.2.2 MRS-GABA, -Glu, SPSQ and IAS

In the TD group, two-tailed correlations were conducted to assess any significant correlations between MRS-GABA and -Glu concentrations with self-report measures of interoceptive and exteroceptive awareness. No significant correlations were identified between MRS-GABA concentrations with SPSQ or IAS scores (p > 0.05). However, a significant correlation was identified between MRS-Glu and SSA scores (r = -0.58, p = 0.031). This suggests that greater MRS-Glu concentrations are associated with reduced thresholds in SSA tasks (Figure 3.8). Correlation statistics are shown in Appendix A.5.

Figure 3.8

Correlation between MRS-Glu concentration and SSA thresholds in the TD control group

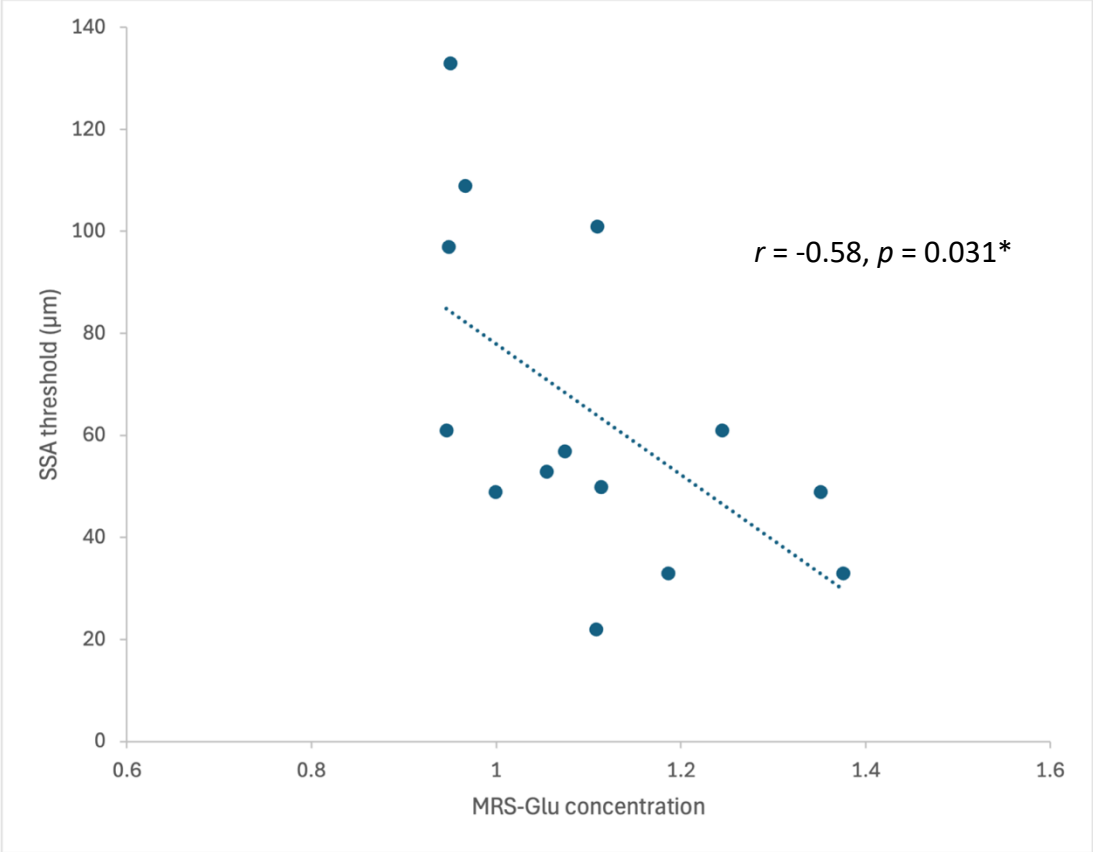

Note. SSA = single-site adaptation threshold. * = p < 0.05

These two-tailed correlations were repeated for the TS group. A significant correlation was identified between MRS-GABA and SPSQ score (r = 0.749, *p* = 0.013), where greater concentrations of MRS-GABA were associated with greater exteroceptive sensitivity as assessed by SPSQ scores (Figure 3.9).

Figure 3.9

Correlation between MRS-GABA concentration and SPSQ scores in the TS group

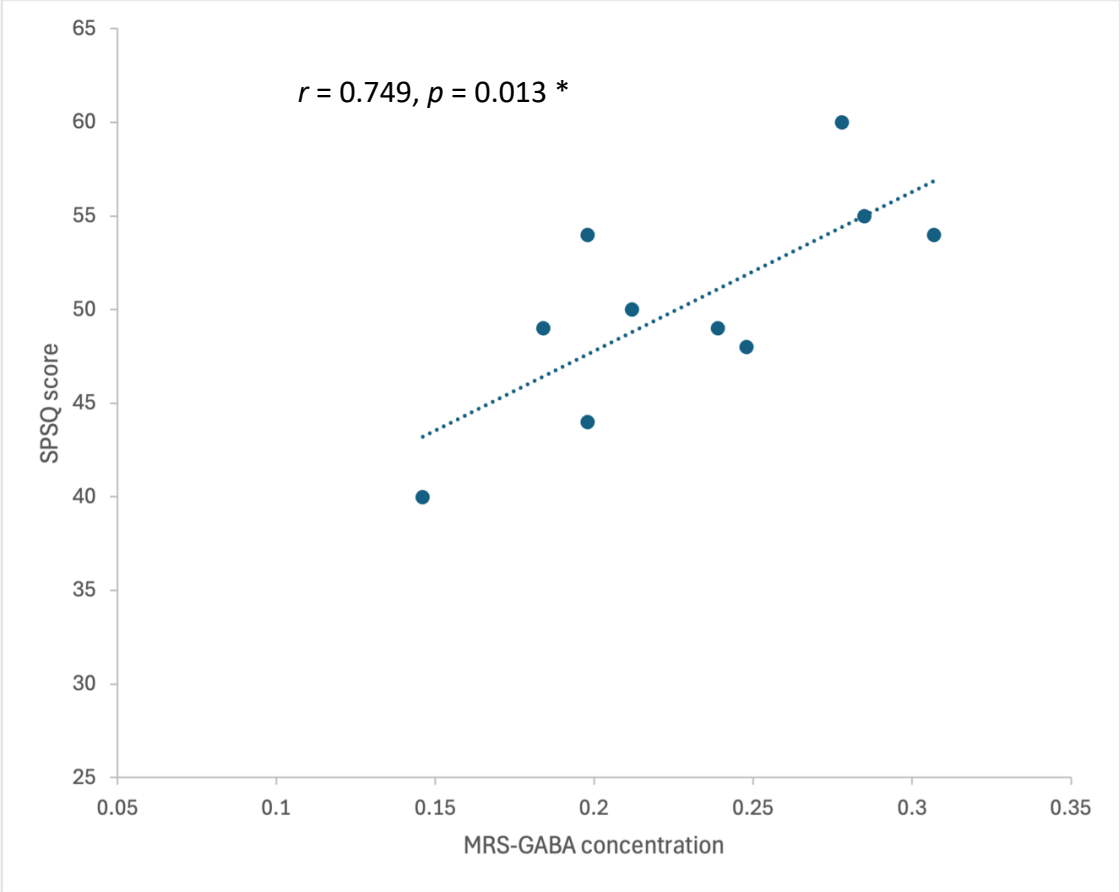

Note. SPSQ = Sensory Processing Sensitivity Questionnaire. * = *p* < 0.05

3.3.2.2.3 MRS-GABA, -Glu and self-report measures

One-tailed correlation analyses were also conducted for the TS group MRS-GABA levels with PUTS-R and YGTSS subscales, however no significant correlations were identified (*p* > 0.05). Two-tailed correlations between MRS-Glu with YGTSS subscales

also showed no significant correlations (p > 0.05), but a significant negative correlation was identified between MRS-Glu and PUTS-R scores (r = -0.597, p = 0.041; Figure 3.10), suggesting lower MRS-Glu concentrations are associated with greater premonitory urge severity. Full correlation analyses are shown in Appendix A.5.

Figure 3.10

Correlation between MRS-Glu concentration and PUTS-R scores in the TS group

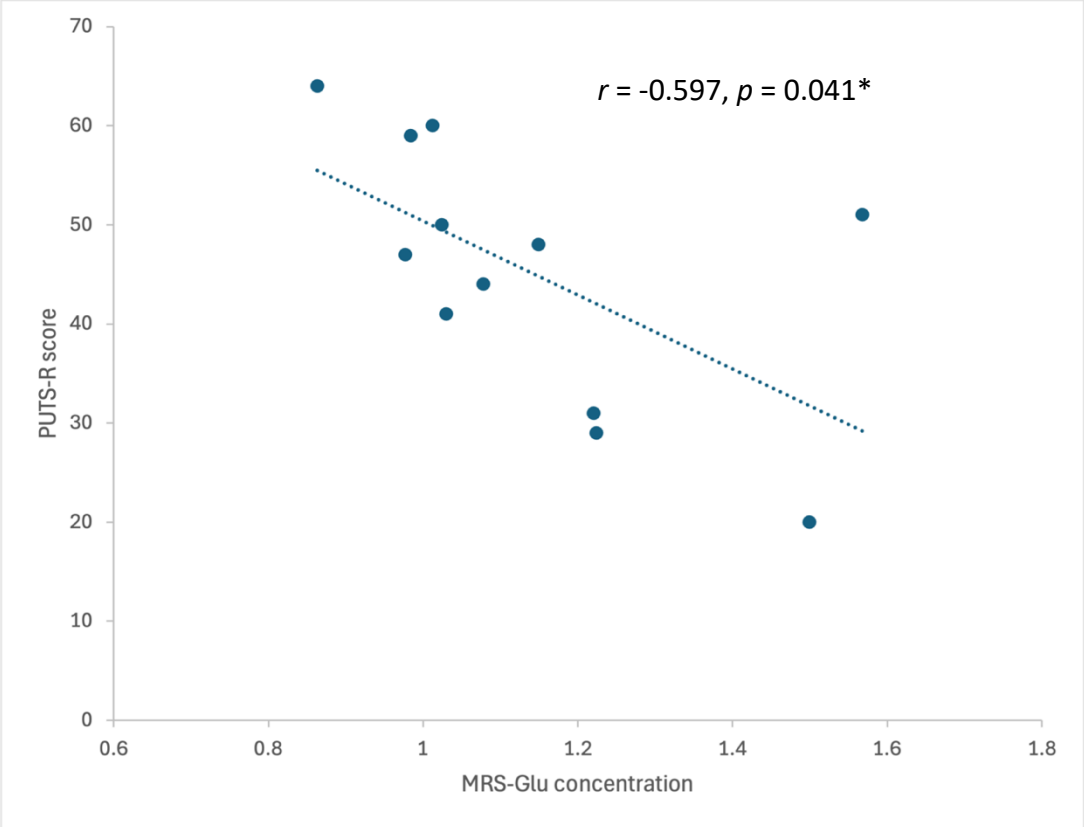

Note. PUTS-R = Premonitory Urges of Tics Score – Revised. * = p < 0.05

3.3.3 Discussion

MRS-GABA measures have previously been linked with sensory processing of tactile stimuli in TD populations (Cassady et al., 2019; Kolasinski et al., 2017; Mikkelsen et al., 2018; Puts et al., 2011, 2015; Puts, Harris, et al., 2017) and in populations with abnormalities in inhibitory mechanisms, such as ASD (Puts et al., 2014; Tommerdahl et al., 2008) and FHD (Antelmi et al., 2017c; Bara–Jimenez et al.,

2000; Bara-Jimenez et al., 2000). However, at the time of writing, only one study has investigated this relationship in TS (Puts et al., 2015). This study therefore used MRS to measure MRS-GABA and MRS-Glu in individuals with TS and a TD control group and correlated these with measures of sensory processing, namely subjective ratings of exteroception and interoceptive accuracy and quantitative tactile sensory thresholds.

Firstly, differences in MRS concentrations of GABA and Glu were assessed, however no significant differences were identified between TD control and TS groups for MRS-Glu concentrations which is inconsistent with previous evidence (Mahone et al., 2018). However, there was a trend for lower concentrations of MRS-GABA in the TS group, with Bayesian inference providing anecdotal evidence in support, signifying abnormalities in inhibitory mechanisms in TS. This trend is in support of previous evidence, which showed that children with TS display reduced GABA in sensorimotor cortices (Puts et al., 2015), however this relationship has not been displayed in recent investigations in children (He et al., 2022), adolescents (Draper et al., 2014) or adults (Tinaz et al., 2014) with TS.

Additionally, quantitative sensory thresholds and self-reported measures of exteroception and interoception were assessed and, although sensory thresholds and SPSQ scores were higher in the TS group, reflecting poorer performance in tactile discrimination and greater experience of sensitivity to external stimuli, no significant differences were identified between groups. This suggests that in the Study 2 cohort, there were no group differences in somatosensory processing. However, this is likely due to the reduced number of participants and therefore, statistical power in analyses.

3.3.3.1 Cortical excitability, inhibition and quantitative sensory thresholds

Correlation analyses revealed no significant correlations between quantitative sensory thresholds with MRS-Glu and -GABA in both TD and TS groups, suggesting measures of cortical excitability and inhibition are not related to sensory processing

of tactile stimuli. For the TS group, this is in line with previous evidence (Puts et al., 2015), which proposes that in TS, GABA is not involved in tactile discrimination and alternative strategies are used to process somatosensory information. This is also supported by evidence of similar adaptation and carrier effects between groups in Study 1 (see discussion in Section 3.2.3). However, while previous research has identified relationships between MRS-GABA and individual tactile sensory thresholds in healthy populations (Cassady et al., 2019; Kolasinski et al., 2017; Puts et al., 2011; Puts, 2015; Puts et al., 2017; Mikkelsen et al., 2018), this study failed to identify any relationship between measures of MRS-GABA in the TD control group with amplitude discrimination, TOJ thresholds or with adaptation and carrier effects. This suggests that although differences in inhibitory functioning have been proposed to underly differences in sensory processing (Kolasinski et al., 2017; Cassady et al., 2019; Kaneko & Hicks, 1990; Hicks & Dykes, 1983), results from the current study suggest that GABA, measured by MRS, is not implicated in quantitative tactile sensory processing. However, the proposed mechanisms behind the discrimination of tactile stimuli are thought to be driven by intracortical inhibitory processes, such as surround inhibition. These processes cannot be reflected in MRS-GABA concentrations, as MRS is the mere summation of neurometabolites within a voxel and is unrelated to intracortical inhibitory measures (Dyke et al., 2017). Instead, measures such as TMS-SICI, which reflect intracortical GABAergic functioning mechanisms, such as surround inhibition, should be utilised to further assess this relationship.

Additionally, there may be too much emphasis on role of GABAergic inhibition in external sensory processing, with other mechanisms proposed to be at play. This is highlighted by the TD control group, who showed a significant relationship between MRS-Glu concentrations and SSA scores, suggesting that greater levels of cortical excitability are associated with better detection of amplitudes after adaptation to a repetitive stimulus. While enhanced detection of discrete stimuli is thought to be driven by increased GABA and more efficient surround inhibition, allowing for enhanced separation of signals, this could instead be attributed to a balance of excitation and inhibition. Alternatively, this could be caused by an increased signal-

to-noise ratio in the sensorimotor cortices. Therefore, abnormalities in sensory processing may instead be influenced by factors such as increased 'noise', where detection of stimulus features may be reduced due to increased noise obscuring the signal of interest. Recent evidence has proposed that neural noise, an EEG measure, is increased in TS and therefore there is a reduced cortical signal-to-noise ratio during information processing (Adelhöfer et al., 2021; Münchau et al., 2021). Therefore, this reduced signal-to-noise ratio may underly differences in behavioural performance, and has been supported in populations with ADHD, where increases in neural noise are evident and reduced levels were associated with better behavioural performance in a response inhibition task (Pertermann et al., 2019). As a result, increased levels of neural noise with TS may be related to reduced precision when detecting amplitude and temporal properties of sensory stimuli.

3.3.3.2 Cortical inhibition and self-reported exteroceptive sensitivity

No significant correlations were identified between MRS-GABA or -Glu and IAS scores in the either group. Interestingly, MRS-GABA was significantly correlated with SPSQ scores in the TS group only, where greater levels of inhibition were related to greater scores of self-reported sensitivities to external stimuli (such as tactile stimuli, light and sound). This relationship has also been demonstrated in ASD, where self-reported hypersensitivity was positively correlated with MRS-GABA concentrations (Sapey-Triomphe et al., 2019). If GABA acts by sharpening acuity to sensory signals, this means that sensitivity to external stimuli would be increased. However, while self-reported hypersensitivity is associated with increased sensorimotor inhibition, this does not explain why quantitative sensory thresholds are poorer in the TS group. Similar mismatching relationships have previously been reported in Belluscio et al. (2011) and mirrors the relationship between self-reported interoception and objective interoceptive accuracy scores in TS (discussed in Section 1.3.2.2), where individuals with TS perceive their interoceptive accuracy as high, yet quantitative measures of interoception are significantly reduced compared to TD controls (Rae, Larsson, et al., 2019). A proposed explanation for this is that top-down predictions of sensory information are abnormal in TS and ASD, with the weight of predictions

thought to be modulated by GABA (Rosenberg et al., 2015). Therefore, prediction errors are common due to abnormal GABAergic modulation, which causes external stimuli to be perceived as unpredicted and leads to perceived hypersensitivity to external stimuli (Rae, Critchley, et al., 2019; Sapey-Triomphe et al., 2021). This Bayesian account of perceived hypersensitivity may account for this relationship in the TS group, were abnormalities in GABA modulation result in prediction errors and therefore, increased hypersensitivity. However, in this cohort, hypersensitivity scores are only slightly elevated in the TS group compared to the TD group, so caution must be taken with further investigation required into this explanation.

3.3.3.3 Cortical excitability and urge severity

Within the TS group, tic and urge severity scores were also input into correlation analyses with neurometabolite concentrations. A significant correlation was identified between MRS-Glu scores and urge severity scores, as assessed with total PUTS-R scores. Specifically, reduced levels of MRS-Glu, reflecting reduced cortical excitability, were associated with greater PU scores. This paradoxical relationship was demonstrated in children with TS with single-pulse measures of cortical excitability and reduced cortical excitability was also modulated by reduced MRS-GABA concentrations in the SMA (Larsh et al., 2023). Reductions in MRS-GABA in the SMA have also been associated with urge severity in TS (He et al., 2022), indicating the presence of abnormalities in connectivity between SMA and M1 in TS. However, He et al. (2022) did not identify any relationships between PU and MRS-Glx (a measure of cortical excitability by combining glutamate and glutamine values) in a larger sample of children with TS (N = 68). However, MRS-Glx was utilised by this group as glutamate cannot be reliably detected at 3T, and therefore may show differences with MRS-Glu which can be resolved at 7T.

3.3.3.4 Limitations

This study has several limitations. Firstly, as discussed in Section 3.1, individuals with ASD and ADHD also show abnormalities in tactile thresholds and MRS-GABA

(Tommerdahl et al., 2008; Puts et al., 2017). These are common co-morbidities in TS, however the impact of these co-morbidities on MRS concentrations and tactile thresholds were not controlled during correlation analyses. Therefore, it is possible that trends in reduced MRS-GABA and increased tactile thresholds may be associated with the presence of co-morbidities. Additionally, TS participants were screened prior to recruitment and were only recruited if they had relatively low tic frequency/intensities, with the absence of frequent or intense facial and head tics. This was to ensure comfort during scanning and reduce the likelihood of movement artefacts impacting data quality, though excludes a subset of the TS population. Additionally, during participant recruitment, a greater number of females expressed interest in taking part and, during screening, displayed low tic frequencies/intensities. As a result, a higher proportion of females were recruited for this study. However, this resulted in a sample not reflective of the estimated male to female ratio of 2-3:1 in adult TS populations (Freeman et al., 2000; Levine et al., 2019). Moreover, females with TS generally display later symptom onset, more complex tics in adulthood and have a greater prevalence of comorbid OCD (Baizabal-Carvallo & Jankovic, 2023; Dy-Hollins et al., 2023), with these sex differences perhaps reflecting different aetiologies, as evidenced by differential treatment response to medication, and evidence of neural dimorphisms in brain structure and functional connectivity (Baizabal-Carvallo & Jankovic, 2023; Garris & Quigg, 2021). Consequently, these results could reflect sensory processing and neurometabolite concentrations in an alternative 'phenotype' of TS. Therefore, the TS group used in this study may not represent that of the general adult population with TS, limiting the generalisability of these results.

Furthermore, MRS was conducted at rest and participants were instructed to be still and actively suppress their tics. As a result, it cannot be ruled out that the trend of reduced GABA in the sensorimotor cortices may be related to suppression of tics during MRS. For instance, it has been proposed that control over motor outputs and suppression of tics involves an increase in tonic inhibition within the SMA, influencing excitability in sensorimotor cortices (Draper et al., 2014; Jackson et al., 2015; Ueda et

al., 2021). This has also been demonstrated by reduced tic severity scores and reduced motor cortex excitability after multiple sessions of 'inhibitory' rTMS to the SMA (Kwon et al., 2011; Le et al., 2013; Mantovani et al., 2007). However, this would not explain the reduction in sensorimotor MRS-GABA identified in this study, as enhanced SMA MRS-GABA has been linked with reduced excitability in the motor cortex in TS (Draper et al., 2014). Nevertheless, as the extent of suppression during MRS was not assessed and SMA MRS was not conducted in this study, the possible influence of suppression on MRS-GABA in this sample is unclear.

Finally, MRS was measured from the left hemisphere, related to the dominant right hand. However, quantitative tactile sensory testing was measured in the index and middle fingers of the non-dominant left hand and selecting responses with the dominant right hand. This mismatch could also explain the absence of relationships between MRS-GABA and sensory discrimination thresholds. However, sensorimotor MRS measures are generally consistent across hemispheres (Puts et al., 2018). Moreover, previous evidence in TS also demonstrated a lack of relationship when measuring tactile discrimination in the left hand and MRS-GABA in the right hemisphere (Puts et al., 2015). Additionally, in TD controls, relationships were discovered between right hand sensorimotor performance and averaged bilateral MRS-GABA (Cassaday et al., 2019). However, while this suggests that laterality of MRS and sensory tasks are unlikely to influence subsequent analyses, it cannot be ruled out.

3.4 Conclusions

Overall, this chapter highlighted the presence of some abnormalities in cortical inhibitory functioning and in tactile discrimination thresholds in individuals with TS, compared to TD controls, although these measures were not correlated with each other in either group. However, it is unlikely that MRS-GABA is reflective of the intracortical inhibitory mechanisms suggested to reflect the proposed role of surround inhibition on tactile discrimination. Nonetheless, associations were identified between urge severity and sensorimotor MRS-Glu, and a positive

relationship was seen between self-reported exteroceptive sensitivity and MRS-GABA concentrations in the TS group only, posing questions into the role of inhibitory functioning on tactile discrimination and self-reported sensory processing. As a negative relationship was highlighted between SSA and MRS-Glu scores in the TD control group, other mechanisms may be at play. Alternative explanations for the abnormalities in central processing of sensory information (such as the contradictory relationship between self-reported and objective sensitivity to external stimuli), should be explored further, with insight into the role of neural noise and Bayesian explanations of hypersensitivity.

4. Chapter 4 - Sensorimotor mapping of digit representations in Tourette Syndrome

Key words: Tourette Syndrome (TS), functional magnetic resonance imaging (fMRI), sensorimotor representations, digits

4.1 Introduction

As reviewed in Chapter 1, cortical sensorimotor representations are thought to be related to GABAergic inhibitory mechanisms. In Chapter 3 of this thesis, a trend for reduced sensorimotor MRS-GABA in the group of individuals with TS compared to the TD control group was shown. Moreover, abnormalities were identified in tactile discrimination tasks, and MRS-GABA was significantly correlated with self-reported hypersensitivity scores in the TS group. This suggests that there may be disruptions to sensory processing, however tactile discrimination thresholds were not associated with MRS-GABA concentrations in either group. This casts doubt on the role of tonic inhibition in shaping somatosensory acuity and discrimination.

GABAergic inhibition has previously been associated with the integrity of cortical representations, as discussed in Section 1.2.1.1, individuals with greater levels of sensorimotor GABA display greater specificity and acuity of cortical sensorimotor representations, of the digits in particular. Specifically, individual concentrations of sensorimotor MRS-GABA have been related to digit activation profiles and the level of sensorimotor network integration (Cassady et al., 2019; Kolasinski et al., 2017). Moreover, TMS SICI has been shown to be a significant predictor of the area of the FDI hand muscle representation, as measured with TMS mapping (Sigurdsson, Molloy, et al., 2020). However, groups with abnormalities in GABAergic inhibition and in movement of the hand have shown abnormalities in digit representations.

FHD is characterised by abnormal cortical inhibitory mechanisms (Beck et al., 2008; Beck & Hallett, 2011; Gallea et al., 2018; Sohn & Hallett, 2004; Stinear & Byblow, 2004) and there is a strong consensus that individuals with FHD show abnormalities in sensorimotor digit representations (Bara-Jimenez et al., 1998; Butterworth et al., 2003; Byl et al., 2000; Byrnes et al., 1998; Elbert et al., 1998; Huber et al., 2023; Meunier et al., 2001; Schabrun et al., 2009). While healthy controls show well defined areas of the sensorimotor cortex associated with each digit or hand muscle, these are less well differentiated and are larger in FHD, with reduced distances between the centres of each representation (Meunier et al., 2001; Schabrun et al., 2009). Additionally, some evidence has demonstrated that digits can be spatially reversed and located more superiorly and medially in Writer's cramp compared to TD control groups (Nelson et al., 2009). This is supported by primate models of FHD, which show enlarged and overlapping receptive fields across the hand and face representations compared to a control primate (Blake et al., 2002), with receptive field size thought to be controlled by GABA and surround inhibition (Beck & Hallett, 2011). As a result, it is proposed that impaired GABA functioning in FHD results in reduced differentiation between different cortical representations due to weakened receptive field tuning and surround inhibition, as seen in animal research after injection of GABA antagonists (Foeller et al., 2005; Jacobs & Donoghue, 1991; Schneider et al., 2002). Therefore, it can be argued that in TS, the identified abnormalities in inhibitory functioning may cause alterations in cortical organisation.

Previous TMS mapping evidence has demonstrated that the FDI hand muscle representation is shifted more medially and reduced in size in individuals with TS compared to TD controls (Sigurdsson, Jackson, et al., 2020). However, these maps were measured with single-pulse TMS at an intensity of 200%RMT. Although this intensity was kept constant when mapping every muscle for each participant to reduce discomfort from long periods of keeping still, this may have been problematic as different sensorimotor areas likely require different stimulation intensities to evoke the same MEP response in different muscles (Menon et al., 2018). Additionally, while MEP responses at an individual's RMT are comparable between populations, above

threshold intensities may instead produce MEPs that are significantly smaller in TS than in the general population. This is because evidence consistently suggests that TMS input-output (IO) curves (indicative of motor gain in the cortex) are reduced in TS (Draper et al., 2014; Orth, 2009; Pépés et al., 2016) and using an intensity for mapping during pre-activation of the muscle may have been more appropriate as this produces similar MEP recruitment between TS and control populations (Orth, 2009). As a result, it is unclear if mapping of the hand and digits truly differ between populations with TS and TD controls.

Moreover, it is not clear if GABAergic inhibition is directly related to the aberrant nature of sensorimotor maps in FHD, as these have not been directly correlated with digit maps in previous research. Additionally, abnormalities in FHD sensorimotor digit maps are generally only associated with the hemisphere of the affected hand, despite evidence of both hemispheres displaying abnormalities in sensorimotor GABAergic inhibition (Ridding et al., 1995; Rona et al., 1998). However, evidence of abnormalities isolated to one hemisphere are generally mixed, as many studies limit investigation to the hemisphere associated with the affected hand (Bara-Jimenez et al., 1998; Butterworth et al., 2003; Elbert et al., 1998; Schabrun et al., 2009), and evidence of bilateral disruptions in digit mapping are thought to be a result of symptom severity and in those who have experienced FHD for long periods (Byrnes et al., 1998; Meunier et al., 2001).

It has been proposed that the abnormalities in digit mapping with FHD are due to the repetitive unilateral movements associated, which drive sensorimotor abnormalities within the sensorimotor cortex of the affected hemisphere. Specifically, while FHD has a genetic component, it is typically developed in those who conduct highly skilled and repetitive use of the hand, such as musicians (Lin & Hallett, 2009). As a result, it has been theorised that FHD is associated with abnormalities in sensory hand representations due to repetitive hand behaviours inducing the creation of abnormal representations, which in turn affect motor control and strengthen these sensory abnormalities in a positive feedback loop (Blake et al., 2002; Evinger, 2005).

This could also explain why abnormalities in digit representations have also been evidenced in individuals with repetitive hand behaviours, such as writing tremor (Byrnes et al., 2005) and carpal tunnel syndrome (Napadow et al., 2006). Therefore, impaired GABA modulation and surround inhibitory mechanisms may provide the ideal environment to create aberrant sensorimotor representations in the hemisphere associated with repetitive movements (i.e. the dystonic limb). This also means that there may be great variability in individual digit maps across individuals depending on their distinct dystonic symptomology. This has been supported by animal models of FHD, where digits showing greater dysfunction could be identified on hand maps (Blake et al., 2002). As a result, although individuals with TS may show trends in reductions in sensorimotor MRS-GABA and TMS-SICI (see Section 1.3.1), as hand tics are not widely reported it can be hypothesised that it is unlikely that differences will be evident in sensorimotor digit representations in TS compared to TD control populations.

Additionally, in TD populations, a mechanistic relationship has been demonstrated between tactile TOJ performance and sensorimotor MRS-GABA concentration, which is mediated by the somatosensory cortical tuning profiles of activity across D2-D5 (Kolasinski et al., 2017). However, although Chapter 3 demonstrated abnormalities in tactile TOJ performance and MRS-GABA concentrations within the TS group, no relationships were evident between these in TD, or TS populations. This lack of association was also demonstrated in children with TS in Puts et al. (2015). Considering this, it is not expected that sensorimotor representations of the digits will show differences between TS and TD groups in this study.

4.2 Aims

This study aimed to investigate the size of fine-grained maps of individual digits of individuals with TS and TD controls in the left sensorimotor cortex (M1 and S1). This is the contralateral cortex to the right (dominant) hand. Previous research has demonstrated that specific digits can be extracted during task fMRI to map the

somatotopy of the digits at high resolution, some even achieving mapping of different parts of a single digit (Besle et al., 2013; Da Rocha Amaral et al., 2020; Kolasinski et al., 2016; O'Neill et al., 2020; Sánchez-Panchuelo et al., 2014; Sánchez-Panchuelo et al., 2010; Sánchez-Panchuelo et al., 2012; Stringer et al., 2011). Digits with the most use are thought to have greater cortical magnification, resulting in D1 and D2 typically showing larger cortical representations compared to D4 and D5 which have reduced cortical representations (Janko et al., 2022). As a result, any nuances in the cortical size of digits can be readily identified across groups. Here, a 7T fMRI phase-encoding travelling wave design was employed for accurate mapping of the digits (see Section 2.1.1.3). It is hypothesised that the voxels assigned to each digit and distances between digits in M1 and S1 will not differ between groups.

4.3 Methods

4.3.1 Participants

Due to the practical limitations (funding availability and timescale) and that this data was collected with sensorimotor MRS (Chapter 3) and fMRI (Chapter 5, Study 2), the target number of participants per group was set at 20 individuals per group (justification for this sample size can be found in Chapter 3). Twenty TD adults and 16 participants with TS or chronic tic disorder were recruited for this study at 7T using online recruitment methods (e.g. social media, mailing lists, charity partners). Participants gave informed consent, and ethics were approved by the local ethics committee (School of Psychology, University of Nottingham: S1500). No participants in the TD group were taking CNS-active drugs and were free from any mood or neurological illness during the experimental timeline. Due to a projector fault and visual impairments preventing viewing of task from scanner bore, seven participants from the TD group and seven participants from the TS group did not complete the digit tapping task. No data was removed due to data quality concerns. Therefore, this study included 13 TD controls and nine TS participants.

Demographic information is displayed in Table 4.1. Age ($t(20) = 1.71$, $p = 0.102$) and sex (X^2 (1, $N = 22$) = 2.01, $p = 0.157$), distributions were not significantly different

between the groups. Clinical questionnaires, as described in Section 3.2.1.2, were also administered to individuals with TS, with all medications, YGTSS and PUTS-R scores for the TS group are displayed in Appendix B.1. All participants were free from any contraindications for MRI, as assessed by completion of an MRI safety screening form. All participants were right-handed as assessed by the Edinburgh handedness questionnaire (Oldfield, 1971).

Table 4.1

Demographic information of TD and TS participants

Group	N	Age	Sex
TD	13	28.46 (±6.5)	5 male, 8 female
TS	9	23.56 (±6.7)	2 male, 7 female

Note. *N* = number of participants, TD = group of typically developing control participants, TS = group of participants with Tourette Syndrome, mean (±standard deviation)

4.3.2 MRI Data Acquisition

This MRI data was collected in a scan session that also comprised of sensorimotor MRS (Chapter 3) and vibrotactile stimulation to three facial regions (Chapter 5). All MRI data was acquired on a 7T Philips Achieva MRI Scanner with a 32-channel head coil at the Sir Peter Mansfield Imaging Centre at the University of Nottingham.

4.3.2.1 fMRI Mapping Paradigm

Two travelling wave fMRI task blocks were acquired with participants visually instructed to tap their right (dominant) hand digit 2 (index finger) at 2Hz for 4 seconds (in time with the visual stimuli presented) followed by digit 3, digit 4, and digit 5 in the “forward” condition resulting in a block length of 16 s, this was repeated for 8

cycles. A second fMRI run was completed with the same tapping parameters as the first run, but performed in the "reverse" condition tapping digit 5 first, then digit 4, digit 3 and digit 2. See Figure 4.1 for a visual depiction of the task.

Figure 4.1

Visual depiction of fMRI travelling wave tapping task

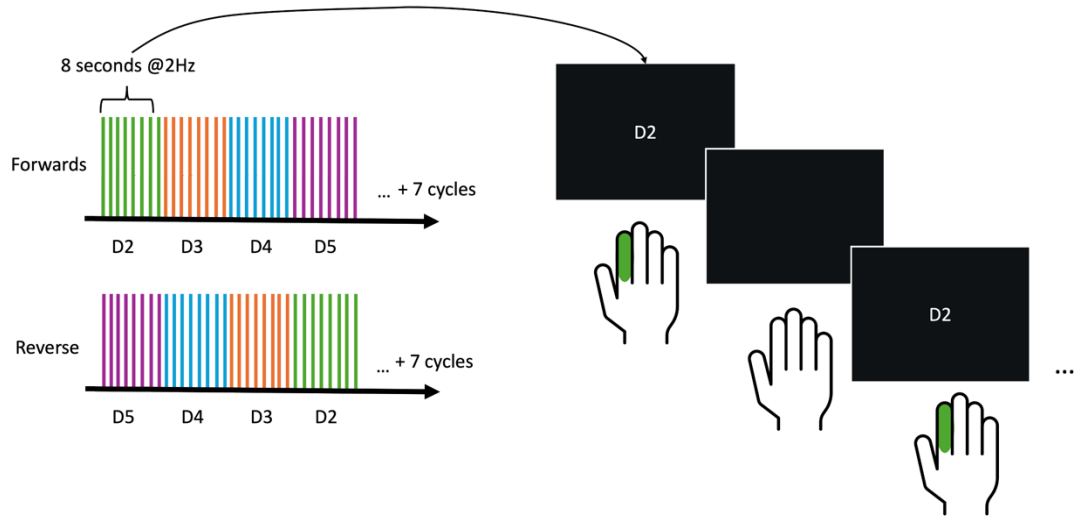

Note. Dx= Digit. Participants were instructed to tap their right-hand digit in time with the presentation of the digit on the screen (2Hz). Forwards cycle: D2, D3, D4, then D5 and reverse cycle: D5, D4, D3, then D2. Each forward and reverse run consisted of 8 cycles total

Each travelling wave task block was visually presented using PsychoPy (Open Science Tools, Ltd.; (Peirce et al., 2019) on a projector screen visible to the participant with Prism glasses. Participants were trained in tapping prior to scanning. Participants tapped using a MR-compatible button box (fORP response button box; Cambridge Research Systems, UK).

The two fMRI runs were conducted using a single-shot 2D T_2*-weighted GE-EPI sequence (voxel 1.5 mm isotropic, matrix size = 128 x 128 x 40, multiband 2, TR/TE = 2000/22 ms, 2.24 minute acquisition time per run). For the fMRI data acquisition both magnitude and phase images were collected, along with a final noise scan dynamic to allow NORDIC PCA image denoising in the analysis pipeline (Moeller et al.,

2021; Vizioli et al., 2021). After the fMRI runs, two additional spin SE-EPI short scans (5 dynamics) with the same acquisition parameters, but with opposing fat shift direction, were collected for EPI distortion correction (see Section 4.3.3.2.1).

4.3.2.2 T1-weighted MRI parameters

Prior to the fMRI runs, a anatomical T_1-weighted 3D gradient echo PSIR scan was acquired (matrix size = 320 x 320, FOV = 224 x 224 x 157 mm, 0.7mm isotropic, 224 slices, TR/TE = 6.3/2.8 ms, flip angle = 5^o, acquisition time 6.25 minutes) with TFE readouts after each inversion pulse at TI1 = 780 ms and TI2 = 2380 ms. This was collected for co-registering with the fMRI runs and with standard template space images to allow for comparison across participants.

4.3.3 Data Analysis

4.3.3.1 T_1-weighted MRI

The two PSIR readouts were converted into T_1-weighted images using an in-house Python (v.3.9.12) script (https://github.com/oliviermougin/PSIR). All PSIR images underwent brain surface extraction implemented on the University of Nottingham's High-Performance Computer using an in-house BRC structural analysis pipeline (Mohammadi-Nejad et al., 2019). This employed FreeSurfer functions (Fischl, 2012) and was completed to extract Broadmann areas (BA) for subsequent masking of fMRI images.

4.3.3.2 BOLD-fMRI analysis

4.3.3.2.1 Pre-processing

fMRI data were distortion corrected using FSL-TOPUP and thermal noise was removed using NORDIC PCAS denoising (Andersson et al., 2003; Moeller et al., 2021; Vizioli et al., 2021). Data was then assessed for any motion artefacts and any fMRI blocks with absolute mean motion displacement above 1.5mm were removed. Due to the low sample size and to preserve as much data as possible, fMRI images that

were contaminated by brief periods of large motion displacement (>1.5mm) for up to 2 cycles had these cycles removed from subsequent analyses using FSL UTILS (Jenkinson et al., 2012). Only Map09 from the TD group had the last cycle of the forward travelling wave run and the first cycle of the reverse travelling wave run removed, resulting in a total of 7 cycles per travelling wave run.

The temporal signal-to-noise ratio (tSNR) of the resulting de-noised fMRI timeseries (tSNR) were assessed in MATLAB (MATLAB_R2019a, Mathworks, Natick, MA) using an in-house quality assurance code fMRI_report_app (https://github.com/nottingham-neuroimaging/qa/tree/master/fMRI_report_app). The mean tSNR for the TD group was 85 with a standard deviation of 2 and the mean tSNR for the TS group was 94 with a standard deviation of 26. Any fMRI scans with tSNR < 30 would have been removed, however none were present in this sample.

The resulting de-noised data were pre-processed using FSL-FEAT (FMRI Expert Analysis Tool; Jenkinson et al., 2012). Motion correction was conducted using FMRIB's linear image registration tool, MCFLIRT, using the middle volume as a reference volume (Jenkinson, 2002). High-pass temporal filtering of 16 s was applied, and spatial smoothing was conducted using a Gaussian kernel of 2.25mm FWHM to account for anatomical differences between participants using the FSL Smallest Univalue Segment Assimilating Nucleus toolbox (SUSAN; Smith & Brady, 1997). Registration of fMRI images to anatomical images was performed using FLIRT (FMRI; Jenkinson et al., 2002; Jenkinson & Smith, 2001) by taking an example volume from the low-resolution fMRI image and registering this to an example volume of the participant's T_1-weighted PSIR high-resolution image.

4.3.3.2.2 fMRI analysis

Data analysis was conducted using the pipeline described in Besle et al. (2013). The aligned and pre-processed travelling wave fMRI data were analysed using mrTools (Gardner et al., 2018) in MATLAB (MATLAB_R2019a, Mathworks, Natick, MA). In-house MATLAB scripts were then used to average the forward and reverse

travelling wave runs and calculate phase and coherence maps, which were threshold to 0.3 (corresponding to p = 0.008). To quantitatively characterise each participant's individual digit region of interest (ROI), travelling wave outputs were masked over individual left hemisphere BA 4 (corresponding to the M1), and individual digits were extracted by dividing phase maps into 4 bins (one for each digit). This employed a 'winner-takes-all' approach, in which each voxel is only assigned to one digit. This process was then repeated for travelling wave outputs masked to individual left hemisphere BA 1, 2, 3a, 3b (analogous to somatosensory cortices and primarily activated in digit mapping; Janko et al., 2022).

4.3.3.2.3 Digit ROI metrics

To quantitatively characterise each participant's digits, voxel counts and 3D coordinates of the centre of gravity (COG) were extracted for each digit ROI for each participant in native space, using FSL functions in FSLUTILS (Jenkinson et al., 2012). 3D COG coordinates are defined in three directions; x (left (-) to right (+), L-R), y (posterior (-) to anterior (+), P-A) and z (inferior (-) to superior (+), I-S).

As datasets were threshold at an individual level prior to extraction of digits, voxel counts will vary between individuals. To account for this, ratios for each digit ROI were calculated, using Equation 4.1, to quantify the proportion of voxels assigned to each digit within individuals.

$$Dx_{Ratio} = \frac{nDx}{(nD1+nD2+nD3+nD4+nD5)} \quad (4.1)$$

where nDx is the number of voxels assigned to the digit in question and $nD1$+ $nD2$ + $nD3$ … is the total number of voxels for all digits. This gives an insight into the size of each digit ROI in comparison to other digits within M1 and S1 ROIs for each individual and allows for comparison across groups.

Finally, as COG coordinates were extracted in native space, to allow comparison between the positioning of digits in relation to other digits, COG coordinates were used to calculate the Euclidean distances (d) between adjacent digits, expressed in Equation 4.2.

$$d = \sqrt{(x2 - x1)^2 + (y2 - y1)^2 + (z2 - z1)^2} \quad (4.2)$$

where $x2$, $y2$, $z2$ are the 3D COG coordinates for one digit and $x1$, $y1$, $z1$ are another digit's 3D COG coordinates.

These were then normalised after outlier removal in Section 4.3.4, using the min-max scaling method in Equation 4.3.

$$x' = \frac{x - \min(x)}{\max(x) - \min(x)} \quad (4.3)$$

where x' is the normalised value, x is the original value, $\min(x)$ is the minimum value in the group and $\max(x)$ is the maximum value in the group.

4.3.4 Statistical analysis

Each digit metric was assessed for extreme outliers. Any datapoint with any value outside of 1.5x the IQR above the third quartile or 1.5x the IQR below the first quartile were classed as an outlier and removed from subsequent analyses. For M1, this resulted in two TD (two from D3) and three TS participants (one from D3, two from D4) removed from digit ratio analyses, and one TD (one from D3-D4), two TS (one from D2-D3, one from D4-D5) from Euclidean distance analyses. For S1, this resulted in three TD (two from D3 and one from D4) and two TS participants (two from D4) removed from digit ratio analyses, and one TS (one from D3-D4) from Euclidean distance analyses.

Independent two-tailed t-tests were then conducted to detect any significant differences between the TD and TS group in: digit ratio and Euclidean distances between digit ROIs. Where data was not normally distributed, independent t-tests were replaced with non-parametric Mann-Whitney *U* tests. A BF_{10} was used with a Cauchy distribution with a scale of γ = 0.707 used as the prior distribution (Rouder et al., 2009). Interpretation of BF_{10} values are shown in Table 3.2. These statistical analyses were conducted using jamovi (v 2.3.28; jamovi.org).

4.4 Results

4.4.1 Motor digit mapping

Here, the results of the motor digit mapping are explored.

4.4.1.1 Digit ratios

To assess whether there were any significant differences in digit ratios between TD and TS groups, two-tailed independent-samples t-tests were conducted. A significant difference in D3 voxel ratios was identified between TD and TS groups, ($U = 4$, $p < .001$, $BF_{10} = 17$). This suggests that the proportion of voxels assigned to D3 in comparison to other digits was higher in the TS group compared to the TD group. No significant differences were identified in D2, D4 or D5 average digit ratios between each group, however Bayesian inference in D4 digit ratios provided anecdotal support for the the alternative hypothesis (see Table 4.2 for means, standard deviations and *t* and Bayesian statistics). This suggests that the TS group have a larger proportion of voxels assigned to D3 and D4 in the left hemisphere motor cortex compared to the TD group.

Table 4.2

Means, standard deviations and statistics for M1 digit ratios in TD and TS groups

	Digit ratios			
Group	**D2**	**D3**	**D4**	**D5**
TD	0.202 (±0.131)	0.048 (±0.035)	0.157 (±0.103)	0.540 (±0.257)
TS	0.167 (±0.119)	0.159 (±0.088)	0.227 (±0.044)	0.396 (±0.209)
N	TD = 12 TS = 9	TD = 10 TS = 8	TD = 12 TS = 9	TD = 12 TS = 9
	$t(19) = 0.64$, $p = 0.532$	$U = 4$, $\mathbf{p < .001}^{**}$	$t(16.0) = -2.05$, $p = 0.057$	$U = 31$, $p = 0.111$
	$BF_{10} = 0.454$	$\mathbf{BF_{10} = 17.02}^{\dagger\dagger\dagger}$	$\mathbf{BF_{10} = 1.059}^{\dagger}$	$BF_{10} = 0.757$

Note. Dx= Digit, TD = typically developing control group, TS = group of participants with Tourette Syndrome, *N* = number of participants, mean (±standard deviation), ** = $p < .001$, † = anecdotal evidence for the alternative hypothesis, ††† = strong evidence for the alternative hypothesis

4.4.1.2 Euclidean distances

Two-tailed independent group t-tests were conducted between TD and TS group Euclidean distances (D2-D3, D3-D4 and D4-D5). No significant differences were identified between groups, as shown in Table 4.3.

Table 4.3

Means, standard deviations and statistics for Euclidean distances between M1 digits in TD and TS groups

	Euclidean distances between COG 3D coordinates (min-max normalised)		
Group	**D2-D3**	**D3-D4**	**D4-D5**
TD	0.44 (±0.29)	0.38 (±0.32)	0.35 (±0.30)
TS	0.36 (±0.34)	0.35 (±0.32)	0.50 (±0.39)
N	TD = 12 TS = 8	TD = 12 TS = 9	TD = 13 TS = 8
	$t(18) = 0.56$, $p = 0.586$	$U = 50$, $p = .803$	$t(19) = -1.02$, $p = 0.321$
	$BF_{10} = 0.449$	$BF_{10} = 0.403$	$BF_{10} = 0.572$

Note. Dx= Digit, TD = group of typically developing control participants, TS = group of participants with Tourette Syndrome, *N* = number of participants, mean (±standard deviation)

4.4.2 Somatosensory digit mapping

Here, the results of the somatosensory digit mapping are explored.

4.4.2.1 Digit ratios

To assess whether there were any significant differences in digit ratios between TD and TS groups, two-tailed independent-samples t-tests were conducted. No significant differences were identified in any average digit ratios between each group, however Bayesian inference provided anecdotal support for the alternative hypothesis in D2 and D3 ratios (see Table 4.4 for means, standard deviations and *t* and Bayesian statistics). This suggests that the TD group have a larger proportion of voxels assigned to D2 in the sensory cortex of the dominant hand compared to the TS group and vice versa for D3.

Table 4.4

Means, standard deviations and associated statistics for S1 digit ratios in TD and TS groups

	Digit ratios			
Group	**D2**	**D3**	**D4**	**D5**
TD	0.285 (±0.133)	0.097 (±0.081)	0.154 (±0.097)	0.394 (±0.222)
TS	0.178 (±0.098)	0.172 (±0.098)	0.198 (±0.052)	0.398 (±0.188)
N	TD = 13 TS = 9	TD = 11 TS = 9	TD = 12 TS = 7	TD = 13 TS = 9
	$t(20) = 2.04$, $p = 0.055$	$t(18) = -1.85$, $p = 0.080$	$t(17) = -1.12$, $p = 0.277$	$t(20) = -0.052$, $p = 0.959$
	$\mathbf{BF_{10} = 1.581}^{\dagger}$	$\mathbf{BF_{10} = 1.254}^{\dagger}$	$BF_{10} = 0.634$	$BF_{10} = 0.390$

Note. Dx= Digit, TD = group of typically developing control participants, TS = group of participants with Tourette Syndrome, *N* = number of participants, mean (±standard deviation), † = anecdotal evidence for the alternative hypothesis

4.4.2.2 Euclidean distances

Two-tailed independent group t-tests were conducted between TD and TS group Euclidean distances (D2-D3, D3-D4 and D4-D5). No significant differences were identified between groups, as shown in Table 4.5.

Table 4.5

Means, standard deviations and associated statistics for Euclidean distances between S1 digits in TD and TS groups

	Euclidean distances between COG 3D coordinates (min-max normalised)		
Group	**D2-D3**	**D3-D4**	**D4-D5**
TD	0.40 (±0.31)	0.48 (±0.33)	0.50 (±0.31)
TS	0.35 (±0.34)	0.52 (±0.34)	0.62 (±0.38)
N	TD = 13 TS = 9	TD = 13 TS = 8	TD = 13 TS = 9
	$t(20) = 0.36$, $p = 0.723$ $BF_{10} = 0.408$	$t(19) = -0.27$, $p = 0.788$ $BF_{10} = 0.409$	$t(20) = -0.82$, $p = 0.406$ $BF_{10} = 0.503$

Note. D*x*= Digit, TD = group of typically developing control participants, TS = group of participants with Tourette Syndrome, *N* = number of participants, mean (±standard deviation)

4.5 Discussion

This study aimed to assess digit representations within the primary motor and somatosensory cortices (M1 and S1) in TD controls and individuals with TS. It was hypothesised that digit maps in the TS group would show no differences from digit maps in the TD control group, as hand tics are not common in TS. This hypothesis was supported in the data as Euclidean distances between adjacent digits did not significantly differ between groups in M1 and S1, but some differences were evident in digit ratios between the groups.

Firstly, the proportion of voxels assigned to each digit (digit ratios) in M1 were significantly larger in D3 for the TS group, with anecdotal evidence for the same pattern in D4 in the TS group. In S1, there was anecdotal evidence for differences in D2 and D3 ratios, where the D2 ratio was smaller and D3 ratio was larger in the TS group compared to the TD control group. This suggests that there are some differences in the size of digits in the dominant hand in contralateral M1 and S1, where D3 (in M1 and S1) and D4 (in M1) in the TS group occupy a larger proportion of M1/S1 and D2 occupies a smaller portion of S1 in comparison to the TD control group.

The differences in digit ratios between groups suggests that abnormalities in cortical representations exist in populations who display alterations in inhibitory functioning and somatosensory processing, such as FHD and TS. Moreover, as hand tics are uncommon in TS, this suggests that these differences may occur regardless of motor pathology. This supports previous evidence that shows when GABAergic inhibition is disrupted after applying a $GABA_A$ antagonist to the sensorimotor system, cortical representations undergo changes in size and location alone (Foeller et al., 2005; Jacobs & Donoghue, 1991; Schneider et al., 2002), without repetitive movements as suggested by the positive feedback loop hypothesis in FHD (Blake et al., 2002; Evinger, 2005). As a result, disruption inhibitory functioning within the sensorimotor cortices may be sufficient to disrupt cortical mapping, without repetitive movements.

4.5.1 Limitations

There are some limitations in this study. Firstly, as noted in Chapter 3, the generalisability of the TS sample used in this study to the general TS population is limited due to the greater prevalence of females within the sample and the recruitment of individuals with low tic frequency and absence of large head and facial tics to preserve data quality. Consequently, this sample may instead reflect a limited population of those with TS, namely those with lower tic frequencies, and females who may evidence differences in brain structure, functional connectivity and aetiologies (see Section 3.3.4.4). Moreover, suppression of tics during the fMRI task could have impacted results in the TS group, as control of motor outputs in TS groups is associated with increased SMA activation, resulting in diminished cortical excitability (Draper et al., 2014; Ueda et al., 2021). Additionally, the extent to which the current TS sample experienced hand tics, and if so, the frequency/intensity of these hand tics, was not measured. Therefore, although generally uncommon in TS, this study cannot rule out any impact of hand tics on resultant digit maps. Finally, measures of inhibitory functioning (such as MRS-GABA or TMS-SICI) and somatosensory functioning were not analysed in relation to digit map properties, and therefore it cannot be concluded that abnormalities in inhibitory and somatosensory functioning are related to the differences evident in TS digit maps.

While traditionally D1 and D2 show greater representations in the sensorimotor cortices (Janko et al., 2022), the number of voxels assigned to D5 in comparison to other digits was much larger and more variable across both groups in this study. This is likely because a considerable amount of the literature measured cortical digit representations by applying vibrotactile stimuli to digits, rather than relying on motor tapping of the digits. While vibrotactile stimulation is a passive task where stimulation is applied to each digit separately, digit tapping tasks are unlikely to accurately separate individual digits, as the movement of one finger inherently causes movement of other fingers (van den Noort et al., 2016). Moreover, although motor tasks may be acceptable for digit mapping, the predictability of the task may not be appropriate. For example, in comparison to a random-order tapping task, 70% more

activation was observed in a sequential tapping task, which was more widespread. This activation included non-specific BOLD responses and reduced the ability to detect separate digits (Olman et al., 2012). As a result, some digits dominated digit maps, which were more evenly distributed in the random-order task. Similar findings were demonstrated in Mastria et al. (2023), where the percentage of ROI volume for each digit was larger in D4 and D5 in a sequential motor tapping task but in a passive vibrotactile task, percentage ROI volumes were larger in D1 and more evenly distributed in D2-D5. This may explain why D4 and D5 in this study dominated digit maps and showed a greater digit ratio in comparison to other digits in each group. Moreover, the D5 representation is generally more variable in comparison to other digits, as it has shown low agreeability over time within subjects (O'Neill et al., 2020). Therefore, to more accurately quantify the ratio of activation in each digit within M1 and S1 and give an insight into the cortical magnification of digits, tasks involving passive stimulation of the digits should be used.

Additionally, although phase-encoding travelling wave fMRI designs come with the benefit of faster acquisition, which reduces patient time in the scanner, and rely on 'winner-takes-all' analyses, these designs are insensitive to the overlapping of representations (Besle et al., 2013). As a result, any overlapping of digit ROIs could not be assessed in this study, and therefore it is still unknown if blurring between digits is evident in the TS group, as illustrated in animal evidence after application of GABA antagonists and in FHD animal models (Blake et al., 2002; Foeller et al., 2005; Jacobs & Donoghue, 1991; Schneider et al., 2002). Overlapping of digits is already underreported in fMRI digit mapping research in TD populations, and therefore event-related or block fMRI designs should be employed in order to determine the level of overlap between digits in both TD control and clinical populations (Janko et al., 2022). Moreover, in this chapter, each digit map analysis was initially performed in native space and then averaged across individuals. However, because individual digit maps vary widely between individuals (Schweizer et al., 2008), group-level analyses have likely masked individual variations in Euclidean distances and digit ratios. As a result,

when assessing fine-grained variable cortical representations, individual comparison to matched controls or to a standard digit map should be considered.

4.6 Conclusions

In conclusion, some differences were identified between TD control and TS group M1 and S1 digit representations. Specifically, M1 D3 and D4 and S1 D3 digit ratios were larger and D2 digit ratios in the S1 were smaller in the TS group in comparison to the TD control group. This suggests that there are differences in the proportion of M1 and S1 associated with different digits and the precise location of those digits between those with TS and TD controls. As a result, GABAergic inhibition and abnormalities in sensory processing may be sufficient to induce abnormalities in cortical representations of the digits. However, MRS-GABA, sensory processing and presence of hand tics were not directly assessed in this study, and therefore this cannot be concluded with certainty. Moreover, methodological limitations of using a movement paradigm and group-level analyses may explain the differences identified in digit ratio and topographical variations between groups.

5. Chapter 5 - Sensorimotor mapping of facial movements and vibrotactile stimulation to three facial locations in Tourette Syndrome

Key words: Tourette Syndrome (TS), functional magnetic resonance imaging (fMRI), sensorimotor representations, facial movements, vibrotactile stimulation

5.1 Introduction

As discussed in Chapter 4, disruption within GABAergic inhibitory mechanisms impact the stability of cortical functional representations (Foeller et al., 2005; Jacobs & Donoghue, 1991; Schneider et al., 2002). In FHD, a condition characterised by involuntary movements/spasms in the hand and associated with abnormalities in sensorimotor inhibition, there is evidence of abnormalities in cortical representations of the digits (Huber et al., 2023). However, in general digit representation abnormalities have only been associated with the hemisphere contralateral to the affected hand, despite abnormalities in inhibition being shown across both hemispheres (Ridding et al., 1995; Rona et al., 1998). Though, some research has evidenced bilateral abnormalities in digit representations in FHD, which have been linked with symptom severity and duration of the condition (Byrnes et al., 1998; Meunier et al., 2001). These aberrant representations, usually localised to one hemisphere, have been proposed to occur due to the abnormalities in cortical inhibition, paired with repetitive behaviours of the hand (Blake et al., 2002; Evinger, 2005).

In Chapter 3, some evidence of abnormalities in GABAergic inhibition in the sensorimotor cortices of the TS group were displayed using MRS-GABA measures. Moreover, despite hand tics being uncommon in TS, alterations in sensorimotor digit representations were evident in the results shown in Chapter 4. It is therefore proposed in this chapter that this environment of altered GABAergic inhibitory processing in TS is sufficient to encourage malleability of cortical representations of

regions commonly involved in facial tics, the most common tics in TS (Baizabal-Carvallo et al., 2023). While previous TMS mapping research has demonstrated that FDI hand muscle representations are smaller in individuals with TS compared to TD controls, maps of different facial muscles did not significantly differ between groups (Sigurdsson, Jackson, et al., 2020). However, the reliability of both hand and facial maps can be questioned, as the TMS intensity used was likely too high. Moreover, this intensity was based on the FDI muscle, but different M1 areas corresponding to different muscles will require different stimulation intensities to evoke the same MEP response (Menon et al., 2018). Moreover, as motor gain excitability is reduced in TS, these increased threshold intensities may produce smaller MEPs in individuals with TS compared to TD controls (Draper et al., 2015; Orth, 2009; Pépés et al., 2016). Additionally, these maps were measured at rest, however individuals with TS have been reported to show differential activation when performing volitional movements, such as reduced motor excitability prior to voluntary movements and enhanced interaction between M1-SMA (Draper et al., 2014; Franzkowiak et al., 2012). As a result, sensorimotor movement representations of common tics may show nuances in activation when a volitional movement is performed in comparison to TD controls.

Many individuals with TS also report feeling uncomfortable urges to tic, which are associated with abnormal sensations, such as tingling or itching. Specifically, individuals report that urges prior to tics are most commonly felt in the face and head, corresponding to tic locations (Essing et al., 2022; McGuire et al., 2016). Additionally, as Chapter 3 demonstrated, sensory processing of tactile stimuli differs between TD control groups and individuals with TS, where individuals with TS displayed some abnormalities in TOJ and amplitude discrimination thresholds. Therefore, sensorimotor activations in response to vibrotactile stimulation to facial regions may also reveal differences in sensory processing in areas of common tics and urges compared to TD controls.

5.2 Aims

This study used fMRI with the aim of investigating the sensorimotor cortical representations relating to facial regions widely involved in tics in individuals with TS and TD controls with. It was hypothesised that there would be differences in the sensorimotor representations of facial movements relating to common tics (blinking, grimacing and jaw clenching) and representations in response to vibrotactile stimulation across different facial areas in comparison to TD controls. In this chapter, Study 1 investigates the sensorimotor representations of facial movements using 3T fMRI, while Study 2 investigates activations in response to vibrotactile stimulation to three facial locations using 7T fMRI.

5.3 Study 1

This study investigates the sensorimotor representations of facial movements using 3T fMRI.

5.3.1 Methods

5.3.1.1 Participants

Twenty participants per group was set as the recruitment target due to funding availability of the 3T MRI scanner. As a result, 20 TD control and 20 participants with TS or chronic tic disorder took part in the study. Four TS participants were excluded from subsequent analysis due to excessive head motion during the fMRI. Demographic information for the remainder of participants in each group are displayed in Table 5.1. Age (U = 127, p = 0.292) and sex (X^2 (1, N = 36) = 0.00, p = 1.00) distributions were not significantly different between groups.

Table 5.1

Demographic information of TD and TS participants in Study 1

Group	N	Age	Sex
TD	20	31.20 (±9.8)	10 male, 10 female
TS	16	35.06 (±12.2)	8 male, 8 female

Note. N = number of participants, TD = group of typically developing control participants, TS = group of participants with Tourette Syndrome, mean (±standard deviation)

Participants gave informed consent, and ethics were approved by the local ethics committee (School of Psychology, University of Nottingham: S1454). No participants in the TD group were taking CNS-active drugs and were free from any mood or neurological illness during the experimental timeline. Clinical questionnaires, as described in Section 3.2.1.2, were also administered to individuals

with TS, with all medications, YGTSS and PUTS-R scores for the TS group displayed in Appendix C.1. All participants were free from any contraindications for MRI, as assessed by completion of an MRI safety screening form. All participants were right-handed, as assessed by the Edinburgh handedness questionnaire (Oldfield, 1971).

5.3.1.2 fMRI Paradigm

Three 4.5 minute fMRI task blocks were acquired with participants visually instructed to perform a facial movement at 1Hz for 8 seconds, with 24 seconds of rest (repeated for 8 cycles). Each movement task block was visually presented using PsychoPy (Open Science Tools, Ltd.; Pierce et al., 2019) on a MR-compatible screen (BOLDscreen 32, Cambridge Research Systems, UK), which was visible to the participant by a mirror mounted to the head coil. Each fMRI task block consisted of a different facial movement in the same order across participants; blinking, grimacing, then jaw clenching. These facial movements are very common tics experienced by those with TS (Baizabal-Carvallo et al., 2023). Participants were trained on each facial movement prior to scanning to ensure conformity across movements.

Video recordings were acquired during scans using a MR compatible camera with integrated LED light, mounted to the head coil (12M-I, MRC systems GmbH). This was used to assess compliance with the cued facial movements and to obtain accurate onset and duration timings of cued movements to enter as a regressor in subsequent GLM analyses. Video recordings were not available for all blocks from one TS participant and six TD controls due to technical issues with the MR-compatible camera or consent. For those not available, the fixed block timings were used.

5.3.1.3 MRI data acquisition

MRI data were acquired on a Philips 3T Ingenia MRI scanner (Philips Healthcare, Best, The Netherlands) using a 32-channel head coil situated in the Sir Peter Mansfield Imaging Centre at the University of Nottingham, Nottingham, UK.

5.3.1.3.1 fMRI parameters

Three BOLD fMRI data sets were acquired using a single-shot 2D T_2*-weighted GE-EPI sequence (voxel 2.5 mm, matrix size = 84 x 83 x 48, multiband 4, TR/TE = 1000/30 ms, 4.32 acquisition time per block). Two additional SE-EPI short scans (5 dynamics) with the same parameters, but with opposing fat shift directions, were collected for distortion correction (see Section 5.3.1.4.1).

5.3.1.3.2 T_1-weighted anatomical parameters

Following acquisition of the fMRI blocks, a T_1-weighted 3D MPRAGE scan was acquired (matrix size = 256 x 256, FOV = 176 x 256 x 256 mm, 1 mm isotropic, 176 slices, TR/TE = 8.1/3.7 ms, flip angle = 8 °, acquisition time 3.35 minutes). This was co-registered with the fMRI data runs and to MNI standard space to allow for comparison across participants.

5.3.1.4 BOLD-fMRI analysis

5.3.1.4.1 Pre-processing

fMRI data were distortion corrected using FSL-TOPUP and thermal noise was removed using NORDIC PCAS denoising (Andersson et al., 2003; Vizioli et al., 2021). Data was then assessed for motion artefacts and any fMRI blocks with absolute mean motion displacement above 2.5mm were removed. In the TS group especially, many blocks were contaminated by brief periods of large motion displacement (>2.5 mm). To preserve as much data as possible, fMRI images that were contaminated by brief periods of large motion displacement (>2.5 mm) for up to three cycles had these cycles removed using FSL functions (Jenkinson et al., 2012) from subsequent analyses. This resulted in the removal of data from three TS in the ‘blink’ blocks, one TD and eight TS from the ‘grimace’ blocks and two TD and six TS from the ‘jaw’ blocks.

The tSNR of the resulting de-noised block fMRI timeseries were assessed in MATLAB (MATLAB_R2019a, Mathworks, Natick, MA) using an in-house quality assurance code fMRI_report_app (https://github.com/nottingham-neuroimaging/qa/tree/master/fMRI_report_app). If present, fMRI blocks with tSNR values <30 would be removed from analyses, however no fMRI blocks had tSNR below this threshold. Final number of participants and mean tSNR and standard deviations for each movement block are presented in Table 5.2.

Table 5.2

Number of participants and tSNR in each block in Study 1

	Blink		Grimace		Jaw clench	
Group	**N**	**tSNR**	**N**	**tSNR**	**N**	**tSNR**
TD	20	134 (±11)	19	115 (±8)	18	113 (±13)
TS	13	98 (±14)	8	99 (±20)	10	96 (±17)

Note. N = number of participants, tSNR = temporal signal-to-noise ratio, TD = group of typically developing control participants, TS = group of participants with Tourette Syndrome, mean (±standard deviation)

Motion correction was conducted using FMRIB's linear image registration tool, MCFLIRT, using the middle volume as a reference volume (Jenkinson et al., 2002). Resulting de-noised data were pre-processed using FSL-FEAT (FMRI Expert Analysis Tool; Jenkinson et al., 2012). High-pass temporal filtering of 32 s was applied, and spatial smoothing was conducted using SUSAN (FMRIB; Smith & Brady, 1997) using a Gaussian kernel of 3.75mm FWHM to account for anatomical differences between participants.

Registration of fMRI images to MNI standard space was also applied using FLIRT (FMRIB; Jenkinson et al., 2002; Jenkinson & Smith, 2001), by taking an example volume from the low-resolution fMRI image and registering this to an example volume of the participant's T1-weighted anatomical high-resolution image. This high-

resolution image is also registered to the MNI standard space. Transformations for both steps are combined and applied so that the low-resolution fMRI images are registered to standard space for group analysis.

5.3.1.4.2 Standard imaging analysis

First and third-level analyses were conducted using FSL-FEAT. Standard and extended motion parameters were applied and an additional confound explanatory variables (EV) was applied to scrub volumes where motion exceeded FD values of over 0.9 mm to avoid motion confounding analysis. Pre-whitening was also applied to remove temporal autocorrelation from the data.

For each fMRI scan, regressors were entered into the GLM design matrix which included onset time and duration of the performed facial movement (blink, grimace or jaw clench) marked from the video recordings (or block timings in absence of video recordings). Regressors were convolved using a double-gamma HRF. Convolution applies blurring and delays to the input waveform (i.e. stimulus timings) and output waveform (i.e. the fMRI haemodynamic response). Double-gamma HRF applies a positive gamma function at a normal lag and a delayed, brief, negative gamma to the input waveform in order to model the late undershoot of the HRF. Contrasts were also set up to identify the movement block for later analyses ('Blink', 'Grimace', or 'Jaw clench').

Finally, third-level analyses were conducted using a mixed-effects analysis (FLAME 1+2) to average responses in TS and TD groups for each facial movement block (blink, grimace, or jaw clench). Results were masked to cover bilateral supplementary motor areas (SMA), and bilateral pre- and post-central gyri as defined by the Harvard-Oxford Cortical Structural atlas, before applying cluster correction determined by a Z-threshold of 2.3 ($p = 0.05$; (Worsley, 2001). The SMA was included in this ROI mask due to its involvement in action initiation and control of action and its reported dysfunction in TS (Jung et al., 2013; Nachev et al., 2008).

5.3.1.4.3 Conjunction analysis

A conjunction analysis was performed for each group. This identified overlapping voxels that passed a voxel-wise p-corrected statistical *t* threshold in all facial movement block contrasts (blink, grimace and jaw clench). This was conducted using AFNI (Cox, 1996; Cox & Hyde, 1997) on thresholded contrast images from first-level FSL-FEAT analyses, creating a conjunction map. With these, *t* thresholds for each group-level facial movement block map were used to identify common voxels within each map that passed the specified threshold of $p = 0.05$. Unique voxels were identified by subtracting the resulting conjunction maps from each group-level facial movement block map. Conjunction maps of common/unique voxels to each facial movement were compared between groups.

5.3.2 Results

5.3.2.1 Cluster-level inferences

Significant cluster activations were identified across the bilateral sensorimotor cortices for blink, grimace, and jaw clench blocks in both the TD and TS groups (Figure 5.1; $Z = 2.3$, $p < 0.05$). However, these clusters did not significantly differ between groups suggesting similar activations within the bilateral sensorimotor cortices and SMA across groups. The number of voxels and COG for each cluster activation are displayed in Appendix C.2.

Figure 5.1

Cluster activations in TD (blue) and TS (red) control groups for (a) Blink, (b) Grimace, and (c) Jaw clench blocks

a.

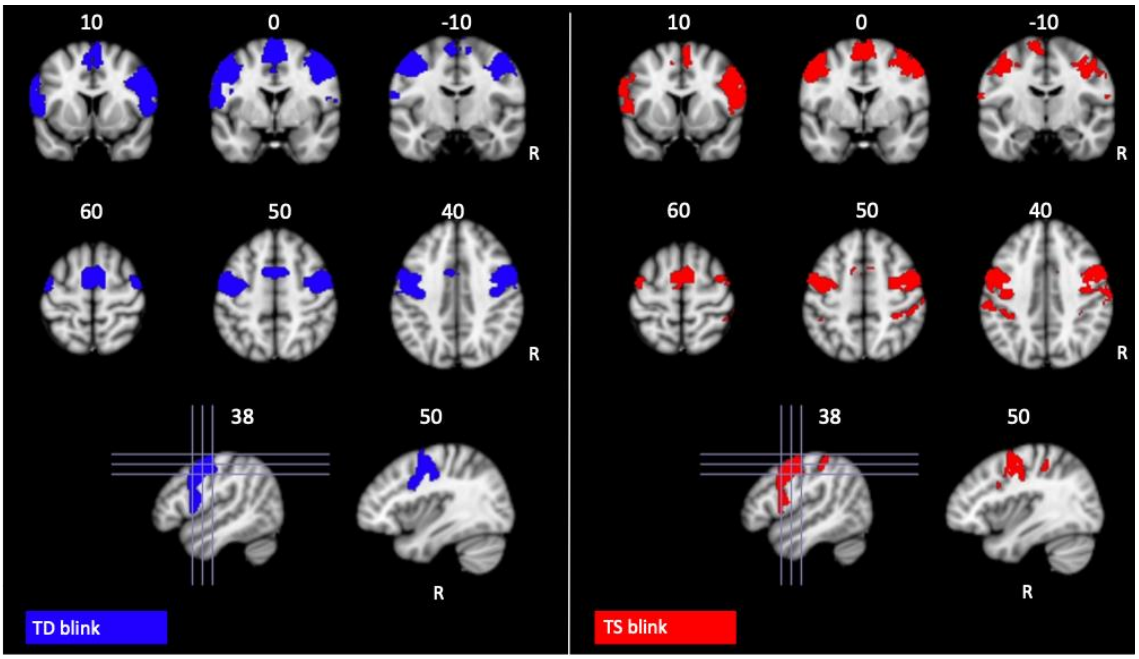

b.

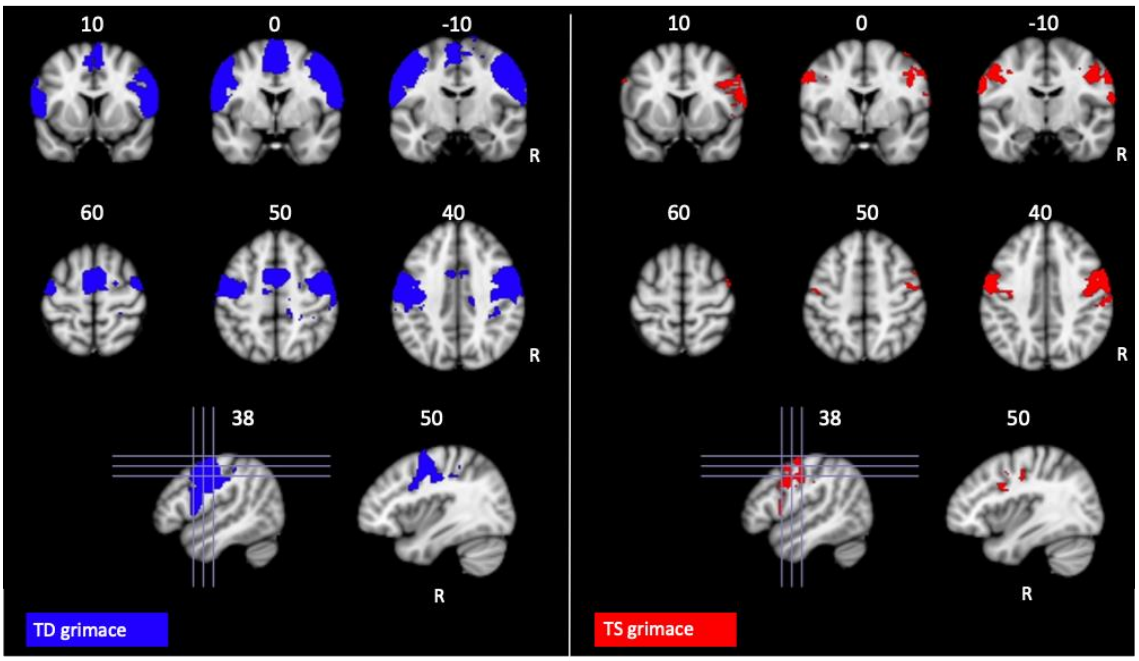

c.

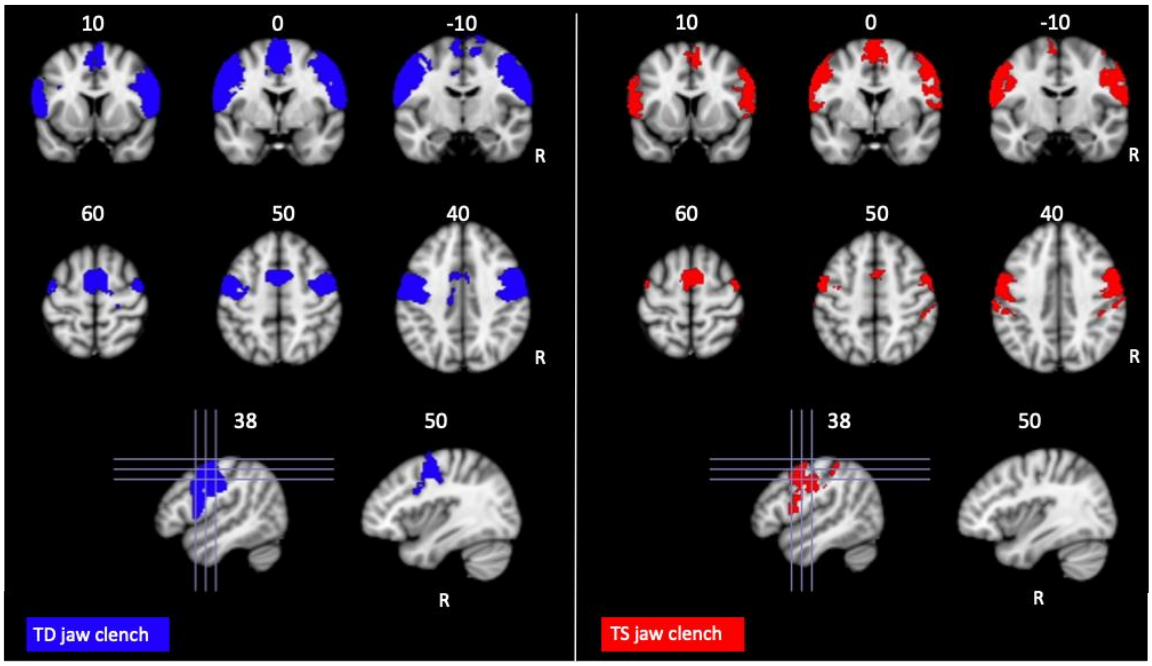

Note. Numbers depict slice number, R = right hemisphere, TD = group of typically developing control participants, TS = group of participants with Tourette Syndrome

5.3.2.2 Conjunction analysis

A conjunction analysis identified unique (Figure 5.2) and common (Figure 5.3) voxels across all facial movements in both groups. Unique voxels for each movement showed overlap with the face region of the M1 in both TD and TS groups (Figure 5.2). Common voxels across all movements in both groups also showed overlap within the sensorimotor face region and SMA, however, more common voxels were identified across movements in the TD group. Moreover, common voxels were only identified in the SMA in the TD group (Figure 5.3).

Figure 5.2

Unique voxels identified in a conjunction analysis for TD (blue) and TS (red) groups in (a) blink, (b) grimace, and (c) jaw clench movement blocks

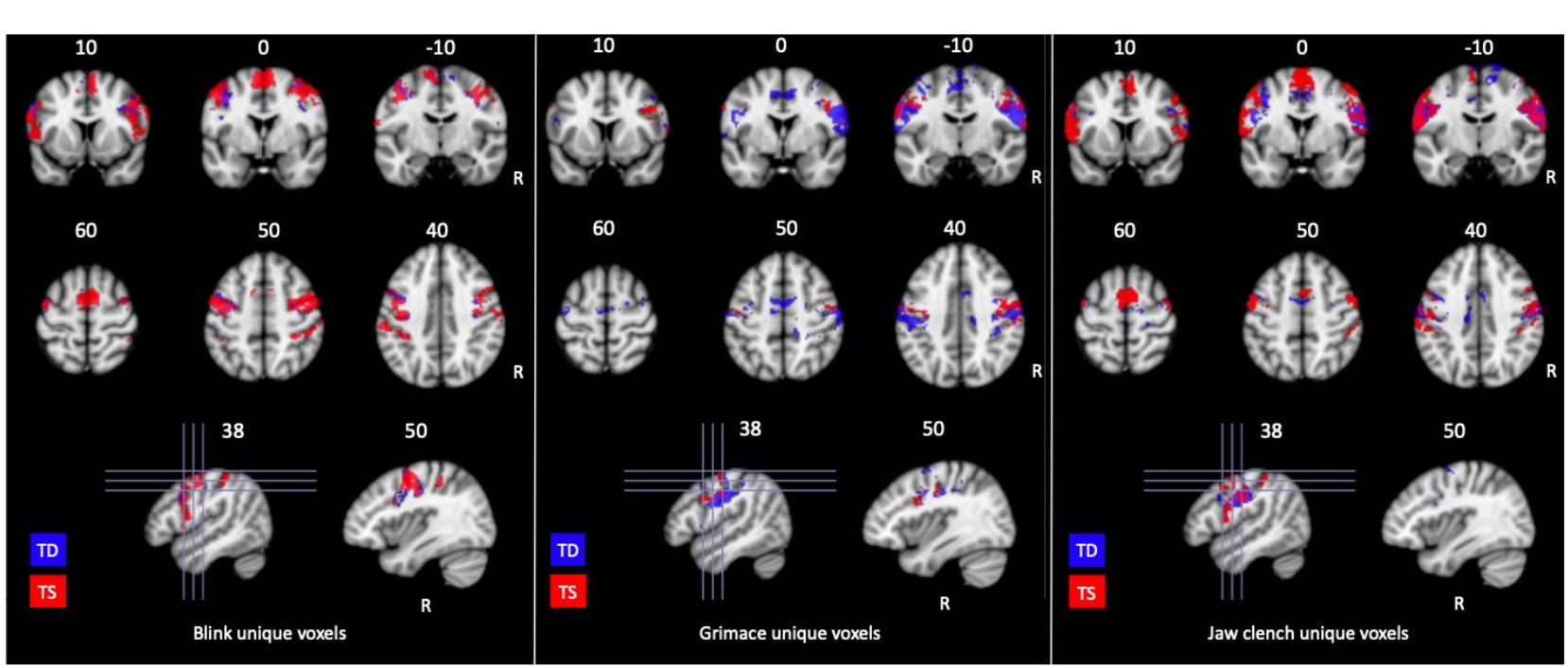

Note. Numbers depict slice number, R = right hemisphere, TD = group of typically developing control participants, TS = group of participants with Tourette Syndrome

Figure 5.3

Common voxels identified in a conjunction analysis for TD (blue) and TS (red) groups across movement blocks (blink, grimace and jaw clench)

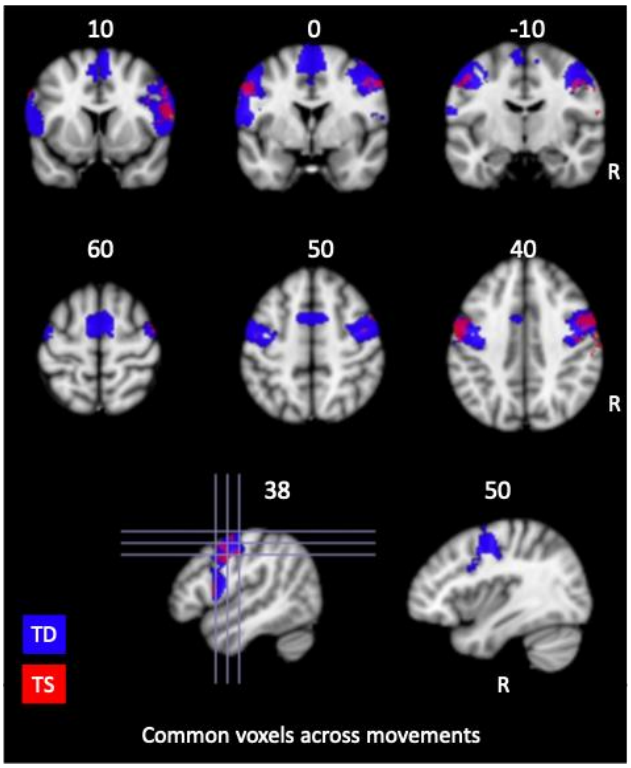

Note. Numbers depict slice number, R = right hemisphere, TD = group of typically developing control participants, TS = group of participants with Tourette Syndrome

5.3.3 Discussion

In Study 1, bilateral cortical maps were extracted for different facial movements relating to common tics (blinking, grimacing and jaw clenching), which activated across a sensorimotor mask encompassing bilateral S1, M1 and SMA. However, no significant differences were identified in cluster activations for any movement between TD and TS groups. This suggests that cued movements mimicking facial tics show comparable activations within the sensorimotor cortices and SMA across groups. This is against predictions that individuals with TS would show aberrant representations due to abnormalities in GABA modulation. However, as MRS-GABA

or TMS-SICI measures of GABAergic inhibition were not taken, the specific role of GABAergic inhibition in sensorimotor maps across groups is not clear.

A conjunction analysis was also employed to assess common and unique activations across all facial movements in each group. Across unique voxels activated for each movement, similarities in patterns are evident across the sensorimotor cortices for each group. However, for common voxels activated across all tasks, there was a greater spread of activation in the TD group compared to the TS group across sensorimotor cortices. This suggests that TD individuals recruit similar regions of the sensorimotor cortex across all cued facial movements, whereas this is more aberrant in TS, evidenced by reduced areas of common voxels activated across movements. Furthermore, while the SMA was consistently activated across tasks in the TD control group, this was not the case in the TS group. This aligns with previous evidence of disordered activity within the SMA during tasks involving cognitive control of movement (Jung et al., 2013). The SMA is a premotor area involved in action initiation and volitional control of action and has been linked to tic suppression in TS (Nachev et al., 2008; Ueda et al., 2021). As the motor tasks in Study 1 required control of movement, with the possibility for tic suppression to better control motor output, the SMA is likely to be recruited in each task. However, differences in activations across tasks could be a result of disordered activity within the SMA.

Upon assessment of cluster activations across each task in the TS group, while SMA activation is present in blink and jaw clench blocks, this is absent in the grimace block. Grimacing is a more complex movement which involves more facial muscles, and therefore requires greater movement coordination. Previous evidence has illustrated that reduced motor cortical excitability are evident during tasks requiring greater cognitive control in TS participants, with reduced motor cortical excitability thought to be a result of increases in SMA MRS-GABA (Heise et al., 2010; Jackson et al., 2015; Jackson et al., 2011, 2013; Jung et al., 2013; Larsh et al., 2023). In TS, SMA MRS-GABA has also previously shown an inverse correlation with SMA fMRI BOLD responses (Draper et al., 2014), suggesting that the absence of activation in the SMA

during the grimacing task may be a result of greater inhibition within the SMA as a control mechanism. Consequently, the absence of activation in the SMA during the grimace task in the TS group may be a result of grimacing requiring more precise control of motor output and the suppression of tics during movements, increasing the difficulty and cognitive control.

Additionally, review of video data during motor blocks highlighted that some facial tics were present during motor blocks, which may also have induced aberrant activation in the SMA. Previous evidence has examined cross-correlation activations between tics in individuals with tic disorders and specific volitional 'tic-like' movements in age- and sex-matched TD controls (Hampson et al., 2009). Similar patterns of cross-correlation were identified in activations from the motor cortex to the rest of the brain, however broader cross-correlations were identified between the motor cortex to the SMA in the group with tic disorders only. This evidence indicated the presence of greater SMA activation prior to and after tic execution compared to volitional movement (Hampson et al., 2009). As a result, the presence of tics is another possible cause of the aberrant activation in the SMA across tasks in the TS group, which is consistently activated across tasks in the TD group. However, as the number of tics and level of suppression during tasks was not quantified, this cannot be concluded.

5.4 Study 2

This study investigated activations in response to vibrotactile stimulation to three facial locations using 7T fMRI.

5.4.1 Methods

5.4.1.1 Participants

Participants were recruited as part of a wider study involving MRS (Chapter 3) and digit mapping (Chapter 4), with a recruitment target of 20 participants per group due to funding limitations of the 7T MRI scanning hours. Seventeen TD adults and ten adults with TS or chronic tic disorder took part in this study. Data from four TS participants were removed due to excessive motion across all blocks in three participants and incorrect voxel placement during fMRI blocks in one participant. The resulting demographic information is displayed in Table 5.3. Age ($t(21) = 0.323$, $p = 0.750$) and sex (X^2 (1, $N = 23$) = 0.727, $p = 0.394$) distributions were not significantly different between groups.

Table 5.3

Demographic information of TD and TS participants in Study 2

Group	N	Age	Sex
TD	17	28.06 (±6.6)	6 male, 11 female
TS	6	27.00 (±7.8)	1 male, 5 female

Note. N = number of participants, TD = group of typically developing control participants, TS = group of participants with Tourette Syndrome, mean (±standard deviation)

Participants gave informed consent, and ethics were approved by the local ethics committee (School of Psychology, University of Nottingham: S1500). No participants in the TD group were taking CNS-active drugs and were free from any

mood or neurological illness during the experimental timeline. All medications and Yale/PUTS-R scores for the TS group are displayed in Appendix C.3. All participants were free from any contraindications for MRI, as assessed by completion of an MRI safety screening form. All participants were right-handed as assessed by the Edinburgh handedness questionnaire (Oldfield, 1971).

5.4.1.2 fMRI paradigm

5.4.1.2.1 Applying somatosensory stimulation using piezo-electric tactors

To study somatosensory stimulation of the face piezo-electric tactors (PiezoTac Mini Tactors, Engineering Acoustics, Inc., EAI, FL, USA) were used. These tactors are made of biocompatible acrylonitrile butadiene styrene plastic and wires were insulated tinsel, however prior to use, the safety of these within the 7T was assessed by collecting heating tests on an agar phantom with fibre optic temperature gauges with < 0.05 °C precision (Luxtron Fluoroptic Thermometry Lab Kit, LumaSense Technologies Inc., CA, USA). This was assessed as there is a risk of interaction between MRI radiofrequency pulses and conductive devices, which can induce electrical currents and heating, with the potential to cause burns and injury (Tang & Yamamoto, 2023). Three fibre optic temperature gauges were placed on the phantom under the piezo-electric tactor plastic, under the wiring and at a control site. Temperatures were monitored during a 9 minute baseline period, during a 2.5 minute fMRI run, a 4.5 minute fMRI run and a 8.5 minute MRS protocol. Low thermal fluctuations were found during the scan sequences (< 0.5 °C), with no difference in temperature change for the test site in comparison to the control site. See Appendix C.4 for average temperature readings and changes in temperature across scans, and Appendix C.5 for temperature across time during scans.

For Study 2, the piezo-electric tactors were attached using medical grade tape to three locations of the left side of the face at the orbicularis oculi (O. oculi), masseter and orbicularis oris (O. oris) before scanning. Figure 5.4 shows the location of each piezo-electric tactor on the face. For each somatosensory block, piezo-electric tactor vibrations were delivered at 35Hz at a constant above-threshold intensity across

participants. This intensity was the highest intensity for a frequency of 35Hz as recommended by the manufacturer. To confirm participants could feel vibrations at this set frequency and intensity, in the scanner vibrations were triggered in each piezo-electric stimulators using an in-house MATLAB script (MATLAB_R2019a, Mathworks, MA, USA) and participants were asked if they could feel vibrations in all three tactors. Furthermore, 35Hz was chosen as the optimal stimulation frequency to trigger Meissner Corpuscles which are responsible for somatosensory discrimination and acuity and are responsible for the detection of stimuli of frequencies between 30-50 Hz (Piccinin et al., 2018; Purves & Williams, 2001). Moreover, previous research in has shown greater fMRI activation in S1 in response to 35Hz stimulation, our target cortical area, in comparison to high frequency stimulation (150 Hz), which activates Pacinian corpuscles and evoke greater fMRI activation in the secondary sensory cortices (Harrington & Hunter Downs, 2001).

Figure 5.4

Image of (a) PiezoTac Mini Tactor (EAI, FL, USA) *and (b) the location of each piezo tactor on the face*

a.

b.

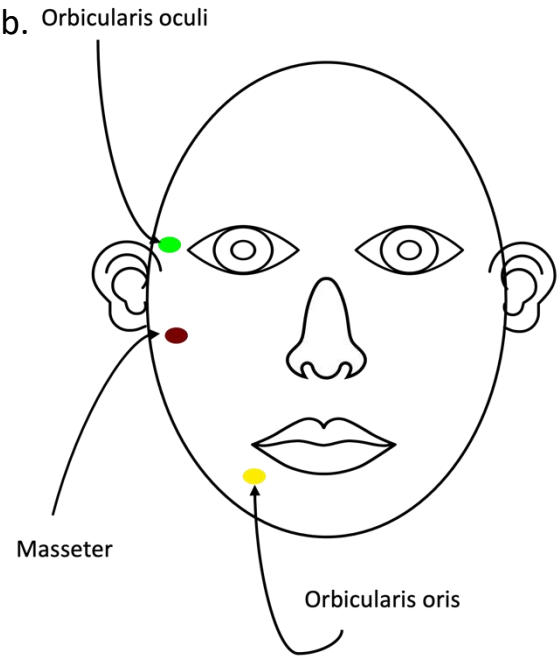

Once confirmed that the participant could feel the stimulation, three fMRI somatosensory blocks were acquired (4.5 minutes each), with participants instructed before scans to relax and concentrate on the piezo-tactor vibration. 500 ms vibrations in each block were performed at one location of the face; O. oculi, masseter or O. oris (see Figure 5.4) at a frequency of 1Hz for 8 seconds, with 24 seconds of rest period, and this was repeated for 8 cycles. Each somatosensory block was triggered using an in-house MATLAB script, controlling the Tactor Interface (EAI, FL, USA).

5.4.1.3 MRI parameters

MRI data were collected on a Philips 7T Achieva MRI scanner (Philips Healthcare, Best, The Netherlands) using a 32-channel head coil situated in the Sir Peter Mansfield Imaging Centre at the University of Nottingham, Nottingham, UK. The scanning that took place in this chapter was part of a wider scanning session, which used fMRI to investigate MRS-GABA and -Glu concentrations (Chapter 3 Study 2) and sensorimotor digit mapping (Chapter 4).

5.4.1.3.1 fMRI parameters

BOLD fMRI data were acquired using a single-shot 2D T_2*-weighted GE-EPI sequence (voxel 1.5 mm, matrix size = 108 x 118 x 40, multiband 2, TR/TE = 2000/22 ms, 4.32 minute acquisition time per block). Two additional short SE-EPI MRI scans (5 dynamics) with the same acquisition parameters, but with opposing fat shift directions, were collected for EPI distortion correction (see Section 5.4.1.4.1).

5.4.1.3.2 T1-weighted anatomical parameters

Prior to fMRI blocks, an anatomical T_1-weighted 3D gradient echo PSIR scan was acquired (matrix size = 320 x 320, FOV = 224 x 224 x 156.8 mm, 0.7mm isotropic, 224 slices, TR/TE = 6.3/2.8 ms, flip angle = 5^o, acquisition time 6.25 minutes). The two PSIR readouts were then converted into T_1-weighted images using an in-house Python

(v.3.9.12) script (https://github.com/oliviermougin/PSIR). This was collected for co-registering with the fMRI runs and with standard template space images to allow for comparison across participants.

5.4.1.4 BOLD-fMRI analysis

5.4.1.4.1 Pre-processing

fMRI data were distortion corrected using FSL-TOPUP and thermal noise was removed using NORDIC PCAS denoising (Andersson et al., 2003; Vizioli et al., 2021). Data was then assessed for any motion artefacts and any fMRI blocks with absolute mean motion displacement above 1.5 mm were removed. In the TS group, many blocks were contaminated by brief periods of large motion displacement (>1.5 mm). In order to preserve as much data as possible, any blocks that included up to two cycles of >1.5 mm absolute motion displacement had contaminated cycles removed from subsequent analyses. If motion displacement was still >1.5 mm after removal of cycles, these blocks were removed from subsequent analysis. This resulted in the removal of two TS 'O. oculi' blocks, one TD and one TS 'masseter' blocks and two TD and one TS 'O. oris' blocks.

The tSNR of the resulting de-noised block fMRI timeseries were assessed were assessed in MATLAB (MATLAB_R2019a, Mathworks, Natick, MA) using an in-house quality assurance code fMRI_report_app (https://github.com/nottingham-neuroimaging/qa/tree/master/fMRI_report_app). If present, fMRI blocks with tSNR values <30 were removed from analyses. No fMRI blocks were removed due to tSNR concerns. fMRI blocks with absolute mean motion displacement above 2.5mm were also removed. Final number of participants and mean tSNR and standard deviations for each movement block are presented in Table 5.4.

Table 5.4

Number of participants and tSNR in each block in Study 1

	Orbicularis oculi		Masseter		Orbicularis oris	
Group	**N**	**tSNR**	**N**	**tSNR**	**N**	**tSNR**
TD	17	97 (±19)	16	82 (±14)	15	83 (±14)
TS	4	97 (±23)	5	103 (±38)	5	106 (±38)

Note. N = number of participants, tSNR = temporal signal-to-noise ratio, TD = group of typically developing control participants, TS = group of participants with Tourette Syndrome, mean (±standard deviation)

Motion correction was conducted using FMRIB's linear image registration tool, MCFLIRT, using the middle volume as a reference volume (Jenkinson, 2002). Resulting de-noised data were pre-processed using FSL-FEAT (FMRI Expert Analysis Tool; Jenkinson et al., 2012). High-pass temporal filtering of 32 s was applied and spatial smoothing using SUSAN (FMRIB; Smith & Brady, 1997) using a Gaussian kernel of 3.75mm FWHM to account for anatomical differences between participants.

Registration of fMRI images to MNI standard space was also applied using FLIRT (FMRIB; Jenkinson & Smith, 2001; Jenkinson et al., 2002). This was conducted by taking an example volume from the low-resolution fMRI image and registering this to an example volume of the participant's T1-weighted anatomical high-resolution image. This high-resolution image is also registered to the MNI standard space. Transformations for both steps are combined and applied so that the low-resolution fMRI images are registered to standard space for group analysis.

5.4.1.4.2 Standard imaging analysis

First and third-level analyses were conducted using FSL-FEAT (Woolrich et al., 2001, 2004). Standard and extended motion parameters were applied and an additional confound EV was applied to scrub volumes where motion exceeded FD

values of over 0.9mm to avoid motion confounding analyses. Pre-whitening was also applied to remove temporal autocorrelation from the data.

For each fMRI scan in first-level analyses, regressors were entered into the GLM design matrix which included onset time and duration of the vibrations at different facial locations (O. oculi, masseter or O. oris). Regressors were convolved using a double-gamma HRF. Convolution applies blurring and delays to the input waveform (i.e. somatosensory stimulus timings) and output waveform (i.e. the fMRI haemodynamic response). Double-gamma HRF applies a positive gamma function at a normal lag and a delayed, brief, negative gamma to the input waveform in order to model the late undershoot of the HRF. Contrasts were also set up to identify the somatosensory block for later analyses ('O. oculi', 'masseter', or 'O. oris').

Finally, third-level analyses were conducted using a mixed-effects analysis (FLAME 1+2) to average responses in TS and TD groups for each somatosensory block (O. oculi, masseter, or O. oris). Results were masked to cover the right SMA and bilateral pre- and post-central gyri as defined by the Harvard-Oxford Cortical Structural atlas, before applying cluster correction determined by a Z-threshold of 2.3 (p = 0.05; Worsley, 2001).

5.4.1.4.3 Conjunction analysis

A conjunction analysis was performed for each group to identify overlapping voxels that pass a voxel-wise p-corrected statistical *t* threshold for all somatosensory block contrasts (O. oculi, masseter, and O. oris). This was conducted using AFNI (Cox, 1996; Cox & Hyde, 1997) in thresholded contrast images from first-level FSL-FEAT analyses. From these, *t* thresholds for each group-level somatosensory block map were used to identify common voxels within each map that passed the specified threshold of p = 0.05, creating a conjunction map. Unique voxels were identified by subtracting the resulting conjunction maps from each group-level somatosensory block map. Conjunction maps of common/unique voxels to each somatosensory block were compared between groups.

5.4.1.4.4 Voxel counts, 3D coordinates of maximum Z statistics and Euclidean distances

The number of voxels and 3D coordinates of the maximum Z statistic centre of gravity (zCOG) were also extracted for each contrast (O. oculi, masseter and O. oris) for each participant. This involved masking first-level thresholded images (Z = 2.3, p < .05) over the right post-central gyrus and extracting voxel counts and 3D zCOG coordinates using FSL functions Featquery and FSLUTILS (Jenkinson et al., 2012). 3D zCOG coordinates are in three directions; x (left (-) to right (+), L-R), y (posterior (-) to anterior (+), P-A) and z (inferior (-) to superior (+), I-S).

3D zCOG coordinates were also used to calculate Euclidean distances (d) between each contrast as outlined in the formula 5.1.

$$d = \sqrt{(x2 - x1)^2 + (y2 - y1)^2 + (z2 - z1)^2} \quad (5.1)$$

Where $x2$, $y2$, $z2$ are coordinates from one contrast's 3D zCOG coordinates and $x1$, $y1$, $z1$ are coordinates from the second contrast's 3D zCOG coordinates.

5.4.1.4.4.1 Statistical analysis

For the O. oculi block, there were 17 TD and four TS datasets, for the masseter block, there were 16 TD and four TS datasets and for the O. oris block, there were 14 TD and four TS datasets. Independent two-tailed *t*-tests were then conducted to detect any significant differences between TD and TS group average voxel counts, zCOG coordinates and Euclidean distances for between 3D zCOG coordinates for contrast. Where data were not normally distributed, Mann-Whitney *U* tests replaced independent *t*-tests. BF_{10} was also used with a Cauchy distribution with a scale of γ = 0.707 used as the prior distribution (Rouder et al., 2009). Interpretation of BF_{10} values are shown in Table 3.2. These statistical analyses were conducted using jamovi (v 2.3.28; jamovi.org).

5.4.2 Results

5.4.2.1 Cluster-level inferences

Significant cluster activations were identified in the right sensorimotor cortex ROI for O. oculi, masseter, and O. oris blocks in the TD control group only (Figure 5.5; $Z = 2.3$, $p < .05$). This is likely due to the very small sample size within the TS group, and therefore insufficient power to detect a group effect. As a result, no comparison between TD and TS group-level cluster contrasts was conducted.

In the TD group for the O. oculi block, a significant cluster was only present within the SMA. For the masseter and O. oris blocks, significant clusters were identified within the face region of the right M1 and in the SMA. The number of voxels and 3D COG coordinates within each cluster activation for each sensory block are displayed in Appendix C.6.

Figure 5.5

Cluster activations in TD group for (a) O. oculi, (b) masseter, and (c) O. oris blocks

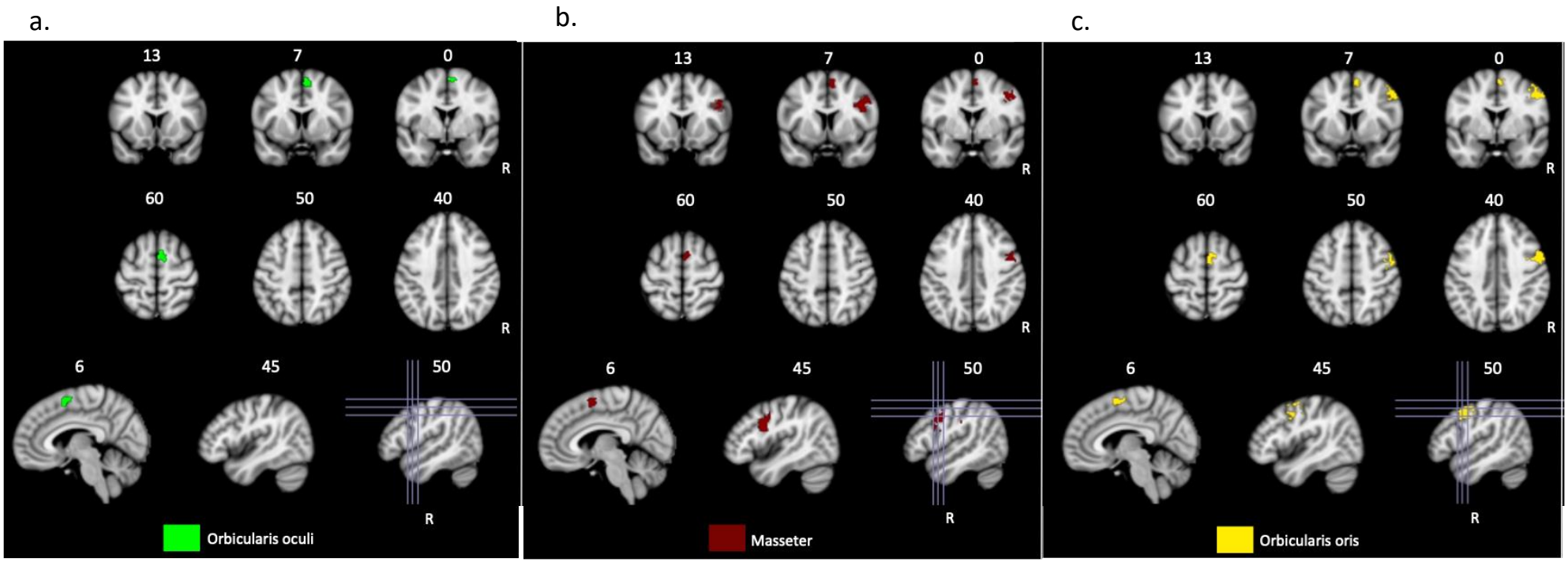

Note. Numbers depict slice number, R = right hemisphere, TD = group of typically developing control participant

5.4.2.2 Conjunction analysis

For the TD control group, a conjunction analysis identified unique (Figure 5.6) and common (Figure 5.7) voxels activated across O. oculi, masseter and O. oris contrasts. Unique voxels for the O. oculi were located in the SMA, and unique voxels for the masseter and O. oris were located in the face region of the M1 and the SMA (Figure 5.6). Common voxels across all movements showed overlap with the SMA only (Figure 5.7).

Figure 5.6

Unique voxels identified in the TD group in O. oculi, masseter, and O. oris blocks in a conjunction analysis

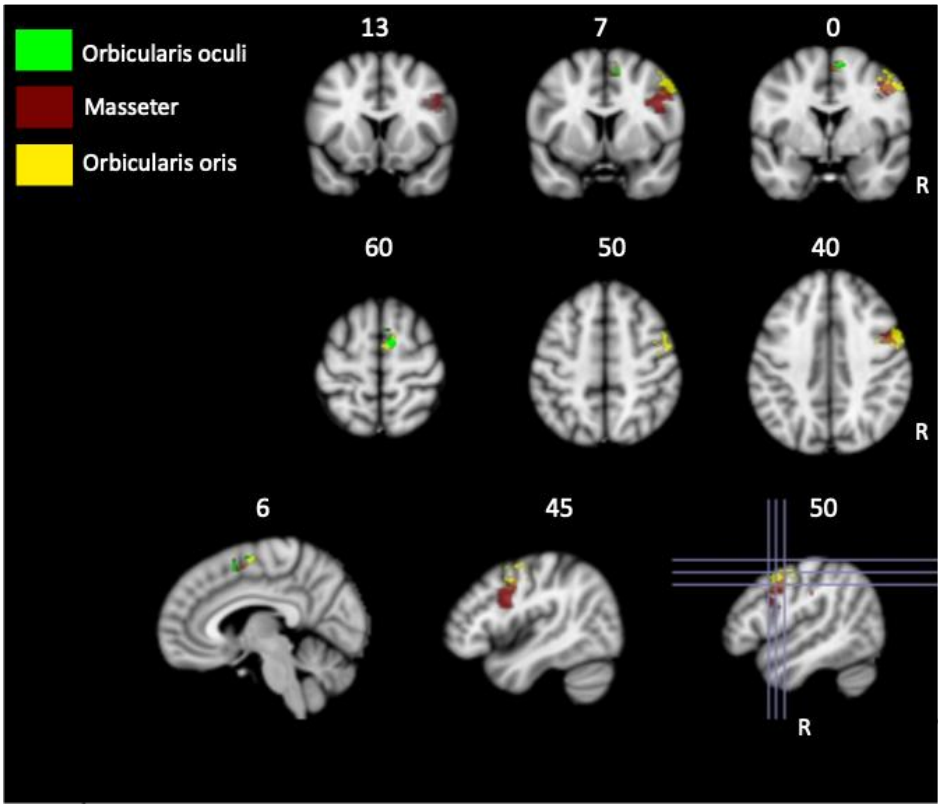

Note. Numbers depict slice number, R = right hemisphere, TD = group of typically developing control participants

.

Figure 5.7

Common voxels identified in the TD group across sensory blocks (O. oculi, masseter and O. oris) in a conjunction analysis

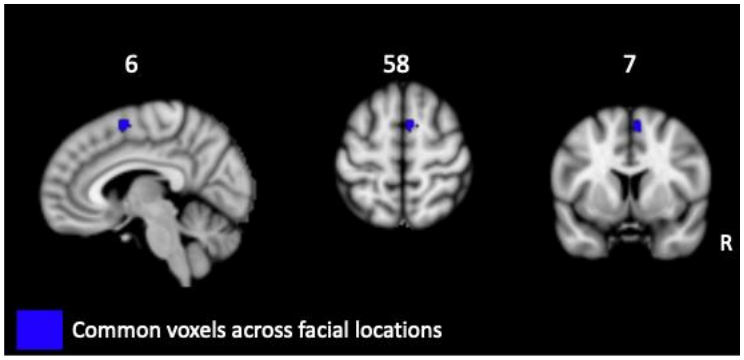

Note. Numbers depict slice number, R = right hemisphere, TD = group of typically developing control participants

5.4.2.3 Voxel counts

Independent *t*-tests were conducted on the number of voxels within thresholded cluster activations (Z = 2.3, $p < .05$) for each participant for each contrast. No significant differences were found in the average number of O. oculi voxels between TD control (M = 1068.53, SD = 1032.3) and TS group (M = 1445.75, SD = 784.9); U = 20, p = 0.237, with Bayesian inference providing anecdotal evidence for the null hypothesis (BF_{10} = 0.529). There were also no significant differences found in the average number of masseter voxels between TD control (M = 916.19, SD = 526.8) and TS group (M = 439.50, SD = 284.9); t(18); = 1.72, p = 0.102. For the average number of O. oris voxels, no significant differences were found between the TD control (M = 1014.87, SD = 559.9) and TS group (M = 494.00, SD = 190.0); t(17); = 1.80, p = 0.090. However, Bayesian statistics provide anecdotal evidence for the alternative hypothesis between the number of voxels for masseter (BF_{10} = 1.135) and O. oris (BF_{10} = 1.225) blocks. This suggests that voxel counts for the masseter and O. oris are reduced in the TS group. Means and standard deviations are illustrated in Figure 5.8.

Figure 5.8

Means and standard deviations (error bars) of number of voxels present activated in TD (blue) and TS (red) groups for each sensory block

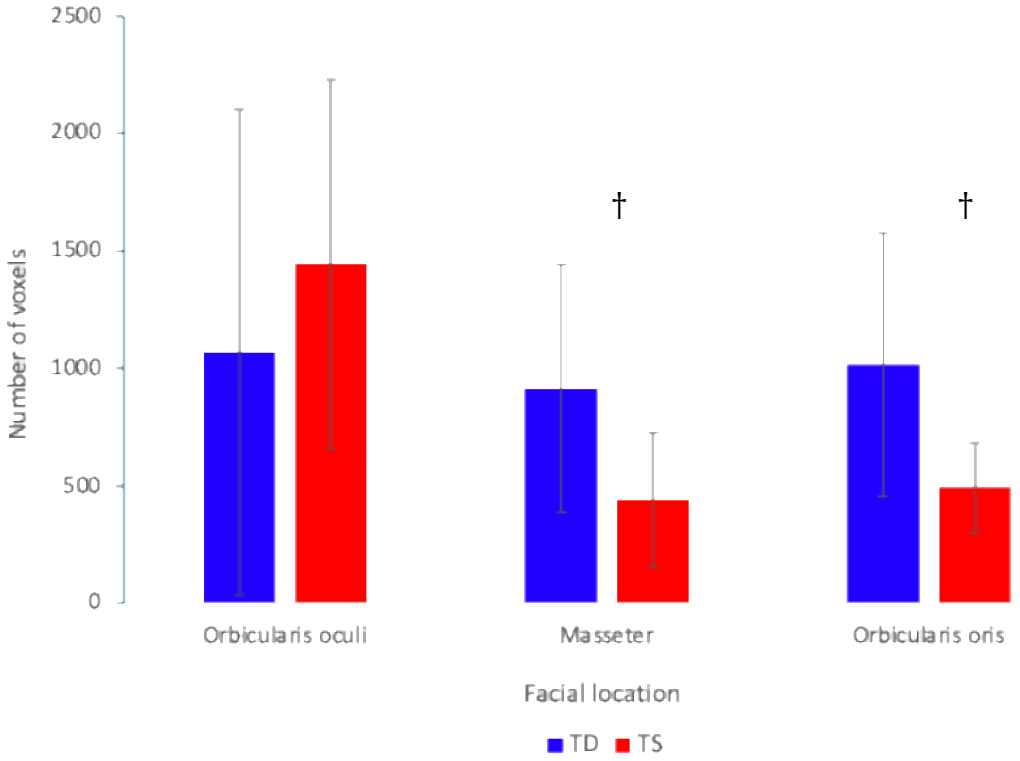

Note. TD = group of typically developing control participants, TS = group of participants with Tourette Syndrome, † = anecdotal support for alternative hypothesis. Group differences are non-significant ($p > 0.05$)

5.4.2.4 3D zCOG coordinates

Independent *t*-tests were conducted on the 3D zCOG coordinates identified in each sensory block between groups (means and standard deviations summarised in Table 5.5). No significant differences were identified between TD and TS group coordinates for O. oculi: L-R ($t(19) = -.798$, $p = 0.435$, $BF_{10} = 0.558$), and A-P ($t(19) = -1.144$, $p = 0.267$, $BF_{10} = 0.688$); Masseter: L-R ($U = 31$, $p = 0.962$, $BF_{10} = 0.465$), P-A ($U = 24$, $p = 0.478$, $BF_{10} = 0.509$) and I-S ($t(18) = 0.139$, $p = 0.891$, $BF_{10} = 0.461$) or O. oris: L-R ($t(16) = -.781$, $p = 0.446$, $BF_{10} = 0.560$), P-A ($U = 25$, $p = 0.798$, $BF_{10} = 0.462$) and I-S ($t(16) = 0.970$, $p = 0.346$, $BF_{10} = 0.620$). However, Bayesian statistics revealed anecdotal evidence in support of the alternative hypothesis, signifying that O. oculi I-

S coordinates were more inferior in the TS group ($t(19) = 1.622$, $p = 0.121$, $BF_{10} = 1.027$).

Table 5.5

Mean and standard deviations of maximum Z statistic 3D coordinates for each sensory block

	Orbicularis oculi			Masseter			Orbicularis oris		
Group	**L-R**	**P-A**	**I-S**†	**L-R**	**P-A**	**I-S**	**L-R**	**P-A**	**I-S**
TD	41.8 (±17.5)	-26.2 (±11.9)	43.1 (±17.0)	48.6 (±17.2)	-20.1 (±13.0)	35.8 (±19.5)	51.0 (±14.7)	-20.1 (±14.4)	40.2 (±15.6)
TS	49.4 (±14.71)	-18.9 (±9.67)	27.8 (±16.54)	50.6 (±12.87)	-24.1 (±9.73)	34.3 (±19.87)	57.2 (±9.57)	-19.9 (±9.59)	32.2 (±8.62)

Note. L-R = left to right, P-A = posterior to anterior, I-S = inferior to superior, TD = group of typically developing control participants, TS = group of participants with Tourette Syndrome, mean (±standard deviation), † = anecdotal support for alternative hypothesis

A scatterplot of individual 2D zCOG coordinates for each block are shown in Figure 5.9. Visual inspection of Figure 5.9 shows that although right M1, S1, and SMA were included in the sensorimotor mask, zCOG coordinates across all movements and groups were located in the right hemisphere S1, clustered into two locations.

Figure 5.9

Scatterplot of individual maximum Z statistic 2D coordinates (x, y) in TD (blue) and TS (red) groups for (a) O. oculi, (b) masseter and (c) O. oris sensory blocks

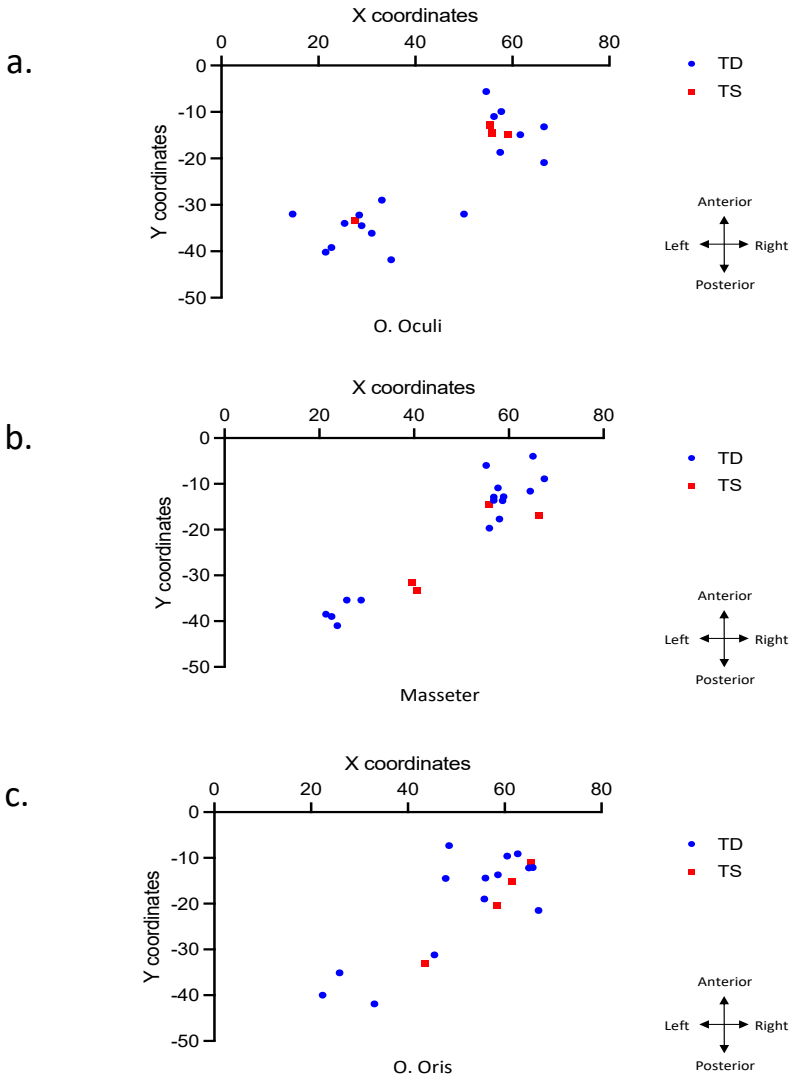

Note. Each point reflects individual participant's maximum Z statistic coordinates (L-R, P-A) for each sensory block, TD = group of typically developing control participants, TS = group of participants with Tourette Syndrome. All coordinates fall within the right post-central gyrus (S1) as assessed using mni2atlas (https://github.com/dmascali/mni2atlas/releases/tag/1.1)

5.4.2.5 Euclidean distances

Independent *t*-tests were conducted on the Euclidean distances identified between groups, based on the 3D coordinates of zCOG for each sensory block within the right post-central gyrus for each participant. The average Euclidean distance between the O. oculi and masseter 3D zCOG coordinates were not significantly different between TD (*M* = 14.3, *SD* = 17.8) and TS (*M* = 10.8, *SD* = 8.40) groups; *U* = 23.0, *p* = 0.955. No significant differences were also found between TD (*M* = 17.1, *SD* = 17.3) and TS (*M* = 29.9, *SD* = 28.39) groups when assessing Euclidean distances between the masseter and O. oris (*U* = 19, *p* = 0.382) and Euclidean distances between the O. oculi and O. oris (*t*(15) = 0.241, *p* = 0.813) in TD (*M* = 18.0, *SD* = 17.4) and TS groups (*M* = 15.5, *SD* = 5.74). Bayesian inference provided anecdotal evidence in support of null hypothesis for O. oculi-masseter (BF_{10} = 0.533), masseter-O. oris (BF_{10} = 0.693) and O. oculi-oris (BF_{10} = 0.503). Means and standard deviations are summarised in Figure 5.10.

Figure 5.10

Means and standard deviations (error bars) of Euclidean distances between maximum Z statistic 3D coordinates (x,y,z) of each sensory block in TD (blue) and TS (red) groups

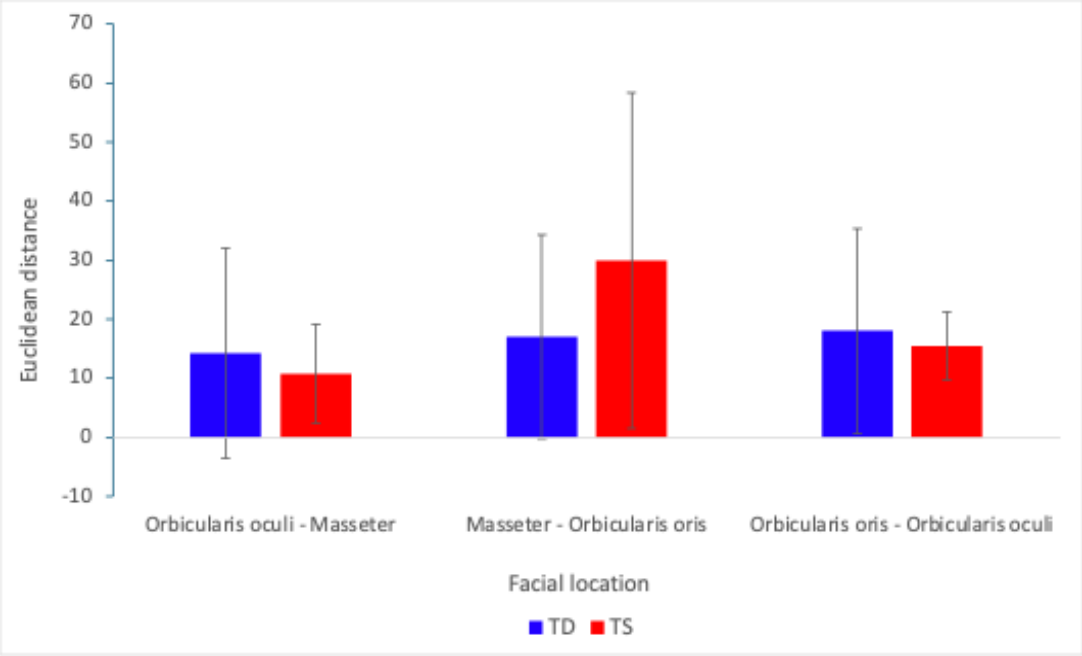

Note. TD = group of typically developing control participants, TS = group of participants with Tourette Syndrome. Group differences are non-significant ($p > 0.05$)

5.4.3 Discussion

In Study 2, right hemisphere sensorimotor representations were extracted in response to vibrotactile stimulation of different regions of the face, namely, the O. oculi, masseter and O. oris. However, while significant cluster activations were identified across the TD control group in each sensory block, no activations were present in the TS group. This is likely due to the low sample size and thus, insufficient power to detect a group effect. Similarly, in the TD group, cluster activations for each sensory block showed activations within the SMA and M1, despite all individuals showing maximum Z statistic activation coordinates (zCOG) located in the S1. Moreover, conjunction analysis identified common voxel activations within the SMA only, which has previously shown to be activated during passive vibrotactile

stimulation (Nelson et al., 2004). This supports the notion that while cortical representations are generally stable within individuals, there is great variation in the shape, position and extent of cortical representations between individuals (Besle et al., 2013; Kikkert et al., 2023; Kolasinski et al., 2016; Sanchez-Panchuelo et al., 2012; Stringer et al., 2011). Therefore, although the same area of the face was stimulated across participants, activations across the S1 show great variation and therefore, are not likely to pass group-level cluster thresholding or show common activations during conjunction analysis.

When assessing individual thresholded cluster activations to vibrotactile stimulation to different areas of the face, it was found that the number of voxels activated in the right hemisphere sensorimotor mask in response to O. oculi vibrotactile stimulation was comparable across TD controls and the TS group. In contrast, for vibrotactile stimulation of the masseter and O. oris, there was anecdotal evidence for group differences, with reduced number of voxels activated evident in the TS group. This reflects the notion that motor gain excitability is reduced in TS and therefore, there may be less activation present in the sensorimotor cortices in comparison to TD controls (Draper et al., 2015; Orth, 2009; Pépés et al., 2016). Additionally, this could suggest that tactile detection of vibrotactile stimuli on the masseter and O. oris are poorer in TS, therefore resulting in a reduction of cortical responses. This also reinforces reports of abnormal somatosensory processing of tactile stimuli in TS, as demonstrated by abnormalities in quantitative sensory thresholds in the TS group within Chapter 3. This could also signify that there are abnormalities in quantitative sensory thresholds of facial regions, the region of the body most commonly associated with tics and PU (Baizabal-Carvallo et al., 2023; Essing et al., 2022; McGuire et al., 2016). However, as evidenced in the absence of group-level cluster activations, the TS group has a low sample size and power. As a result, there is reduced reliability of these results reflecting a true effect due to the enhanced likelihood of Type I and Type II errors. Additionally, there is large variability of individual voxel activations demonstrated within each group. Consequently, these findings should be taken with caution.

Interestingly, although no significant differences were identified in 3D zCOG coordinates across groups, except anecdotal evidence of inferior O. oris representations in the TS group, all individuals showed maximum activations within the S1. However, these appeared to be clustered into two groups across all participants. This suggests that there may be two sites of S1 that are activated during vibrotactile stimulation of the O. oculi, masseter and O. oris.

This mirrors recent evidence presented by Gordon et al. (2023), which proposed that topography within the M1 is not structured as first proposed by Penfield and Boldrey (1937; see Figure 1.2), but instead is organised in three distinct concentrically organised effector-specific regions (face, hand and leg) which are interleaved by 'body-action' regions (Gordon et al., 2023). Within the effector-specific regions, fMRI activation profiles of movements across the body were assessed and showed differential activations. In the face region, while one-peak gaussian curves better fit the activation profiles of movement in the tongue, two-peak gaussian curves better fit activation profiles of movement in areas further from the tongue, such as the jaw, nostrils and eyelids (Gordon et al., 2023). This was also found in the foot and hand effector regions, where toes and hand show one-peak activations, the ankle, knee, hip and wrist, elbow, shoulder evoked two-peak activation profiles. This suggests that while M1 cortical areas relating to the tongue/toes/hand show one site of activation, cortical areas of more distal parts of the body show two sites of possible activation (each surrounding above and below the central activation peak). This indicates that effector-specific regions are concentrically organised, with proximal-distal organisation (Gordon et al., 2023). Specifically, in the effector-specific region, the tongue is represented in the centre of effector region and is surrounded by concentric zones relating to the jaw, nostrils and eyelids. In the data presented in Study 2 within the S1 (Figure 5.9), the presence of two clustered sites of zCOGs in each sensory block across participants could suggest that activation profiles of the O. oculi, masseter and O. oris show two-peak activations. This supports the novel concentric organisation of effector specific regions proposed by Gordon et al. (2023). However, activation

profiles of each individual's response to vibrotactile stimulation to each facial region must be analysed further to assess their fit with one- and two-peak Gaussian activation profiles before this can be concluded within this data.

5.5 Limitations

There are several limitations within this chapter. Firstly, it would have been useful to compare group differences between the intensity of BOLD activations. However, in Study 1, it is likely that the intensity of movements would have varied between individuals. If measured with EMG, this could allow for normalisation of BOLD activation across individuals depending on the strength of EMG output to provide some insight into BOLD activation intensities across groups. Moreover, in Study 2, vibrotactile stimulation was not thresholded to individual detection levels. Instead, to reduce set-up time, a suprathreshold intensity of vibrotactile stimulation was implemented consistently across individuals and therefore, individuals may have differential BOLD activation profiles depending on individual detection thresholds. This could also have accounted for the variability in the number of voxel activations present within each group. Additionally, different areas of the face have been shown to have different detection thresholds (Komiyama & De Laat, 2005) and, as demonstrated in Chapter 3, there are differences in quantitative sensory thresholds between TS and TD controls. This may explain why group-level cluster activations were absent in the TS group, as individuals with TS are less responsive to low-intensity vibrotactile stimuli**.** Alternatively, this could be explained by suppression of tics during tasks has been associated with reductions in M1 cortical excitability, however, suppression was not directly measured (Draper et al., 2014; Jackson et al., 2015). In future, these EMG and thresholding of vibrotactile stimuli should be implemented to provide an insight into the strength of BOLD activations within sensorimotor cortices. Additional measures into the extent of suppression during tasks may also reveal differences in BOLD activations during fMRI tasks, which could be controlled for during analyses.

An additional drawback is the averaging of responses within groups. While the somatotopic organisation of the digits are well documented within the sensorimotor cortices (Janko et al., 2022), evidence of the precise somatotopic organisation of the face is mixed. For instance, while some studies have reported an upright homunculus, where the mouth is inferior to the eye representation (Krippl et al., 2015; Penfield & Boldrey, 1937) others have demonstrated the opposite (Servos et al., 1999), or even where the chin is superior to the lip but inferior to the forehead (Kikkert et al., 2023) or the nose is represented inferior to the to the jaw or superior to the eye (DaSilva et al., 2002; Moulton et al., 2009). Consequently, it may be more beneficial to statistically investigate maps on an individual basis. As a result, assuming homogeneity of samples and performing group analyses could mask individual variability as although maps are stable within individuals, they vary greatly across individuals.

Additionally, in the TS group, differences in sensorimotor activations in each study may have been influenced by individual GABA functioning and particular symptom phenomenology, such as tic severity and PU severity. As discussed in Section 5.1, bilateral abnormalities in the digit representations of individuals with FHD were evident in patients with greater symptom severity and durations of FHD (Byrnes et al., 1998; Meunier et al., 2001). Additionally, repetitive behaviours of the hand, paired with abnormalities in cortical inhibition, were proposed to drive the abnormalities demonstrated in sensorimotor digit representations (Blake et al., 2002; Evinger, 2005). However, in this chapter, levels of cortical inhibition, facial tic severity and PU severity were not assessed alongside individual features of sensorimotor representations. Therefore, it cannot be concluded that the presence and individual severity of facial tics are associated with the differences identified in sensorimotor representations between each group.

5.6 Conclusions

Overall, this chapter has uncovered some abnormalities in the representations of facial movements and in processing vibrotactile stimulation across different facial

locations in individuals with TS compared with a TD control group. Study 1 highlighted possible differences in the sensorimotor mapping of facial movements, specifically differential SMA activation during volitional movements in the TS group. This was suggested to be a result of abnormalities within SMA activations and due to variables, such as task complexity, tic execution and tic suppression. Study 2 showed that vibrotactile stimulation to different areas of the face revealed that the number of sensorimotor voxels activated in response to O. oculi vibrotactile stimulation was comparable across TD controls and the TS group, but vibrotactile stimulation of the masseter and O. oris displayed reduced voxel counts in the TS group. This may reflect reduced motor gain excitability as previously reported in TS (Draper et al., 2015; Orth, 2009; Pépés et al., 2016), or differences in the processing of somatosensory stimuli.

However, it should be noted that there was great variability within voxel counts for somatosensory representations within each group, therefore it may be more beneficial to assess somatosensory representations on an individual level with individually-thresholded vibrotactile stimuli. Moreover, increased sample size within the TS group is required. Interestingly, across all tasks and groups, participants displayed zCOG activations within one of two clusters of the S1. This may reflect a concentric organisation of effector-specific regions in the sensorimotor cortices as proposed by Gordon et al. (2023). However, further analyses of activation profiles for each sensory block are required before this can be concluded.

6. Chapter 6 - The influence of intermittent theta-burst stimulation on cortical digit representations using TMS and fMRI

Key words: Repetitive transcranial magnetic stimulation (rTMS), intermittent theta-burst stimulation (iTBS), γ-aminobutyric acid (GABA), short-interval intracortical inhibition (SICI), input-output curve (IO curve), TMS mapping, functional magnetic resonance imaging (fMRI), primary motor cortex (M1)

Note: Data collection was part of my undergraduate project and was completed during this PhD

6.1 Introduction

The inhibitory neurotransmitter GABA is heavily implicated in the shaping and maintenance of cortical motor representations (Jacobs & Donoghue, 1991; James Kolasinski et al., 2017). So far, this thesis has demonstrated that within TS, there is a trend of reduced MRS-GABA inhibition, reflecting a reduction of neuro-metabolite tonic inhibition, (Chapter 3) and some alterations in cortical digit and facial representations in the sensorimotor cortices (Chapters 4 and Chapter 5) in comparison to TD control groups. Therefore, tonic inhibition may play a role in the maintenance of cortical representations, as in groups where inhibition is disrupted, cortical representations are disrupted. However, MRS-GABA was not assessed in all individuals and were not correlated with features of sensorimotor maps, so this cannot be concluded. Moreover, MRS-GABA is not correlated with SICI, a TMS protocol proposed to reflect mechanisms of phasic inhibition and thought to shape cortical representations; surround inhibition and receptive field tuning (Dyke et al., 2017; Foeller et al., 2005; Jacobs & Donoghue, 1991; Schneider et al., 2002).

One way we can assess the role of phasic inhibition on cortical representations is by directly manipulating GABAergic mechanisms using rTMS. Much evidence heavily implicates GABA and glutamate as the main physiological drivers responsible for the induction of rTMS after-effects. For instance, glutamatergic synaptic

neurotransmission act through NMDA receptors. As discussed in Section 2.3.3.2, NMDA receptor antagonists have been found to block TBS after-effects (Huang et al., 2007; Labedi et al., 2014). NMDA receptors are also implicated in the LTP and LTD processes TBS is thought to initiate, due to their abilities to trigger influxes of Ca^{2+} (Huang et al., 2007). Also, as previously discussed in Section 2.3.3.2, $GABA_A$ receptors are understood to have a role in LTP plasticity. We may, therefore, expect that GABAergic function is disrupted to allow for this enhanced cortical excitability. For example, $GABA_A$ receptor antagonists have been demonstrated to enhance LTP-like responses after excitatory rTMS in rat hippocampal tissue and M1, implicating GABAergic mechanisms are involved in the after-effects of rTMS (Grover & Yan, 1999; Hess et al., 1996). $GABA_A$ antagonists have also resulted in the alteration of cortical motor representations (Foeller et al., 2005; Jacobs & Donoghue, 1991; Schneider et al., 2002), with recent evidence suggesting that SICI is a predictor of the FDI muscle motor representation area (Sigurdsson, Molloy, et al., 2020). As a result, if rTMS protocol truly influences SICI, this technique may have the ability to alter functional representations within the motor system.

The notion that rTMS-induced weakened inhibition may be a driver for increased excitability and LTP-like facilitation, driving malleability of cortical representations, has been supported in recent animal research. 10Hz rTMS to the visual cortex of a cat resulted in the weakening of intracortical inhibitory mechanisms which, in turn, weakened cortical map integrity, enhanced spontaneous activity and increased cortical excitability and plasticity (Kozyrev et al., 2014, 2018). Moreover, this 10Hz rTMS disrupted visual cortical maps, which became more malleable and biased to visual input. Specifically, after stimulation, passive viewing of visual stimuli of a specific orientation led to map reorganization, with greater representation and preference for the viewed orientation lasting around six hours (Kozyrev et al., 2018). Moreover, limb stimulation paired with 10Hz rTMS of the rat sensory cortex has previously resulted in short-term plasticity after a single session, and long-term changes when this protocol was repeated for five days (Zhong et al., 2021). This plasticity was shown by an increase in the number of activated fMRI voxels after

cortical sensory mapping of the forepaw after 10Hz rTMS. Additionally, long-term changes were not present with limb sensory stimulation alone but were with 10Hz rTMS. This further suggests that high-frequency rTMS can enhance excitability and cortical representations of the stimulated region, especially when combined with sensory stimulation (Zhong et al., 2021)

Furthermore, one human study has used 20Hz excitatory rTMS over the M1 hand area which significantly expanded somatosensory hand representations (Houzé et al., 2013). Moreover, two human studies have used 5Hz excitatory rTMS to the left primary somatosensory cortex (S1) index finger representation, which resulted in a transient increase of the associated cortical fMRI S1 digit map compared to sham rTMS (Pleger et al., 2006; Tegenthoff et al., 2005). While cortical inhibitory mechanisms were not assessed, one group previously found that this 5Hz rTMS protocol resulted in a sustained reduction of paired-pulse inhibition (Ragert et al., 2004), which may suggest that changes in cortical representations may be a result of disturbance to inhibition. As a result, this suggests that excitatory rTMS may induce plasticity mechanisms in cortical maps by acting on intracortical inhibition, allowing maps to become malleable and biased to training and learning input.

If excitatory rTMS does, in fact, reduce GABA-related inhibition, it may hold therapeutic promise. For example**,** in a post-stroke animal model where motor function was affected, increased inhibition was evident (Clarkson et al., 2010). By disrupting GABA mechanisms responsible for this tonic inhibition, recovery of motor function was promoted (Clarkson et al., 2010). Similarly in human research, decreases in MRS-GABA are associated with greater improvements in motor function post-stroke (Blicher et al., 2015). As preliminary data has suggested, excitatory-rTMS may be able to reduce MRS-GABA, indicating its potential therapeutic potential (Gröhn et al., 2019). However, while animal evidence strongly supports that excitatory rTMS acts through the weakening of intracortical inhibition to manipulate cortical representations, the impact of rTMS on inhibitory mechanisms in human evidence is mixed. For instance, while some show reduced SICI after excitatory rTMS application

(Peinemann et al., 2000; Quartarone et al., 2005; Wu et al., 2000), other studies have demonstrated that SICI remains relatively unchanged (Chung et al., 2016; Murakami et al., 2012; Tse et al., 2018). Therefore, while glutamate and GABA are implicated in excitatory rTMS after-effects, the precise physiological mechanisms in which rTMS acts upon are still unclear, especially as after-effects are highly variable across individuals (Hamada et al., 2013; Suppa et al., 2016).

6.2 Aims

This study aimed to investigate the influence of excitatory rTMS to the M1 hand area, or the vertex as a control site, on cortical motor representations of the hand in TD populations across two studies. While there is some evidence to suggest that iTBS is inferior to 20Hz rTMS on cortical mapping (Houzé et al., 2013), iTBS was specifically chosen as rat models have previously determined that cortical inhibitory cells are most sensitive to iTBS protocols (Funke & Benali, 2011). To expand on previous research, multiple hand muscles and digit representations were explored with TMS and fMRI, as iTBS effects have been shown to extend beyond the initial site of stimulation (Morris et al., 2019). As these representations are close to the FDI M1 target of stimulation, it is expected that these maps would also show some differences after active stimulation.

In Study 1, the ability of active M1 iTBS to modulate TMS measures of cortical excitability (IO curve slopes) and inhibition (TMS-SICI) was investigated and compared to control vertex iTBS. Stimulating the vertex in rTMS paradigms has been shown not to influence activity within the motor system, making it an ideal control site for stimulation (Jung et al., 2016). Further to cortical excitability and inhibitory measures, TMS corticospinal excitability maps of three hand muscles were collected before and after active or control iTBS to detect any changes in the area, 3D COG coordinates and Euclidean distances in relation to other representations for each muscle. TMS mapping is described in Section 2.3.2.3 and has previously been shown to be sensitive to changes in cortical mapping between clinical populations such as in patients who have experienced a stroke (Freundlieb et al., 2015), Tourette Syndrome (Sigurdsson,

Jackson, et al., 2020), or after amputation (Gunduz et al., 2020) and immobilization of limbs (Liepert et al., 1995; Zanette et al., 2004). It was hypothesised that active iTBS would increase IO curve slopes and SICI values (indicating reduced inhibition) whereas the control group would show no change. For TMS maps, it was hypothesised that cortical representations will show a larger magnitude of change after active compared to control stimulation in line with previous evidence (Houzé et al., 2013; Pleger et al., 2006; Tegenthoff et al., 2005).

In Study 2, fMRI was employed to measure digit maps before and after active or control iTBS; specifically, the ratio of voxels assigned to each digit ROI (digit ratios), and the Euclidean distances between digit COGs before and after iTBS. Again, it was hypothesised that cortical representations will show a larger magnitude of change after active iTBS compared to control iTBS.

6.3 Study 1

This study assessed the effect of active and control iTBS on M1 cortical excitability, inhibition and TMS map measures of three hand muscles.

6.3.1 Methods

6.3.1.1 Participants

Twenty-six participants took part in this study. An initial recruitment target of ten participants per condition was chosen due to a limited undergraduate project timescale, subsequent COVID-19 restrictions and Study 2 funding limitations (see Section 6.4.1.1). Recruitment was increased after COVID-19 restrictions were lifted to account for any instances of poor data quality and to strengthen reliability of results, but was paused to prioritise other projects in this thesis due to delays in testing human participants after COVID-19. For this preliminary dataset, data from one participant from the control group was removed due to a diagnosis of ADHD. Participants gave informed consent and ethics were approved by the local ethics committee (School of Psychology, University of Nottingham: F1095). No participants were taking CNS-active drugs and were free from any mood or neurological illness during the experimental timeline. In the final dataset, there were 14 participants in the active condition and 11 participants in the control condition. A subset of eight participants from the active group and seven participants from the control group took part in TMS mapping measures.

Demographic information is displayed in Table 6.1. for active and control groups. Age ($U = 74.5$, $p = 0.913$) and sex (X^2 (1, $N = 25$) = 0.070, $p = 0.792$) distributions were not significantly different between groups. All participants were free from any contraindications for MRI and TMS, as assessed by completion of MRI and TMS safety screening forms. All participants were right-handed as assessed by the Edinburgh handedness questionnaire (Oldfield, 1971).

Table 6.1

Demographics of participants in active and control groups in Study 1

Group	N	Age	Sex
Active	14	22.52 (±3.2)	2 male, 12 female
Control	11	23.01 (±4.2)	2 male, 9 female

Note. N = number of participants, mean (±standard deviation)

6.3.1.2 Electromyography

Subjects were seated in a chair with their right arm and elbow placed in a comfortable position on the desk in front of them and disposable Ag-AgCl surface electromyography (EMG) electrodes for MEP recording were attached. Electrodes were placed securely on the right hand in a belly-tendon montage targeting the FDI hand muscle, with the ground electrode placed on the right ulna (Figure 6.1). Participants were asked to keep their hand in a relaxed position, palm facing down, throughout the experiment and were given breaks throughout if needed. For TMS motor mapping, two further sets of electrodes were attached to the right hand, targeting the abductor pollicis brevis (APB) and abductor digiti minimi (ADM) muscles in a belly tendon montage (Figure 6.1). Three hand muscles were chosen as iTBS effects have been shown to extend beyond the initial FDI site of stimulation (Morris et al., 2019). These electrodes were only attached during TMS mapping and participants were asked to keep their hand in a relaxed position with their palm facing up and supported by a pillow. EMG signals were amplified and bandpass filtered (10Hz-2kHz, with a sampling rate of 2kHz) and then digitized using Brain Amp ExG (Brain Products, GmbH, Gilching, Germany), controlled by Brain Vision Recorder (Brain Products, GmbH, Gilching, Germany).

Figure 6.1

EMG set up over the FDI, APB and ADM in a belly-tendon montage

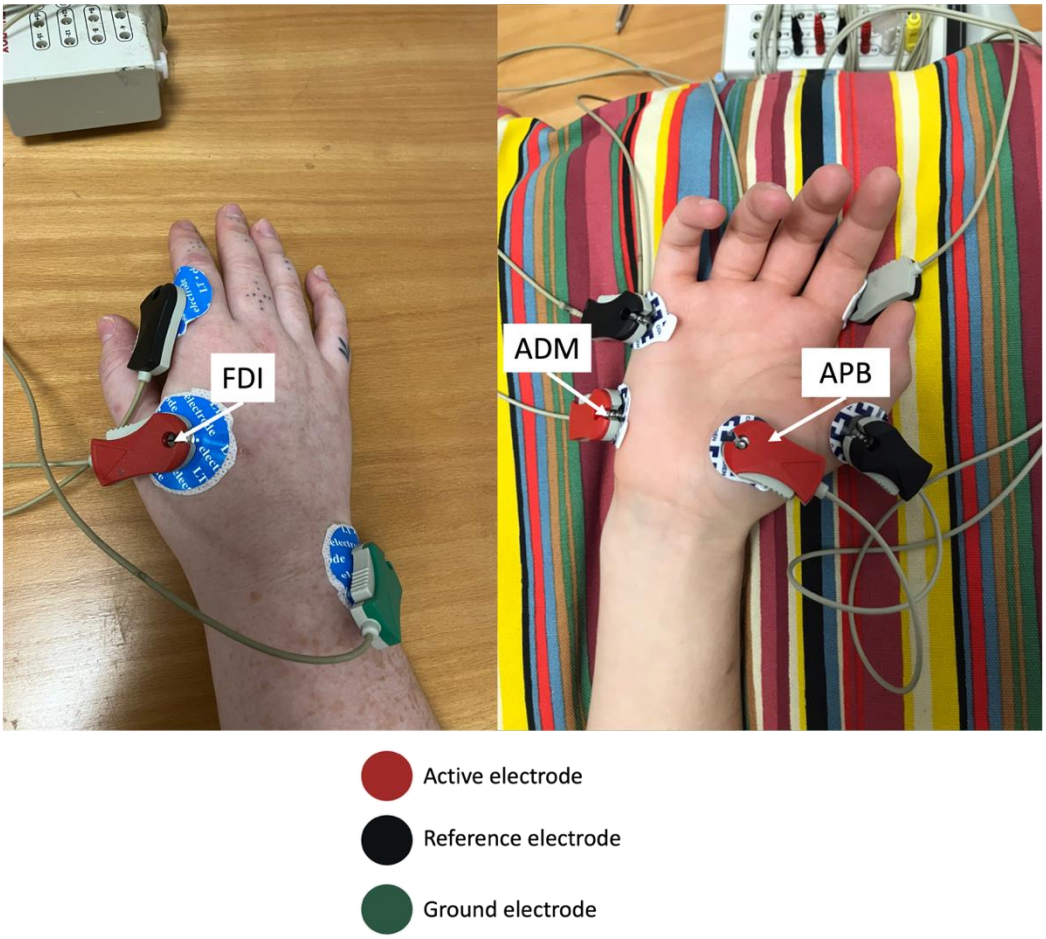

Note. FDI = first dorsal interosseous, ADM = abductor digiti minimi, APB = abductor pollicis brevis

6.3.1.3 TMS protocol

6.3.1.3.1 Hotspotting and thresholding

TMS hotspotting, thresholding, TMS cortical mapping, SICI and IO curve measures were performed using a Magstim-Bistim operating system (Magstim, Whiteland, Dyfed, UK) using a 50mm figure-of-eight coil and neuronavigation was conducted using BrainSight software (Rogue Research Inc., Montreal, Quebec, Canada).

Neuronavigation was conducted using BrainSight software (Rogue Research Inc., Montreal, Quebec, Canada). Neuronavigation was based on each participant's individual T_1-weighted anatomical MRI scans (for acquisition parameters, see Section 6.4.1.2.2) to allow for accurate coil orientation and location over the left M1. Within BrainSight, scans underwent skin reconstruction and the precentral gyrus 'hand knob' anatomical landmark in the left motor cortex was targeted (Yousry et al., 1997). Around this hand knob target, a square 5 x 5 cm grid (consisting of four target corners) was superimposed on the skull above the 'hand' area of the motor cortex on BrainSight. This grid allows us to conduct mapping within set bounds for each participant.

Before delivering pulses to the scalp, a neuronavigation tracking headband was securely and comfortably attached to participant's heads. Participants also had the opportunity to ask questions and feel a test pulse of TMS on the palm of their hand once the procedure (Figure 6.2) was explained to them. Once participants were ready to begin, suprathreshold pulses were delivered to the left M1 hand area 'hotspot', defined as the location that consistently evoked the largest MEPs in the right FDI muscle. Coil orientation was maintained at 45 degrees from the midline with current flowing in a posterior-anterior direction, which has been shown to evoke optimal MEP responses in the FDI muscle (Adank et al., 2018). Pulses were recorded on BrainSight and once the hotspot was found, this area was landmarked to ensure this hotspot area was consistently targeted at the correct orientation throughout the experiment and allowed participants to take breaks if they requested one. If this

hotspot was outside or near to the boundaries of the superimposed grid, the grid would be moved, and the new 'hotspot' hand target would become the centre target for the grid.

All trials had an interval of 5 seconds between them and were operated using an in-house program written with MATLAB (MATLAB_R2019a, Mathworks, MA, USA). Following hotspotting, RMT and SI1mV thresholds were determined for each participant based on EMG responses from the FDI muscle. The full procedure is illustrated in Figure 6.2. Following the study, participants were requested to fill in a questionnaire the day after their participation, allowing them to report any experienced side-effects in the 24 hours following TMS.

Figure 6.2

Study 1 procedure

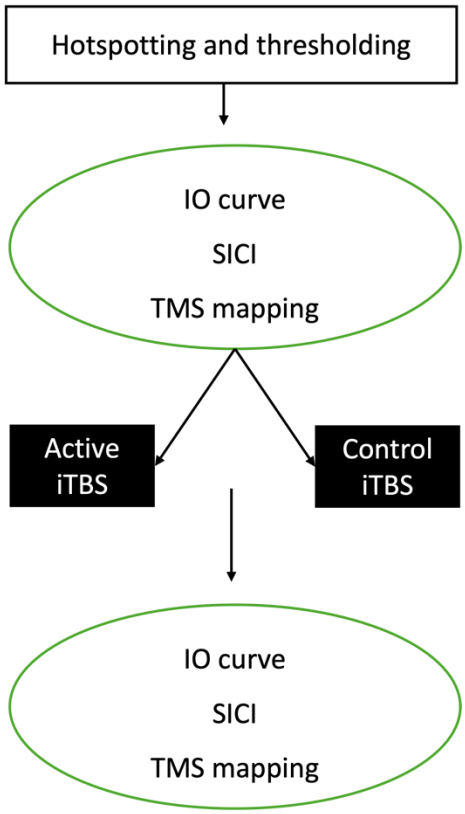

Note. IO curve = input-output curve, SICI = short-interval intracortical inhibition, TMS = transcranial magnetic stimulation, iTBS = intermittent theta burst stimulation

6.3.1.3.2 RMT and SI1mV

RMT is defined as the TMS stimulation intensity as a percentage of maximum stimulator output (%MSO) needed to evoke a peak-to-peak MEP amplitude of between 50-100 μv in the FDI muscle in ~5 out of 10 trials (Rossini et al., 2015). 1mV thresholds (SI1mV) were also determined; this is the optimal TMS stimulation intensity (%MSO) to consistently evoke a peak-to-peak amplitude of 1mV, on average, in the FDI muscle.

6.3.1.3.3 Input-output curves

IO curve measures were conducted using RMT intensities of 100, 110, 120, 130, 140 and 150%. 15 trials per intensity were conducted in a randomized order using a bespoke MATLAB script, giving a total of 90 pulses with 5 seconds between trials. Both of these measures have been shown to have moderate-excellent reliability (Dyke et al., 2018).

6.3.1.3.4 Short-interval intracortical inhibition

3 ms short-interval intracortical inhibition (SICI) was determined using a paired-pulse TMS protocol. The test stimulus (TS) was set at SI1mV and conditioned stimulus (CS) intensities were set at 65%, 70% and 75% of each participant's RMT. 15 trials at each TS-CS intensity pairing with an inter-stimulus interval (ISI) of 3 ms and 30 unconditioned trials were conducted in a randomized order using a bespoke MATLAB script, giving a total of 75 paired-pulses with 5 seconds between trials.

6.3.1.3.5 TMS motor mapping

TMS cortical motor maps were acquired using a rapid acquisition method where MEPs are sampled pseudorandomly over the cortex, within the bounds of the 5 x 5 cm grid superimposed over each participant's 'hand' area within BrainSight. TMS maps were acquired with stimulus intensity of 120% of RMT with 120 pulses recorded in total, with 6 second gaps between pulses.

6.3.1.4 iTBS parameters

iTBS was performed using a Magstim Rapid^2 system (Magstim, Whiteland, Dyfed, UK) and 70mm figure-of-eight coil. Prior to repetitive stimulation, each participant underwent hotspotting again to determine the optimal site of stimulation targeting the FDI muscle and RMT was defined as the TMS stimulation intensity (as %MSO) needed to evoke a visible twitch in the FDI muscle in ~ 5 out of 10 of trials. These preliminary measures were conducted again due to the use of a different coil and operating system.

iTBS was either applied at the optimal left M1 site with an intensity of 70% RMT (active condition) or to the vertex control site (control condition) with an intensity of 30% RMT (control condition). The vertex site was measured prior to stimulation by measuring between the midpoint the participant's nasion and inion and left and right pre-auricular and marking this location with a pen. Fourteen participants were assigned to the active condition and 11 participants were assigned to the control condition. The pattern of iTBS performed involved 3 pulses every 200 ms at a frequency of 50Hz, repeated 20 times with a 10 second ISI, giving a total of 600 pulses (~ 3.5 minutes).

Following iTBS, TMS mapping, IO curve and SICI protocols were repeated, and MEP responses were recorded. Timings were recorded at the start of each protocol after iTBS to assess for any differences in timings between groups. The time to start TMS mapping after iTBS did not significantly differ between the active (*M* = 3.21 minutes, *SD* = 2.89) and control groups (*M* = 3.18 minutes, *SD* = 1.40); *U* = 66, *p* = 0.525. Moreover, the time to start IO curves after iTBS did not significantly differ between active (*M* = 20.46 minutes, *SD* = 7.23) and control groups (*M* = 19.90 minutes, *SD* = 6.33); *U* = 57.5, *p* = 0.662. Finally, the time to start SICI after iTBS in the active (*M* = 26.08 minutes, *SD* = 4.39) and control group (*M* = 27.27 minutes, *SD* = 5.18) did not significantly differ; *U* = 54, *p* = 0.322.

6.3.1.5 Data analysis

6.3.1.5.1 Electromyography

EMG data from each participant and trial was visually inspected within inhouse software (written in MATLAB_R2019a); if FDI pre-contraction or noise was present 500 ms before an MEP, that trial was excluded from analysis. Peak-to-peak MEP amplitudes were measured within this software. For each TMS intensity (%MSO), median MEP amplitude values were collected from each participant and the mean of these medians were collated across participants.

6.3.1.5.2 RMT and SI1mV

Independent *t*-tests indicated that RMT values (%MSO) were not significantly different between the active (M = 51.43, SD = 7.39) and control group (M = 53.73, SD = 8.30); $t(23) = -0.73$, $p = 0.472$. SI1mV values (%MSO) were also not significantly different between active (M = 63.36, SD = 9.16) and control group (M = 66.09, SD = 9.78); $t(23) = -0.72$, $p = 0.479$.

6.3.1.5.3 Input-output curve

IO curves were calculated by computing each participant's median MEP amplitude for each TMS intensity (100-150%RMT); group data involved averaging these median MEP amplitudes for each intensity. In line with previous research, MEP amplitudes increased in response to increasing TMS intensities – group IO curve data can be seen in Figure 3 (Ridding & Rothwell, 1997). Although IO curves are typically sigmoidal in shape due to a steep increase in MEP amplitudes with a plateau at higher intensities (Kemlin et al., 2019), this range of TMS intensities used in this study (100-150%RMT) are not sufficient to capture this sigmoid shape. Therefore, linear functions were fit to the curves and the IO curve slope was calculated from the resulting gradient. Percentage change between before and after iTBS IO curve slopes were also calculated.

Due to noise contaminating >50% of trials, one dataset was removed from before iTBS measures in the control group and two datasets were removed from after iTBS measures (one from the active group and one from the control group). For remaining data, any datapoint outside 1.5x the IQR above the third quartile or 1.5x the IQR below the first quartile were removed from further analyses. Across all before/after/percentage change measures, this included one dataset from the before iTBS timepoint in the active group and one dataset from the percentage change in slope in the active group, which were subsequently removed. Pre-analysis checks using independent *t*-tests showed that before iTBS IO curve slopes between the active group (M = 58.1, SD = 32.9) and control group (M = 67.6, SD = 47.4) were not significantly different; $t(21) = -0.57$, $p = 0.576$.

6.3.1.5.4 Short-interval intracortical inhibition

SICI ratios, i.e. the ratio of unconditioned MEP amplitudes to conditioned MEP amplitudes, were calculated using each participant's median MEP amplitude for the given CS intensities (65- 75%RMT). Each CS intensity median MEP amplitude was then divided by the participant's median MEP amplitude for TS trials, creating a SICI ratio for each intensity. The median of the resulting three ratios was then selected for each participant and group SICI ratios were calculated as the mean of median ratios. Ratios closer to 0 indicate greater inhibition, whereas ratios closer to 1.0 indicate less inhibition. Absolute percentage change between before and after iTBS median inhibition were also calculated.

Due to noise contaminating >50% of trials, two datasets were removed from before iTBS measures in the active group. For remaining data, any datapoint outside 1.5x the IQR above the third quartile or 1.5x the IQR below the first quartile were removed from subsequent analyses. Across all before/after/percentage change measures, this included one dataset from active group in the pre timepoint and three datasets from the percentage change measure (one from the active group and two from the control group), which were subsequently removed. Pre-analysis checks confirmed no significant difference in the before iTBS SICI ratios between the active

group (*M* = 0.23, *SD* = 0.16) and control group (*M* = 0.43, *SD* = 0.33); *t*(4) = -1.87, *p* = 0.082.

6.3.1.5.5 TMS mapping

TMS motor mapping and calculation of each TMS map metric was determined using a bespoke in-house MATLAB (MATLAB_R2019a, Mathworks, MA, USA) script in MNI standard space, as described in Sigurdsson et al. (2020). Firstly, MEPs from the FDI, ADM and APB muscles were time-locked and linked to BrainSight neuronavigation 3D coordinates, before standardising using a z-transformation. 3D coordinates were then projected to a 2D plane and re-sampled to a grid (see example map in Figure 6.3). Each pixel in the grid is appointed an approximated MEP based on the nearest MEP datapoint, using a triangular interpolation.

Figure 6.3

TMS map of the FDI muscle in P01 (active group) within 2D grid of coordinates

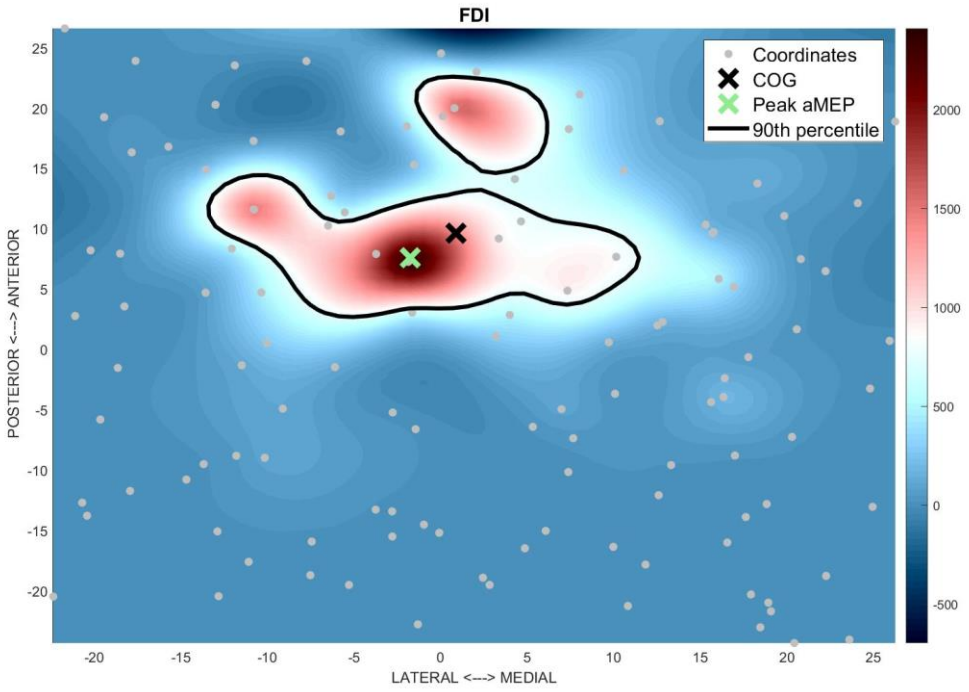

Note. FDI = first dorsal interosseous, COG = centre of gravity, Peak aMEP = peak amplitude of motor-evoked potential. Scale denotes amplitude of motor-evoked potentials

The TMS map metrics calculated for FDI, APB and ADM TMS maps in this study were the 2D COG coordinates, the area and the Euclidean distances (described in Sigurdsson et al., 2020). The 2D (x: - to +, L-R; y: - to +, P-A) COG coordinates were calculated as the mean position of the map, based on MEP amplitude-weighted mean intensity of each pixel within the superimposed grid (van de Ruit et al., 2015). Euclidean distances were calculated with Equation 6.1 for pairs of 2D COG coordinates (FDI-ADM, APB-FDI and ADM-APB) before and after control or active iTBS.

$$d = \sqrt{(x2 - x1)^2 + (y2 - y1)^2} \tag{6.1}$$

where $x2$, $y2$ are coordinates from 2D COG coordinates of one TMS map and $x1$, $y1$ are coordinates from the 2D COG coordinates of another TMS map. Finally, the area of each TMS map was calculated as the number of pixels in each map, normalised by dividing the total number of pixels in the grid.

Due to noise contaminating >50% of trials, one dataset was removed from after iTBS FDI TMS mapping measures in the control group. For remaining data, any datapoint outside 1.5x the IQR above the third quartile or 1.5x the IQR below the first quartile were removed from subsequent analyses. These are specified in Appendix D.1. Pre-analysis checks confirmed no significant difference in baseline L-R COG, P-A COG, Euclidean distances and areas between active and control groups in the FDI (all $p > 0.16$), APB (all $p > 0.15$) and ADM maps (all $p > 0.21$).

6.3.1.6 Statistical analysis

Parametric paired-groups *t*-tests were conducted to assess within-group differences in IO curve, SICI and TMS mapping measures before and after iTBS in active and control groups. Firstly, for IO curve and SICI measures, one-tailed paired-group *t*-tests were performed on the active group and two-tailed for the control group, as only the active group was predicted to show an increase in IO slopes and SICI inhibition in response to iTBS. Additionally, two-tailed paired *t*-tests were conducted on 2D COG coordinates, area and Euclidean distances before and after iTBS

in each group for each muscle, as while the active group are expected to show differences in TMS map properties before and after iTBS, the direction of this change is not clear.

To assess between-group differences, one-tailed independent *t*-tests were also performed to establish if there was a significant difference in the percentage change between before and after iTBS measures of SICI and IO curve slopes between the active and control groups. This would provide insight as to whether active-iTBS and control-iTBS show differences in the average direction of change in inhibition and excitability within each group.

To assess between-group differences in TMS map measures, the absolute change between L-R COG coordinates, P-A COG coordinates and Euclidean distances before and after iTBS were calculated. The absolute percentage change between TMS map areas before and after iTBS were also calculated. For TMS map properties, each change was converted into absolute values to assess the magnitude of change in TMS map properties between each group, rather than the direction of change. One-tailed independent *t*-tests were conducted for absolute changes in map properties between active and control groups, as it is expected that the active group will show a greater change in map properties than the control group.

Where data did not pass normality checks, independent t-tests were replaced with non-parametric Mann-Whitney *U* tests and paired *t*-tests were replaced with non-parametric Wilcoxon signed-rank test. BF_{10} was used with a Cauchy distribution with a scale of γ = 0.707 used as the prior distribution. Interpretation of BF_{10} values are shown in Table 3.2 (Rouder et al., 2009). All statistical analyses were conducted using jamovi (v 2.3.28; jamovi.org).

6.3.2 Results

No side effects in response to TMS were reported.

6.3.2.1 Input-output curve slopes

6.3.2.1.1 Within-group differences

A one-tailed paired *t*-test revealed no significant difference between IO curve slopes before (*M* = 54.3, *SD* = 31.3) and after (*M* = 81.4, *SD* = 43.6) iTBS in the active group; W = 20, *p* = 0.076. However, Bayesian inference revealed anecdotal evidence in support of the alternative hypothesis, suggesting that IO curve slopes showed some evidence of increasing after active iTBS (BF_{10} = 1.37). In the control group, a two-tailed paired *t*-test revealed no significant differences between IO curve slopes before (*M* = 72.3, *SD* = 47.8) and after (*M* = 67.6, *SD* = 65.6) control iTBS; *t*(8) = 0.45, *p* = 0.664, BF_{10} = 0.351. This provides evidence to suggest that control iTBS has no effect on IO curve slopes.

6.3.2.1.2 Between-group differences

A one-tailed independent *t*-test revealed in percentage change in IO curve slopes were significantly greater after iTBS in the active group (*M* = 48.4%, *SD* = 81.3%) compared to the control group (*M* = -15.7%, *SD* = 56.5%); *U* = 31.0, *p* = 0.029, BF_{10} = 2.925. The active group showed an average percentage change of 48.4% in IO curve slopes after active iTBS, whereas the control group showed an average percentage change of 15% in IO curve slopes. Means and standard deviations are shown in Figure 6.4.

Figure 6.4

Means and standard deviations (error bars) of percentage change in IO curve slopes before and after iTBS in active and control groups

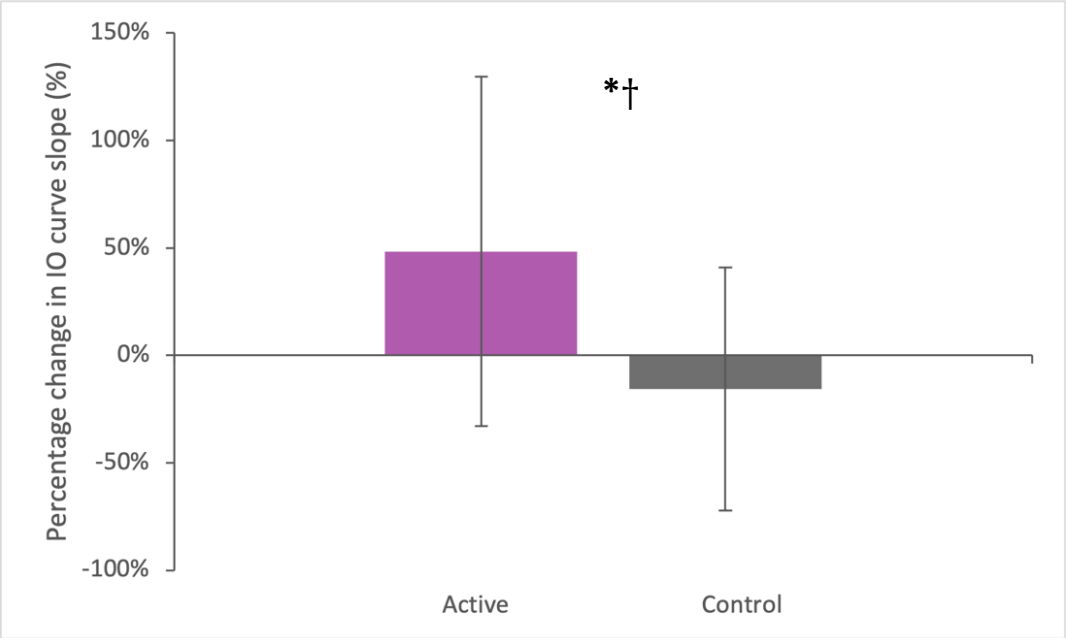

Note. IO curve = input output curve, * = $p < 0.05$, † = anecdotal support for the alternative hypothesis

6.3.2.2 Short-interval intracortical inhibition

6.3.2.2.1 Within-group differences

A one-tailed paired *t*-test revealed a significant difference between SICI before ($M = 0.23$, $SD = 0.16$) and after ($M = 0.35$, $SD = 0.21$) iTBS in the active group; $t(11) = -4.44$, $p < 0.001$. Bayesian inference revealed very strong evidence in support of the alternative hypothesis ($BF_{10} = 79.82$), suggesting that active iTBS significantly reduces inhibition (where numbers closer to 1 = less inhibition). In the control group, a two-tailed paired *t*-test revealed no significant differences between SICI before ($M = 0.43$, $SD = 0.33$) and after ($M = 0.45$, $SD = 0.26$) iTBS; $t(10) = -0.36$, $p = 0.724$. Bayesian inference evidenced moderate support for the null hypothesis ($BF_{10} = 0.315$). This provides evidence to suggest that control iTBS has no effect on SICI.

6.3.2.2.2 Between-group differences

A one-tailed independent *t*-test highlighted that percentage change in SICI were not significantly larger before and after iTBS in the active group (M = 38.3%, SD = 51.2%) compared to the control group (M = 18.6%, SD = 84.9%); U = 33.0, p = 0.074, BF_{10} = 0.649. Means and standard deviations are shown in Figure 6.5

Figure 6.5

Means and standard deviations (error bars) of percentage change in SICI before and after iTBS in active and control groups

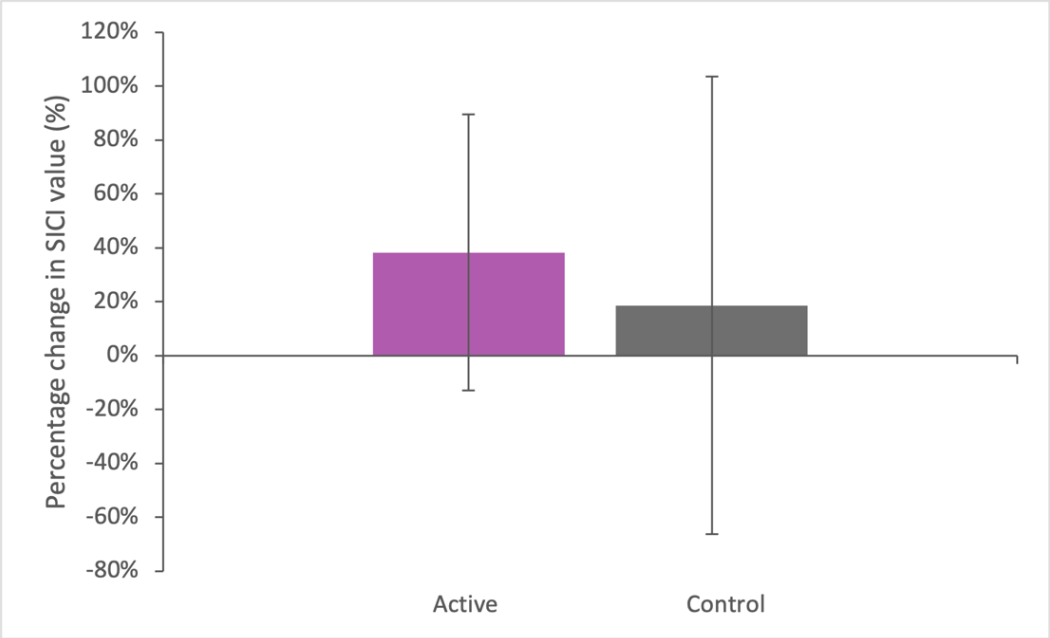

Note. SICI = short-interval intracortical inhibition. Group differences are non-significant (one-tailed, $p > 0.05$)

6.3.2.3 TMS mapping

6.3.2.3.1 2D COG coordinates: Within-group differences

6.3.2.3.1.1 FDI

Means and standard deviations for FDI 2D COG coordinates before and after iTBS are shown in Table 6.2, with an additional scatterplot including individual 2D COG coordinates in Figure 6.6.

In the active group, two-tailed paired *t*-tests revealed no significant differences between before and after iTBS L-R COG locations ($t(4) = -2.04$, $p = 0.111$). However, Bayesian statistics revealed anecdotal support for the alternative hypothesis, suggesting that the FDI COG shifted towards the right after active iTBS ($BF_{10} = 1.27$). There was no significant difference or Bayesian support for the alternative hypothesis between P-A COG locations before and after active-iTBS ($t(6) = -0.06$, $p = 0.957$, $BF_{10} = 0.354$). Overall, there is a small amount of evidence to suggest that the FDI COGx coordinate shifted towards the right after active iTBS.

In the control group, two tailed paired *t*-tests showed no significant differences in the position of L-R COG coordinates ($W = 10$, $p = 1.00$) or P-A COG coordinates ($t(3) = 1.67$, $p = 0.193$). Bayesian evidence revealed anecdotal support for the null hypothesis (L-R COG $BF_{10} = 0.526$; P-A COG $BF_{10} = 0.956$). This suggests that control iTBS had no influence on the location of FDI 2D COG coordinates.

Table 6.2

Means and standard deviations of TMS FDI map 2D COG coordinates in active and control groups

	FDI 2D COG coordinates			
	Active		Control	
Group	L-R †	P-A	L-R	P-A
Pre	-0.97 (±1.37)	8.69 (±3.17)	-2.65 (±3.48)	4.63 (±6.49)
Post	2.76 (±2.96)	8.77 (±2.23)	-1.21 (±6.21)	1.28 (±2.54)
N = Pre	5	7	6	4
N = Post	5	7	6	4

Note. FDI = first dorsal interosseous, COG = centre of gravity, *N* = number of participants, mean (±standard deviation). † = anecdotal support for the alternative hypothesis. Differences before and after iTBS for all coordinates and groups are non-significant (two-tailed, $p > 0.05$)

Figure 6.6

Scatterplot of individual and mean FDI map 2D COG coordinates before and after iTBS in the (a) active and (b) control group

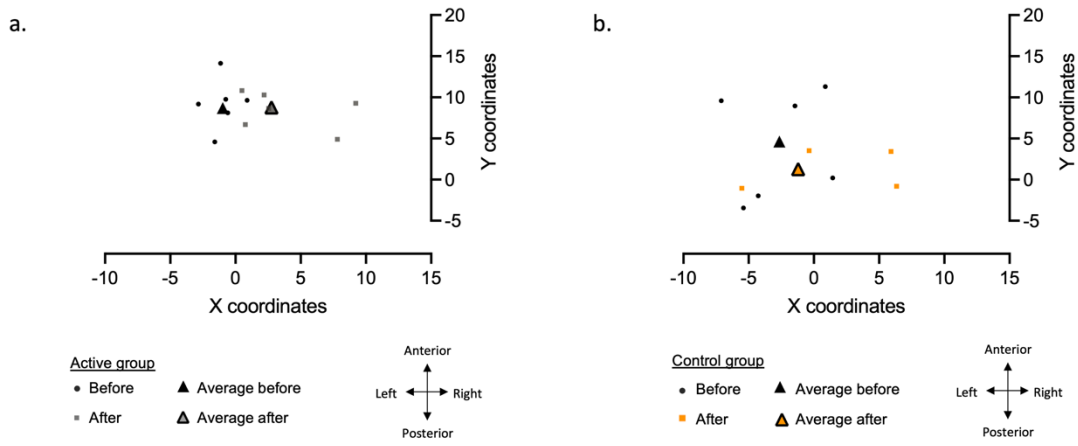

Note. See Table 6.2 for statistical results

6.3.2.3.1.2 APB

Means and standard deviations for APB 2D COG coordinates before and after iTBS are shown in Table 6.3, with an additional scatterplot including individual 2D COG coordinates in Figure 6.7.

In the active group, no significant differences were identified in two-tailed paired *t*-tests in the location of L-R COG coordinates ($t(6) = -0.43$, $p = 0.68$) or P-A coordinates ($t(6) = 0.06$, $p = 0.951$) of the APB map before and after active iTBS. Bayesian inference also provided anecdotal support for the null hypothesis (L-R COG $BF_{10} = 0.382$; P-A COG $BF_{10} = 0.354$). This suggests that active iTBS has no influence on APB map COG locations.

In the control group, two-tailed paired *t*-tests revealed no significant differences before and after control iTBS in the location of L-R COG coordinates ($t(6) = -0.50$, $p = 0.636$) or P-A COG coordinates ($W = 9$, $p = 0.844$). This was supported by Bayesian anecdotal evidence for the null hypothesis (L-R COG $BF_{10} = 0.391$; P-A COG $BF_{10} = 0.447$). This suggests that control iTBS has no influence on COG locations of the APB map.

Table 6.3

Means and standard deviations of TMS APB map 2D COG coordinates in active and control groups

	APB 2D COG coordinates			
	Active		Control	
Group	L-R	P-A	L-R	P-A
Pre	-0.39 (±3.52)	7.27 (±2.86)	-0.55 (±3.76)	4.56 (±5.70)
Post	0.42 (±3.93)	7.19 (±2.15)	0.04 (±5.28)	3.35 (±4.17)
N = Pre	7	7	7	6
N = Post	7	7	7	6

Note. APB = abductor pollicis brevis, COG = centre of gravity, *N* = number of participants, mean (±standard deviation). Differences before and after iTBS for all coordinates and groups are non-significant (two-tailed, $p > 0.05$)

Figure 6.7

Scatterplot of individual and mean APB map 2D COG coordinates before and after iTBS in the (a) active and (b) control group

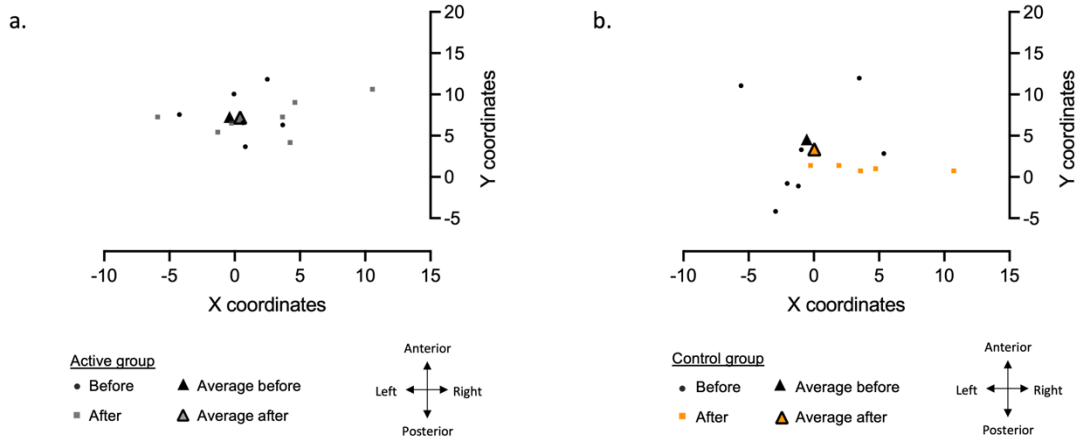

Note. See Table 6.3 for statistical results

6.3.2.3.1.3 ADM

Means and standard deviations for ADM 2D COG coordinates before and after iTBS are shown in Table 6.4, with an additional scatterplot including individual 2D COG coordinates in Figure 6.8.

The active group showed no significant differences before and after active iTBS in the location of ADM L-R COG coordinates ($t(4) = -0.41$, $p = 0.705$) or P-A COG coordinates ($t(6) = 0.004$, $p = 0.996$). This was supported with anecdotal evidence for the null hypothesis assessed with Bayesian statistics (L-R COG $BF_{10} = 0.426$; P-A COG $BF_{10} = 0.353$). This suggests that active iTBS has no influence on ADM map COG coordinates.

The control group also showed no significant differences before and after control iTBS, with Bayesian anecdotal support for the null hypothesis, in the location of ADM L-R COG coordinates ($t(6) = -0.84$, $p = 0.435$, $BF_{10} = 0.467$) and P-A COG coordinates ($t(4) = 1.16$, $p = 0.309$, $BF_{10} = 0.645$). This suggests that L-R COG and P-A COG coordinates of the ADM map did not change in response to control iTBS.

Table 6.4

Means and standard deviations of TMS ADM map 2D COG coordinates in active and control groups

	ADM 2D COG coordinates			
	Active		Control	
Group	L-R	P-A	L-R	P-A
Pre	0.12 (±1.33)	7.83 (±4.00)	-1.79 (±5.31)	4.13 (±6.02)
Post	0.67 (±1.80)	7.82 (±2.57)	-0.28 (±5.69)	1.67 (±2.39)
N = Pre	5	7	7	5
N = Post	5	7	7	5

Note. ADM = abductor digiti minimi, COG = centre of gravity, *N* = number of participants, mean (±standard deviation). Differences before and after iTBS for all coordinates and groups are non-significant (two-tailed, $p > 0.05$)

Figure 6.8

Scatterplot of individual and mean ADM map 2D COG coordinates before and after iTBS in the (a) active and (b) control group

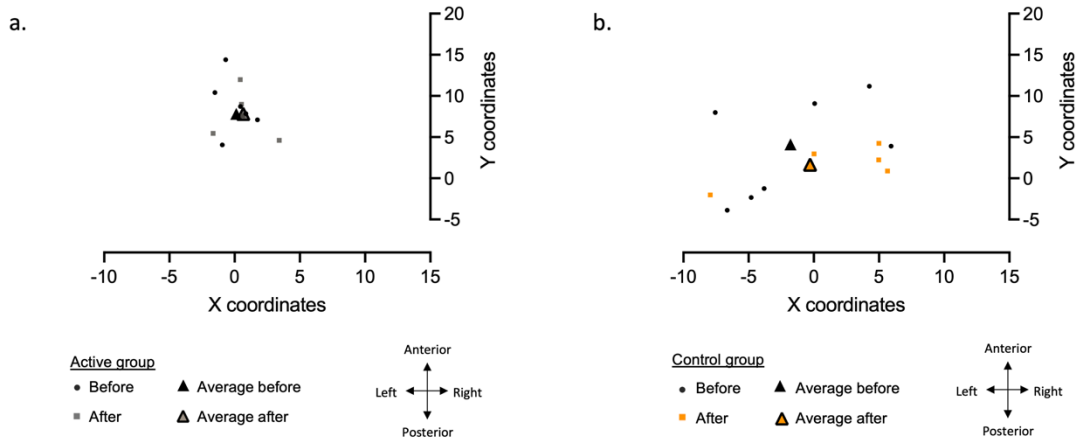

Note. See Table 6.4 for statistical results

6.3.2.3.2 2D COG coordinates: Between-group differences

One-tailed independent *t*-tests were conducted between active and control groups on the absolute change in L-R COG and P-A COG coordinates before and after iTBS. Mean and standard deviation of absolute changes are reflected in Figure 6.9.

Figure 6.9.

Means and standard deviations (error bars) of absolute change in (a) L-R COG and (b) P-A COG coordinates before and after iTBS in active and control groups

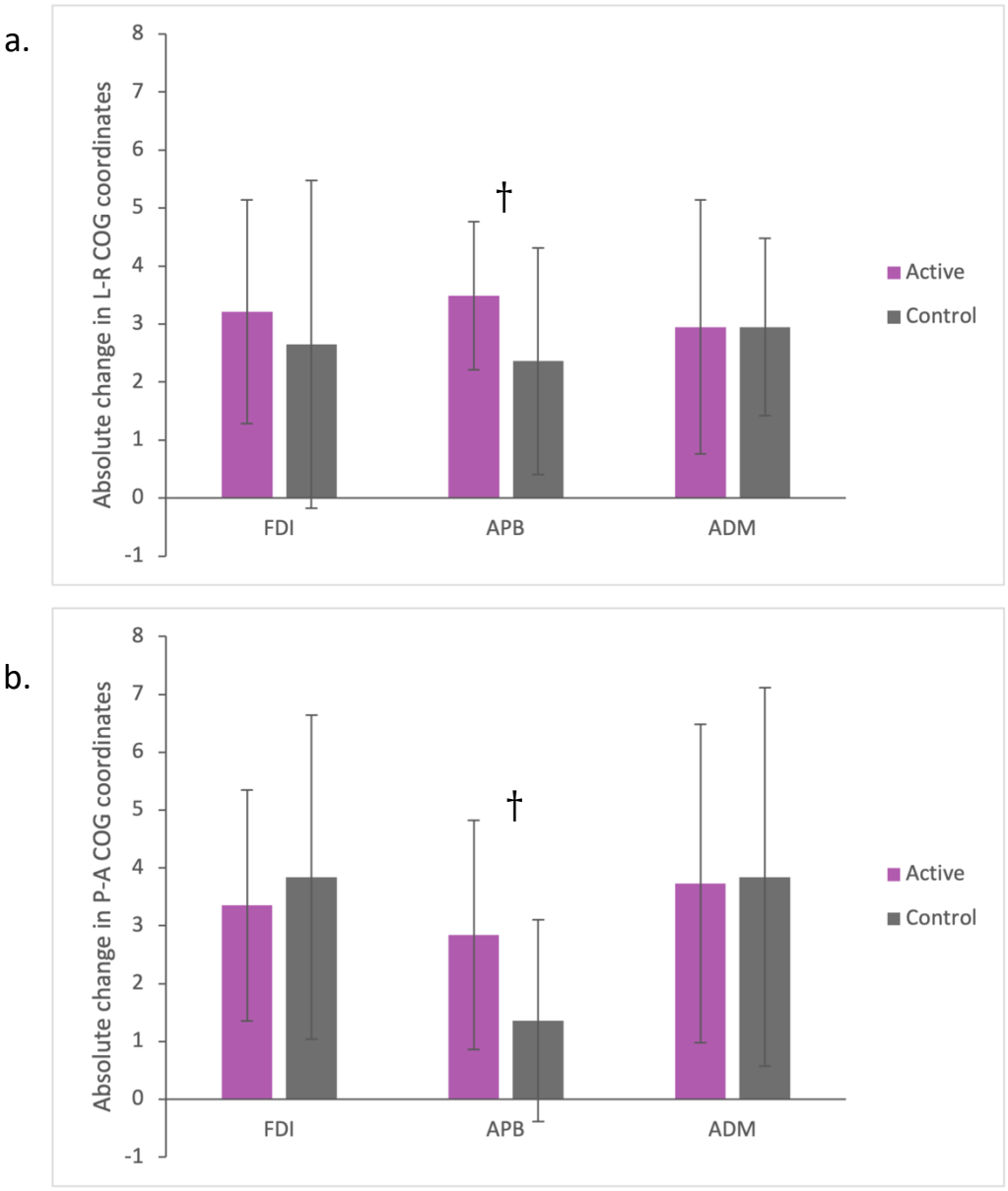

Note. FDI = first dorsal interosseous, APB = abductor pollicis brevis, ADM = abductor digiti minimi, COG = centre of gravity. † = anecdotal support for the alternative hypothesis. Group differences are non-significant (one-tailed, $p > 0.05$)

6.3.2.3.2.1 FDI

One-tailed independent *t*-tests revealed that the active group (*M* = 3.21, *SD* = 1.93) did not show significantly greater absolute change in FDI L-R COG coordinates in comparison to the control group (*M* = 2.65, *SD* = 2.83); *t*(11) = 0.421, *p* = 0.341. Bayesian evidence revealed anecdotal support for the null hypothesis (BF_{10} = 0.608). For the absolute change in FDI P-A COG coordinates, the active group (*M* = 3.35, *SD* = 2.00) did not show greater absolute change in comparison to the control group (*M* = 3.84, *SD* = 2.80), with anecdotal support for the null hypothesis; *t*(12) = -0.386, *p* = 0.647, BF_{10} = 0.359. This indicates that there are active iTBS does not influence the position of L-R COG or P-A COG coordinates of FDI maps more than control iTBS.

6.3.2.3.2.2 APB

The active group (*M* = 3.49, *SD* = 1.28) did not show significantly greater absolute change in APB L-R COG coordinates compared to the control group (*M* = 2.36, *SD* = 1.95); *t*(12) = 1.28, *p* = 0.112. However, Bayesian statistics revealed anecdotal support for the alternative hypothesis (BF_{10} = 1.261). For absolute changes in P-A COG coordinates between active (*M* = 2.84, *SD* = 1.98) and control groups (*M* = 1.36, *SD* = 1.74), no significantly greater absolute change was identified in the active group; *t*(12) = 1.45, *p* = 0.086. However, Bayesian statistics revealed anecdotal support for the alternative hypothesis (BF_{10} = 1.499). This provides some evidence to suggest that absolute changes in L-R COG and P-A COG positions were influenced by active iTBS more in comparison to control iTBS.

6.3.2.3.2.3 ADM

No significantly greater absolute changes in ADM L-R COG coordinates were identified in the active group (*M* = 2.95, *SD* = 2.19) compared to the control group (*M* = 2.95, *SD* = 1.53); *t*(12) = -0.001, *p* = 0.500. Absolute change in P-A COG coordinates in the active group (*M* = 3.73, *SD* = 2.75) were also not significantly greater compared to the control group (*M* = 3.84, *SD* = 3.27); *t*(13) = -0.07, *p* = 0.528. This was supported

with Bayesian inference, which provided anecdotal support for the null hypothesis (L-R COG BF_{10} = 0.448; P-A COG BF_{10} = 0.418). This suggests that active iTBS does not evoke a larger effect than control iTBS on L-R COG and P-A COG coordinates of ADM maps.

6.3.2.3.3 Euclidean distances: Within-group differences

The Euclidean distances of each TMS map COG coordinates in relation to other TMS map COG coordinates were assessed before and after active or control iTBS with two-tailed independent *t*-tests and Bayesian statistics. Means and standard deviations for each COG coordinate are shown in Table 6.5.

Table 6.5

Means and standard deviations of Euclidean distances between TMS map 2D COG coordinates in active and control groups

	Euclidean distances between 2D COG coordinates					
	FDI-ADM		APB-FDI		ADM-APB	
Timepoint	**Active** * †	**Control**	**Active**	**Control** * ††	**Active**	**Control**
Pre	1.48 (±0.69)	1.70 (±1.01)	2.85 (±1.29)	3.13 (±1.27)	2.82 (±1.14)	2.82 (±1.60)
Post	2.16 (±1.16)	1.94 (±0.83)	3.20 (±1.95)	1.22 (±0.33)	2.64 (±1.66)	1.65 (±0.66)
N = Pre	7	5	8	5	8	6
N = Post	7	5	8	5	8	6

Note. FDI = first dorsal interosseous, APB = abductor pollicis brevis, ADM = abductor digiti minimi, COG = centre of gravity, *N* = number of participants, mean (±standard deviation). * = $p < 0.05$, † = anecdotal evidence for the alternative hypothesis**,** †† = moderate evidence for the alternative hypothesis

6.3.2.3.3.1 FDI-ADM

In the active group, a two-tailed paired *t*-test revealed a significant difference in FDI Euclidean distances before and after iTBS with anecdotal evidence in support from Bayesian statistics (W = 2.00, p = 0.047, BF_{10} = 1.214). This suggests that the distances between FDI COG and ADM COG coordinates increased after active iTBS.

In the control group, no significant differences were identified between FDI Euclidean distances before and after control iTBS and Bayesian inference revealed anecdotal support for the null hypothesis ($t(4)$ = -0.30, p = 0.781; BF_{10} = 0.412). This suggests that Euclidean distances between FDI and ADM COG coordinates did not change in response to control iTBS.

6.3.2.3.3.2 APB-FDI

In the active group, no significant differences were revealed between APB Euclidean distances before and after active iTBS ($t(7)$ = -0.41, p = 0.693). This was supported by anecdotal evidence in Bayesian statistics for the null hypothesis (BF_{10} = 361). This provides evidence to suggest that the Euclidean distance between APB and FDI maps is comparable before and after active iTBS.

In the control group, a significant difference was revealed between APB-FDI Euclidean distances before and after control iTBS ($t(4)$ = 3.52, p = 0.024). This was supported by moderate evidence in Bayesian statistics for the alternative hypothesis (BF_{10} = 3.704). This provides evidence to suggest that the Euclidean distance between APB and FDI muscles is reduced after control iTBS.

6.3.2.3.3.3 ADM-APB

In the active group, no significant differences were identified between ADM Euclidean distances before and after active iTBS, with anecdotal support for the null hypothesis from Bayesian statistics; $t(7)$ = 0.26, p = 0.806, BF_{10} = 0.346. This suggests

that active iTBS does not alter Euclidean distances between ADM and APB COG coordinates.

Likewise, the control group showed no significant differences between ADM Euclidean distances before and after control iTBS, with Bayesian statistics providing anecdotal support for the null hypothesis; $t(5) = 1.56$, $p = 0.179$, $BF_{10} = 0.852$. This infers that control iTBS does not influence the Euclidean distances between ADM and APB COG coordinates.

6.3.2.3.4 Euclidean distances: Between-group differences

Absolute change in Euclidean distances between each TMS map pair were assessed between groups using one-tailed independent *t*-tests. Means and standard deviations are depicted in Figure 6.10.

Figure 6.10

Means and standard deviations (error bars) of absolute change in Euclidean distances before and after iTBS in active and control groups

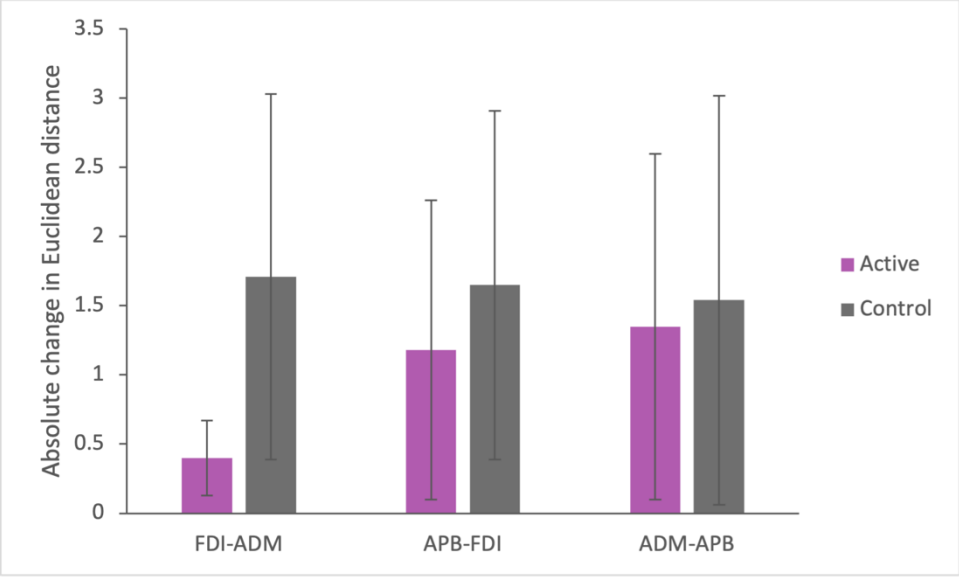

Note. FDI = first dorsal interosseous, APB = abductor pollicis brevis, ADM = abductor digiti minimi. Differences between groups are non-significant (one-tailed, $p > 0.05$)

6.3.2.3.4.1 FDI-ADM

No significantly larger absolute change in Euclidean distances between FDI and ADM maps in the active group were identified after a one-tailed independent t-test between the active (*M* = 0.40, *SD* = 0.27) and control group (*M* = 1.71, *SD* = 1.32); *t*(5.36) = -2.39, *p* = 0.970. Bayesian inference revealed moderate support for the null hypothesis (BF_{10} = 0.187). This suggests that the absolute change between Euclidean distances of FDI maps in relation to ADM maps were not significantly larger in the active iTBS group compared to the control group.

6.3.2.3.4.2 APB-FDI

The active group (*M* = 1.18, *SD* = 1.08) did not show significantly greater absolute change of Euclidean distances between APB and FDI maps when compared to the control group (*M* = 1.65, *SD* = 1.26) in the; *t*(11) = -0.722, *p* = 0.757. This was supported by Bayesian inference, which provided moderate evidence for the null hypothesis (BF_{10} = 0.312). This suggests that the absolute change between Euclidean distances of APB maps in relation to FDI maps were not significantly larger in the active iTBS group compared to the control group.

6.3.2.3.4.3 ADM-APB

The active group (*M* = 1.35, *SD* = 1.25) did not show significantly greater absolute change of Euclidean distances between ADM and APB maps compared to the control group (*M* = 1.54, *SD* = 1.48); *U* = 21, *p* = 0.669. This is supported by Bayesian inference which provided anecdotal support for the null hypothesis (BF_{10} = 0.385). As a result, this indicated that the absolute change between Euclidean distances of ADM maps in relation to APB maps were not significantly larger in the active iTBS group compared to the control group.

6.3.2.3.5 Area: Within-group differences

Two-tailed paired *t*-tests and Bayesian statistics were performed to assess the difference in the area of TMS maps before and after active or control iTBS. All means and standard deviations are shown in Table 6.6.

Table 6.6

Means and standard deviations of TMS map areas in active and control groups

	Area					
	FDI		APB		ADM	
Timepoint	**Active**	**Control**	**Active** †	**Control**	**Active**	**Control**
Pre	283.9 (±31.4)	294.3 (±28.8)	307.3 (±23.6)	307.8 (±14.0)	312.9 (±23.7)	297.1 (±20.8)
Post	296.4 (±20.4)	297.8 (±33.1)	312.6 (±29.0)	307.0 (±11.6)	315.00 (±22.2)	300.4 (±21.1)
N = Pre	8	6	8	6	7	7
N = Post	8	6	8	6	7	7

Note. FDI = first dorsal interosseous, APB = abductor pollicis brevis, ADM = abductor digiti minimi, *N* = number of participants, mean (±standard deviation). † = anecdotal evidence for the alternative hypothesis. Differences before and after iTBS for all coordinates and groups are non-significant (two-tailed, $p > 0.05$)

6.3.2.3.5.1 FDI

In the active group, no significant differences were identified between the area of the FDI map before and after iTBS, with Bayesian anecdotal support for the null hypothesis; $t(7) = -1.12$, $p = 0.298$, $BF_{10} = 0.551$. This suggests that active iTBS does not influence the area of FDI maps.

In the control group, no significant differences were identified between the area of the FDI map before and after iTBS, with Bayesian anecdotal support for the null hypothesis; $t(5) = -0.422$, $p = 0.690$, $BF_{10} = 0.402$. This indicates that control iTBS does not influence the area of FDI maps.

6.3.2.3.5.2 APB

For the area of the APB, no significant differences were identified before and after active iTBS; $t(7) = -2.35$, $p = 0.051$. However, Bayesian inference revealed anecdotal evidence in support of the alternative hypothesis ($BF_{10} = 1.875$), providing some evidence that the area of the APB map increased in response to active iTBS.

In the control group, no significant differences were revealed before and after control iTBS; $t(5) = 0.12$, $p = 0.912$. Bayesian statistics also supported the null hypothesis with anecdotal evidence ($BF_{10} = 0.375$). This suggests that the area of the APB in the control group were comparable before and after control iTBS.

6.3.2.3.5.3 ADM

The area of the ADM did not significantly differ before and after active iTBS; $t(6) = -0.27$, $p = 0.795$. Bayesian inference also supported this notion, with anecdotal evidence for the null hypothesis ($BF_{10} = 0.364$). This suggests that active iTBS does not influence the area of ADM maps.

For the control group, no significant differences were found between ADM maps before and after control iTBS, supported with anecdotal evidence for the null

hypothesis by Bayesian inference; $t(6) = -0.41$, $p = 0.696$, $BF_{10} = 0.379$. This provides evidence to suggest that control iTBS does not influence the area of ADM maps.

6.3.2.3.6 Area: Between-group differences

The absolute percentage change in the area in each TMS map were assessed between groups with one-tailed independent *t*-tests. Means and standard deviations are illustrated in Figure 6.11.

Figure 6.11

Means and standard deviations (error bars) of absolute percentage change in the area of TMS maps before and after iTBS in active and control groups

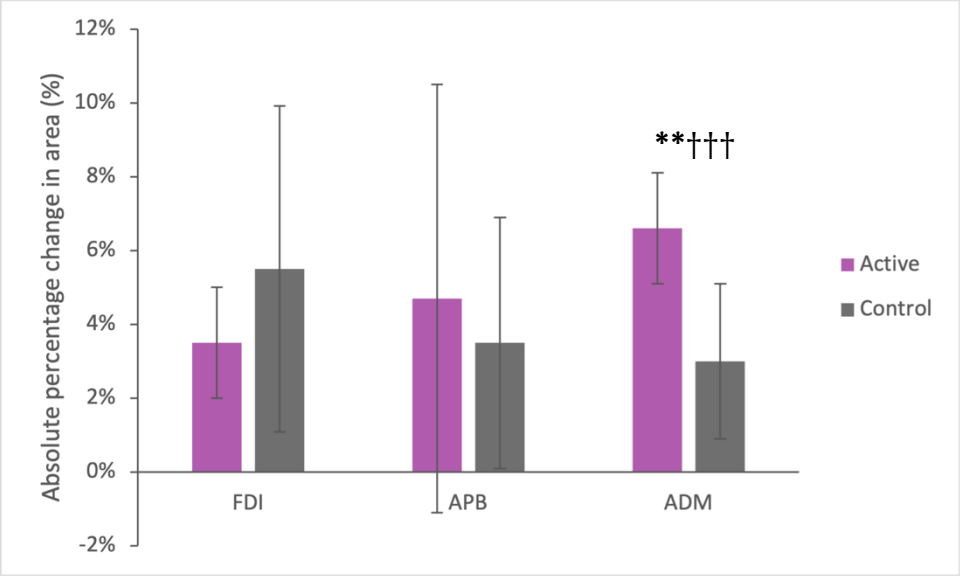

Note. FDI = first dorsal interosseous, APB = abductor pollicis brevis, ADM = abductor digiti minimi. ** = $p < 0.01$, ††† = strong evidence for alternative hypothesis

6.3.2.3.6.1 FDI

The absolute percentage change in the area of the FDI map was not significantly greater in the active group (*M* = 3.5%, *SD* = 1.5%) compared to the control group (*M* = 5.5%, *SD* = 4.41%); *t*(10) = -1.06, *p* = 0.843. Bayesian evidence provided moderate support for the null hypothesis (BF_{10} = 0.280). This suggests that active iTBS did not influence on FDI maps more than control iTBS.

6.3.2.3.6.2 APB

Absolute percentage changes in APB map areas were not significantly greater in the active group (*M* = 4.7%, *SD* = 5.8%) in comparison to the control group (*M* = 3.5%, *SD* = 3.4%), with Bayesian evidence providing anecdotal support for the null hypothesis (BF_{10} = 0.615). This suggests that active iTBS did not influence APB map areas more than control iTBS.

6.3.2.3.6.3 ADM

A significant difference was identified in the absolute percentage changes of ADM map areas between active (*M* = 6.6%, *SD* = 1.5%) and control group (*M* = 3.0%, *SD* = 2.1%); *t*(10) = 3.47, *p* = 0.003. Bayesian inference supported this with strong support for the alternative hypothesis; BF_{10} = 14.806. This strongly suggests that active iTBS has a larger effect on ADM map areas in comparison to control iTBS.

6.3.3 Discussion

Study 1 aimed to assess the influence of active and control iTBS on TMS measures of cortical excitability and inhibition, namely IO curve slopes and SICI, and cortical mapping of hand muscles after active or control stimulation.

6.3.3.1 Effect of iTBS on IO curve slopes

This study demonstrated that although IO curve slopes were generally steeper in response to active iTBS, this increase was not significant. This is likely due to the high variability seen within the data. However, Bayesian inference provided anecdotal support in the increase of IO curve slopes after active iTBS, providing some support for the notion that iTBS facilitates cortical excitability. In the control group, there was no significant change in IO curve slopes for the control group. Despite this, a significant difference was seen between the magnitude of change in slopes for active and control groups, suggesting that active iTBS has some facilitatory influence on cortical excitability (evidenced by an average 48.4% increase in IO curve slopes) compared to control iTBS (with an average 15.7% decrease in IO curve slopes). This result supports previous findings that iTBS may generally enhance M1 cortical excitability, but high interindividual variability in after-effects are evident (Chung et al., 2016; Huang et al., 2017; López-Alonso et al., 2018; Wischnewski & Schutter, 2015).

6.3.3.2 Effect of iTBS on SICI

In the active group, a significant increase in SICI values was demonstrated in response to active iTBS, indicative of a reduction in cortical inhibition. Bayesian statistics supported this effect with very strong evidence for the alternative hypothesis, providing support for the notion that active iTBS results in the reduction of cortical inhibitory functioning. This effect was not shown in the control iTBS group. This aligns with previous research who have demonstrated that 'excitatory' effects of high frequency rTMS (such as iTBS) are driven by a disruption in GABAergic inhibitory processing (Kozyrev et al., 2014, 2018; Ragert et al., 2004). This indicates that iTBS may be sufficient to induce changes in cortical motor mapping by altering cortical inhibitory processes involved in the maintenance of functional representations (Foeller et al., 2005; Jacobs & Donoghue, 1991; Kozyrev et al., 2014, 2018; Schneider et al., 2002; Sigurdsson, Molloy, et al., 2020; Zhong et al., 2021)

However, the differences in the percentage change in SICI values were not significantly greater in the active group (38.3%) compared to the control group (18.6%), though there was a trend towards significance. Again, it is possible that a difference was not evident due to the high variability within the data, as standard deviations in the active group were 51.2% and in the control group, 84.9%. On the other hand, methodology could explain changes observed in SICI after iTBS. After iTBS, SI1mV and RMT thresholds were not recalibrated to account for iTBS-induced changes, due to time constraints and the prioritisation of TMS mapping after iTBS. However, previous research has heavily stressed the dependence of SICI on the intensity of the TMS test pulse (Garry & Thomson, 2009; Roshan et al., 2003). Therefore, altering test pulses is essential as RMT/SI1mV thresholds may change after iTBS and subsequent post-iTBS SICI measures may not be accurate or comparable to pre-iTBS SICI measures. For instance, researchers have demonstrated that test pulse TMS intensities less than 110%RMT do not induce the inhibitory SICI response (Garry & Thomson, 2009). In the current study, test pulses were based on SI1mV thresholds, which are usually larger than 110%RMT. However, if these thresholds changed after iTBS, or even over time, then baseline SI1mV thresholds may no longer be sufficient to evoke the same extent of MEP inhibition. To provide confidence that the level of SICI induced inhibition of MEP amplitudes are consistent between groups, further investigation into the IO curve data is required to determine if SI1mV thresholds were above 110%RMT post-stimulation.

6.3.3.3 Effect of iTBS on TMS mapping

In the active group, some anecdotal support was evident for changed in the position of COG coordinates in the FDI only, however absolute changes in COG coordinates for FDI TMS maps were not significantly larger in the active group compared to the control group. However, additional anecdotal evidence was found supporting that absolute changes in COG coordinates of the APB TMS map was larger for the active group. This provides some evidence that active iTBS may influence the locations of COG coordinates for FDI and APB TMS maps after active iTBS, both close to the initial FDI site of stimulation.

For Euclidean distances between FDI and ADM TMS maps, two-tailed investigations revealed that distances differed before and after active iTBS, indicating an increase in distances. However, for APB-FDI maps in the control group, Euclidean distances significantly reduced after control iTBS. Moreover, the absolute change in Euclidean distances were not significant larger in the active group. This suggests that active iTBS likely has no influence on the distance between hand muscle representations.

For TMS map areas, there was Bayesian anecdotal evidence supporting an increase in APB map areas after active iTBS, suggesting that active iTBS may increase the corticospinal excitability of the APB hand muscle. However, the absolute percentage change in APB map areas was not significantly larger in the active group when compared to the control group. However, a significantly larger absolute percentage change was demonstrated in ADM TMS maps after active iTBS (6.6%) compared to control iTBS (3.0%), with strong Bayesian support. This demonstrates that while active iTBS may not show a larger influence on FDI or APB map areas, it has shown a significantly larger effect on ADM maps.

However, the changes evoked in TMS maps may be unreliable, due to the low sample size of each group and the known variability in response to rTMS protocols (Chung et al., 2016; Huang et al., 2017; López-Alonso et al., 2018; Wischnewski & Schutter, 2015). Moreover, the methods in collecting TMS maps, although chosen to prioritise the fast collection of TMS maps after iTBS, may have been problematic. Specifically, the TMS coil was consistently angled 45 degrees from the midline (current flowing posterior-anterior direction) during mapping protocols. However, while this angle is optimal for evoking MEPs in the FDI and APB hand muscles (Adank et al., 2018), this may not be optimal for the ADM muscle which has previously been shown to evoke optimal MEP responses between 0 and 45 degrees from the midline (Bashir et al., 2013). Nevertheless, as angles were kept consistent in mapping before and after iTBS, nuances in cortical maps should be comparable before and after iTBS.

Moreover, as hand maps were restricted to a 5 x 5 cm grid surrounding the FDI hotspot, this was not always sufficient to record the extent of APB and ADM muscle map, with some maps showing activation at edges of the grid. Additionally, the intensity used during mapping was based on 120%RMT of the FDI hand muscle, and while RMTs have previously been found to be similar across FDI, APB and ADM muscles (Kaelin-Lang et al., 2002; Ziemann, 2004), RMTs were not measured for each muscle. This could have amplified or diminished differences the spread of corticospinal excitability in APB/ADM maps if RMT for these muscles are different, as this will produce MEP responses of different sizes. However, although it may be more consistent to collect TMS maps from one muscle at a time at specific angles and use individual RMTs for each map RMTs, this could be problematic due to the transient nature of iTBS and therefore any iTBS-induced effects could disappear before each TMS map is collected. However, rTMS-induced effects to cortical mapping, though transient, may last as long as two hours (Pleger et al., 2006; Tegenthoff et al., 2005). As a result, for this study, where rapid collection of TMS maps was prioritised, results should be taken with caution.

Overall, Study 1 has provided strong evidence that active iTBS can induce reductions in GABAergic intracortical inhibitory processes, as measured with SICI. Moreover, there is some evidence to suggest that IO curve slopes become steeper after active iTBS. However, there is only anecdotal evidence to suggest that active iTBS induces changes in cortical mapping of hand muscles, including those beyond the target FDI site. As this evidence is not consistent across within- and between-group statistics, it cannot be concluded that active iTBS can alter cortical representations, despite altering GABAergic mechanisms. A larger cohort of participants is also required in order to account for the vast variability in iTBS-induced responses. This will also allow for investigation into relationships between iTBS-induced disruptions in inhibition with alterations in TMS maps.

6.4 Study 2

This study aimed to assess the influence of active and control iTBS on fMRI-measured cortical representations of the digits.

6.4.1 Methods

6.4.1.1 Participants

Twenty-one healthy right-handed participants took part in Study 2, with an initial recruitment aim of ten participants per condition. This could not be extended due to COVID-19 restrictions and 7T MRI funding limitations. One participant was removed from the control group due to a diagnosis of ADHD. Participants gave informed consent and ethics were approved by the local ethics committee (School of Psychology, University of Nottingham: F1095). No remaining participants were taking CNS-active drugs and were free from any mood or neurological illness during the experimental timeline. Ten participants were assigned to the active condition and ten participants were assigned to the control condition.

Demographic information is displayed in Table 6.7 for active and control groups. Age ($U = 45.5$, $p = 0.762$) and sex (X^2 (1, $N = 20$) = 0.392, $p = 0.531$) distributions were not significantly different between groups. All participants were free from any contraindications for MRI and TMS, as assessed by completion of MRI and TMS safety screening forms. All participants were right-handed as assessed by the Edinburgh handedness questionnaire (Oldfield, 1971).

Table 6.7

Demographic information of active and control groups in Study 2

Group	N	Age	Sex
Active	10	23.26 (±3.4)	1 male, 9 female
Control	10	23.19 (±4.4)	2 male, 8 female

Note. N = number of participants, mean (±standard deviation)

6.4.1.2 MRI Data Acquisition

All MRI data was acquired on a 7T Philips Achieva MRI Scanner with a 32-channel head coil at the Sir Peter Mansfield Imaging Centre at the University of Nottingham.

6.4.1.2.1 fMRI mapping paradigm

Two travelling wave fMRI task blocks were acquired with participants visually instructed to tap their right (dominant) hand digit 1 (D1; thumb) at 2Hz for 4 seconds in time with visual presentation (shown in Figure 6.12b). This was followed by digit 2 (D2), digit 3 (D3), digit 4 (D4), and digit 5 (D5) in the "forward" condition resulting in a block length of 20 s, this was repeated for 8 cycles. The second fMRI run was completed with the same tapping timings, but performed in reverse (tapping D5 first, then D4, D3, D2 and D1). All digits were assessed as iTBS effects have been shown to extend beyond the initial FDI (D1) site of stimulation (Morris et al., 2019).

Each travelling wave task block was visually presented using Presentation software (Neurobehavioral Systems, Inc.) on a projector screen visible to the participant with Prism glasses. Participants were trained in tapping prior to scanning. Participants were instructed to tap with their right hand rested on their right leg.

The two fMRI runs were conducted using a single-shot 2D T2*-weighted gradient-echo echo-planar-imaging (EPI) sequence (voxel 1.5 mm isotropic, matrix size = 128 x 128 x 26, TR/TE = 2000/25 ms, 2.52 minute acquisition time per run). After fMRI runs, two additional short scans (5 dynamics) with the same acquisition parameters, but opposing fat shift direction, were collected for EPI distortion correction.

6.4.1.2.2 T1-weighted MRI parameters

Prior to the fMRI runs, an anatomical T1-weighted 3D gradient echo PSIR scan was acquired conducted on a 7T Philips Achieva MRI Scanner with a 32-channel head coil (matrix size = 320 x 320, FOV = 224 x 224 x 157 mm, 0.7mm isotropic, 224 slices, TR/TE = 6.3/2.7 ms, flip angle = 5^{o}, acquisition time = 6.15 minutes), with two turbo field echo (TFE) readouts after each inversion pulse at TI1 = 780 ms and TI2 = 2380 ms. This was collected for co-registering with the fMRI runs and with standard template space images to allow for comparison across participants.

6.4.1.3 iTBS Parameters

iTBS was conducted using a Magstim Rapid2 system (Dyfed, UK), with a 70mm figure-of-eight coil. iTBS parameters for active and control groups are identical to those shown in Section 6.3.1.4.

Before delivering pulses to the scalp, participants had the opportunity to ask questions and feel a test pulse of TMS on the palm of their hand once the procedure was explained to them. Once participants were ready to begin, suprathreshold pulses were delivered to the left M1 hand area 'hotspot', defined as the location that consistently evoked the largest MEPs in the right FDI muscle. Coil orientation was maintained at 45 degrees from the midline with current flowing in a posterior-anterior direction, which has been shown to evoke optimal MEP responses in the FDI muscle (Adank et al., 2018). RMT was also measured and was defined as the TMS stimulation intensity (%MSO) needed to evoke a visible twitch in the FDI muscle in ~ 5 out of 10 trials.

6.4.1.4 Procedure

The experimental procedure for this study is illustrated in Figure 6.12. The time between iTBS application and the start of the after iTBS fMRI travelling wave run

were not significantly different between active (*M* = 8.21, *SD* = 1.41) and control (*M* = 8.19, *SD* = 1.05) groups; *t*(17) = 0.032, *p* = 0.974.

Figure 6.12

(a) Procedure for Study 2 with (b) travelling wave tapping task paradigm

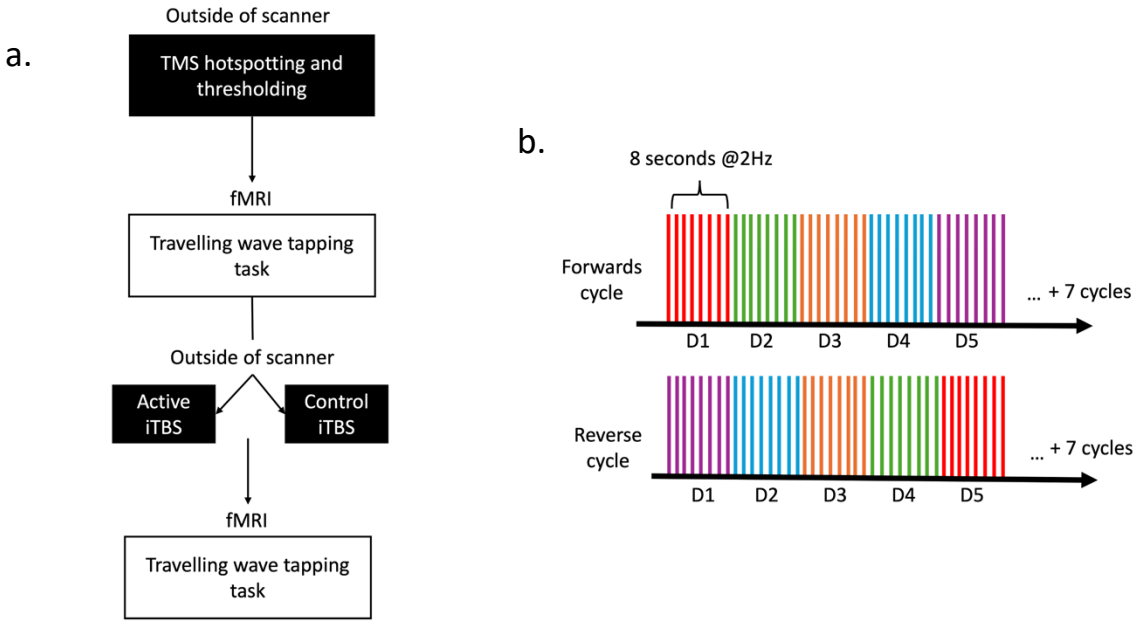

Note. TMS = transcranial magnetic stimulation, fMRI = functional magnetic resonance imaging, iTBS = intermittent theta burst stimulation, D*x*= Digit. Active and control iTBS parameters are listed in Section 6.3.1.4

6.4.1.5 Data analysis

Data analysis of T1-weighted images and fMRI runs were the same as described in Chapter 4 (Section 4.3.3), with an additional digit (D1) measured in this study. This means that in pre-processing, high-pass temporal filtering was set to 20 s and all travelling wave runs before and after iTBS were aligned to the same native space in each individual to allow comparison across the same individual. Individual

digits were extracted by dividing phase maps into 5 bins, one for each digit. Results were masked over the left M1 (BA 4).

Due to the low sample size and to preserve as much data as possible, fMRI images that were contaminated by brief periods of large motion displacement (>1.5mm) for up to 2 cycles had these cycles removed using FSL UTILS functions (Jenkinson et al., 2012). At the before iTBS timepoint in the active group, P08 had the seventh cycle of each travelling wave run removed, P12 had the second cycle of each travelling wave run and at the after iTBS timepoint in the control group, P16 had the third cycle removed from each travelling wave run. Each of these participants had a resulting total of 7 cycles per travelling wave run.

6.4.1.5.1 Digit ROI metrics

To quantitatively characterise each participant's digits, voxel counts and 3D coordinates of the COG were extracted for each digit ROI for each participant before and after iTBS, using FSL functions in FSLUTILS (Jenkinson et al., 2012). 3D COG coordinates are defined in three directions; x (left (-) to right (+), L-R), y (posterior (-) to anterior (+), P-A) and z (inferior (-) to superior (+), I-S).

As datasets were thresholded at an individual level prior to extraction of digits, voxel counts will vary between individuals. To account for this, ratios for each digit ROI were calculated, using Equation 6.2, to quantify the proportion of voxels assigned to each digit within individuals.

$$Dx_{Ratio} = \frac{nDx}{(nD1+nD2+nD3+nD4+nD5)} \quad (6.2)$$

where nDx is the number of voxels assigned to the digit in question and $nD1+ nD2 + nD3$ … is the total number of voxels for all digits. This gives an insight into the size of each digit ROI in comparison to other digits within M1 for each individual and allows for comparison across groups.

To determine any alterations in the COG of each digit ROI from baseline after active- and control-iTBS, the Euclidean distances (d) were calculated. 3D COG coordinates are used to calculate Euclidean distances between each digit ROI before and after iTBS, expressed in Equation 6.3.

$$d = \sqrt{(x2 - x1)^2 + (y2 - y1)^2 + (z2 - z1)^2} \quad (6.3)$$

where $x2$, $y2$, $z2$ are coordinates from the before iTBS 3D COG coordinates of one digit and $x1$, $y1$, $z1$ are coordinates from the after iTBS 3D COG coordinates of the same digit.

Any datapoint outside 1.5x the IQR above the third quartile or 1.5x the IQR below the first quartile were classed as an outlier and removed from further analyses. These are specified in Appendix D.2.

Pre-analysis independent *t*-tests were conducted to highlight any significant differences between groups in average digit ratios before iTBS. A significant difference was apparent in D2 digit ratios between groups ($t(13.2) = -2.37$, $p = 0.034$). Therefore, before and after iTBS digit ratios and Euclidean distances for each group were normalised using the min-max scaling method, outlined in Equation 6.3:

$$x' = \frac{x - \min(x)}{\max(x) - \min(x)} \quad (6.3)$$

where x' is the normalised value, x is the original value, $\min(x)$ is the minimum value in the group and $\max(x)$ is the maximum value in the group.

6.4.1.6 Statistical analysis

To assess within-group differences, two-tailed paired *t*-tests were then conducted to detect any significant differences in digit ratios between pre-stimulation and post-stimulation in active-iTBS and control-iTBS groups. Two-tailed tests were

implemented as the direction of change in each digit ratio before and after iTBS in each group is not clear.

To assess between-group differences, absolute percentage change was calculated between raw digit ratios before and after iTBS for each digit for each group. Digit ratio change was converted into absolute values to assess the magnitude of change in digit map properties between each group, rather than the direction of change. With these, one-tailed independent *t*-tests were conducted to determine any significant differences in the absolute percentage change in digit ratios between active and control groups. One-tailed tests were conducted as it is hypothesised that the active group will display a larger change in response to iTBS compared to the control group. Min-max scaled Euclidean distances between before and after iTBS digit ROIs were also input into two-tailed independent *t*-tests to compare between active and control groups (i.e. before iTBS D1 and after iTBS D1, before iTBS D2 and after iTBS D2, etc.). Two-tailed tests were implemented as the direction of change in digit ROI COG coordinates before and after iTBS is not clear.

Where data did not pass normality checks, independent *t*-tests were replaced with non-parametric Mann-Whitney *U* tests and paired *t*-tests were replaced with non-parametric Wilcoxon signed-rank test. BF_{10} was used with a Cauchy distribution with a scale of γ = 0.707 used as the prior distribution. Interpretation of BF_{10} values are shown in Table 3.2 (Rouder et al., 2009). All statistical analyses were conducted using jamovi (v 2.3.28; jamovi.org).

6.4.2 Results

No side effects in response to TMS were reported.

6.4.2.1 Digit ratios: Within-group differences

Two-tailed paired *t*-tests were conducted between min-max normalized digit ratios before and after iTBS in each group. Means, standard deviations and associated statistics are presented in Table 6.8.

In the active group, no significant differences were identified before and after active iTBS, suggesting active iTBS did not influence digit ratios for any digit. However, Bayesian inference detected anecdotal evidence for the alternative hypothesis in the active group between before and after iTBS D3 ratios (BF_{10} = 1.163). This provides some evidence to suggest that the proportion of voxels assigned to D3 was greater after active iTBS.

In the control group, no significant differences were identified before and after control iTBS, suggesting that the proportion of voxels assigned to each digit does not change after control iTBS.

Table 6.8

Means, standard deviations and statistics of min-max normalised digit ratios before and after iTBS in active and control groups

	Digit ratios (min-max normalised)									
	Active					Control				
Timepoint	**D1**	**D2**	**D3**	**D4**	**D5**	**D1**	**D2**	**D3**	**D4**	**D5**
Pre	0.43 (±0.33)	0.60 (±0.35)	0.51 (±0.31)	0.48 (±0.35)	0.46 (±0.32)	0.35 (±0.36)	0.50 (±0.35)	0.44 (±0.39)	0.42 (±0.34)	0.52 (±0.35)
Post	0.31 (±0.31)	0.36 (±0.31)	0.25 (±0.32)	0.43 (±0.35)	0.61 (±0.33)	0.30 (±0.29)	0.37 (±0.34)	0.29 (±0.34)	0.47 (±0.35)	0.38 (±0.36)
N = Pre N = Post	9 9	7 7	8 8	9 9	8 8	9 9	10 10	10 10	10 10	10 10
	$t(8) = 0.91$ $p = 0.388$	$t(6) = 1.49$ $p = 0.187$	$t(7) = 1.91$ $p = 0.098$	$t(8) = 0.37$ $p = 0.723$	$t(7) = -1.23$ $p = 0.259$	$t(8) = 0.32$ $p = 0.755$	$t(9) = 0.95$ $p = 0.365$	$W = 26.0$ $p = 0.722$	$t(9) = -0.42$ $p = 0.684$	$t(9) = 0.83$ $p = 0.43$
	$BF_{10} = 0.452$	$BF_{10} = 0.780$	$\mathbf{BF_{10} = 1.163}^{\dagger}$	$BF_{10} = 0.341$	$BF_{10} = 0.600$	$BF_{10} = 0.336$	$BF_{10} = 0.449$	$BF_{10} = 0.505$	$BF_{10} = 333$	$BF_{10} = 0.410$

Note. D*x*= Digit, *N* = number of participants. † = anecdotal evidence for alternative hypothesis, mean (±standard deviation). Differences before and after iTBS for all digit ratios and groups are non-significant (two-tailed, $p > 0.05$)

6.4.2.2 Digit ratios: Between-group differences

One-tailed independent *t*-tests were conducted between active and control groups to assess the absolute percentage change in digit ratios before and after iTBS.

One-tailed independent *t*-tests demonstrated significant differences between groups in the percentage change in digit ratios ($p > 0.07$). However, Bayesian statistics provided anecdotal evidence for the alternative hypothesis in the absolute percentage change in D1 ratios and in D5 ratios. This provides some evidence to suggest that the change in digit ratios before and after iTBS is greater in the active group than the control group. Means and standard deviations and all statistics are displayed in Table 6.9. Means and standard deviations are illustrated in Figure 6.13.

Table 6.9

Means, standard deviations and associated statistics of absolute percentage change in raw digit ratios before and after iTBS in active and control groups

	Absolute percentage change in digit ratios				
Group	**D1**	**D2**	**D3**	**D4**	**D5**
Active	61.6% (±21.8%)	54.1% (±40.7%)	45.0% (±25.4%)	52.4% (±35.7%)	63.2% (±40.7%)
Control	42.3% (±27.9%)	52.9% (±27.6%)	85.0% (±75.2%)	37.1% (±34.9%)	39.1% (±36.1%)
N = Active N = Control	8 9	8 8	8 9	8 9	10 9
	$t(15) = 1.57$ $p = 0.068$ $\mathbf{BF_{10} = 1.678}$ †	$t(14) = 0.07$ $p = 0.471$ $BF_{10} = 0.448$	$U = 25$ $p = 0.862$ $BF_{10} = 0.214$	$t(15) = 0.89$ $p = 0.193$ $BF_{10} = 0.839$	$t(17) = 1.36$ $p = 0.097$ $\mathbf{BF_{10} = 1.303}$ †

Note. D*x*= Digit, *N* = number of participants. † = anecdotal evidence for alternative hypothesis, mean (±standard deviation). Differences before and after iTBS for all digit ratios and groups are non-significant (one-tailed, $p > 0.05$)

Figure 6.13

Mean and standard deviations (error bars) of absolute percentage change in digit ratios before and after iTBS in active and control groups

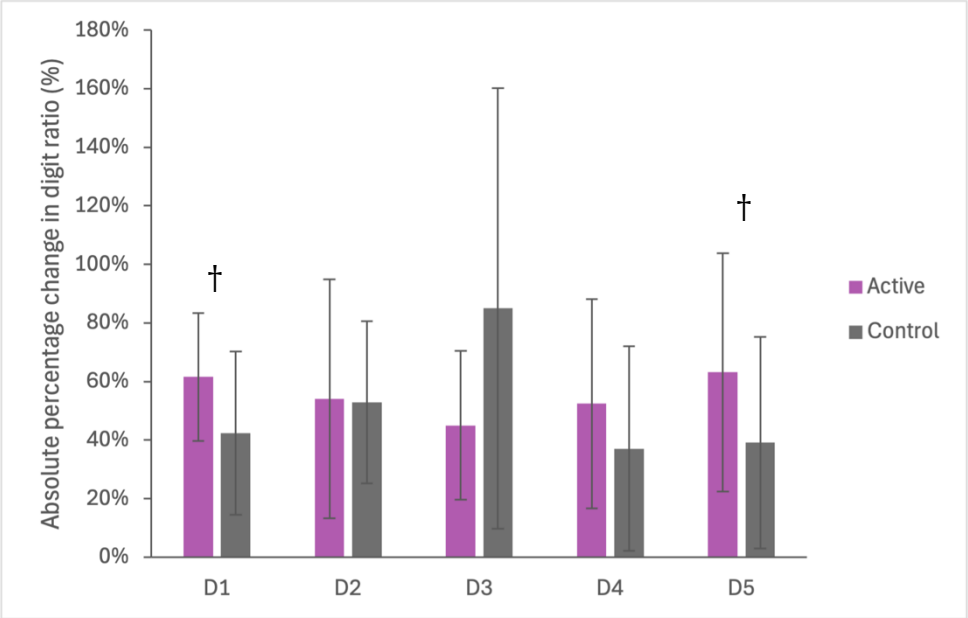

Note. D*x* = Digit. † = anecdotal evidence for alternative hypothesis. Group differences are non-significant (one-tailed, $p > 0.05$)

6.4.2.3 Euclidean distances: Between-group differences

Two-tailed independent *t*-tests were conducted between active and control groups to assess Euclidean distances between 3D COG coordinates before and after iTBS.

No significant differences were identified in Euclidean distances between 3D COG coordinates before and after active or control iTBS in D1, D2, D3 or D4 digit ROIs (all $p > 0.47$). This was supported with Bayesian statistics, which provided anecdotal evidence for the null hypothesis across all groups. However, significant differences were identified between active and control group in Euclidean distances between D5 3D COG coordinates. This was supported by Bayesian inference of anecdotal support

for the alternative hypothesis. This suggests that Euclidean distances between D5 3D COG coordinates are further from baseline after control iTBS compared to active iTBS. Means and standard deviations are illustrated in Figure 6.14 and all statistics are displayed in Table 6.10.

Table 6.10

Means, standard deviations and associated statistics of Euclidean distances between digit 3D COG coordinates before and after iTBS in active and control groups

	Euclidean distances between 3D COG coordinates before and after iTBS (mix-max normalised)				
Group	**D1-D1**	**D2-D2**	**D3-D3**	**D4-D4**	**D5-D5**
Active	0.43 (±0.32)	0.41 (±0.38)	0.36 (±0.37)	0.31 (±0.33)	0.36 (±0.33)
Control	0.51 (±0.32)	0.42 (±0.39)	0.35 (±0.31)	0.52 (±0.41)	0.65 (±0.36)
N = Active N = Control	10 9	9 10	9 10	9 9	9 7
	$t(17) = -0.54$ $p = 0.596$	$t(17) = -0.10$ $p = 0.921$	$U = 43$ $p = 0.902$	$U = 29$ $p = 0.331$	$t(14) = -1.68$ $p = 0.114$
	$BF_{10} = 0.448$	$BF_{10} = 0.406$	$BF_{10} = 0.405$	$BF_{10} = 0.690$	$\mathbf{BF_{10} = 1.058}$ †

Note. D*x*= Digit, *N* = number of participants, COG = centre of gravity, mean (±standard deviation). † = anecdotal evidence for alternative hypothesis. Group differences are non-significant (two-tailed, $p > 0.05$)

Figure 6.14

Mean and standard deviations (error bars) of Euclidean distances between digit ROIs before and after iTBS in active and control groups

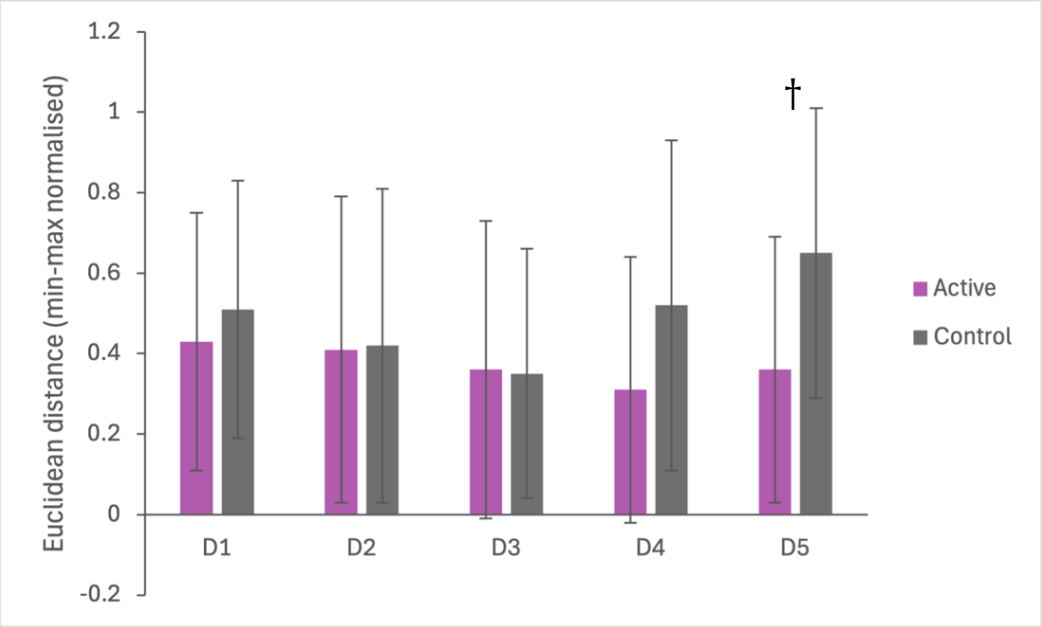

Note. Dx= Digit. † = anecdotal evidence for alternative hypothesis. Group differences are non-significant (two-tailed, $p > 0.05$)

6.4.3 Discussion

Study 2 aimed to assess the influence of active and control iTBS on the cortical representations of digits as assessed with fMRI, with metrics including digit ratios and Euclidean distances between digits before and after iTBS.

For digit ratios, the active group displayed anecdotal evidence for a reduction in voxels associated to D3 after iTBS, suggesting that the D3 representation reduced in relation to other digits. However, this was not evident in between-group analyses, suggesting that any changes in D3 representations due to active iTBS were not larger than that of control iTBS. Moreover, there was anecdotal evidence for a greater absolute percentage change in D1 digit ratios after active iTBS (61.6%) compared to control iTBS (42.3%), and in D5 digit ratios between active (63.2%) and control groups (39.1%). However, while changes may be larger for these digits in the active group, changes in digit ratios after control iTBS are still evident and there was large variability within each group. This suggests that the digit ratios are not an ideal measure of assessing the size of each digit representation in relation to other digits, as these may be highly variable measures over time.

In the control group, there was evidence of greater Euclidean distances between D5 COG coordinates before and after control iTBS in comparison to active iTBS. This indicates that control iTBS may induce a shift in D5 digit representations while digit representations after active iTBS are generally stable. However, previous research has indicated little agreement in individual D5 representations over time, and therefore the differences identified in Euclidean distances may reflect the individual variability of the D5 representation (O'Neill et al., 2020)

Limitations of the methods in Study 2 are evident and similar to those described in Chapter 4. A travelling wave design was chosen as it is a fast acquisition fMRI method which would therefore allow for the rapid measurement of digit representations after iTBS, which has transient after-effects. However, as discussed in Chapter 4, phase-encoding travelling wave fMRI designs are insensitive to the

overlapping of representations due to the 'winner-takes-all' analyses (Besle et al., 2013). As a result, any blurring of digit ROIs that may have been induced by iTBS could not be assessed in this study. Additionally, the digit ratio metric is a highly variable measure within individuals over time and was initially calculated as the number of voxels extracted for each digit was not comparable across individuals. This is because thresholding of digit maps was completed individually for each participant. However, as the number of voxels assigned to each digit was calculated using the 'winner-takes-all' measure of phase-encoded travelling wave analyses (see Section 4.3.3.2.2), there is likely some level of variation in the exact number of voxels assigned to each digit at each timepoint. The digit ratio metric could also have been influenced by the predictive, sequential nature of the tapping task, which shows greater and more widespread activation in the sensorimotor cortices compared to a random-order tapping task and vibrotactile task (Olman et al., 2013; Mastria et al., 2023). This made it difficult to separate digits in analysis and resulted in some digits dominating digit maps, which were more evenly spread in the random-order and vibrotactile tasks (Mastria et al., 2023; Olman et al., 2012). Consequently, future research should use block or event-related vibrotactile tasks in order to more accurately quantify the size of digit representations in M1 within each individual, and give insight to the blurring of maps, as 'winner-takes-all' analyses would be redundant.

Overall, this study suggests that there are great variations in fMRI digit maps across time in both active and control groups when measured using a phase-encoded travelling wave design. Coupled with the known variability in response to iTBS (Chung et al., 2016; Huang et al., 2017; López-Alonso et al., 2018; Wischnewski & Schutter, 2015), it is unclear if the differences detected in digit maps iTBS are a result of active iTBS itself, or the variability in digit maps over time. Future research should employ block or event-related fMRI tasks in order to more accurately detect any differences in digit representations after iTBS. Although these fMRI tasks would take longer to require, rTMS-induced changes in somatosensory representations have previously lasted up to two hours after rTMS application (Pleger et al., 2006; Tegenthoff et al., 2005) and these fMRI tasks would offer greater confidence in any differences

detected after active iTBS, with additional metrics, such as overlap and size of representations.

6.5 Conclusions

Overall, this chapter demonstrates that in comparison to control iTBS, active iTBS increases cortical excitability as measured by IO curve slopes, and reduces GABAergic inhibitory mechanisms as measured with TMS-SICI, though responses are variable. However, while inhibitory mechanisms thought to play a role in the maintenance of cortical representations are disrupted (Foeller et al., 2005; Jacobs & Donoghue, 1991; Schneider et al., 2002; Sigurdsson, Molloy, et al., 2020), the extent to which active iTBS influences the integrity of cortical mapping can be questioned. While some differences in cortical TMS and fMRI maps of different hand muscles and digits were detected after active iTBS, there is great variation and inconsistencies between active and control groups. Overall, due to the low number of participants per group indicating low statistical power, coupled with variability within and between groups and methodological limitations of travelling wave designs, it cannot be concluded with confidence that active iTBS can reliably disrupt cortical representations.

Additionally, iTBS as a method of rTMS may not be sufficient to disrupt cortical representations. As previous human and animal research has indicated, 5-20Hz rTMS can interrupt cortical map integrity (Houzé et al., 2013; Kozyrev et al., 2014, 2018; Pleger et al., 2006; Tegenthoff et al., 2005; Zhong et al., 2021). However, one study has indicated that 20Hz rTMS may more effectively disrupt cortical representations in comparison to iTBS, as 20Hz matches intrinsic M1 frequencies, which oscillate around 20Hz (Houzé et al., 2013). Subsequently, this questions the mechanisms involved in the stability and maintenance of cortical representations. While disruptive of GABAergic mechanisms, iTBS may not disrupt the specific mechanisms pertaining to the integrity of cortical representations. However, as individual GABA/SICI levels were not measured across both studies or directly correlated in relation to changes in cortical representations, the relationship between individual GABA and cortical mapping after-effects cannot be determined.

7. Chapter 7 - General discussion

This thesis has explored inhibitory functioning and its relationship to somatosensory processing in adults with TS and TD controls. Cortical sensorimotor representations of the digits and face have also been examined in adults with TS, in comparison to TD controls, utilising the multimodal neuroimaging methods MRS, fMRI and TMS. Finally, the impact of rTMS on TMS and fMRI cortical motor representations were also explored.

This chapter will summarise the findings of this thesis to answer research aims indicated in Section 1.5, in three sections, with limitations and considerations for future research:

Section 7.1 - Inhibitory functioning and somatosensory processing in TS

- Do measures of cortical inhibition and sensory processing differ between TS and TD controls? Are these measures correlated in both groups? Do tic and urge features correlate with these measures?

Section 7.2 - Sensorimotor representations of the digits and face in TS

- Do fine-grained sensorimotor representations of non-tic-related movements (finger tapping) differ between TS and TD controls?
- Do sensorimotor functional representations of tic-related facial movements and responses to low-frequency vibration of facial areas differ between TS and TD controls?

Section 7.3 - Disrupting cortical representations with iTBS.

- Can functional representations be manipulated with rTMS?

7.1 Inhibitory functioning and somatosensory processing in Tourette Syndrome

Abnormalities in sensory processing are commonly experienced in TS (Isaacs & Riordan, 2020). However, while research has addressed interoceptive PU domains of sensory processing, exteroceptive alterations have been greatly neglected despite being the self-reported cause of considerable discomfort for individuals with TS (Isaacs & Riordan, 2020).

One physiological mechanism thought to be disrupted in TS, which is theorised to be responsible for abnormalities in sensory processing, is that of cortical inhibition and GABA. Differences in sensory processing and performance in quantitative tactile tasks are thought to depend on individual levels of GABA and surround inhibition; with greater levels thought to shape cortical neuron responses by enhancing receptive field size and activation thresholds in response to peripheral stimulation (Chowdhury & Rasmusson, 2002; Hicks & Dykes, 1983; Kaneko & Hicks, 1990; Oka et al., 1986). Enhanced tonic GABAergic inhibition has also been linked to sensory processing by enhancing sensorimotor network integration and tuning cortical activity (Cassady et al., 2019; Kolasinski et al., 2017).

In TS, MRS-GABA in the SMA and sensorimotor cortices has been linked to PU and tic severity scores (Draper et al., 2014; Puts et al., 2015; He et al., 2022). Coupled with reports of enhanced external hypersensitivity (Issacs & Riordan, 2020), quantitative sensory thresholds are hypothesised to show abnormalities in TS. However, only three studies have measured quantitative tactile sensory thresholds in TS, which have provided mixed results (Belluscio et al., 2011; Puts et al., 2015; Schunke et al., 2016). Moreover, while evidence of disruptions to phasic TMS-SICI inhibition are generally consistent across the literature (Heise et al., 2010; Orth, 2009; Orth et al., 2005, 2008; Ziemann et al., 1997), evidence of abnormalities in tonic MRS-GABA inhibitory functioning across premotor, SMA and sensorimotor cortices are largely contradictory (He et al., 2022; Mahone et al., 2018; Puts et al., 2015; Tinaz et

al., 2014). A recent study has investigated the relationship between tic phenomenology, MRS-GABA and quantitative sensory thresholds in children with TS and TD controls (Puts et al., 2015). However, while sensorimotor GABA was reduced and impaired performance was evident in tactile detection and adaptation tasks in the TS group, only the TD group showed significant correlations between GABA and tactile performance (Puts et al., 2015). Therefore, in TS, sensory thresholds may rely on other means such as cortical excitability measured with MRS-Glu, evidenced to be increased and associated with behavioural performance in TS (Mahone et al., 2018). Overall, the specific processes underlying abnormalities in sensory processing in TS are unclear.

As a result, Chapter 3 aimed to address if, in Study 1, quantitative tactile sensory thresholds differed between adults with TS and TD control participants. In Study 2, levels of MRS-GABA and MRS-Glu within the sensorimotor cortex and quantitative and self-reported measures of sensory processing were assessed between groups. These were also input into correlation analyses in each group to uncover any relationships with somatosensory processing. Additionally, PU and tic severity scores were also correlated with MRS-GABA and MRS-Glu in the TS group.

Study 1 demonstrated that there are some abnormalities in the somatosensory system in TS, as evidenced by increased tactile discrimination thresholds. Specifically, TOJ and cTOJ thresholds are significantly greater in TS compared to TD controls. Moreover, there is some anecdotal evidence supporting differences in simAD and SSA thresholds, with higher thresholds present in the TS group. This supports that tactile discrimination, thought to be reflected by intracortical inhibitory mechanisms, are disrupted in TS. However, while it was predicted that the percentage change in response to adaptation and carrier stimuli would be reduced in the TS group, as evidenced in previous research in TS (Puts et al., 2015) and in common comorbidities ADHD (Puts, Harris, et al., 2017) and ASD (Puts et al., 2014; Tommerdahl et al., 2008), these did not differ between TD and TS groups. Therefore, mechanisms involved in

adaptation and carrier effects, such as the synchronisation of sensory activity, may not be disrupted in TS.

In Study 2, there was some support for the initial hypothesis of abnormalities in sensorimotor inhibition, with a trend for reduced sensorimotor MRS-GABA in the TS group, however MRS-Glu concentrations were comparable across TS and TD groups, contradicting previous evidence (Mahone et al., 2018). Moreover, GABA concentrations were not related to quantitative tactile sensory thresholds which are seen in other conditions with disruptions in GABA such as FHD (Antelmi et al., 2017) and ASD (Puts et al., 2014). In contrast with previous evidence, MRS-GABA was also not related to quantitative tactile sensory thresholds in the TD control group (Cassady et al., 2019; Kolasinski et al., 2017). This suggests that measures reflecting intracortical inhibitory mechanisms implicated in sensory discrimination performance (i.e. surround inhibition and receptive field tuning) such as TMS-SICI, should be utilised instead. Alternatively, MRS-Glu was negatively correlated with SSA performance in the TD group, indicating that other mechanisms may be involved in sensory discrimination abilities. One mechanism proposed is that of increased neural noise, reflecting the signal-to-noise ratio in the sensorimotor system and the ability to separate incoming sensory signals. This has recently been evidenced to be disrupted in TS (Adelhöfer et al., 2021; Münchau et al., 2021).

Interestingly, a positive relationship was identified between MRS-GABA and SPSQ scores in the TS group only. This relationship has also been demonstrated in ASD (Sapey-Triomphe et al., 2019) and is reminiscent of the paradoxical relationship between self-reported interoception and objective interoceptive acuity (Rae, Larsson, et al., 2019). This provides support for the Bayesian account of TS, which proposes that top-down predictions, modulated by GABA, of sensory information are abnormal (Rae, Critchley, et al., 2019; Rosenberg et al., 2015). As a result, abnormalities in sensorimotor GABA modulation may result in increased prediction errors and therefore, enhanced perceived hypersensitivity. However, SPSQ scores did not significantly differ between TS and TD groups, so the extent to which hypersensitivity

is increased in TS is unclear. Additionally, a significant relationship was demonstrated between MRS-Glu and urge severity, where reduced MRS-Glu was associated with greater urge severity. This has previously been demonstrated in TMS evidence and suggests that sensorimotor excitability has a role in the pathology of PU (Larsh et al., 2023).

Overall, Chapter 3 identified some evidence reflecting the presence of reductions in sensorimotor inhibition and poorer tactile discrimination thresholds in TS in comparison to TD controls. However, these measures were not significantly related in either group.

7.1.1 Limitations and future considerations

While this absence of relationships between MRS-GABA and tactile processing in TS and TD control groups could suggest that GABA is not involved in tactile processing, it could also reflect the notion that tonic inhibition is not an accurate reflection of the GABAergic phasic mechanisms implicated in sensory processing, such as surround inhibition (Dyke et al., 2017). As a result, future work should investigate sensory processing in relation to TMS-SICI measures, which has shown some relationship with surround inhibition during movement initiation (Beck et al., 2008; Leodori et al., 2019; Molloy et al., 2003; Premoli et al., 2014; Stinear & Byblow, 2003). Additionally, as relationships have not been demonstrated between MRS-GABA and tactile discrimination in children, and now adults, with TS, the role of inhibitory mechanisms in sensory processing may be overstated (Puts et al., 2015). Instead, the reduced ability to separate of sensory signals (previously attributed to poor surround inhibitory mechanisms) could be a result of decreased signal-to-noise (increased neural noise) in the sensorimotor system. As neural noise is thought to be increased in TS (Adelhöfer et al., 2021; Münchau et al., 2021), this could result in a poorer precision during tactile discrimination due to the reduced ability to separate signals within the sensorimotor cortices. Future work should aim to investigate the role of neural noise with EEG and TMS-SICI in sensory processing in TS and TD controls to

further clarify the role of inhibition and noise in tactile discrimination and sensory processing.

Co-morbidities were also not controlled in these studies, which could explain the differences identified in tactile discrimination and MRS-GABA, as individuals with ASD and ADHD also show abnormalities in tactile thresholds and MRS-GABA (Puts, Wodka, et al., 2017; Tommerdahl et al., 2008). These are common co-morbidities in TS, however the impact of these co-morbidities on MRS concentrations and tactile thresholds are not clear. Future work with larger samples should aim to clarify if abnormalities are demonstrated in TS alone or are a result of co-morbidities. Moreover, TS participants were screened prior to recruitment and were only recruited if they had relatively low tic frequency/intensities, with the absence of frequent or intense facial and head tics. This was to ensure comfort during MRS scanning and reduce the likelihood of movement artefacts impacting data quality. However, this means that this sample is not likely to be representative of the general adult population with TS. Additionally, reduced tic frequencies and greater response to online recruitment resulted in more females participating in these studies. As a result, the resultant TS group did not reflect the estimated 2-3:1 male to female ratio in adult TS populations (Freeman et al., 2000; Levine et al., 2019). This data may therefore reflect female populations with TS, who are thought to display differences in aetiology, tic phenomenology, comorbidities and neural structure and function (Baizabal-Carvallo & Jankovic, 2023; Dy-Hollins et al., 2023; Garris & Quigg, 2021). As a result, this limits the generalisability of these results to the overall TS population.

Suppression of tics during MRS collection could also have impacted measures of sensorimotor MRS-GABA. This is because control of motor outputs in TS has been linked to increases in SMA MRS-GABA (Draper et al., 2014; Jackson et al., 2015). However, increases in SMA MRS-GABA have previously been linked with a reduction in motor cortical excitability in TS, and therefore this is unlikely to explain the reduced level of MRS-GABA evident in TS (Draper et al., 2014). Moreover, laterality of sensory tasks and MRS voxel placement may have impacted subsequent analyses, though

previous investigations have found that sensorimotor MRS are significantly correlated across hemispheres (Puts et al., 2018). Nevertheless, the impact of suppression and laterality cannot be ruled out, and to minimise the potential impact, future research should measure the extent to which individuals with TS suppress during MRS scans and aim to keep laterality of sensory measures and MRS voxels consistent.

7.2 Sensorimotor representations of the digits and face in Tourette Syndrome

As indicated in Chapter 3, there is some evidence to suggest that sensorimotor inhibition is disrupted in TS. Sensorimotor GABA has also been associated with the cortical representations of digit profiles and the hand muscle of TD individuals (Cassady et al., 2019; Kolasinski et al., 2017; Sigurdsson, Molloy, et al., 2020). In disorders with alterations in GABAergic inhibition such as FHD (Beck et al., 2008; Beck & Hallett, 2011; Gallea et al., 2018; Sohn & Hallett, 2004; Stinear & Byblow, 2004), abnormalities in digit representations are evident (Bara-Jimenez et al., 1998; Butterworth et al., 2003; Byl et al., 2000; Byrnes et al., 1998; Elbert et al., 1998; Huber et al., 2023; Meunier et al., 2001; Schabrun et al., 2009). However, there are questions as to whether these disruptions in cortical representations are evident across both hemispheres. For example, while disordered inhibition is displayed bilaterally (Ridding et al., 1995; Rona et al., 1998), investigations into cortical hand mapping are usually limited to the hemisphere of the affected hand (Bara-Jimenez et al., 1998; Butterworth et al., 2003; Elbert et al., 1998; Schabrun et al., 2009), and evidence of bilateral abnormalities in hand representations are suspected to relate with duration of FHD and severity of symptoms (Byrnes et al., 1998; Meunier et al., 2001). As a result, it is proposed that while inhibitory mechanisms involved in the maintenance of cortical representations are impaired bilaterally, repetitive movements of the dystonic limb are unilateral. This results in abnormalities to one hemisphere only, with variability depending on distinct dystonic symptoms (Blake et al., 2002). However, despite abnormalities in cortical inhibition and the presence of repetitive movements, cortical sensorimotor representations have not been investigated in TS.

It was therefore hypothesised in Chapter 4 that while there are disruptions in sensorimotor GABA associated with TS, as hand tics are not widely reported then sensorimotor digit representations would be comparable to TD control participants. Alternatively, in Chapter 5, it was hypothesised that differences would be apparent in sensorimotor representations in areas of the body associated with tics, such as facial areas (Baizabal-Carvallo et al., 2023).

Chapter 4 used a phase-encoded travelling wave fMRI paradigm at 7T to investigate the fine-grained M1 and S1 representations of digits 2-4 in the dominant hand of individuals with TS and TD controls. The proportion of voxels assigned to each digit representation (digit ratios) and Euclidean distances between adjacent digits were determined for each individual and compared across groups. However, while Euclidean distances did not differ between the TS group and TD control group, significant differences were identified in digit ratios. Specifically, D3 (in M1 and S1) and D4 (in M1) occupy a greater proportion of M1/S1 and D2 (in S1) occupies a smaller proportion of S1 in the TS group, compared to the control group. Against the initial hypothesis, this suggests that abnormalities in digit representations exist in TS populations, despite hand tics being uncommon in TS. As a result, disrupted inhibitory functioning within sensorimotor cortices may be sufficient to disrupt cortical representations.

In Chapter 5, Study 1 measured sensorimotor representations of three volitional facial tic-like movements in individuals with TS and TD controls with 3T fMRI; this included blinking, grimacing and jaw clenching. Each fMRI movement map was compared across groups, however no significant differences were identified. This suggests that movements associated with common tics activate similar areas across bilateral sensorimotor cortices and SMA in individuals with TS and TD controls. Further analyses input each movement map into conjunction analyses in each group to identify common voxels activated across all movements and voxels that were unique to each movement. Patterns of unique voxels identified for each movement were similar across groups, showing activations within the sensorimotor cortices.

However, for common voxel maps, the TD group displayed a greater spread of activation across sensorimotor cortices, whereas the TS group displayed reduced areas of common voxels across movements. This indicates that the TD group recruit similar regions of the sensorimotor cortex across movements, whereas this may be more aberrant in the TS group. Moreover, while the SMA was consistently activated across movements and included in the common voxel map for the TD group, this was absent in the TS group. Upon inspection of cluster maps for each movement, SMA activation is absent in the grimace task which involves greater coordination of facial muscles. This results in greater cognitive control of movement and perhaps, greater suppression of tics, which are thought to be associated with greater levels of MRS-GABA in the SMA as a form of control over motor cortical hyperexcitability (Heise et al., 2010; Jackson et al., 2015; Jackson et al., 2011, 2013; Jung et al., 2013; Larsh et al., 2023). As SMA MRS-GABA has shown a significant inverse relationship with SMA BOLD activation (Draper et al., 2014), the absence of SMA activation in the grimace task may reflect compensatory strategies over motor control. Consequently, while sensorimotor representations of facial movements may not show overt differences between individuals with TS and TD controls, the execution and control of volitional movements may result in differential patterns of activation within the SMA.

Finally, in Chapter 5 Study 2, right hemisphere sensorimotor representations were extracted in response to vibrotactile stimulation to different regions of the face, specifically, the O. oculi, masseter and O. oris. While group cluster activations were not present for the TS group, likely due to insufficient statistical power, these were evident for the TD control group. Moreover, conjunction analyses in the TD control group for each sensory block identified common voxels in the SMA, in line with previous evidence which displayed SMA activation during passive vibrotactile stimulation (Nelson et al., 2004). However, despite all participants showing maximum activation coordinates within S1, unique voxels across each movement were only evident in the SMA and M1. This may indicate and support the notion that sensorimotor representations display great inter-individual variability in the sensorimotor cortices (Besle et al., 2013; Kikkert et al., 2023; Kolasinski et al., 2016;

Sanchez-Panchuelo et al., 2012; Stringer et al., 2011), and therefore do not pass group-level cluster thresholding. As a result, it may be more appropriate to assess sensorimotor representations individually.

When assessing individual thresholded cluster activations, the number of voxels activated within the right hemisphere sensorimotor mask were comparable across groups for O. oculi block, but anecdotal evidence was evident for a reduction in masseter and O. oris block activated voxels in the TS group compared to TD controls. This could reflect the notion that the gain in excitability is reduced in the M1 in TS in comparison to TD controls (Draper et al., 2015; Orth, 2009; Pépés et al., 2016). Alternatively, this could reflect differences in tactile quantitative sensory thresholds between groups, as a consistent suprathreshold vibrotactile stimulus was used across participants. However, more evidence is required to increase the statistical power in the TS group in order to more accurately compare responses across groups and confidently state that results reflect a true effect.

An interesting outcome of this study was that the locations of maximum voxel activation coordinates appeared to be split into two clustered locations of the S1 in both groups across all sensory blocks. This could indicate that there are two S1 sites that are activated during facial regions such as the O. oculi, masseter and O. oris, and which may provide support that the S1 is organised in a similar manner to that as described in the novel proposal the M1 is organised into concentric effector-specific regions, interleaved by body-action zones (Gordon et al., 2023). For the face effector region, this means that the tongue is in the centre of the effector region (a one peak activation site) and is surrounded by the jaw, nostrils and eyelids (two peak activation sites). However, further investigation is required before determining if this data supports this organisation in the S1. This will be investigated by assessing activation profiles for each sensory block and determining if each profile better fits a one-peak or two-peak gaussian curve. As the O. oculi, masseter and O. oris are beyond the activation peak (tongue), it is hypothesised that two-peak gaussian curves will better fit these activation profiles.

Overall, it has been shown that some differences were present in sensorimotor digit and vibrotactile facial representations between individuals with TS and TD controls. However, while no differences were identified across groups in volitional facial movements that relate to facial tics, differences may be evident in the SMA between groups. Specifically, the absence of SMA activation within the TS group is proposed to be a result of task complexity, suppression and cognitive control of action.

7.2.1 Limitations and future considerations

Some limitations are associated with the methods discussed in Chapter 4. Namely, the predictability of the travelling wave tapping task is associated with greater activation in the sensorimotor cortices compared to random-order tapping tasks or passive vibrotactile stimulation. This resulted in the reduced ability to separate digits, and the overrepresentation of specific digits in subsequent analyses (Mastria et al., 2023; Olman et al., 2012). This could explain the finding that D4 and D5 had greater digit ratios in both groups, rather than D1/D2 as demonstrated in previous research (Janko et al., 2022). Additionally, while rapid acquisition is beneficial in reducing patient time in the MRI scanner, travelling wave task analyses are insensitive to overlapping of digit representations due to 'winner-takes-all' analyses (Besle et al., 2013). This means that blurring of digit representations (as demonstrated after application of inhibitory GABA antagonists and in FHD animal models; Blake et al., 2002; Foeller et al., 2005; Jacobs & Donoghue, 1991; Schneider et al., 2002) could not be assessed. As a result, future research should utilise event-related or block fMRI with vibrotactile tasks to more reliably quantify the size of digit representations and to assess overlapping representations in patient groups. Additionally, due to the great inter-individual variability across sensorimotor representations, it may be more appropriate to assess representations on an individual level, as assuming homogeneity across samples and performing group analyses has likely masked individual differences within groups.

As in Section 7.1.1., co-morbidities were not controlled for so the impact of these on sensorimotor representations and movement activations are unknown. Also, in both Chapter 4 and Chapter 5, the extent to which individuals in the TS group experienced hand tics and facial tics was not measured. As a result, it cannot be determined if digit map and facial maps showed abnormalities despite the presence of hand tics and due to the presence of facial tics in the sample. Finally, it was assumed that disruptions in sensorimotor inhibition were present in samples from Chapter 4 and Chapter 5, however these were not assessed in all individuals or correlated with individual sensorimotor maps. Future work assessing digit and facial representations should assess the frequency and intensity of hand/facial tics and sensorimotor inhibition to determine if features of representations are related to individual tic profiles and GABA concentrations.

Strength of fMRI BOLD activations could also not be compared across groups as the intensity of finger tapping/facial movements likely varied across individuals. Moreover, findings in Chapter 3 suggest that individual thresholds of facial vibrotactile stimulation are likely to vary between groups, however these were set at a consistent intensity across all participants. When conducting similar tasks in the future, EMG should be used in movement tasks to allow for normalisation of BOLD activations across individuals depending on EMG-informed strength of movements. Moreover, BOLD activations in vibrotactile stimulation blocks should be controlled for by measuring individual facial thresholds to vibrotactile stimulation and basing block stimulation on a consistent percentage above this threshold across participants. Additionally, further investigation is needed into the impact of tic suppression, as any impact of suppression during fMRI tasks on sensorimotor excitability and BOLD responses is unclear (Draper et al., 2014)

Additionally, the extent to which results from Chapter 4 and Chapter 5 can be generalised is limited. This is because of the limited recruitment of TS participants to those who experience low tic frequencies/intensities, especially of facial and head tics. This was because large head and facial tics may result in fMRI motion artefacts

and data quality concerns. Moreover, the male to female ratio within our TS sample are unlikely to reflect that of the general TS population and may reflect an alternative TS phenotype due to possible sex differences in aetiology, clinical presentation, neural structure and function (Baizabal-Carvallo & Jankovic, 2023; Garris & Quigg, 2021). To detect differences in sensorimotor maps in a more representative TS population, imaging techniques that are less susceptible to motion artefacts should be utilised, such as TMS and optically pumped magnetometer magnetoencephalography (OPM-MEG). This would also reduce the impact of movement on data quality and sample size, as evidenced in Chapter 5, with removal of seven TS datasets in Study 1 and six TS datasets in Study 2.

Finally, practical limitations of studies (funding timescales and limitations, and equipment failures), and data quality concerns (such as movement artefacts) resulted in low sample sizes throughout studies within this thesis. This has greatly limited the statistical power and enhanced susceptibility to Type I/II errors, reducing the likelihood that findings are reflective of a true effect. Using a sensitivity power analysis (G*Power; Faul et al., 2007), the target sample size of 20 participants per group within this thesis in studies conducting *t*-tests only holds sufficient power (0.8; alpha of 0.05) for detecting large effects (Cohen's $d > 0.8$). However, the effect size in psychological research is estimated to be an average of $d = 0.4$ (small-medium; Brysbaert, 2019). As a result, this data does not have sufficient power to detect smaller effects with *t*-tests, which would requiring group sizes of 79 (one-tailed) or 100 (two-tailed) to detect effect sizes above $d = 0.4$ with comparable power (0.8). While smaller effects and their practical relevance can be questioned, the valid detection of these effects requires more data to increase the statistical power and thus, the confidence that a statistical result reflects a true effect. This will allow greater reliability and confidence in the results and subsequent conclusions that are drawn.

7.3 Disrupting cortical motor representations with iTBS

Previous evidence has indicated that rTMS may operate through NMDA and GABAergic mechanisms in order to drive LTP and LTD-like after-effects (Grover & Yan, 1999; Hess et al., 1996; Huang et al., 2007; Labedi et al., 2014). For example, $GABA_A$ receptor antagonists have been shown to enhance LTP-like after-effects of excitatory stimulation (Grover & Yan, 1999; Hess et al., 1996). Additionally, cortical motor representations have also shown alterations after application of $GABA_A$ antagonists (Foeller et al., 2005; Jacobs & Donoghue, 1991; Schneider et al., 2002). Consequently, previous animal and human research have demonstrated that excitatory rTMS protocols can alter cortical representations in the S1 and the visual cortex by weakening intracortical inhibitory mechanisms, driving cortical map variability (Houzé et al., 2013; Kozyrev et al., 2014, 2018; Pleger et al., 2006; Tegenthoff et al., 2005; Zhong et al., 2021). However, the extent to which rTMS can reliably weaken inhibitory mechanisms is unclear, with human evidence showing either reductions or no change in TMS-SICI after excitatory rTMS (Murakami et al., 2012; Peinemann et al., 2000; Quartarone et al., 2005; Tse et al., 2018; Wu et al., 2000).

As a result, Chapter 6 aimed to assess the impact of iTBS, an 'excitatory' rTMS protocol, on intracortical inhibitory mechanisms (measured with TMS-SICI) and TMS mapping of three hand muscles and fMRI digit mapping. iTBS was either delivered at 70% RMT to the M1 hand area (active group) or at 30% RMT to the vertex (control group). iTBS was chosen as animal research has previously shown that cortical inhibitory cells are most sensitive to iTBS protocols (Funke & Benali, 2011). Study 1 investigated the impact of active and control iTBS on measures of cortical excitability (IO curve slopes), cortical inhibition (TMS-SICI) and on the TMS corticospinal excitability mapping of three hand muscles. Study 2 investigated the impact of active and control iTBS on fMRI maps of digits 1-5, measured with a phase-encoded travelling wave tapping task. Expanding on previous research, multiple muscles were investigated, beyond the target site of M1 stimulation (FDI/D1-D2), as iTBS effects have been shown to extend beyond the initial stimulation site (Morris et al., 2019). It was hypothesised that IO curve slopes and SICI values would show significant

increases after active-iTBS (reflecting greater excitability and reduced inhibition). It was also proposed that TMS maps would show greater absolute changes in the active group compared to the control group.

Study 1 evidenced that while IO curve slopes were generally steeper after active iTBS, this was not a significant increase. However, there was some anecdotal support for this effect in Bayesian inference. The control group also showed no significant change in IO curve slopes after control iTBS. However, a significant difference was evident between the absolute percentage change in IO curve slopes between groups, indicating that active iTBS had a facilitatory influence on cortical excitability. Moreover, the active group evidenced a significant increase in SICI values with very strong Bayesian support, indicating a reduction in cortical inhibition. However, while this effect was absent in the control group, a one-tailed independent t-test revealed that the percentage change in SICI values before and after active iTBS were not significantly larger than that of the control group. It is proposed that this may be a result of the known variability in after-effects to rTMS, paired with variability in SICI values in both the active and control group (Chung et al., 2016; Hamada et al., 2013; López-Alonso et al., 2018; Wischnewski & Schutter, 2015).

While there some evidence of increases in IO curve slopes and increases in SICI values (indicating reduced intracortical inhibition) after active iTBS, there was no clear influence of active iTBS on TMS maps. For instance, some Bayesian support was evidenced for active iTBS inducing a larger effect on positions of L-R COG and P-A COG coordinates compared to the control group. However, while the distance between FDI-ADM TMS maps increased after active iTBS, the control group showed a decrease in Euclidean distances between APB-FDI maps. Moreover, absolute changes in Euclidean distances were not significantly larger in the active group compared to the control group. This suggests that active iTBS has no influence on Euclidean distances between different maps. Finally, the absolute percentage change in map areas were only significantly larger after active iTBS compared to control iTBS for ADM maps. Overall, Study 1 has indicated that there may be some influence of active iTBS on

cortical mapping of the hand and digits. However, the direction of this change and precise influence of iTBS on mapping is unclear due to low sample sizes, variability in iTBS after-effects and the variability in TMS maps across groups.

In Study 2, the control group showed some evidence of larger changes compared to the active group in D5 Euclidean distances before and after iTBS. However, the reliability of this result can be questioned, as the D5 representation has previously shown to be variable over time (O'Neill et al., 2020). Moreover, while D1 and D5 digit ratios showed a greater percentage change in the active group compared to the control group, changes in the control group were still evident when these were hypothesised to remain stable after iTBS. Great variability in digit ratios were also demonstrated across both groups, suggesting that the digit ratio metric may not be an accurate measure of the size of each digit relative to other digits.

Nevertheless, Study 1 demonstrated that SICI values are significantly increased after iTBS in the active group, indicating that iTBS can induce a reduction in inhibition in the M1. However, while previous evidence has demonstrated that weakened intracortical inhibition may be the driver of disruptions in cortical mapping, no decisive evidence of changes to TMS or fMRI mapping in response to active iTBS were evident in this study. However, the extent to which individual SICI values are related to changes in cortical mapping is unclear, as the sample size is insufficient to reliably determine this in correlation or regression analyses. Consequently, with the low statistical power, coupled with variability within and between groups, it cannot be decisively concluded that active iTBS can disrupt cortical representations.

7.3.1 Limitations and future considerations

Recalibrating RMT/SI1mV thresholds may be essential when measuring SICI after an intervention, as the inhibitory effect of SICI is dependent on the test pulse intensity (Garry & Thomson, 2009; Roshan et al., 2003). This is because SI1mV thresholds may change after active iTBS, and subsequent post-iTBS SICI values could no longer be sufficient to evoke the same extent of inhibition in MEP amplitudes. As rapid

measurement of TMS maps was a priority in Chapter 6, the SI1mV threshold was not recalibrated. As a result, future research should control for this by assessing SI1mV after iTBS. Differences in RMT between each muscle representation may have also impacted TMS maps, as the 120% FDI RMT TMS mapping pulses may result in larger/smaller MEP amplitudes in other muscles if they have lower/greater RMTs. Additionally, individually collecting muscle maps while using the optimal angle to evoke MEPs in each muscle may produce more accurate representations (Bashir et al., 2013). However, despite the time cost of measuring each threshold and collecting individual maps, previous literature has reported that rTMS after-effects have persisted in TMS maps for up to two hours (Pleger et al., 2006; Tegenthoff et al., 2005). Therefore, future investigations should consider thresholding individual muscle representation RMTs and recalibrating SI1mV thresholds to ensure reliable measures of TMS maps and SICI. With these limitations in mind, and the additional issues of variability in response to rTMS and low sample sizes, these results should be taken with caution.

As in Section 7.2.1, while travelling wave fMRI tasks allow for the rapid acquisition of digit maps after iTBS, phase-encoded fMRI tasks may be limiting as 'winner-takes-all' analyses are insensitive to overlapping of digits (Besle et al., 2013) and the sequential tapping tasks are more likely to misrepresent the size of digits than random-order tapping or passive vibrotactile stimulation (Mastria et al., 2023; Olman et al., 2012). Consequently, future research assessing the influence of iTBS on fMRI digit mapping should utilise block or event-related vibrotactile tasks to more accurately quantify the size of each digit in the cortex and give insight to any changes in the overlapping of digit representations.

Finally, while excitatory 5Hz-20Hz rTMS has previously been evidenced to alter cortical representations within the human and animal S1 and visual cortices, iTBS may not disrupt the specific mechanisms involved in the maintenance of cortical representations (Houzé et al., 2013; Kozyrev et al., 2014, 2018; Pleger et al., 2006; Tegenthoff et al., 2005; Zhong et al., 2021). Specifically, one study demonstrated that

iTBS was less effective at disrupting cortical representations in comparison to 20Hz rTMS (Houzé et al., 2013). As a result, while active iTBS can weaken M1 GABAergic inhibition, it is unlikely that these inhibitory mechanisms are the only mechanism involved in maintenance of cortical representations.

7.4 Overall conclusions

In conclusion, this thesis has demonstrated that quantitative tactile sensory thresholds are altered in adults with TS. However, while there is some evidence to suggest sensorimotor inhibition is reduced in adults with TS in comparison to TD controls, this is not related to quantitative sensory thresholds in TS or TD groups. This indicates that quantitative sensory discrimination thresholds may be instead more likely to correlate with measures reflecting surround inhibitory mechanisms, such as TMS-SICI. Alternatively, other mechanisms that may allow for the discrimination of sensory input, such as sensorimotor signal-to-noise ratios, should be explored. Moreover, GABA concentrations were significantly associated with self-reported levels of hypersensitivity in the TS group, suggesting top-down predictions of sensory information are abnormal in TS. There is also some evidence to indicate that sensorimotor representations of the digits are disrupted in TS, despite hand tics being relatively uncommon. This indicates that disordered inhibition may be sufficient to alter sensorimotor representations. However, the extent to which differences in representations are due to disruption of cortical inhibition is unclear, as this was not measured. Additionally, while the representation of facial movements relating to common tics do not significantly differ between TS and TD control groups, there is some evidence of differences in SMA activation during more complex volitional movements. Additionally, while sample sizes and variability of cortical facial representations prevented the accurate comparison of different sensorimotor representations of the face in response to vibrotactile stimulation, peak activation coordinates for each facial location were dispersed into two clustered locations of S1. This warrants further investigation into whether this reflects a concentric organisation of the face region in S1. Finally, while M1 iTBS may evoke an increase in cortical excitability and decrease in GABAergic inhibition, due to the low sample sizes,

variability within and between groups, and methodological limitations, there is no decisive evidence to suggest that iTBS can reliably influence M1 cortical representations of hand muscles and digits.

Bibliography

Adank, P., Kennedy-Higgins, D., Maegherman, G., Hannah, R., & Nuttall, H. E. (2018). Effects of coil orientation on motor evoked potentials from orbicularis oris. *Frontiers in Neuroscience*, *12*, 1–8. https://doi.org/10.3389/fnins.2018.00683

Adelhöfer, N., Paulus, T., Mückschel, M., Bäumer, T., Bluschke, A., Takacs, A., Tóth-Fáber, E., Tárnok, Z., Roessner, V., Weissbach, A., Münchau, A., & Beste, C. (2021). Increased scale-free and aperiodic neural activity during sensorimotor integration—a novel facet in Tourette syndrome. *Brain Communications*, *3*(4). https://doi.org/10.1093/braincomms/fcab250

Albin, R. L., & Mink, J. W. (2006). Recent advances in Tourette syndrome research. *Trends Neurosci*, *29*(3), 175–182. https://doi.org/10.1016/j.tins.2006.01.001

Albin, R. L., Young, A. B., & Penney, J. B. (1989). *The functional anatomy of basal ganglia disorders*.

Alexander, G. E., DeLong, M. R., & Strick, P. L. (1986). Parallel Organization of Functionally Segregated Circuits Linking Basal Ganglia and Cortex. *Annual Review of Neuroscience*, *9*(1), 357–381. https://doi.org/10.1146/annurev.ne.09.030186.002041

American Psychiatric Association. (2013). *Diagnostic and statistical manual of mental disorders DSM-5.* (5th ed.). American Psychiatric Association.

Andersson, J. L. R., Skare, S., & Ashburner, J. (2003). How to correct susceptibility distortions in spin-echo echo-planar images: Application to diffusion tensor imaging. *NeuroImage*, *20*(2), 870–888. https://doi.org/10.1016/S1053-8119(03)00336-7

Antelmi, E., Erro, R., Rocchi, L., Liguori, R., Tinazzi, M., Di Stasio, F., Berardelli, A., Rothwell, J. C., & Bhatia, K. P. (2017). Neurophysiological correlates of abnormal somatosensory temporal discrimination in dystonia. *Movement Disorders*, *32*(1), 141–148. https://doi.org/10.1002/mds.26804

Arthurs, O. J., & Boniface, S. (2002). How well do we understand the neural origins of the fMRI BOLD signal? *Trends in Neurosciences*, *25*(1), 27–31. https://doi.org/10.1016/S0166-2236(00)01995-0

Baizabal-Carvallo, J. F., Alonso-Juarez, M., & Jankovic, J. (2023). Oromandibular tics associated with Tourette syndrome. *Journal of Neurology*, *270*(5), 2591–2596. https://doi.org/10.1007/s00415-023-11583-8

Baizabal-Carvallo, J. F., & Jankovic, J. (2023). Sex differences in patients with Tourette syndrome. *CNS Spectrums, 28*(2), 205–211. doi:10.1017/S1092852922000074

Banaschewski, T., Woerner, W., & Rothenberger, A. (2003). Premonitory sensory phenomena and suppressibility of tics in Tourette syndrome: Developmental aspects in children and adolescents. *Developmental Medicine and Child Neurology*, *45*(10), 700–703. https://doi.org/10.1017/S0012162203001294

Bara-Jimenez, W., Catalan, M. J., Hallett, M., & Gerloff, C. (1998). Abnormal somatosensory homunculus in dystonia of the hand. *Annals of Neurology*, *44*(5), 828–831. https://doi.org/10.1002/ana.410440520

Bara–Jimenez, W., Shelton, P., & Hallett, M. (2000). Spatial discrimination is abnormal in focal hand dystonia. *Neurology*, *55*(12), 1869–1873. https://doi.org/10.1212/WNL.55.12.1869

Bara-Jimenez, W., Shelton, P., Sanger, T. D., & Hallett, M. (2000). Sensory discrimination capabilities in patients with focal hand dystonia. *Annals of Neurology*, *47*(3), 377–380. https://doi.org/10.1002/1531-8249(200003)47:3<377::AID-ANA16>3.0.CO;2-2

Bashir, S., Perez, J. M., Horvath, J. C., & Pascual-Leone, A. (2013). Differentiation of Motor Cortical Representation of Hand Muscles by Navigated Mapping of Optimal TMS Current Directions in Healthy Subjects. *Journal of Clinical Neurophysiology*, *30*(4), 390–395. https://doi.org/10.1097/WNP.0b013e31829dda6b

Batschelett, M. A., Huddleston, D. A., Crocetti, D., Horn, P. S., Mostofsky, S. H., & Gilbert, D. L. (2023). Biomarkers of tic severity in children with Tourette syndrome: Motor cortex inhibition measured with transcranial magnetic stimulation. *Developmental Medicine and Child Neurology*, *65*(10), 1321–1331. https://doi.org/10.1111/dmcn.15578

Bäumer, T., Thomalla, G., Kroeger, J., Jonas, M., Gerloff, C., Hummel, F. C., Müller-Vahl, K., Schnitzler, A., Siebner, H. R., Orth, M., & Münchau, A. (2010).

Interhemispheric motor networks are abnormal in patients with Gilles de la Tourette syndrome. *Movement Disorders*, *25*(16), 2828–2837. https://doi.org/10.1002/mds.23418

Baumung, L., Müller-Vahl, K., Dyke, K., Jackson, G., Jackson, S., Golm, D., Münchau, A., & Brandt, V. (2021). Developing the Premonitory Urges for Tic Disorders Scale–Revised (PUTS-R). *Journal of Neuropsychology*, *15*(1), 129–142. https://doi.org/10.1111/jnp.12216

Beck, S., & Hallett, M. (2011). Surround inhibition in the motor system. *Experimental Brain Research*, *210*(2), 165–172. https://doi.org/10.1007/s00221-011-2610-6

Beck, S., Richardson, S. P., Shamim, E. A., Dang, N., Schubert, M., & Hallett, M. (2008). Short Intracortical and Surround Inhibition Are Selectively Reduced during Movement Initiation in Focal Hand Dystonia. *Journal of Neuroscience*, *28*(41), 10363–10369. https://doi.org/10.1523/JNEUROSCI.3564-08.2008

Belluscio, B. A., Jin, L., Watters, V., Lee, T. H., & Hallett, M. (2011). Sensory sensitivity to external stimuli in Tourette syndrome patients. *Movement Disorders*, *26*(14), 2538–2543. https://doi.org/10.1002/mds.23977

Bernard, B. A., Stebbins, G. T., Siegel, S., Schultz, T. M., Hays, C., Morrissey, M. J., Leurgans, S., & Goetz, C. G. (2009). Determinants of quality of life in children with Gilles de la Tourette syndrome. *Movement Disorders*, *24*(7), 1070–1073. https://doi.org/10.1002/mds.22487

Besle, J., Sánchez-Panchuelo, R. M., Bowtell, R., Francis, S., & Schluppeck, D. (2013). Single-subject fMRI mapping at 7 T of the representation of fingertips in S1: A comparison of event-related and phase-encoding designs. *Journal of Neurophysiology*, *109*(9), 2293–2305. https://doi.org/10.1152/jn.00499.2012

Blake, D. T., Byl, N. N., Cheung, S., Bedenbaugh, P., Nagarajan, S., Lamb, M., & Merzenich, M. (2002). Sensory representation abnormalities that parallel focal hand dystonia in a primate model. *Somatosensory & Motor Research*, *19*(4), 347–357. https://doi.org/10.1080/0899022021000037827

Blicher, J. U., Near, J., Næss-Schmidt, E., Stagg, C. J., Johansen-Berg, H., Nielsen, J. F., Østergaard, L., & Ho, Y. C. L. (2015). GABA levels are decreased after stroke and GABA changes during rehabilitation correlate with motor improvement.

Neurorehabilitation and Neural Repair, *29*(3), 278–286. https://doi.org/10.1177/1545968314543652

Bliss, T. V. P., & Cooke, S. F. (2011). Long-term potentiation and long-term depression: A clinical perspective. *Clinics*, *66*(SUPPL.1), 3–17. https://doi.org/10.1590/S1807-59322011001300002

Bloch, M. H., & Leckman, J. F. (2009). Clinical course of Tourette syndrome. *Journal of Psychosomatic Research*, *67*(6), 497–501. https://doi.org/10.1016/j.jpsychores.2009.09.002

Bohlhalter, S., Goldfine, A., Matteson, S., Garraux, G., Hanakawa, T., Kansaku, K., Wurzman, R., & Hallett, M. (2006). Neural correlates of tic generation in Tourette syndrome: an event-related functional MRI study. *Brain*, *129*(Pt 8), 2029–2037. https://doi.org/10.1093/brain/awl050

Borghetti, D., Sartucci, F., Petacchi, E., Guzzetta, A., Piras, M. F., Murri, L., & Cioni, G. (2008). Transcranial magnetic stimulation mapping: A model based on spline interpolation. *Brain Research Bulletin*, *77*(2–3), 143–148. https://doi.org/10.1016/j.brainresbull.2008.06.001

Brabson, L. A., Brown, J. L., Capriotti, M. R., Ramanujam, K., Himle, M. B., Nicotra, C. M., Ostrander, R., Kelly, L. M., Grados, M. A., Walkup, J. T., Perry-Parrish, C., Reynolds, E. K., Hankinson, J. C., & Specht, M. W. (2016). Patterned changes in urge ratings with tic suppression in youth with chronic tic disorders. *Journal of Behavior Therapy and Experimental Psychiatry*, *50*, 162–170. https://doi.org/10.1016/j.jbtep.2015.07.004

Brandt, V. C., Beck, C., Sajin, V., Baaske, M. K., Bäumer, T., Beste, C., Anders, S., & Münchau, A. (2016). Temporal relationship between premonitory urges and tics in Gilles de la Tourette syndrome. *Cortex*, *77*, 24–37. https://doi.org/10.1016/j.cortex.2016.01.008

Bronfeld, M., Belelovsky, K., & Bar-Gad, I. (2011). Spatial and Temporal Properties of Tic-Related Neuronal Activity in the Cortico-Basal Ganglia Loop. *Journal of Neuroscience*, *31*(24), 8713–8721. https://doi.org/10.1523/JNEUROSCI.0195-11.2011

Bronfeld, M., Israelashvili, M., & Bar-Gad, I. (2013). Pharmacological animal models of Tourette syndrome. *Neuroscience & Biobehavioral Reviews*, *37*(6), 1101–1119. https://doi.org/10.1016/j.neubiorev.2012.09.010

Bronfeld, M., Yael, D., Belelovsky, K., & Bar-Gad, I. (2013). Motor tics evoked by striatal disinhibition in the rat. *Frontiers in Systems Neuroscience*, *7*. https://doi.org/10.3389/fnsys.2013.00050

Brownjohn, P. W., Reynolds, J. N. J., Matheson, N., Fox, J., & Shemmell, J. B. H. (2014). The effects of individualized theta burst stimulation on the excitability of the human motor system. *Brain Stimulation*, *7*(2), 260–268. https://doi.org/10.1016/j.brs.2013.12.007

Bruce, A. B., Yuan, W., Gilbert, D. L., Horn, P. S., Jackson, H. S., Huddleston, D. A., & Wu, S. W. (2021). Altered frontal-mediated inhibition and white matter connectivity in pediatric chronic tic disorders. *Experimental Brain Research*, *239*(3), 955–965. https://doi.org/10.1007/s00221-020-06017-0

Brysbaert, M. (2019). How many participants do we have to include in properly powered experiments? A tutorial of power analysis with reference tables. *Journal of Cognition, 2*(1), 16. https://doi.org/10.5334/joc.72

Butterworth, S., Francis, S., Kelly, E., McGlone, F., Bowtell, R., & Sawle, G. V. (2003). Abnormal cortical sensory activation in dystonia: An fMRI study. *Movement Disorders*, *18*(6), 673–682. https://doi.org/10.1002/mds.10416

Buxton, R. B. (2013). The physics of functional magnetic resonance imaging (fMRI). *Reports on Progress in Physics*, *76*(9). https://doi.org/10.1088/0034-4885/76/9/096601

Buzsáki, G., Anastassiou, C. A., & Koch, C. (2012). The origin of extracellular fields and currents — EEG, ECoG, LFP and spikes. *Nature Reviews Neuroscience*, *13*(6), 407–420. https://doi.org/10.1038/nrn3241

Byl, N. N., McKenzie, A., & Nagarajan, S. S. (2000). Differences in somatosensory hand organization in a healthy flutist and a flutist with focal hand dystonia: A case report. *Journal of Hand Therapy*, *13*(4), 302–309. https://doi.org/10.1016/S0894-1130(00)80022-8

Byrnes, M. L., Mastaglia, F. L., Walters, S. E., Archer, S.-A. R., & Thickbroom, G. W. (2005). Primary writing tremor: motor cortex reorganisation and disinhibition. *Journal of Clinical Neuroscience*, *12*(1), 102–104. https://doi.org/10.1016/j.jocn.2004.08.004

Byrnes, M. L., Thickbroom, G. W., Wilson, S. A., Sacco, P., Shipman, J. M., Stell, R., & Mastaglia, F. L. (1998). The corticomotor representation of upper limb muscles in writer's cramp and changes following botulinum toxin injection. *Brain*, *121*(5), 977–988. https://doi.org/10.1093/brain/121.5.977

Cassady, K., Gagnon, H., Lalwani, P., Simmonite, M., Foerster, B., Park, D., Peltier, S. J., Petrou, M., Taylor, S. F., Weissman, D. H., Seidler, R. D., & Polk, T. A. (2019). Sensorimotor network segregation declines with age and is linked to GABA and to sensorimotor performance. *NeuroImage*, *186*, 234–244. https://doi.org/10.1016/j.neuroimage.2018.11.008

Catani, M. (2017). A little man of some importance. *Brain*, *140*(11), 3055–3061. https://doi.org/10.1093/brain/awx270

Cavanna, A. E., Black, K. J., Hallett, M., & Voon, V. (2017). Neurobiology of the Premonitory Urge in Tourette's Syndrome: Pathophysiology and Treatment Implications. *The Journal of Neuropsychiatry and Clinical Neurosciences*, *29*(2), 95–104. https://doi.org/10.1176/appi.neuropsych.16070141

Cavanna, A. E., Servo, S., Monaco, F., & Robertson, M. M. (2009). The Behavioral Spectrum of Gilles de la Tourette Syndrome. *The Journal of Neuropsychiatry and Clinical Neurosciences*, *21*(1), 13–23. https://doi.org/10.1176/jnp.2009.21.1.13

Chappell, M., Okell, T., & Jenkinson, M. (2020). Short introduction to MRI Physics for Neuroimaging. In M. Jenkinson & M. Chappell (Eds.), *Oxford Neuroimaging Primers* (pp. 1–25). Oxford University Press.

Chavhan, G. B., Babyn, P. S., Thomas, B., Shroff, M. M., & Mark Haacke, E. (2009). Principles, techniques, and applications of T2*-based MR imaging and its special applications. *Radiographics*, *29*(5), 1433–1449. https://doi.org/10.1148/rg.295095034

Chen, J. E., & Glover, G. H. (2015). Functional Magnetic Resonance Imaging Methods. *Neuropsychology Review*, *25*(3), 289–313. https://doi.org/10.1007/s11065-015-9294-9

Chen, Y. J., Huang, Y. Z., Chen, C. Y., Chen, C. L., Chen, H. C., Wu, C. Y., Lin, K. C., & Chang, T. L. (2019). Intermittent theta burst stimulation enhances upper limb motor function in patients with chronic stroke: A pilot randomized controlled trial. *BMC Neurology*, *19*(1), 1–10. https://doi.org/10.1186/s12883-019-1302-x

Chouinard, S., & Ford, B. (2000). Adult onset tic disorders. *Journal of Neurology, Neurosurgery & Psychiatry*, *68*(6), 738–743. https://doi.org/10.1136/jnnp.68.6.738

Chowdhury, S. A., & Rasmusson, D. D. (2002). Effect of GABAB receptor blockade on receptive fields of raccoon somatosensory cortical neurons during reorganization. *Experimental Brain Research*, *145*(2), 150–157. https://doi.org/10.1007/s00221-002-1130-9

Chung, S. W., Hill, A. T., Rogasch, N. C., Hoy, K. E., & Fitzgerald, P. B. (2016). Use of theta-burst stimulation in changing excitability of motor cortex: A systematic review and meta-analysis. *Neuroscience and Biobehavioral Reviews*, *63*, 43–64. https://doi.org/10.1016/j.neubiorev.2016.01.008

Clarke, R. A., Lee, S., & Eapen, V. (2012). Pathogenetic model for Tourette syndrome delineates overlap with related neurodevelopmental disorders including Autism. *Transl Psychiatry*, *2*, e158. https://doi.org/10.1038/tp.2012.75

Clarkson, A. N., Huang, B. S., MacIsaac, S. E., Mody, I., & Carmichael, S. T. (2010). Reducing excessive GABA-mediated tonic inhibition promotes functional recovery after stroke. *Nature*, *468*(7321), 305–309. https://doi.org/10.1038/nature09511

Cohen, A. J., & Leckman, J. F. (1992). Sensory phenomena associated with Gilles de la Tourette's syndrome. *Journal of Clinical Psychiatry*, *53*(9), 319–323.

Cohen, S. C., Leckman, J. F., & Bloch, M. H. (2013). Clinical assessment of Tourette syndrome and tic disorders. *Neuroscience & Biobehavioral Reviews*, *37*(6), 997–1007. https://doi.org/10.1016/j.neubiorev.2012.11.013

Cohrs, S., Rasch, T., Altmeyer, S., Kinkelbur, J., Kostanecka, T., Rothenberger, A., Rüther, E., & Hajak, G. (2001). Decreased sleep quality and increased sleep related movements in patients with Tourette's syndrome. *Journal of Neurology Neurosurgery and Psychiatry*, *70*(2), 192–197. https://doi.org/10.1136/jnnp.70.2.192

Conelea, C. A., & Woods, D. W. (2008). The influence of contextual factors on tic expression in Tourette's syndrome: A review. *Journal of Psychosomatic Research*, *65*(5), 487–496. https://doi.org/10.1016/j.jpsychores.2008.04.010

Conelea, C. A., Woods, D. W., Zinner, S. H., Budman, C. L., Murphy, T. K., Scahill, L. D., Compton, S. N., & Walkup, J. T. (2013). The impact of tourette syndrome in adults: Results from the tourette syndrome impact survey. *Community Mental Health Journal*, *49*(1), 110–120. https://doi.org/10.1007/s10597-011-9465-y

Conelea, C. A., Woods, D. W., Zinner, S. H., Budman, C., Murphy, T., Scahill, L. D., Compton, S. N., & Walkup, J. (2011). Exploring the impact of chronic tic disorders on youth: Results from the Tourette syndrome impact survey. *Child Psychiatry and Human Development*, *42*(2), 219–242. https://doi.org/10.1007/s10578-010-0211-4

Cox, R. W. (1996). AFNI: Software for Analysis and Visualization of Functional Magnetic Resonance Neuroimages. *Computers and Biomedical Research*, *29*(3), 162–173. https://doi.org/10.1006/cbmr.1996.0014

Cox, R. W., & Hyde, J. S. (1997). Software tools for analysis and visualization of fMRI data. *NMR in Biomedicine*, *10*(4–5), 171–178. https://doi.org/10.1002/(SICI)1099-1492(199706/08)10:4/5<171::AID-NBM453>3.0.CO;2-L

Da Rocha Amaral, S., Sanchez Panchuelo, R. M., & Francis, S. (2020). A Data-Driven Multi-scale Technique for fMRI Mapping of the Human Somatosensory Cortex. *Brain Topography*, *33*(1), 22–36. https://doi.org/10.1007/s10548-019-00728-6

Daniela, M., Călin, C., Bogdan, I., Radu, M., Matei, D., Corciovă, C., Ignat, B., & Matei, R. (2018). Transcranial magnetic stimulation in stroke rehabilitation. *Balneo Research Journal*, *9*(3), 264–269. https://doi.org/10.12680/balneo.2018.193

DaSilva, A. F. M., Becerra, L., Makris, N., Strassman, A. M., Gonzalez, R. G., Geatrakis, N., & Borsook, D. (2002). Somatotopic Activation in the Human Trigeminal Pain Pathway. *The Journal of Neuroscience*, *22*(18), 8183–8192. https://doi.org/10.1523/JNEUROSCI.22-18-08183.2002

de la Cruz, L. F., & Mataix-Cols, D. (2020). General health and mortality in Tourette syndrome and chronic tic disorder: A mini-review. *Neuroscience & Biobehavioral Reviews*, *119*, 514–520. https://doi.org/10.1016/j.neubiorev.2020.11.005

D'Esposito, M., Deouell, L. Y., & Gazzaley, A. (2003). Alterations in the BOLD fMRI signal with ageing and disease: A challenge for neuroimaging. *Nature Reviews Neuroscience*, *4*(11), 863–872. https://doi.org/10.1038/nrn1246

Di Lazzaro, V., Oliviero, A., Profice, P., Pennisi, M. A., Pilato, F., Zito, G., Dileone, M., Nicoletti, R., Pasqualetti, P., & Tonali, P. A. (2003). Ketamine increases human motor cortex excitability to transcranial magnetic stimulation. *The Journal of Physiology*, *547*(2), 485–496. https://doi.org/10.1113/jphysiol.2002.030486

Di Lazzaro, V., Oliviero, A., Saturno, E., Dileone, M., Pilato, F., Nardone, R., Ranieri, F., Musumeci, G., Fiorilla, T., & Tonali, P. (2005). Effects of lorazepam on short latency afferent inhibition and short latency intracortical inhibition in humans. *The Journal of Physiology*, *564*(2), 661–668. https://doi.org/10.1113/jphysiol.2004.061747

Di Lazzaro, V., Pilato, F., Dileone, M., Profice, P., Oliviero, A., Mazzone, P., Insola, A., Ranieri, F., Meglio, M., Tonali, P. A., & Rothwell, J. C. (2008). The physiological basis of the effects of intermittent theta burst stimulation of the human motor cortex. *The Journal of Physiology*, *586*(16), 3871–3879. https://doi.org/10.1113/jphysiol.2008.152736

Di Lazzaro, V., Pilato, F., Dileone, M., Profice, P., Ranieri, F., Ricci, V., Bria, P., Tonali, P. A., & Ziemann, U. (2007). Segregating two inhibitory circuits in human motor cortex at the level of GABAA receptor subtypes: A TMS study. *Clinical Neurophysiology*, *118*(10), 2207–2214. https://doi.org/10.1016/j.clinph.2007.07.005

Di Lazzaro, V., Pilato, F., Dileone, M., Ranieri, F., Ricci, V., Profice, P., Bria, P., Tonali, P. A., & Ziemann, U. (2006). GABA A receptor subtype specific enhancement of inhibition in human motor cortex. *The Journal of Physiology*, *575*(3), 721–726. https://doi.org/10.1113/jphysiol.2006.114694

Di Lazzaro, V., Pilato, F., Dileone, M., Tonali, P. A., & Ziemann, U. (2005). Dissociated effects of diazepam and lorazepam on short-latency afferent inhibition. *The Journal of Physiology*, *569*(1), 315–323. https://doi.org/10.1113/jphysiol.2005.092155

Di Lazzaro, V., & Rothwell, J. C. (2014). Corticospinal activity evoked and modulated by non-invasive stimulation of the intact human motor cortex. *Journal of Physiology*, *592*(19), 4115–4128. https://doi.org/10.1113/jphysiol.2014.274316

Di Lazzaro, V., & Ziemann, U. (2013). The contribution of transcranial magnetic stimulation in the functional evaluation of microcircuits in human motor cortex. In *Frontiers in Neural Circuits* (Issue JAN). https://doi.org/10.3389/fncir.2013.00018

Dice, L. R. (1945). Measures of the Amount of Ecologic Association Between Species. *Ecology*, *26*(3), 297–302. https://doi.org/10.2307/1932409

Dowdle, L. T., Vizioli, L., Moeller, S., Akçakaya, M., Olman, C., Ghose, G., Yacoub, E., & Uğurbil, K. (2023). Evaluating increases in sensitivity from NORDIC for diverse fMRI acquisition strategies. *NeuroImage*, *270*. https://doi.org/10.1016/j.neuroimage.2023.119949

Draper, A., Jackson, G. M., Morgan, P. S., & Jackson, S. R. (2016). Premonitory urges are associated with decreased grey matter thickness within the insula and sensorimotor cortex in young people with Tourette syndrome. *Journal of Neuropsychology*, *10*(1), 143–153. https://doi.org/10.1111/jnp.12089

Draper, A., Jude, L., Jackson, G. M., & Jackson, S. R. (2015). Motor excitability during movement preparation in Tourette syndrome. *J Neuropsychol*, *9*(1), 33–44. https://doi.org/10.1111/jnp.12033

Draper, A., Stephenson, M. C., Jackson, G. M., Pépés, S., Morgan, P. S., Morris, P. G., & Jackson, S. R. (2014). Increased GABA contributes to enhanced control over

motor excitability in Tourette syndrome. *Curr Biol*, *24*(19), 2343–2347. https://doi.org/10.1016/j.cub.2014.08.038

Dy-Hollins, M., Chibnik, L., Osiecki, L., Sharma, N., Mathews, C., & Scharf, J. (2023). Assessing Sex Differences in Individuals with Tourette Syndrome and Persistent Motor or Vocal Tic Disorder (S42. 009). *Neurology*, *100*(17,2), 1948. https://doi.org/10.1212/WNL.0000000000202217

Dyke, K., Kim, S., Jackson, G. M., & Jackson, S. R. (2018). Reliability of single and paired pulse transcranial magnetic stimulation parameters across eight testing sessions. *Brain Stimulation*, *11*(6), 1393–1394. https://doi.org/10.1016/j.brs.2018.08.008

Dyke, K., Pépés, S. E., Chen, C., Kim, S., Sigurdsson, H. P., Draper, A., Husain, M., Nachev, P., Gowland, P. A., Morris, P. G., & Jackson, S. R. (2017). Comparing GABA-dependent physiological measures of inhibition with proton magnetic resonance spectroscopy measurement of GABA using ultra-high-field MRI. *NeuroImage*, *152*, 360–370. https://doi.org/10.1016/j.neuroimage.2017.03.011

Eapen, V., Cavanna, A. E., & Robertson, M. M. (2016). Comorbidities, social impact, and quality of life in tourette syndrome. *Frontiers in Psychiatry*, *7*(JUN), 97. https://doi.org/10.3389/fpsyt.2016.00097

Eddy, C. M., Rickards, H. E., & Cavanna, A. E. (2014). Physiological Awareness Is Negatively Related to Inhibitory Functioning in Tourette Syndrome. *Behavior Modification*, *38*(2), 319–335. https://doi.org/10.1177/0145445513504431

Edelstein, W. A., Glover, G. H., Hardy, C. J., & Redington, R. W. (1986). The intrinsic signal-to-noise ratio in NMR imaging. *Magnetic Resonance in Medicine*, *3*(4), 604–618. https://doi.org/10.1002/mrm.1910030413

Elbert, T., Candia, V., Altenmüller, E., Rau, H., Sterr, A., Rockstroh, B., Pantev, C., & Taub, E. (1998). Alteration of digital representations in somatosensory cortex in focal hand dystonia. *NeuroReport*, *9*(16), 3571–3575. https://doi.org/10.1097/00001756-199811160-00006

Essing, J., Jakubovski, E., Psathakis, N., Cevirme, S. N., Leckman, J. F., & Müller-Vahl, K. R. (2022). Premonitory Urges Reconsidered: Urge Location Corresponds to

Tic Location in Patients With Primary Tic Disorders. *Journal of Movement Disorders*, *15*(1), 43–52. https://doi.org/10.14802/jmd.21045

Evans, J., Seri, S., & Cavanna, A. E. (2016). The effects of Gilles de la Tourette syndrome and other chronic tic disorders on quality of life across the lifespan: a systematic review. In *European Child and Adolescent Psychiatry* (Vol. 25, Issue 9, pp. 939–948). Dr. Dietrich Steinkopff Verlag GmbH and Co. KG. https://doi.org/10.1007/s00787-016-0823-8

Evinger, C. (2005). Animal models of focal dystonia. *NeuroRX*, *2*(3), 513–524. https://doi.org/10.1602/neurorx.2.3.513

Faul, F., Erdfelder, E., Lang, A.-G., & Buchner, A. (2007). G*Power 3: A flexible statistical power analysis program for the social, behavioral, and biomedical sciences. *Behavior Research Methods*, *39*, 175-191. https://doi.org/10.3758/bf03193146

Fernández de la Cruz, L., Rydell, M., Runeson, B., Brander, G., Rück, C., D'Onofrio, B. M., Larsson, H., Lichtenstein, P., & Mataix-Cols, D. (2017). Suicide in Tourette's and Chronic Tic Disorders. *Biological Psychiatry*, *82*(2), 111–118. https://doi.org/10.1016/j.biopsych.2016.08.023

Fischl, B. (2012). FreeSurfer. *NeuroImage*, *62*(2), 774–781. https://doi.org/10.1016/j.neuroimage.2012.01.021

Fitzgerald, P. B., Fountain, S., & Daskalakis, Z. J. (2006). A comprehensive review of the effects of rTMS on motor cortical excitability and inhibition. In *Clinical Neurophysiology* (Vol. 117, Issue 12, pp. 2584–2596). https://doi.org/10.1016/j.clinph.2006.06.712

Foeller, E., Celikel, T., & Feldman, D. E. (2005). Inhibitory Sharpening of Receptive Fields Contributes to Whisker Map Plasticity in Rat Somatosensory Cortex. *Journal of Neurophysiology*, *94*(6), 4387–4400. https://doi.org/10.1152/jn.00553.2005

Franzkowiak, S., Pollok, B., Biermann-Ruben, K., Südmeyer, M., Paszek, J., Thomalla, G., Jonas, M., Orth, M., Münchau, A., & Schnitzler, A. (2012). Motor-Cortical Interaction in Gilles de la Tourette Syndrome. *PLoS ONE*, *7*(1), e27850. https://doi.org/10.1371/journal.pone.0027850

Freeman, R. D., Fast, D. K., Burd, L., Kerbeshian, J., Robertson, M. M., & Sandor, P. (2000). An international perspective on Tourette syndrome: Selected findings from 3500 individuals in 22 countries. *Developmental Medicine and Child Neurology*, *42*, 436–447.

Freundlieb, N., Philipp, S., Drabik, A., Gerloff, C., Forkert, N. D., & Hummel, F. C. (2015). Ipsilesional motor area size correlates with functional recovery after stroke: A 6-month follow-up longitudinal TMS motor mapping study. *Restorative Neurology and Neuroscience*, *33*(2), 221–231. https://doi.org/10.3233/RNN-140454

Friston, K. J., Holmes, A. P., Poline, J.-B., Grasby, P. J., Williams, S. C. R., Frackowiak, R. S. J., & Turner, R. (1995). Analysis of fMRI Time-Series Revisited. *NeuroImage*, *2*(1), 45–53. https://doi.org/10.1006/nimg.1995.1007

Friston, K. J., Holmes, A., Poline, J.-B., Price, C. J., & Frith, C. D. (1996). *Detecting Activations in PET and fMRI: Levels of Inference and Power*.

Friston, K. J., Worsley, K. J., Frackowiak, R. S. J., Mazziotta, J. C., & Evans, A. C. (1994). Assessing the significance of focal activations using their spatial extent. *Human Brain Mapping*, *1*(3), 210–220. https://doi.org/10.1002/hbm.460010306

Funke, K., & Benali, A. (2011). Modulation of cortical inhibition by rTMS - findings obtained from animal models. *Journal of Physiology*, *589*(18), 4423–4435. https://doi.org/10.1113/jphysiol.2011.206573

Gallea, C., Herath, P., Voon, V., Lerner, A., Ostuni, J., Saad, Z., Thada, S., Solomon, J., Horovitz, S. G., & Hallett, M. (2018). Loss of inhibition in sensorimotor networks in focal hand dystonia. *NeuroImage: Clinical*, *17*, 90–97. https://doi.org/10.1016/j.nicl.2017.10.011

Ganos, C., Asmuss, L., Bongert, J., Brandt, V., Munchau, A., & Haggard, P. (2015). Volitional action as perceptual detection: predictors of conscious intention in adolescents with tic disorders. *Cortex*, *64*, 47–54. https://doi.org/10.1016/j.cortex.2014.09.016

Ganos, C., Bongert, J., Asmuss, L., Martino, D., Haggard, P., & Münchau, A. (2015). The somatotopy of tic inhibition: Where and how much? *Movement Disorders*, *30*(9), 1184–1189. https://doi.org/10.1002/mds.26188

Ganos, C., Garrido, A., Navalpotro-Gómez, I., Ricciardi, L., Martino, D., Edwards, M. J., Tsakiris, M., Haggard, P., & Bhatia, K. P. (2015). Premonitory urge to tic in tourette's is associated with interoceptive awareness. *Movement Disorders*, *30*(9), 1198–1202. https://doi.org/10.1002/mds.26228

Ganos, C., Kahl, U., Schunke, O., Kühn, S., Haggard, P., Gerloff, C., Roessner, V., Thomalla, G., & Münchau, A. (2012). Are premonitory urges a prerequisite of tic inhibition in Gilles de la Tourette syndrome? *Journal of Neurology, Neurosurgery and Psychiatry*, *83*(10), 975–978. https://doi.org/10.1136/jnnp-2012-303033

Gardner, J. L., Merriam, E. P., Schluppeck, D., Besle, J., & Heeger, D. J. (2018). mrTools: Analysis and visualization package for functional magnetic resonance imaging data. *Zendo*. https://doi.org/10.5281/ZENODO.1299483

Garris, J., & Quigg, M. (2021). The female Tourette patient: sex differences in Tourette disorder. *Neuroscience & Biobehavioral Reviews, 129*, 261-268. https://doi.org/10.1016/j.neubiorev.2021.08.001

Garry, M. I., & Thomson, R. H. S. (2009). The effect of test TMS intensity on short-interval intracortical inhibition in different excitability states. *Experimental Brain Research*, *193*(2), 267–274. https://doi.org/10.1007/s00221-008-1620-5

Gilbert, D. L., Bansal, A. S., Sethuraman, G., Sallee, F. R., Zhang, J., Lipps, T., & Wassermann, E. M. (2004). Association of cortical disinhibition with tic, ADHD, and OCD severity in Tourette syndrome. *Movement Disorders*, *19*(4), 416–425. https://doi.org/10.1002/mds.20044

Gilbert, D. L., Sallee, F. R., Zhang, J., Lipps, T. D., & Wassermann, E. M. (2005). Transcranial Magnetic Stimulation-Evoked Cortical Inhibition: A Consistent Marker of Attention-Deficit/Hyperactivity Disorder Scores in Tourette Syndrome. *Biological Psychiatry*, *57*(12), 1597–1600. https://doi.org/10.1016/j.biopsych.2005.02.022

Gittis, A. H., & Kreitzer, A. C. (2012). Striatal microcircuitry and movement disorders. *Trends in Neurosciences*, *35*(9), 557–564. https://doi.org/10.1016/j.tins.2012.06.008

Glover, G. H. (2011). Overview of functional magnetic resonance imaging. *Neurosurgery Clinics of North America*, *22*(2), 133–139. https://doi.org/10.1016/j.nec.2010.11.001

Gordon, E. M., Chauvin, R. J., Van, A. N., Rajesh, A., Nielsen, A., Newbold, D. J., Lynch, C. J., Seider, N. A., Krimmel, S. R., Scheidter, K. M., Monk, J., Miller, R. L., Metoki, A., Montez, D. F., Zheng, A., Elbau, I., Madison, T., Nishino, T., Myers, M. J., … Dosenbach, N. U. F. (2023). A somato-cognitive action network alternates with effector regions in motor cortex. *Nature*. https://doi.org/10.1038/s41586-023-05964-2

Graybiel, A. M. (2008). Habits, rituals, and the evaluative brain. *Annu Rev Neurosci*, *31*, 359–387. https://doi.org/10.1146/annurev.neuro.29.051605.112851

Greene, D. J., Koller, J. M., Robichaux-Viehoever, A., Bihun, E. C., Schlaggar, B. L., & Black, K. J. (2015). Reward enhances tic suppression in children within months of tic disorder onset. *Developmental Cognitive Neuroscience*, *11*, 65–74. https://doi.org/10.1016/j.dcn.2014.08.005

Gröhn, H., Gillick, B. T., Tkáč, I., Bednařík, P., Mascali, D., Deelchand, D. K., Michaeli, S., Meekins, G. D., Leffler-McCabe, M. J., MacKinnon, C. D., Eberly, L. E., & Mangia, S. (2019). Influence of repetitive transcranial magnetic stimulation on human neurochemistry and functional connectivity: A pilot MRI/MRS study at 7 T. *Frontiers in Neuroscience*, *13*, 1–13. https://doi.org/10.3389/fnins.2019.01260

Grover, L. M., & Yan, C. (1999). Blockade of GABAA receptors facilitates induction of NMDA receptor-independent long-term potentiation. *Journal of Neurophysiology*, *81*(6), 2814–2822. https://doi.org/10.1152/jn.1999.81.6.2814

Gu, Y., Li, Y., & Cui, Y. (2020). Correlation between premonitory urges and tic symptoms in a Chinese population with tic disorders. *PEDIATRIC INVESTIGATION*, *4*(2), 86–90. https://doi.org/10.1002/ped4.12189

Gulisano, M., Calì, P., Palermo, F., Robertson, M., & Rizzo, R. (2015). Premonitory Urges in Patients with Gilles de la Tourette Syndrome: An Italian Translation and

a 7-Year Follow-up. *Journal of Child and Adolescent Psychopharmacology*, *25*(10), 810–816. https://doi.org/10.1089/cap.2014.0154

Gunduz, M. E., Pinto, C. B., Saleh Velez, F. G., Duarte, D., Pacheco-Barrios, K., Lopes, F., & Fregni, F. (2020). Motor Cortex Reorganization in Limb Amputation: A Systematic Review of TMS Motor Mapping Studies. *Frontiers in Neuroscience*, *14*. https://doi.org/10.3389/fnins.2020.00314

Haas, M., Jakubovski, E., Fremer, C., Dietrich, A., Hoekstra, P. J., Jäger, B., & Müller-Vahl, K. R. (2021). Yale Global Tic Severity Scale (YGTSS): Psychometric Quality of the Gold Standard for Tic Assessment Based on the Large-Scale EMTICS Study. *Frontiers in Psychiatry*, *12*. https://doi.org/10.3389/fpsyt.2021.626459

Hajnal, J. V., Myers, R., Oatridge, A., Schwieso, J. E., Young, I. R., & Bydder, G. M. (1994). Artifacts due to stimulus correlated motion in functional imaging of the brain. *Magnetic Resonance in Medicine*, *31*(3), 283–291. https://doi.org/10.1002/mrm.1910310307

Hallett, M. (2000). Transcranial magnetic stimulation and the human brain. *Nature*, *406*(6792), 147–150. https://doi.org/10.1038/35018000

Hallett, M. (2007). Transcranial magnetic stimulation: a primer. *Neuron*, *55*(2), 187–199. https://doi.org/10.1016/j.neuron.2007.06.026

Hamada, M., Murase, N., Hasan, A., Balaratnam, M., & Rothwell, J. C. (2013). The role of interneuron networks in driving human motor cortical plasticity. *Cerebral Cortex*, *23*(7), 1593–1605. https://doi.org/10.1093/cercor/bhs147

Hamdy, S., Aziz, Q., Rothwell, J. C., Power, M., Singh, K. D., Nicholson, D. A., Tallis, R. C., & Thompson, D. G. (1998). Recovery of swallowing after dysphagic stroke relates to functional reorganization in the intact motor cortex. *Gastroenterology*, *115*(5), 1104–1112. https://doi.org/10.1016/S0016-5085(98)70081-2

Hampson, M., Tokoglu, F., King, R. A., Constable, R. T., & Leckman, J. F. (2009). Brain Areas Coactivating with Motor Cortex During Chronic Motor Tics and Intentional Movements. *Biological Psychiatry*, *65*(7), 594–599. https://doi.org/10.1016/j.biopsych.2008.11.012

Harrington, G. S., & Hunter Downs, J. (2001). FMRI mapping of the somatosensory cortex with vibratory stimuli. *Brain Research*, *897*(1–2), 188–192. https://doi.org/10.1016/S0006-8993(01)02139-4

He, J. L., Mikkelsen, M., Huddleston, D. A., Crocetti, D., Cecil, K. M., Singer, H. S., Edden, R. A. E., Gilbert, D. L., Mostofsky, S. H., & Puts, N. A. J. (2022). Frequency and Intensity of Premonitory Urges-to-Tic in Tourette Syndrome Is Associated With Supplementary Motor Area GABA+ Levels. *Movement Disorders*, *37*(3), 563–573. https://doi.org/10.1002/mds.28868

Heise, K. F., Steven, B., Liuzzi, G., Thomalla, G., Jonas, M., Muller-Vahl, K., Sauseng, P., Munchau, A., Gerloff, C., & Hummel, F. C. (2010). Altered modulation of intracortical excitability during movement preparation in Gilles de la Tourette syndrome. *Brain*, *133*, 580–590. https://doi.org/10.1093/brain/awp299

Hess, G., Aizenman, C. D., & Donoghue, J. P. (1996). Conditions for the induction of long-term potentiation in layer II/III horizontal connections of the rat motor cortex. *Journal of Neurophysiology*, *75*(5), 1765–1778. https://doi.org/10.1152/jn.1996.75.5.1765

Hicks, T. P., & Dykes, R. W. (1983). Receptive field size for certain neurons in primary somatosensory cortex is determined by GABA-mediated intracortical inhibition. In *Brain Research* (Vol. 274).

Hillman, E. M. C. (2014). Coupling Mechanism and Significance of the BOLD Signal: A Status Report. *Annual Review of Neuroscience*, *37*(1), 161–181. https://doi.org/10.1146/annurev-neuro-071013-014111

Hinder, M. R., Goss, E. L., Fujiyama, H., Canty, A. J., Garry, M. I., Rodger, J., & Summers, J. J. (2014). Inter- and intra-individual variability following intermittent theta burst stimulation: Implications for rehabilitation and recovery. *Brain Stimulation*, *7*(3), 365–371. https://doi.org/10.1016/j.brs.2014.01.004

Hodgkin, A. L., & Huxley, A. F. (1952). A quantitative description of membrane current and its application to conduction and excitation in nerve. *The Journal of Physiology*, *117*(4), 500–544. https://doi.org/10.1113/jphysiol.1952.sp004764

Houlgreave, M. (2023). *Investigating the neural correlates of urge and the modulatory effects of median nerve stimulation in the context of Tourette syndrome*. University of Nottingham.

Houzé, B., Bradley, C., Magnin, M., & Garcia-Larrea, L. (2013). Changes in Sensory Hand Representation and Pain Thresholds Induced by Motor Cortex Stimulation in Humans. *Cerebral Cortex*, *23*(11), 2667–2676. https://doi.org/10.1093/cercor/bhs255

Hsieh, T. H., Huang, Y. Z., Rotenberg, A., Pascual-Leone, A., Chiang, Y. H., Wang, J. Y., & Chen, J. J. J. (2015). Functional dopaminergic neurons in substantia nigra are required for transcranial magnetic stimulation-induced motor plasticity. *Cerebral Cortex*, *25*(7), 1806–1814. https://doi.org/10.1093/cercor/bht421

Huang, Y. Z., Chen, R. S., Rothwell, J. C., & Wen, H. Y. (2007). The after-effect of human theta burst stimulation is NMDA receptor dependent. *Clinical Neurophysiology*, *118*(5), 1028–1032. https://doi.org/10.1016/j.clinph.2007.01.021

Huang, Y. Z., Edwards, M. J., Rounis, E., Bhatia, K. P., & Rothwell, J. C. (2005). Theta burst stimulation of the human motor cortex. *Neuron*, *45*(2), 201–206. https://doi.org/10.1016/j.neuron.2004.12.033

Huang, Y. Z., Lu, M. K., Antal, A., Classen, J., Nitsche, M., Ziemann, U., Ridding, M., Hamada, M., Ugawa, Y., Jaberzadeh, S., Suppa, A., Paulus, W., & Rothwell, J. (2017). Plasticity induced by non-invasive transcranial brain stimulation: A position paper. In *Clinical Neurophysiology* (Vol. 128, Issue 11, pp. 2318–2329). Elsevier Ireland Ltd. https://doi.org/10.1016/j.clinph.2017.09.007

Huang, Y. Z., Rothwell, J. C., Chen, R. S., Lu, C. S., & Chuang, W. L. (2011). The theoretical model of theta burst form of repetitive transcranial magnetic stimulation. *Clinical Neurophysiology*, *122*(5), 1011–1018. https://doi.org/10.1016/j.clinph.2010.08.016

Huber, L., Kassavetis, P., Gulban, O. F., Hallett, M., & Horovitz, S. G. (2023). Laminar VASO fMRI in focal hand dystonia patients. *Dystonia*, *2*. https://doi.org/10.3389/dyst.2023.10806

Isaacs, D., & Riordan, H. (2020). Sensory hypersensitivity in Tourette syndrome: A review. *Brain and Development*, *42*(9), 627–638. https://doi.org/10.1016/j.braindev.2020.06.003

Jackson, G. M., Draper, A., Dyke, K., Pépés, S. E., & Jackson, S. R. (2015). Inhibition, Disinhibition, and the Control of Action in Tourette Syndrome. *Trends Cogn Sci*, *19*(11), 655–665. https://doi.org/10.1016/j.tics.2015.08.006

Jackson, S. R., Loayza, J., Crighton, M., Sigurdsson, H. P., Dyke, K., & Jackson, G. M. (2020). The role of the insula in the generation of motor tics and the experience of the premonitory urge-to-tic in Tourette syndrome. *Cortex*, *126*, 119–133. https://doi.org/10.1016/j.cortex.2019.12.021

Jackson, S. R., Parkinson, A., Kim, S. Y., Schuermann, M., & Eickhoff, S. B. (2011). On the functional anatomy of the urge-for-action. *Cogn Neurosci*, *2*(3–4), 227–243. https://doi.org/10.1080/17588928.2011.604717

Jackson, S. R., Parkinson, A., Manfredi, V., Millon, G., Hollis, C., & Jackson, G. M. (2013). Motor excitability is reduced prior to voluntary movements in children and adolescents with Tourette syndrome. *Journal of Neuropsychology*, *7*(1), 29–44. https://doi.org/10.1111/j.1748-6653.2012.02033.x

Jackson, S., Sigurdsson, H., Dyke, K., Condon, M., & Jackson, G. The role of the cingulate cortex in the generation of motor tics and the experience of the premonitory urge-to-tic in Tourette syndrome. *BioRxiv*. https://doi.org/10.1101/2020.01.29.924399

Jacobs, K., & Donoghue, J. (1991). Reshaping the cortical motor map by unmasking latent intracortical connections. *Science*, *251*(4996), 944–947. https://doi.org/10.1126/science.2000496

Jalenques, I., Galland, F., Malet, L., Morand, D., Legrand, G., Auclair, C., Hartmann, A., Derost, P., & Durif, F. (2012). Quality of life in adults with Gilles de la Tourette Syndrome. *BMC Psychiatry*, *12*(1), 109. https://doi.org/10.1186/1471-244X-12-109

Janko, D., Thoenes, K., Park, D., Willoughby, W. R., Horton, M., & Bolding, M. (2022). Somatotopic Mapping of the Fingers in the Somatosensory Cortex Using

Functional Magnetic Resonance Imaging: A Review of Literature. *Frontiers in Neuroanatomy*, *16*. https://doi.org/10.3389/fnana.2022.866848

Janssen, A. M., Oostendorp, T. F., & Stegeman, D. F. (2015). The coil orientation dependency of the electric field induced by TMS for M1 and other brain areas. *Journal of NeuroEngineering and Rehabilitation*, *12*(1). https://doi.org/10.1186/s12984-015-0036-2

Jenkinson, M., Bannister, P., Brady, M., & Smith, S. (2002). Improved Optimization for the Robust and Accurate Linear Registration and Motion Correction of Brain Images. *NeuroImage*, *17*(2), 825–841. https://doi.org/10.1016/S1053-8119(02)91132-8

Jenkinson, M., Beckmann, C. F., Behrens, T. E. J., Woolrich, M. W., & Smith, S. M. (2012). FSL. *NeuroImage*, *62*(2), 782–790. https://doi.org/10.1016/j.neuroimage.2011.09.015

Jenkinson, M., Bijsterbosch, J., Chappell, M., & Winkler, A. (2020). Short introduction to the General Linear Model for Neuroimaging. In M. Jenkinson & M. Chappell (Eds.), *Oxford Neuroimaging Primers* (pp. 1–31). Oxford University Press.

Jenkinson, M., & Smith, S. (2001). A global optimisation method for robust affine registration of brain images. *Medical Image Analysis*, *5*(2), 143–156. https://doi.org/10.1016/S1361-8415(01)00036-6

Jezzard, P. (2012). Correction of geometric distortion in fMRI data. *NeuroImage*, *62*(2), 648–651. https://doi.org/10.1016/j.neuroimage.2011.09.010

Jiménez-Jiménez, F. J., Alonso-Navarro, H., García-Martín, E., & Agúndez, J. A. G. (2020). Sleep disorders in tourette syndrome. In *Sleep Medicine Reviews* (Vol. 53, p. 101335). W.B. Saunders Ltd. https://doi.org/10.1016/j.smrv.2020.101335

Jones, E. G. (1993). Gabaergic neurons and their role in cortical plasticity in primates. *Cerebral Cortex*, *3*(5), 361–372. https://doi.org/10.1093/cercor/3.5.361-a

Juchem, C., & Rothman, D. L. (2014). Basis of Magnetic Resonance. In C. Stagg & D. Rothman (Eds.), *Magnetic Resonance Spectroscopy* (pp. 3–14). Elsevier. https://doi.org/10.1016/B978-0-12-401688-0.00001-X

Julkunen, P. (2014). Methods for estimating cortical motor representation size and location in navigated transcranial magnetic stimulation. *Journal of Neuroscience Methods*, *232*, 125–133. https://doi.org/10.1016/j.jneumeth.2014.05.020

Jung, J., Bungert, A., Bowtell, R., & Jackson, S. R. (2016). Vertex Stimulation as a Control Site for Transcranial Magnetic Stimulation: A Concurrent TMS/fMRI Study. *Brain Stimulation*, *9*(1), 58–64. https://doi.org/10.1016/j.brs.2015.09.008

Jung, J., Jackson, S. R., Parkinson, A., & Jackson, G. M. (2013). Cognitive control over motor output in Tourette syndrome. *Neuroscience & Biobehavioral Reviews*, *37*(6), 1016–1025. https://doi.org/10.1016/j.neubiorev.2012.08.009

Kaelin-Lang, A., Luft, A. R., Sawaki, L., Burstein, A. H., Sohn, Y. H., & Cohen, L. G. (2002). Modulation of human corticomotor excitability by somatosensory input. *The Journal of Physiology*, *540*(2), 623–633. https://doi.org/10.1113/jphysiol.2001.012801

Kalanithi, P. S. A., Zheng, W., Kataoka, Y., DiFiglia, M., Grantz, H., Saper, C. B., Schwartz, M. L., Leckman, J. F., & Vaccarino, F. M. (2005). Altered parvabumin-positive neuron distribution in basal ganglia of individuals with Tourette syndrome. *PNAS*, *102*(37), 13307–13312.

Kalisch, T., Tegenthoff, M., & Dinse, H. R. (2008). Improvement of sensorimotor functions in old age by passive sensory stimulation. *Clinical Interventions in Aging*, *3*(4), 673–690. https://doi.org/10.2147/cia.s3174

Kane, M. J. (1994). Premonitory urges as “attentional tics” in Tourette’s syndrome. *J Am Acad Child Adolesc Psychiatry*, *33*(6), 805–808.

Kaneko, T., & Hicks, T. P. (1990). GABA(B)-related activity involved in synaptic processing of somatosensory information in S1 cortex of the anaesthetized cat. *British Journal of Pharmacology*, *100*(4), 689–698. https://doi.org/10.1111/j.1476-5381.1990.tb14077.x

Kemlin, C., Moulton, E., Leder, S., Houot, M., Meunier, S., Rosso, C., & Lamy, J.-C. (2019). Redundancy among parameters describing the input-output relation of motor evoked potentials in healthy subjects and stroke patients. *Frontiers in Neurology*, *10*, 1–8. https://doi.org/10.3389/fneur.2019.00535

Kikkert, S., Sonar, H. A., Freund, P., Paik, J., & Wenderoth, N. (2023). Hand and face somatotopy shown using MRI-safe vibrotactile stimulation with a novel soft pneumatic actuator (SPA)-skin interface. *NeuroImage*, *269*, 119932. https://doi.org/10.1016/j.neuroimage.2023.119932

Kim, S., Greene, D. J., Robichaux-Viehoever, A., Bihun, E. C., Koller, J. M., Acevedo, H., Schlaggar, B. L., & Black, K. J. (2019). Tic Suppression in Children With Recent-Onset Tics Predicts 1-Year Tic Outcome. *Journal of Child Neurology*, *34*(12), 757–764. https://doi.org/10.1177/0883073819855531

Klomjai, W., Katz, R., & Lackmy-Vallée, A. (2015). Basic principles of transcranial magnetic stimulation (TMS) and repetitive TMS (rTMS). In *Annals of Physical and Rehabilitation Medicine* (Vol. 58, Issue 4, pp. 208–213). Elsevier Masson SAS. https://doi.org/10.1016/j.rehab.2015.05.005

Kohn, A., & Whitsel, B. L. (2002). Sensory cortical dynamics. *Behavioural Brain Research*, *135*(1–2), 119–126. https://doi.org/10.1016/S0166-4328(02)00139-0

Kolasinski, J., Logan, J. P., Hinson, E. L., Manners, D., Divanbeighi Zand, A. P., Makin, T. R., Emir, U. E., & Stagg, C. J. (2017). A Mechanistic Link from GABA to Cortical Architecture and Perception. *Current Biology*, *27*(11), 1685-1691.e3. https://doi.org/10.1016/j.cub.2017.04.055

Kolasinski, J., Makin, T. R., Jbabdi, S., Clare, S., Stagg, C. J., & Johansen-Berg, H. (2016). Investigating the Stability of Fine-Grain Digit Somatotopy in Individual Human Participants. *The Journal of Neuroscience*, *36*(4), 1113–1127. https://doi.org/10.1523/JNEUROSCI.1742-15.2016

Kolb, B., & Whishaw, I. Q. (1998). Brain plasticity and behavior. *Annual Review of Psychology*, *49*(1), 43–64. https://doi.org/10.1146/annurev.psych.49.1.43

Koller, W. C., & Biary, N. M. (1989). Volitional control of involuntary movements. *Movement Disorders*, *4*(2), 153–156. https://doi.org/10.1002/mds.870040207

Komiyama, O., & De Laat, A. (2005). Tactile and pain thresholds in the intra- and extra-oral regions of symptom-free subjects. *Pain*, *115*(3), 308–315. https://doi.org/10.1016/j.pain.2005.03.006

Konakanchi, D., de Jongh Curry, A. L., Waters, R. S., & Narayana, S. (2020). Focality of the induced e-field is a contributing factor in the choice of tms parameters:

Evidence from a 3d computational model of the human brain. *Brain Sciences*, *10*(12), 1–17. https://doi.org/10.3390/brainsci10121010

Kostanecka-Endress, T., Banaschewski, T., Kinkelbur, J., Wüllner, I., Lichtblau, S., Cohrs, S., Rüther, E., Woerner, W., Hajak, G., & Rothenberger, A. (2003). Disturbed sleep in children with Tourette syndrome A polysomnographic study. *Journal of Psychosomatic Research*, *55*(1), 23–29. https://doi.org/10.1016/S0022-3999(02)00602-5

Kozyrev, V., Eysel, U. T., & Jancke, D. (2014). Voltage-sensitive dye imaging of transcranial magnetic stimulation-induced intracortical dynamics. *Proceedings of the National Academy of Sciences of the United States of America*, *111*(37), 13553–13558. https://doi.org/10.1073/pnas.1405508111

Kozyrev, V., Staadt, R., Eysel, U. T., & Jancke, D. (2018). TMS-induced neuronal plasticity enables targeted remodeling of visual cortical maps. *Proceedings of the National Academy of Sciences of the United States of America*, *115*(25), 6476–6481. https://doi.org/10.1073/pnas.1802798115

Krippl, M., Karim, A. A., & Brechmann, A. (2015). Neuronal correlates of voluntary facial movements. *Frontiers in Human Neuroscience*, *9*. https://doi.org/10.3389/fnhum.2015.00598

Kujirai, T., Caramia, M. D., Rothwell, J. C., Day, B. L., Thompson, P. D., Ferbert, A., Wroe, S., Asselman, P., & Marsden, C. D. (1993). Corticocortical inhibition in human motor cortex. *The Journal of Physiology*, *471*(1), 501–519. https://doi.org/10.1113/jphysiol.1993.sp019912

Kwak, C., Dat Vuong, K., & Jankovic, J. (2003). Premonitory sensory phenomenon in Tourette's syndrome. *Movement Disorders*, *18*(12), 1530–1533. https://doi.org/10.1002/mds.10618

Kwon, H. J., Lim, W. S., Lim, M. H., Lee, S. J., Hyun, J. K., Chae, J.-H., & Paik, K. C. (2011). 1-Hz low frequency repetitive transcranial magnetic stimulation in children with Tourette's syndrome. *Neuroscience Letters*, *492*(1), 1–4. https://doi.org/10.1016/j.neulet.2011.01.007

Labedi, A., Benali, A., Mix, A., Neubacher, U., & Funke, K. (2014). Modulation of Inhibitory Activity Markers by Intermittent Theta-burst Stimulation in Rat

Cortex is NMDA-receptor Dependent. *Brain Stimulation*, *7*(3), 394–400. https://doi.org/10.1016/j.brs.2014.02.010

Lane, R. D., & Schwartz, G. E. (1987). Levels of emotional awareness: a cognitive-developmental theory and its application to psychopathology. *American Journal of Psychiatry*, *144*(2), 133–143. https://doi.org/10.1176/ajp.144.2.133

Larsh, T. R., Huddleston, D. A., Horn, P. S., Wu, S. W., Cecil, K. M., Jackson, H. S., Edden, R. A. E., Mostofsky, S. H., & Gilbert, D. L. (2023). From urges to tics in children with Tourette syndrome: associations with supplementary motor area GABA and right motor cortex physiology. *Cerebral Cortex*, *33*(7), 3922–3933. https://doi.org/10.1093/cercor/bhac316

Lazzaro, V. Di, Ziemann, U., & Lemon, R. N. (2008). State of the art: Physiology of transcranial motor cortex stimulation. *Brain Stimulation*, *1*(4), 345–362. https://doi.org/10.1016/j.brs.2008.07.004

Le, K., Liu, L., Sun, M., Hu, L., & Xiao, N. (2013). Transcranial magnetic stimulation at 1Hertz improves clinical symptoms in children with Tourette syndrome for at least 6 months. *Journal of Clinical Neuroscience*, *20*(2), 257–262. https://doi.org/10.1016/j.jocn.2012.01.049

Leckman, J. F. (2002). Tourette's syndrome. *The Lancet*, *360*(9345), 1577–1586. https://doi.org/10.1016/S0140-6736(02)11526-1

Leckman, J. F., Bloch, M. H., Scahill, L., & King, R. A. (2006). Tourette Syndrome: The Self Under Siege. *J Child Neurol*, *21*, 642–649. https://doi.org/10.2310/7010.2006.00167

Leckman, J. F., & Riddle, M. A. (2000). Tourette's syndrome: When habit-forming systems form habits of their own? *Neuron*, *28*, 349–354.

Leckman, J. F., Riddle, M. A., Hardin, M. T., Ort, S. I., Swartz, K. L., Stevenson, J., & Cohen, D. J. (1989). The Yale Global Tic Severity Scale: Initial testing of a clinician-rated scale of tic severity. *J Am Acad Child Adolesc Psychiatry*, *28*(4), 566–573.

Leckman, J. F., Walker, D. E., & Cohen, D. J. (1993). Premonitory urges in Tourette's syndrome. *American Journal of Psychiatry*, *150*(1), 98–102. https://doi.org/10.1176/ajp.150.1.98

Leckman, J. F., Zhang, H., Vitale, A., Lahnin, F., Lynch, K., Bondi, C., Kim, Y.-S., & Peterson, B. S. (1998). Course of Tic Severity in Tourette Syndrome: The First Two Decades. *Pediatrics*, *102*(1), 14–19. https://doi.org/10.1542/peds.102.1.14

Leodori, G., Thirugnanasambandam, N., Conn, H., Popa, T., Berardelli, A., & Hallett, M. (2019). Intracortical inhibition and surround inhibition in the motor cortex: A tms-EEG study. *Frontiers in Neuroscience*, *13*(JUN), 612. https://doi.org/10.3389/FNINS.2019.00612/BIBTEX

Levine, J. L. S., Szejko, N., & Bloch, M. H. (2019). Meta-analysis: Adulthood prevalence of Tourette syndrome. In *Progress in Neuro-Psychopharmacology and Biological Psychiatry* (Vol. 95, p. 109675). Elsevier Inc. https://doi.org/10.1016/j.pnpbp.2019.109675

Li, H., Heise, K. F., Chalavi, S., Puts, N. A. J., Edden, R. A. E., & Swinnen, S. P. (2022). The role of MRS-assessed GABA in human behavioral performance. In *Progress in Neurobiology* (Vol. 212). Elsevier Ltd. https://doi.org/10.1016/j.pneurobio.2022.102247

Li, Y., Wang, F., Liu, J., Wen, F., Yan, C., Zhang, J., Lu, X., & Cui, Y. (2019). The Correlation between the Severity of Premonitory Urges and Tic Symptoms: A Meta-Analysis. In *Journal of Child and Adolescent Psychopharmacology* (Vol. 29, Issue 9, pp. 652–658). Mary Ann Liebert Inc. https://doi.org/10.1089/cap.2019.0048

Lichter, D. G., & Finnegan, S. G. (2015). Influence of gender on Tourette syndrome beyond adolescence. *Eur Psychiatry*, *30*(2), 334–340. https://doi.org/10.1016/j.eurpsy.2014.07.003

Liepert, J., Tegenthoff, M., & Malin, J.-P. (1995). Changes of cortical motor area size during immobilization. *Electroencephalography and Clinical Neurophysiology/Electromyography and Motor Control*, *97*(6), 382–386. https://doi.org/10.1016/0924-980X(95)00194-P

Lin, P. T., & Hallett, M. (2009). The Pathophysiology of Focal Hand Dystonia. *Journal of Hand Therapy*, *22*(2), 109–114. https://doi.org/10.1016/j.jht.2008.10.008

Liu, J., Feng, X., Wang, Y., Xia, X., & Zheng, J. C. (2022). Astrocytes: GABAceptive and GABAergic Cells in the Brain. *Frontiers in Cellular Neuroscience*, *16*. https://doi.org/10.3389/fncel.2022.892497

Logothetis, N. K. (2003). The Underpinnings of the BOLD Functional Magnetic Resonance Imaging Signal. *The Journal of Neuroscience*, *23*(10), 3963–3971. https://doi.org/10.1523/JNEUROSCI.23-10-03963.2003

Logothetis, N. K., Pauls, J., Augath, M., Trinath, T., & Oeltermann, A. (2001). *Neurophysiological investigation of the basis of the fMRI signal*. www.nature.com

Logothetis, N. K., & Wandell, B. A. (2004). Interpreting the BOLD Signal. *Annual Review of Physiology*, *66*(1), 735–769. https://doi.org/10.1146/annurev.physiol.66.082602.092845

López-Alonso, V., Cheeran, B., Río-Rodríguez, D., & Fernández-Del-Olmo, M. (2014). Inter-individual variability in response to non-invasive brain stimulation paradigms. *Brain Stimulation*, *7*(3), 372–380. https://doi.org/10.1016/j.brs.2014.02.004

López-Alonso, V., Liew, S. L., del Olmo, M. F., Cheeran, B., Sandrini, M., Abe, M., & Cohen, L. G. (2018). A preliminary comparison of motor learning across different non-invasive brain stimulation paradigms shows no consistent modulations. *Frontiers in Neuroscience*, *12*(APR), 1–12. https://doi.org/10.3389/fnins.2018.00253

Lotze, M., Erb, M., Flor, H., Huelsmann, E., Godde, B., & Grodd, W. (2000). fMRI Evaluation of Somatotopic Representation in Human Primary Motor Cortex. *NeuroImage*, *11*(5), 473–481. https://doi.org/10.1006/nimg.2000.0556

Maeda, F., & Pascual-Leone, A. (2003). Transcranial magnetic stimulation: Studying motor neurophysiology of psychiatric disorders. In *Psychopharmacology* (Vol. 168, Issue 4, pp. 359–376). https://doi.org/10.1007/s00213-002-1216-x

Mahone, E. M., Puts, N. A., Edden, R. A. E., Ryan, M., & Singer, H. S. (2018). GABA and glutamate in children with Tourette syndrome: A 1 H MR spectroscopy study at 7 T. *Psychiatry Research - Neuroimaging*, *273*, 46–53. https://doi.org/10.1016/j.pscychresns.2017.12.005

Malinakova, K., Novak, L., Trnka, R., & Tavel, P. (2021). Sensory Processing Sensitivity Questionnaire: A Psychometric Evaluation and Associations with Experiencing the COVID-19 Pandemic. *International Journal of Environmental Research and Public Health*, *18*(24), 12962. https://doi.org/10.3390/ijerph182412962

Mantovani, A., Leckman, J. F., Grantz, H., King, R. A., Sporn, A. L., & Lisanby, S. H. (2007). Repetitive Transcranial Magnetic Stimulation of the Supplementary Motor Area in the treatment of Tourette Syndrome: Report of two cases. *Clinical Neurophysiology*, *118*(10), 2314–2315. https://doi.org/10.1016/j.clinph.2007.07.011

Martino, D., Cavanna, A. E., Robertson, M. M., & Orth, M. (2012). Prevalence and phenomenology of eye tics in Gilles de la Tourette syndrome. *Journal of Neurology*, *259*(10), 2137–2140. https://doi.org/10.1007/s00415-012-6470-1

Martino, D., & Hedderly, T. (2019). Tics and stereotypies: A comparative clinical review. *Parkinsonism and Related Disorders*, *59*, 117–124. https://doi.org/10.1016/j.parkreldis.2019.02.005

Mastria, G., Scaliti, E., Mehring, C., Burdet, E., Becchio, C., Serino, A., & Akselrod, M. (2023). Morphology, Connectivity, and Encoding Features of Tactile and Motor Representations of the Fingers in the Human Precentral and Postcentral Gyrus. *The Journal of Neuroscience*, *43*(9), 1572–1589. https://doi.org/10.1523/JNEUROSCI.1976-21.2022

Matsuda, N., Nonaka, M., Kono, T., Fujio, M., Nobuyoshi, M., & Kano, Y. (2020). Premonitory Awareness Facilitates Tic Suppression: Subscales of the Premonitory Urge for Tics Scale and a New Self-Report Questionnaire for Tic-Associated Sensations. *Frontiers in Psychiatry*, *11*, 1. https://doi.org/10.3389/fpsyt.2020.00592

Matsumura, M., Sawaguchi, T., Oishi, T., Ueki, K., & Kubota, K. (1991). Behavioral deficits induced by local injection of bicuculline and muscimol into the primate motor and premotor cortex. *Journal of Neurophysiology*, *65*(6), 1542–1553. https://doi.org/10.1152/jn.1991.65.6.1542

McCairn, K. W., Bronfeld, M., Belelovsky, K., & Bar-Gad, I. (2009). The neurophysiological correlates of motor tics following focal striatal disinhibition. *Brain*, *132*(8), 2125–2138. https://doi.org/10.1093/brain/awp142

McCairn, K. W., Iriki, A., & Isoda, M. (2013). Global Dysrhythmia of Cerebro-Basal Ganglia-Cerebellar Networks Underlies Motor Tics following Striatal Disinhibition. *Journal of Neuroscience*, *33*(2), 697–708. https://doi.org/10.1523/JNEUROSCI.4018-12.2013

McCairn, K. W., & Isoda, M. (2013). Pharmacological Animal Models of Tic Disorders. In *International Review of Neurobiology* (Vol. 112, pp. 179–209). https://doi.org/10.1016/B978-0-12-411546-0.00007-X

McGuire, J. F., McBride, N., Piacentini, J., Johnco, C., Lewin, A. B., Murphy, T. K., & Storch, E. A. (2016). The premonitory urge revisited: An individualized premonitory urge for tics scale. *Journal of Psychiatric Research*, *83*, 176–183. https://doi.org/10.1016/j.jpsychires.2016.09.007

McKenzie, A. L., Nagarajan, S. S., Roberts, T. P. L., Merzenich, M. M., & Byl, N. N. (2003). Somatosensory Representation of the Digits and Clinical Performance in Patients with Focal Hand Dystonia. *American Journal of Physical Medicine & Rehabilitation*, *82*(10), 737–749. https://doi.org/10.1097/01.PHM.0000087458.32122.14

McRobbie, D. W., Moore, E. A., Graves, M. J., & Prince, M. R. (2017). MRI from Picture to Proton. In *American Journal of Roentgenology* (2nd ed., Vol. 182, Issue 3). Cambridge University Press. https://doi.org/10.1017/9781107706958

Menon, P., Kiernan, M. C., & Vucic, S. (2018). Cortical excitability varies across different muscles. *Journal of Neurophysiology*, *120*(3), 1397–1403. https://doi.org/10.1152/jn.00148.2018

Meunier, S., Garnero, L., Ducorps, A., Maziè, L., Lehéricy, S., Tézenas Du Montcel, S., Renault, B., & Vidailhet, M. (2001). Human Brain Mapping in Dystonia Reveals Both Endophenotypic Traits and Adaptive Reorganization. *Ann Neurol*, *50*, 521–527. https://doi.org/10.1002/aon.1234

Meunier, S., Lehéricy, S., Garnero, L., & Vidailhet, M. (2003). Dystonia: Lessons from Brain Mapping. *The Neuroscientist*, *9*(1), 76–81. https://doi.org/10.1177/1073858402239593

Mikkelsen, M., Harris, A. D., Edden, R. A. E., & Puts, N. A. J. (2018). Macromolecule-suppressed GABA measurements correlate more strongly with behavior than macromolecule-contaminated GABA+ measurements. *Brain Research*, *1701*, 204–211. https://doi.org/10.1016/j.brainres.2018.09.021

Miniussi, C., & Rossini, P. M. (2011). Transcranial magnetic stimulation in cognitive rehabilitation. *Neuropsychological Rehabilitation*, *21*(5), 579–601. https://doi.org/10.1080/09602011.2011.562689

Mink, J. W. (2001). *Basal Ganglia Dysfunction in Tourette's Syndrome: A New Hypothesis*.

Mink, J. W. (2003). The Basal Ganglia and Involuntary Movements. *Archives of Neurology*, *60*(10), 1365. https://doi.org/10.1001/archneur.60.10.1365

Miyachi, S., Lu, X., Imanishi, M., Sawada, K., Nambu, A., & Takada, M. (2006). Somatotopically arranged inputs from putamen and subthalamic nucleus to primary motor cortex. *Neuroscience Research*, *56*(3), 300–308. https://doi.org/10.1016/j.neures.2006.07.012

Moeller, S., Pisharady, P. K., Ramanna, S., Lenglet, C., Wu, X., Dowdle, L., Yacoub, E., Uğurbil, K., & Akçakaya, M. (2021). NOise reduction with DIstribution Corrected (NORDIC) PCA in dMRI with complex-valued parameter-free locally low-rank processing. *NeuroImage*, *226*. https://doi.org/10.1016/j.neuroimage.2020.117539

Moeller, S., Yacoub, E., Olman, C. A., Auerbach, E., Strupp, J., Harel, N., & Uğurbil, K. (2010). Multiband multislice GE-EPI at 7 tesla, with 16-fold acceleration using partial parallel imaging with application to high spatial and temporal whole-brain fMRI. *Magnetic Resonance in Medicine*, *63*(5), 1144–1153. https://doi.org/10.1002/mrm.22361

Mohammadi-Nejad, A., Pszczolkowski, S., Auer, D., & Sotiropoulos, S. (2019). *Multi-modal neuroimaging pipelines for data preprocessing [Computer software].* . https://doi.org/10.5281/zenodo.3624973

Mol Debes, N. M. M. (2013). Co-morbid disorders in Tourette syndrome. *Behavioural Neurology*, *27*, 7–14. https://doi.org/10.3233/BEN-120275

Moll, G. H., Wischer, S., Heinrich, H., Tergau, F., Paulus, W., & Rothenberger, A. (1999). Deficient motor control in children with tic disorder: evidence from transcranial magnetic stimulation. *Neuroscience Letters*, *272*(1), 37–40. https://doi.org/10.1016/S0304-3940(99)00575-3

Molloy, F. M. (2003). Abnormalities of spatial discrimination in focal and generalized dystonia. *Brain*, *126*(10), 2175–2182. https://doi.org/10.1093/brain/awg219

Molloy, F. M., Carr, T. D., Zeuner, K. E., Dambrosia, J. M., & Hallett, M. (2003). Abnormalities of spatial discrimination in focal and generalized dystonia. *Brain*, *126*(10), 2175–2182. https://doi.org/10.1093/brain/awg219

Morris, T. P., Davila-Pérez, P., Jannati, A., Menardi, A., Pascual-Leone, A., & Fried, P. J. (2019). Aftereffects of intermittent theta-burst stimulation in adjacent, non-target muscles. *Neuroscience*, *418*, 157–165. https://doi.org/10.1016/j.neuroscience.2019.08.043

Moulton, E. A., Pendse, G., Morris, S., Aiello-Lammens, M., Becerra, L., & Borsook, D. (2009). Segmentally arranged somatotopy within the face representation of human primary somatosensory cortex. *Human Brain Mapping*, *30*(3), 757–765. https://doi.org/10.1002/hbm.20541

Müller-Vahl, K. R., Riemann, L., & Bokemeyer, S. (2014). Tourette patients' misbelief of a tic rebound is due to overall difficulties in reliable tic rating. *Journal of Psychosomatic Research*, *76*(6), 472–476. https://doi.org/10.1016/j.jpsychores.2014.03.003

Münchau, A., Colzato, L. S., AghajaniAfjedi, A., & Beste, C. (2021). A neural noise account of Gilles de la Tourette syndrome. *NeuroImage: Clinical*, *30*, 102654. https://doi.org/10.1016/j.nicl.2021.102654

Murakami, T., Müller-Dahlhaus, F., Lu, M. K., & Ziemann, U. (2012). Homeostatic metaplasticity of corticospinal excitatory and intracortical inhibitory neural circuits in human motor cortex. *Journal of Physiology*, *590*(22), 5765–5781. https://doi.org/10.1113/jphysiol.2012.238519

Murphy, J., Brewer, R., Plans, D., Khalsa, S. S., Catmur, C., & Bird, G. (2020). Testing the independence of self-reported interoceptive accuracy and attention. *Quarterly Journal of Experimental Psychology*, *73*(1), 115–133. https://doi.org/10.1177/1747021819879826

Nachev, P., Kennard, C., & Husain, M. (2008). Functional role of the supplementary and pre-supplementary motor areas. *Nature Reviews Neuroscience*, *9*(11), 856–869. https://doi.org/10.1038/nrn2478

Nakamura, H., Kitagawa, H., Kawaguchi, Y., & Tsuji, H. (1997). Intracortical facilitation and inhibition after transcranial magnetic stimulation in conscious humans. *The Journal of Physiology*, *498*(3), 817–823. https://doi.org/10.1113/jphysiol.1997.sp021905

Napadow, V., Kettner, N., Ryan, A., Kwong, K. K., Audette, J., & Hui, K. K. S. (2006). Somatosensory cortical plasticity in carpal tunnel syndrome-a cross-sectional fMRI evaluation. *NeuroImage*, *31*(2), 520–530. https://doi.org/10.1016/j.neuroimage.2005.12.017

Nelson, A. J., Blake, D. T., & Chen, R. (2009). Digit-specific aberrations in the primary somatosensory cortex in Writer's cramp. *Annals of Neurology*, *66*(2), 146–154. https://doi.org/10.1002/ana.21626

Nelson, A. J., Staines, W. R., Graham, S. J., & McIlroy, W. E. (2004). Activation in SI and SII; the influence of vibrotactile amplitude during passive and task-relevant stimulation. *Cognitive Brain Research*, *19*(2), 174–184. https://doi.org/10.1016/j.cogbrainres.2003.11.013

Nettekoven, C., Volz, L. J., Kutscha, M., Pool, E. M., Rehme, A. K., Eickhoff, S. B., Fink, G. R., & Grefkes, C. (2014). Dose-dependent effects of theta burst rTMS on cortical excitability and resting-state connectivity of the human motor system. *Journal of Neuroscience*, *34*(20), 6849–6859. https://doi.org/10.1523/JNEUROSCI.4993-13.2014

Neuner, I., Werner, C. J., Arrubla, J., Stöcker, T., Ehlen, C., Wegener, H. P., Schneider, F., & Jon Shah, N. (2014). Imaging the where and when of tic generation and resting state networks in adult Tourette patients. *Frontiers in Human Neuroscience*, *8*(MAY), 1–16. https://doi.org/10.3389/fnhum.2014.00362

Niccolai, V., Korczok, S., Finis, J., Jonas, M., Thomalla, G., Siebner, H. R., Müller-Vahl, K., Münchau, A., Schnitzler, A., & Biermann-Ruben, K. (2019). A peek into premonitory urges in Tourette syndrome: Temporal evolution of neurophysiological oscillatory signatures. *Parkinsonism & Related Disorders*, *65*, 153–158. https://doi.org/10.1016/j.parkreldis.2019.05.039

Numssen, O., van der Burght, C. L., & Hartwigsen, G. (2023). Revisiting the focality of non-invasive brain stimulation – Implications for studies of human cognition. In *Neuroscience and Biobehavioral Reviews* (Vol. 149). Elsevier Ltd. https://doi.org/10.1016/j.neubiorev.2023.105154

Numssen, O., Zier, A. L., Thielscher, A., Hartwigsen, G., Knösche, T. R., & Weise, K. (2021). Efficient high-resolution TMS mapping of the human motor cortex by nonlinear regression. *NeuroImage*, *245*. https://doi.org/10.1016/j.neuroimage.2021.118654

Nutt, D. J., & Malizia, A. L. (2001). New insights into the role of the GABAA-benzodiazepine receptor in psychiatric disorder. *British Journal of Psychiatry*, *179*(NOV.), 390–396. https://doi.org/10.1192/bjp.179.5.390

Obeso, J. A., Rodríguez-Oroz, M. C., Benitez-Temino, B., Blesa, F. J., Guridi, J., Marin, C., & Rodriguez, M. (2008). Functional organization of the basal ganglia: Therapeutic implications for Parkinson's disease. *Movement Disorders*, *23*(SUPPL. 3). https://doi.org/10.1002/mds.22062

Oka, J.-I., Jang, E. K., & Hicks, T. P. (1986). Benzodiazepine receptor involvement in the control of receptive field size and responsiveness in primary somatosensory cortex. In *Brain Research* (Vol. 376).

Oldfield, R. C. (1971). The assessment and analysis of handedness: The Edinburgh inventory. *Neuropsychologia*, *9*(1), 97–113. https://doi.org/10.1016/0028-3932(71)90067-4

Olman, C. A., Pickett, K. A., Schallmo, M., & Kimberley, T. J. (2012). Selective BOLD responses to individual finger movement measured with fMRI at 3T. *Human Brain Mapping*, *33*(7), 1594–1606. https://doi.org/10.1002/hbm.21310

O'Neill, G. C., Sengupta, A., Asghar, M., Barratt, E. L., Besle, J., Schluppeck, D., Francis, S. T., & Sanchez Panchuelo, R. M. (2020). A probabilistic atlas of finger

dominance in the primary somatosensory cortex. *NeuroImage*, *217*, 116880. https://doi.org/10.1016/j.neuroimage.2020.116880

O'Neill, J., Piacentini, J. C., & Peterson, B. S. (2019). Cingulate role in Tourette syndrome. In *Handbook of Clinical Neurology* (166th ed., pp. 165–221). https://doi.org/10.1016/B978-0-444-64196-0.00011-X

Opitz, A., Legon, W., Rowlands, A., Bickel, W. K., Paulus, W., & Tyler, W. J. (2013). Physiological observations validate finite element models for estimating subject-specific electric field distributions induced by transcranial magnetic stimulation of the human motor cortex. *NeuroImage*, *81*, 253–264. https://doi.org/10.1016/j.neuroimage.2013.04.067

Orth, M. (2009). Transcranial magnetic stimulation in Gilles de la Tourette syndrome. *Journal of Psychosomatic Research*, *67*(6), 591–598. https://doi.org/10.1016/j.jpsychores.2009.07.014

Orth, M., Amann, B., Robertson, M. M., & Rothwell, J. C. (2005). Excitability of motor cortex inhibitory circuits in Tourette syndrome before and after single dose nicotine. *Brain*, *128*(Pt 6), 1292–1300. https://doi.org/10.1093/brain/awh473

Orth, M., Münchau, A., & Rothwell, J. C. (2008). Corticospinal System Excitability at Rest Is Associated with Tic Severity in Tourette Syndrome. *Biological Psychiatry*, *64*(3), 248–251. https://doi.org/10.1016/j.biopsych.2007.12.009

Pascual-Leone, A., Walsh, V., & Rothwell, J. (2000). Transcranial magnetic stimulation in cognitive neuroscience – virtual lesion, chronometry, and functional connectivity. *Current Opinion in Neurobiology*, *10*(2), 232–237. https://doi.org/10.1016/S0959-4388(00)00081-7

Patel, N., Jankovic, J., & Hallett, M. (2014). Sensory aspects of movement disorders. *The Lancet Neurology*, *13*(1), 100–112. https://doi.org/10.1016/s1474-4422(13)70213-8

Peinemann, A., Lehner, C., Mentschel, C., Münchau, A., Conrad, B., & Siebner, H. R. (2000). Subthreshold 5-Hz repetitive transcranial magnetic stimulation of the human primary motor cortex reduces intracortical paired-pulse inhibition. *Neuroscience Letters*, *296*(1), 21–24. https://doi.org/10.1016/S0304-3940(00)01616-5

Peirce, J., Gray, J. R., Simpson, S., MacAskill, M., Höchenberger, R., Sogo, H., Kastman, E., & Lindeløv, J. K. (2019). PsychoPy2: Experiments in behavior made easy. *Behavior Research Methods*, *51*(1), 195–203. https://doi.org/10.3758/s13428-018-01193-y

Penfield, W., & Boldrey, E. (1937). Somatic motor and sensory representation in man. *Brain*, *60*(4), 389–443. https://doi.org/10.1093/brain/60.4.389

Pépés, S. E., Draper, A., Jackson, G. M., & Jackson, S. R. (2016). Effects of age on motor excitability measures from children and adolescents with Tourette syndrome. *Dev Cogn Neurosci*, *19*, 78–86. https://doi.org/10.1016/j.dcn.2016.02.005

Pertermann, M., Mückschel, M., Adelhöfer, N., Ziemssen, T., & Beste, C. (2019). On the interrelation of 1/ *f* neural noise and norepinephrine system activity during motor response inhibition. *Journal of Neurophysiology*, *121*(5), 1633–1643. https://doi.org/10.1152/jn.00701.2018

Piccinin, M. A., Miao, J. H., & Schwartz, J. (2018). Histology, Meissner Corpuscle. In *StatPearls*. StatPearls Publishing LLC.

Pile, V., Lau, J. Y. F., Topor, M., Hedderly, T., & Robinson, S. (2018). Interoceptive Accuracy in Youth with Tic Disorders: Exploring Links with Premonitory Urge, Anxiety and Quality of Life. *Journal of Autism and Developmental Disorders*, *48*(10), 3474–3482. https://doi.org/10.1007/s10803-018-3608-8

Pineiro, R., Pendlebury, ; S, Johansen-Berg, ; H, & Matthews, ; P M. (2002). *Altered Hemodynamic Responses in Patients After Subcortical Stroke Measured by Functional MRI*. www.frmib.ox.ac.uk/fsl/

Pitcher, J. B., Doeltgen, S. H., Goldsworthy, M. R., Schneider, L. A., Vallence, A. M., Smith, A. E., Semmler, J. G., McDonnell, M. N., & Ridding, M. C. (2015). A comparison of two methods for estimating 50% of the maximal motor evoked potential. *Clinical Neurophysiology*, *126*(12), 2337–2341. https://doi.org/10.1016/j.clinph.2015.02.011

Platz, T., Adler-Wiebe, M., Roschka, S., & Lotze, M. (2018). Enhancement of motor learning by focal intermittent theta burst stimulation (iTBS) of either the primary motor (M1) or somatosensory area (S1) in healthy human subjects.

Restorative Neurology and Neuroscience, *36*(1), 117–130. https://doi.org/10.3233/RNN-170774

Pleger, B., Blankenburg, F., Bestmann, S., Ruff, C. C., Wiech, K., Stephan, K. E., Friston, K. J., & Dolan, R. J. (2006). Repetitive transcranial magnetic stimulation-induced changes in sensorimotor coupling parallel improvements of somatosensation in humans. *Journal of Neuroscience*, *26*(7), 1945–1952. https://doi.org/10.1523/JNEUROSCI.4097-05.2006

Plessen, K. J. (2013). Tic disorders and Tourette's syndrome. *European Child & Adolescent Psychiatry*, *22*(S1), 55–60. https://doi.org/10.1007/s00787-012-0362-x

Plewes, D. B., & Kucharczyk, W. (2012). Physics of MRI: A primer. *Journal of Magnetic Resonance Imaging*, *35*(5), 1038–1054. https://doi.org/10.1002/jmri.23642

Polanía, R., Nitsche, M. A., & Ruff, C. C. (2018). Studying and modifying brain function with non-invasive brain stimulation. *Nature Neuroscience*, *21*(2), 174–187. https://doi.org/10.1038/s41593-017-0054-4

Poldrack, R. A., Mumford, J. A., & Nichols, T. E. (2011). *Handbook of Functional MRI Data Analysis*. Cambridge University Press.

Porges, E. C., Jensen, G., Foster, B., Edden, R. A. E., & Puts, N. A. J. (2020). The trajectory of cortical GABA levels across the lifespan: An individual participant data meta-analysis of edited MRS studies. *BioRxiv*. https://doi.org/10.1101/2020.07.23.218792

Porges, E. C., Jensen, G., Foster, B., Edden, R. A. E., & Puts, N. A. J. (2021). The trajectory of cortical gaba across the lifespan, an individual participant data meta-analysis of edited mrs studies. *ELife*, *10*. https://doi.org/10.7554/eLife.62575

Power, J. D., Barnes, K. A., Snyder, A. Z., Schlaggar, B. L., & Petersen, S. E. (2012). Spurious but systematic correlations in functional connectivity MRI networks arise from subject motion. *NeuroImage*, *59*(3), 2142–2154. https://doi.org/10.1016/j.neuroimage.2011.10.018

Premoli, I., Castellanos, N., Rivolta, D., Belardinelli, P., Bajo, R., Zipser, C., Espenhahn, S., Heidegger, T., Müller-Dahlhaus, F., & Ziemann, U. (2014). TMS-EEG

Signatures of GABAergic Neurotransmission in the Human Cortex. *The Journal of Neuroscience*, *34*(16), 5603–5612. https://doi.org/10.1523/JNEUROSCI.5089-13.2014

Purves, D., & Williams, S. M. (2001). Mechanoreceptors Specialized to Receive Tactile Information. In P. Dale, A. George J, F. David, K. Lawrence C, L. Anthony-Samuel, M. James O, & W. S Mark (Eds.), *Neuroscience* (2nd ed.). Sinauer Associates.

Puts, N. A., & Edden, R. A. (2012). In vivo magnetic resonance spectroscopy of GABA: a methodological review. *Prog Nucl Magn Reson Spectrosc*, *60*, 29–41. https://doi.org/10.1016/j.pnmrs.2011.06.001

Puts, N. A. J., Edden, R. A. E., John Evans, C., McGlone, F., & McGonigle, D. J. (2011). Regionally specific human GABA concentration correlates with tactile discrimination thresholds. *Journal of Neuroscience*, *31*(46), 16556–16560. https://doi.org/10.1523/JNEUROSCI.4489-11.2011

Puts, N. A. J., Harris, A. D., Crocetti, D., Nettles, C., Singer, H. S., Tommerdahl, M., Edden, R. A. E., & Mostofsky, S. H. (2015). Reduced GABAergic inhibition and abnormal sensory symptoms in children with Tourette syndrome. *Journal of Neurophysiology*, *114*(2), 808–817. https://doi.org/10.1152/jn.00060.2015

Puts, N. A. J., Harris, A. D., Mikkelsen, M., Tommerdahl, M., Edden, R. A. E., & Mostofsky, S. H. (2017). Altered tactile sensitivity in children with attention-deficit hyperactivity disorder. *Journal of Neurophysiology*, *118*(5), 2568–2578. https://doi.org/10.1152/jn.00087.2017

Puts, N. A. J., Heba, S., Harris, A. D., Evans, C. J., McGonigle, D. J., Tegenthoff, M., Schmidt-Wilcke, T., & Edden, R. A. E. (2018). GABA Levels in Left and Right Sensorimotor Cortex Correlate across Individuals. *Biomedicines*, *6*(3), 80. https://doi.org/10.3390/biomedicines6030080

Puts, N. A. J., Wodka, E. L., Harris, A. D., Crocetti, D., Tommerdahl, M., Mostofsky, S. H., & Edden, R. A. E. (2017). Reduced GABA and altered somatosensory function in children with autism spectrum disorder. *Autism Research*, *10*(4), 608–619. https://doi.org/10.1002/aur.1691

Puts, N. A. J., Wodka, E. L., Tommerdahl, M., Mostofsky, S. H., & Edden, R. A. E. (2014). Impaired tactile processing in children with autism spectrum disorder. *Journal of Neurophysiology*, *111*(9), 1803–1811. https://doi.org/10.1152/jn.00890.2013

Quartarone, A., Bagnato, S., Rizzo, V., Morgante, F., Sant'Angelo, A., Battaglia, F., Messina, C., Siebner, H. R., & Girlanda, P. (2005). Distinct changes in cortical and spinal excitability following high-frequency repetitive TMS to the human motor cortex. *Experimental Brain Research*, *161*(1), 114–124. https://doi.org/10.1007/s00221-004-2052-5

Rae, C. D. (2014). A guide to the metabolic pathways and function of metabolites observed in human brain 1H magnetic resonance spectra. *Neurochem Res*, *39*(1), 1–36. https://doi.org/10.1007/s11064-013-1199-5

Rae, C. L., Critchley, H. D., & Seth, A. K. (2019). A Bayesian Account of the Sensory-Motor Interactions Underlying Symptoms of Tourette Syndrome. *Frontiers in Psychiatry*, *10*. https://doi.org/10.3389/fpsyt.2019.00029

Rae, C. L., Larsson, D. E. O., Garfinkel, S. N., & Critchley, H. D. (2019). Dimensions of interoception predict premonitory urges and tic severity in Tourette syndrome. *Psychiatry Research*, *271*, 469–475. https://doi.org/10.1016/j.psychres.2018.12.036

Rae, C. L., Parkinson, J., Betka, S., Gouldvan Praag, C. D., Bouyagoub, S., Polyanska, L., Larsson, D. E. O., Harrison, N. A., Garfinkel, S. N., & Critchley, H. D. (2020). Amplified engagement of prefrontal cortex during control of voluntary action in Tourette syndrome. *Brain Communications*, *2*(2). https://doi.org/10.1093/braincomms/fcaa199

Rae, C., Nasrallah, F. A., Griffin, J. L., & Balcar, V. J. (2009). Now I know my ABC. A systems neurochemistry and functional metabolomic approach to understanding the GABAergic system. *Journal of Neurochemistry*, *109*(SUPPL. 1), 109–116. https://doi.org/10.1111/j.1471-4159.2009.05803.x

Ragert, P., Becker, M., Tegenthoff, M., Pleger, B., & Dinse, H. R. (2004). Sustained increase of somatosensory cortex excitability by 5 Hz repetitive transcranial magnetic stimulation studied by paired median nerve stimulation in humans.

Neuroscience Letters, *356*(2), 91–94. https://doi.org/10.1016/j.neulet.2003.11.034

Ramamoorthi, K., & Lin, Y. (2011). The contribution of GABAergic dysfunction to neurodevelopmental disorders. *Trends in Molecular Medicine*, *17*(8), 452–462. https://doi.org/10.1016/j.molmed.2011.03.003

Reese, H. E., Scahill, L., Peterson, A. L., Crowe, K., Woods, D. W., Piacentini, J., Walkup, J. T., & Wilhelm, S. (2014). The Premonitory Urge to Tic: Measurement, Characteristics, and Correlates in Older Adolescents and Adults. *Behavior Therapy*, *45*(2), 177–186. https://doi.org/10.1016/j.beth.2013.09.002

Ricketts, E. J., Woods, D. W., Espil, F. M., McGuire, J. F., Stiede, J. T., Schild, J., Yadegar, M., Bennett, S. M., Specht, M. W., Chang, S., Scahill, L., Wilhelm, S., Peterson, A. L., Walkup, J. T., & Piacentini, J. (2022). Childhood Predictors of Long-Term Tic Severity and Tic Impairment in Tourette's Disorder. *Behavior Therapy*, *53*(6), 1250–1264. https://doi.org/10.1016/j.beth.2022.07.002

Ridding, M. C., & Rothwell, J. C. (1997). Stimulus/response curves as a method of measuring motor cortical excitability in man. *Electroencephalography and Clinical Neurophysiology/Electromyography and Motor Control*, *105*(5), 340–344. https://doi.org/10.1016/S0924-980X(97)00041-6

Ridding, M. C., & Rothwell, J. C. (2007). Is there a future for therapeutic use of transcranial magnetic stimulation? *Nature Reviews Neuroscience*, *8*(7), 559–567. https://doi.org/10.1038/nrn2169

Ridding, M. C., Sheean, G., Rothwell, J. C., Inzelberg, R., & Kujirai, T. (1995). Changes in the balance between motor cortical excitation and inhibition in focal, task specific dystonia. *Journal of Neurology, Neurosurgery & Psychiatry*, *59*(5), 493–498. https://doi.org/10.1136/jnnp.59.5.493

Robertson, M. M. (2006). Mood disorders and Gilles de la Tourette's syndrome: an update on prevalence, etiology, comorbidity, clinical associations, and implications. *Journal of Psychosomatic Research*, *61*(3), 349–358. https://doi.org/10.1016/j.jpsychores.2006.07.019

Robertson, M. M. (2008). The prevalence and epidemiology of Gilles de la Tourette syndrome. *Journal of Psychosomatic Research*, *65*(5), 461–472. https://doi.org/10.1016/j.jpsychores.2008.03.006

Robertson, M. M., Channon, S., Baker, J., & Flynn, D. (1993). The Psychopathology of Gilles de la Tourette's Syndrome. *British Journal of Psychiatry*, *162*(1), 114–117. https://doi.org/10.1192/bjp.162.1.114

Rocchi, L., Casula, E., Tocco, P., Berardelli, A., & Rothwell, J. (2016). Somatosensory Temporal Discrimination Threshold Involves Inhibitory Mechanisms in the Primary Somatosensory Area. *The Journal of Neuroscience*, *36*(2), 325–335. https://doi.org/10.1523/JNEUROSCI.2008-15.2016

Rona, S., Berardelli, A., Vacca, L., Inghilleri, M., & Manfredi, M. (1998). Alterations of motor cortical inhibition in patients with dystonia. *Movement Disorders*, *13*(1), 118–124. https://doi.org/10.1002/mds.870130123

Rooney, W. D., Johnson, G., Li, X., Cohen, E. R., Kim, S., Ugurbil, K., & Springer, C. S. (2007). Magnetic field and tissue dependencies of human brain longitudinal 1H2O relaxation in vivo. *Magnetic Resonance in Medicine*, *57*(2), 308–318. https://doi.org/10.1002/mrm.21122

Rosenberg, A., Patterson, J. S., & Angelaki, D. E. (2015). A computational perspective on autism. *Proceedings of the National Academy of Sciences*, *112*(30), 9158–9165. https://doi.org/10.1073/pnas.1510583112

Roshan, L., Paradiso, G. O., & Chen, R. (2003). Two phases of short-interval intracortical inhibition. *Experimental Brain Research*, *151*(3), 330–337. https://doi.org/10.1007/s00221-003-1502-9

Rossini, P. M., Burke, D., Chen, R., Cohen, L. G., Daskalakis, Z., Di Iorio, R., Di Lazzaro, V., Ferreri, F., Fitzgerald, P. B., George, M. S., Hallett, M., Lefaucheur, J. P., Langguth, B., Matsumoto, H., Miniussi, C., Nitsche, M. A., Pascual-Leone, A., Paulus, W., Rossi, S., … Ziemann, U. (2015). Non-invasive electrical and magnetic stimulation of the brain, spinal cord, roots and peripheral nerves: Basic principles and procedures for routine clinical and research application. An updated report from an I.F.C.N. Committee. *Clinical Neurophysiology*, *126*(6), 1071–1107. https://doi.org/10.1016/j.clinph.2015.02.001

Rosso, C., Perlbarg, V., Valabregue, R., Obadia, M., Kemlin-Méchin, C., Moulton, E., Leder, S., Meunier, S., & Lamy, J.-C. (2017). Anatomical and functional correlates of cortical motor threshold of the dominant hand. *Brain Stimulation*, *10*(5), 952–958. https://doi.org/10.1016/j.brs.2017.05.005

Rotenberg, A., Horvath, J. C., & Pascual-Leone, A. (2014). The Transcranial Magnetic Stimulation (TMS) Device and Foundational Techniques. In A. Rotenberg, J. C. Horvath, & A. Pascual-Leone (Eds.), *Transcranial Magnetic Stimulation*. Springer New York.

Röther, J., Knab, R., Hamzei, F., Fiehler, J., Reichenbach, J. R., Büchel, C., & Weiller, C. (2002). Negative dip in BOLD fMRI is caused by blood flow - Oxygen consumption uncoupling in humans. *NeuroImage*, *15*(1), 98–102. https://doi.org/10.1006/nimg.2001.0965

Rouder, J. N., Speckman, P. L., Sun, D., Morey, R. D., & Iverson, G. (2009). Bayesian t tests for accepting and rejecting the null hypothesis. *Psychonomic Bulletin & Review*, *16*(2), 225–237. https://doi.org/10.3758/PBR.16.2.225

Sambrani, T., Jakubovski, E., & Müller-Vahl, K. R. (2016). New Insights into Clinical Characteristics of Gilles de la Tourette Syndrome: Findings in 1032 Patients from a Single German Center. *Frontiers in Neuroscience*, *10*(SEP), 415. https://doi.org/10.3389/fnins.2016.00415

Sánchez-Panchuelo, R. M., Besle, J., Beckett, A., Bowtell, R., Schluppeck, D., & Francis, S. (2012). Within-digit functional parcellation of brodmann areas of the human primary somatosensory cortex using functional magnetic resonance imaging at 7 tesla. *Journal of Neuroscience*, *32*(45), 15815–15822. https://doi.org/10.1523/JNEUROSCI.2501-12.2012

Sánchez-Panchuelo, R. M., Francis, S., Bowtell, R., & Schluppeck, D. (2010). Mapping Human Somatosensory Cortex in Individual Subjects With 7T Functional MRI. *Journal of Neurophysiology*, *103*(5), 2544–2556. https://doi.org/10.1152/jn.01017.2009

Sánchez-Panchuelo, R.-M., Besle, J., Mougin, O., Gowland, P., Bowtell, R., Schluppeck, D., & Francis, S. (2014). Regional structural differences across functionally parcellated Brodmann areas of human primary somatosensory

cortex. *NeuroImage*, *93*, 221–230. https://doi.org/10.1016/j.neuroimage.2013.03.044

Sapey-Triomphe, L., Lamberton, F., Sonié, S., Mattout, J., & Schmitz, C. (2019). Tactile hypersensitivity and GABA concentration in the sensorimotor cortex of adults with autism. *Autism Research*, *12*(4), 562–575. https://doi.org/10.1002/aur.2073

Sapey-Triomphe, L.-A., Temmerman, J., Puts, N. A. J., & Wagemans, J. (2021). Prediction learning in adults with autism and its molecular correlates. *Molecular Autism*, *12*(1), 64. https://doi.org/10.1186/s13229-021-00470-6

Scahill, L., Specht, M., & Page, C. (2014). The prevalence of tic disorders and clinical characteristics in children. *Journal of Obsessive-Compulsive and Related Disorders*, *3*(4), 394–400. https://doi.org/10.1016/j.jocrd.2014.06.002

Schabrun, S. M., & Ridding, M. C. (2007). The influence of correlated afferent input on motor cortical representations in humans. *Experimental Brain Research*, *183*(1), 41–49. https://doi.org/10.1007/s00221-007-1019-8

Schabrun, S. M., Stinear, C. M., Byblow, W. D., & Ridding, M. C. (2009). Normalizing motor cortex representations in Focal Hand Dystonia. *Cerebral Cortex*, *19*(9), 1968–1977. https://doi.org/10.1093/cercor/bhn224

Schmidt-Wilcke, T., Fuchs, E., Funke, K., Vlachos, A., Müller-Dahlhaus, F., Puts, N. A. J., Harris, R. E., & Edden, R. A. E. (2018). GABA—from inhibition to cognition: Emerging concepts. *The Neuroscientist*, *24*(5), 501–515. https://doi.org/10.1177/1073858417734530

Schneider, C., Devanne, H., Lavoie, B. A., & Capaday, C. (2002). Neural mechanisms involved in the functional linking of motor cortical points. *Experimental Brain Research*, *146*(1), 86–94. https://doi.org/10.1007/s00221-002-1137-2

Schönbrodt, F. D., & Wagenmakers, E.-J. (2018). Bayes factor design analysis: Planning for compelling evidence. *Psychonomic Bulletin & Review*, *25*(1), 128–142. https://doi.org/10.3758/s13423-017-1230-y

Schott, G. D. (1993). Penfield's homunculus: A note on cerebral cartography. *Journal of Neurology Neurosurgery and Psychiatry*, *56*(4), 329–333. https://doi.org/10.1136/jnnp.56.4.329

Schulz, S. E., Luszawski, M., Hannah, K. E., & Stevenson, R. A. (2023). Sensory Gating in Neurodevelopmental Disorders: A Scoping Review. *Research on Child and Adolescent Psychopathology*, *51*(7), 1005–1019. https://doi.org/10.1007/s10802-023-01058-9

Schunke, O., Grashorn, W., Kahl, U., Schöttle, D., Haggard, P., Münchau, A., Bingel, U., & Ganos, C. (2016). Quantitative Sensory Testing in adults with Tourette syndrome. *Parkinsonism and Related Disorders*, *24*, 132–136. https://doi.org/10.1016/j.parkreldis.2016.01.006

Schweizer, R., Voit, D., & Frahm, J. (2008). Finger representations in human primary somatosensory cortex as revealed by high-resolution functional MRI of tactile stimulation. *NeuroImage*, *42*(1), 28–35. https://doi.org/10.1016/j.neuroimage.2008.04.184

Servos, P., Engel, S. A., Gati, J., & Menon, R. (1999). fMRI evidence for an inverted face representation in human somatosensory cortex. *NeuroReport*, *10*(7), 1393–1395. https://doi.org/10.1097/00001756-199905140-00002

Sharma, H. A. (2009). MRI physics–basic principles. *Acta Neuropsychiatrica*, *21*(4), 200–201. https://doi.org/10.1111/j.1601-5215.2009.00404.x

Siebner, H. R., Funke, K., Aberra, A. S., Antal, A., Bestmann, S., Chen, R., Classen, J., Davare, M., Di Lazzaro, V., Fox, P. T., Hallett, M., Karabanov, A. N., Kesselheim, J., Beck, M. M., Koch, G., Liebetanz, D., Meunier, S., Miniussi, C., Paulus, W., … Ugawa, Y. (2022). Transcranial magnetic stimulation of the brain: What is stimulated? – A consensus and critical position paper. In *Clinical Neurophysiology* (Vol. 140, pp. 59–97). Elsevier Ireland Ltd. https://doi.org/10.1016/j.clinph.2022.04.022

Siebner, H. R., Hartwigsen, G., Kassuba, T., & Rothwell, J. C. (2009). How does transcranial magnetic stimulation modify neuronal activity in the brain? Implications for studies of cognition. *Cortex*, *45*(9), 1035–1042. https://doi.org/10.1016/j.cortex.2009.02.007

Sigurdsson, H. P., Jackson, S. R., Kim, S., Dyke, K., & Jackson, G. M. (2020). A feasibility study for somatomotor cortical mapping in Tourette syndrome using

neuronavigated transcranial magnetic stimulation. *Cortex*, *129*, 175–187. https://doi.org/10.1016/j.cortex.2020.04.014

Sigurdsson, H. P., Molloy, K., & Jackson, S. R. (2020). Somatomotor cortical representations are predicted by levels of short-interval intracortical inhibition. *BioRxiv*. https://doi.org/https://doi.org/10.1101/2020.04.24.057331

Sillito, A. M. (1975). The contribution of inhibitory mechanisms to the receptive field properties of neurones in the striate cortex of the cat. *Journal of Physiology*, *250*, 305–329.

Smith, C. M., Sigurdsson, H. P., Dyke, K., Panchuelo, R. S., Francis, S. T., Jackson, G. M., & Jackson, S. R. (2022). Somatomotor cortical mapping in Tourette syndrome using neuro-navigated transcranial magnetic stimulation. In *International Review of Movement Disorders* (Vol. 3, pp. 321-341). Academic Press. Chicago

Smith, S. M. (2004). Overview of fMRI analysis. In *British Journal of Radiology* (Vol. 77, Issue SPEC. ISS. 2). https://doi.org/10.1259/bjr/33553595

Smith, S. M., & Brady, J. M. (1997). SUSAN—A New Approach to Low Level Image Processing. *International Journal of Computer Vision*, *23*(1), 45–78. https://doi.org/10.1023/A:1007963824710

Sohn, YoungH., & Hallett, M. (2004). Surround inhibition in human motor system. *Experimental Brain Research*, *158*(4), 397–404. https://doi.org/10.1007/s00221-004-1909-y

Soltysik, D. A., Peck, K. K., White, K. D., Crosson, B., & Briggs, R. W. (2004). Comparison of hemodynamic response nonlinearity across primary cortical areas. *NeuroImage*, *22*(3), 1117–1127. https://doi.org/10.1016/j.neuroimage.2004.03.024

Song, A. W., Huettel, S. A., & Mccarthy, G. (2006). Functional Neuroimaging: Basic Principles of Functional MRI. In *Handbook of Functional Neuroimaging of Cognition*. The MIT Press. https://doi.org/10.7551/mitpress/3420.003.0004

Sowell, E. R., Kan, E., Yoshii, J., Thompson, P. M., Bansal, R., Xu, D., Toga, A. W., & Peterson, B. S. (2008). Thinning of sensorimotor cortices in children with

Tourette syndrome. *Nature Neuroscience*, *11*(6), 637–639. https://doi.org/10.1038/nn.2121

Spampinato, D. A., Ibanez, J., Rocchi, L., & Rothwell, J. (2023). Motor potentials evoked by transcranial magnetic stimulation: interpreting a simple measure of a complex system. *The Journal of Physiology*, *601*, 2827–2851. https://doi.org/10.1113/JP281885#support-information-section

Specht, M. W., Nicotra, C. M., Kelly, L. M., Woods, D. W., Ricketts, E. J., Perry-Parrish, C., Reynolds, E., Hankinson, J., Grados, M. A., Ostrander, R. S., & Walkup, J. T. (2014). A Comparison of Urge Intensity and the Probability of Tic Completion During Tic Freely and Tic Suppression Conditions. *Behavior Modification*, *38*(2), 297–318. https://doi.org/10.1177/0145445514537059

Specht, M. W., Woods, D. W., Nicotra, C. M., Kelly, L. M., Ricketts, E. J., Conelea, C. A., Grados, M. A., Ostrander, R. S., & Walkup, J. T. (2013). Effects of tic suppression: Ability to suppress, rebound, negative reinforcement, and habituation to the premonitory urge. *Behaviour Research and Therapy*, *51*(1), 24–30. https://doi.org/10.1016/j.brat.2012.09.009

Stagg, C. J. (2014). Magnetic Resonance Spectroscopy as a tool to study the role of GABA in motor-cortical plasticity. *NeuroImage*, *86*, 19–27. https://doi.org/10.1016/j.neuroimage.2013.01.009

Stagg, C. J., Bestmann, S., Constantinescu, A. O., Moreno Moreno, L., Allman, C., Mekle, R., Woolrich, M., Near, J., Johansen-Berg, H., & Rothwell, J. C. (2011). Relationship between physiological measures of excitability and levels of glutamate and GABA in the human motor cortex. *The Journal of Physiology*, *589*(23), 5845–5855. https://doi.org/10.1113/jphysiol.2011.216978

Stehling, M. K., Turner, R., & Mansfield, P. (1991). Echo-Planar Imaging: Magnetic Resonance Imaging in a Fraction of a Second. *Science*, *254*(5028), 43–50. https://doi.org/10.1126/science.1925560

Steinberg, T., Shmuel Baruch, S., Harush, A., Dar, R., Woods, D., Piacentini, J., & Apter, A. (2010). Tic disorders and the premonitory urge. *Journal of Neural Transmission*, *117*(2), 277–284. https://doi.org/10.1007/s00702-009-0353-3

Stinear, C. M., & Byblow, W. D. (2003). Role of Intracortical Inhibition in Selective Hand Muscle Activation. *Journal of Neurophysiology*, *89*(4), 2014–2020. https://doi.org/10.1152/jn.00925.2002

Stinear, C. M., & Byblow, W. D. (2004). Elevated threshold for intracortical inhibition in focal hand dystonia. *Movement Disorders*, *19*(11), 1312–1317. https://doi.org/10.1002/mds.20160

Storch, E. A., Murphy, T. K., Geffken, G. R., Sajid, M., Allen, P., Roberti, J. W., & Goodman, W. K. (2005). Reliability and validity of the Yale Global Tic Severity Scale. *Psychological Assessment*, *17*(4), 486–491. https://doi.org/10.1037/1040-3590.17.4.486

Stringer, E. A., Chen, L. M., Friedman, R. M., Gatenby, C., & Gore, J. C. (2011). Differentiation of somatosensory cortices by high-resolution fMRI at 7T. *NeuroImage*, *54*(2), 1012–1020. https://doi.org/10.1016/j.neuroimage.2010.09.058

Suppa, A., Huang, Y. Z., Funke, K., Ridding, M. C., Cheeran, B., Di Lazzaro, V., Ziemann, U., & Rothwell, J. C. (2016). Ten years of theta burst stimulation in humans: established knowledge, unknowns and prospects. *Brain Stimulation*, *9*(3), 323–335. https://doi.org/10.1016/j.brs.2016.01.006

Sutherland Owens, A. N., Miguel, E. C., & Swerdlow, N. R. (2011). Sensory Gating Scales and Premonitory Urges in Tourette Syndrome. *The Scientific World JOURNAL*, *11*, 736–741. https://doi.org/10.1100/tsw.2011.57

Talelli, P., Greenwood, R. J., & Rothwell, J. C. (2007). Exploring theta burst stimulation as an intervention to improve motor recovery in chronic stroke. *Clinical Neurophysiology*, *118*(2), 333–342. https://doi.org/10.1016/j.clinph.2006.10.014

Tamburin, S., Fiaschi, A., Andreoli, A., Marani, S., & Zanette, G. (2005). Sensorimotor integration to cutaneous afferents in humans: the effect of the size of the receptive field. *Experimental Brain Research*, *167*(3), 362–369. https://doi.org/10.1007/s00221-005-0041-y

Tang, M., & Yamamoto, T. (2023). Progress in Understanding Radiofrequency Heating and Burn Injuries for Safer MR Imaging. *Magnetic Resonance in*

Medical Sciences, *22*(1), rev.2021-0047. https://doi.org/10.2463/mrms.rev.2021-0047

Tannan, V., Simons, S., Dennis, R. G., & Tommerdahl, M. (2007). Effects of adaptation on the capacity to differentiate simultaneously delivered dual-site vibrotactile stimuli. *Brain Research*, *1186*, 164–170. https://doi.org/10.1016/j.brainres.2007.10.024

Tegenthoff, M., Ragert, P., Pleger, B., Schwenkreis, P., Förster, A. F., Nicolas, V., & Dinse, H. R. (2005). Improvement of tactile discrimination performance and enlargement of cortical somatosensory maps after 5 Hz rTMS. *PLoS Biology*, *3*(11), 2031–2040. https://doi.org/10.1371/journal.pbio.0030362

Tinaz, S., Belluscio, B. A., Malone, P., van der Veen, J. W., Hallett, M., & Horovitz, S. G. (2014). Role of the sensorimotor cortex in tourette syndrome using multimodal imaging. *Human Brain Mapping*, *35*(12), 5834–5846. https://doi.org/10.1002/hbm.22588

Tinaz, S., Malone, P., Hallett, M., & Horovitz, S. G. (2015). Role of the right dorsal anterior insula in the urge to tic in tourette syndrome. *Movement Disorders*, *30*(9), 1190–1197. https://doi.org/10.1002/mds.26230

Tkáč, I., Deelchand, D., Dreher, W., Hetherington, H., Kreis, R., Kumaragamage, C., Považan, M., Spielman, D. M., Strasser, B., & de Graaf, R. A. (2021). Water and lipid suppression techniques for advanced 1H MRS and MRSI of the human brain: Experts' consensus recommendations. *NMR in Biomedicine*, *34*(5). https://doi.org/10.1002/nbm.4459

Tkáč, I., & Gruetter, R. (2005). In vivo 1H NMR spectroscopy and neurochemistry. Quantification matters. *Magnetic Resonance in Medicine*, *54*(4), 1048–1049. https://doi.org/10.1002/mrm.20658

Tkáč, I., Oz, G., Adriany, G., Ugurbil, K., & Gruetter, R. (2009). In vivo 1H NMR spectroscopy of the human brain at high magnetic fields: metabolite quantification at 4T vs. 7T. *Magn Reson Med*, *62*(4), 868–879. https://doi.org/10.1002/mrm.22086

Tkác, I., Starcuk, Z., Choi, I.-Y., & Gruetter, R. (1999). In vivo1H NMR spectroscopy of rat brain at 1 ms echo time. *Magnetic Resonance in Medicine*, *41*(4), 649–656.

https://doi.org/10.1002/(SICI)1522-2594(199904)41:4<649::AID-MRM2>3.0.CO;2-G

Tognarelli, J. M., Dawood, M., Shariff, M. I. F., Grover, V. P. B., Crossey, M. M. E., Cox, I. J., Taylor-Robinson, S. D., & McPhail, M. J. W. (2015). Magnetic Resonance Spectroscopy: Principles and Techniques: Lessons for Clinicians. *Journal of Clinical and Experimental Hepatology*, *5*(4), 320–328. https://doi.org/10.1016/j.jceh.2015.10.006

Tommerdahl, M., Lensch, R., Francisco, E., Holden, J., & Favorov, O. (2019). The Brain Gauge: a novel tool for assessing brain health. *The Journal of Science and Medicine*, *1*(1), 1–19. https://doi.org/10.37714/josam.v1i1.4

Tommerdahl, M., Tannan, V., Holden, J. K., & Baranek, G. T. (2008). Absence of stimulus-driven synchronization effects on sensory perception in autism: Evidence for local underconnectivity? *Behavioral and Brain Functions*, *4*. https://doi.org/10.1186/1744-9081-4-19

Tommerdahl, M., Tannan, V., Zachek, M., Holden, J. K., & Favorov, O. V. (2007). Effects of stimulus-driven synchronization on sensory perception. *Behavioral and Brain Functions*, *3*(1), 61. https://doi.org/10.1186/1744-9081-3-61

Tremblay, S., Beaulé, V., Proulx, S., de Beaumont, L., Marjańska, M., Doyon, J., Pascual-Leone, A., Lassonde, M., Théoret, H., Beaule, V., Proulx, S., de Beaumont, L., Marjanska, M., Doyon, J., Pascual-Leone, A., Lassonde, M., & Theoret, H. (2013). Relationship between transcranial magnetic stimulation measures of intracortical inhibition and spectroscopy measures of GABA and glutamate+glutamine. *Journal of Neurophysiology*, *109*(5), 1343–1349. https://doi.org/10.1152/jn.00704.2012

Tse, N. Y., Goldsworthy, M. R., Ridding, M. C., Coxon, J. P., Fitzgerald, P. B., Fornito, A., & Rogasch, N. C. (2018). The effect of stimulation interval on plasticity following repeated blocks of intermittent theta burst stimulation. *Scientific Reports*, *8*(1), 1–10. https://doi.org/10.1038/s41598-018-26791-w

Tsvetanov, K. A., Henson, R. N. A., Jones, P. S., Mutsaerts, H., Fuhrmann, D., Tyler, L. K., & Rowe, J. B. (2021). The effects of age on resting-state BOLD signal

variability is explained by cardiovascular and cerebrovascular factors. *Psychophysiology*, *58*(7). https://doi.org/10.1111/psyp.13714

Ueda, K., Kim, S., Greene, D. J., & Black, K. J. (2021). Correlates and Clinical Implications of Tic Suppressibility. *Current Developmental Disorders Reports*, *8*(2), 112–120. https://doi.org/10.1007/s40474-021-00230-4

Ueno, S., Matsuda, T., & Fujiki, M. (1990). Functional mapping of the human motor cortex obtained by focal and vectorial magnetic stimulation of the brain. *IEEE Transactions on Magnetics*, *26*(5), 1539–1544. https://doi.org/10.1109/20.104438

Ueno, S., & Sekino, M. (2021). Figure-Eight Coils for Magnetic Stimulation: From Focal Stimulation to Deep Stimulation. In *Frontiers in Human Neuroscience* (Vol. 15). Frontiers Media S.A. https://doi.org/10.3389/fnhum.2021.805971

van de Ruit, M., & Grey, M. J. (2016). The TMS Map Scales with Increased Stimulation Intensity and Muscle Activation. *Brain Topography*, *29*(1), 56–66. https://doi.org/10.1007/s10548-015-0447-1

van De Ruit, M., Perenboom, M. J. L., & Grey, M. J. (2015). TMS brain mapping in less than two minutes. *Brain Stimulation*, *8*(2), 231–239. https://doi.org/10.1016/j.brs.2014.10.020

van der Zwaag, W., Francis, S., Head, K., Peters, A., Gowland, P., Morris, P., & Bowtell, R. (2009). fMRI at 1.5, 3 and 7 T: Characterising BOLD signal changes. *NeuroImage*, *47*(4), 1425–1434. https://doi.org/10.1016/j.neuroimage.2009.05.015

Vizioli, L., Moeller, S., Dowdle, L., Akçakaya, M., De Martino, F., Yacoub, E., & Uğurbil, K. (2021). Lowering the thermal noise barrier in functional brain mapping with magnetic resonance imaging. *Nature Communications*, *12*(1), 5181. https://doi.org/10.1038/s41467-021-25431-8

Wassermann, E. M., McShane, L. M., Hallett, M., & Cohen, L. G. (1992). Noninvasive mapping of muscle representations in human motor cortex. *Electroencephalography and Clinical Neurophysiology/ Evoked Potentials*, *85*(1), 1–8. https://doi.org/10.1016/0168-5597(92)90094-R

Wilson, S. A., Thickbroom, G. W., & Mastaglia, F. L. (1993). Transcranial magnetic stimulation mapping of the motor cortex in normal subjects. The representation of two intrinsic hand muscles. *Journal of the Neurological Sciences*, *118*(2), 134–144. https://doi.org/10.1016/0022-510X(93)90102-5

Wischnewski, M., & Schutter, D. J. L. G. (2015). Efficacy and time course of theta burst stimulation in healthy humans. *Brain Stimulation*, *8*(4), 685–692. https://doi.org/10.1016/j.brs.2015.03.004

Woo, C. W., Krishnan, A., & Wager, T. D. (2014). Cluster-extent based thresholding in fMRI analyses: Pitfalls and recommendations. *NeuroImage*, *91*, 412–419. https://doi.org/10.1016/j.neuroimage.2013.12.058

Woods, D. W., Piacentini, J. C., Himle, M. B., & Chang, S. (2005). Premonitory Urge for Tics Scale (PUTS): Initial Psychometric Results and Examination of the Premonitory Urge Phenomenon in Youths with Tic Disorders. [Article]. *Journal of Developmental & Behavioral Pediatrics*, *26*(6), 397–403. https://doi.org/10.1097/00004703-200512000-00001

Woods, D. W., Piacentini JOHN, HimleI, M. B., & Chang, S. (2005). Premonitory Urge for Tics Scale (PUTS). *Journal of Developmental & Behavioral Pediatrics*, *26*(6), 397–403. https://doi.org/10.1097/00004703-200512000-00001

Woolrich, M. W., Behrens, T. E. J., Beckmann, C. F., Jenkinson, M., & Smith, S. M. (2004). Multilevel linear modelling for FMRI group analysis using Bayesian inference. *NeuroImage*, *21*(4), 1732–1747. https://doi.org/10.1016/j.neuroimage.2003.12.023

Woolrich, M. W., Ripley, B. D., Brady, M., & Smith, S. M. (2001). Temporal Autocorrelation in Univariate Linear Modeling of FMRI Data. *NeuroImage*, *14*(6), 1370–1386. https://doi.org/10.1006/nimg.2001.0931

Worbe, Y., Baup, N., Grabli, D., Chaigneau, M., Mounayar, S., McCairn, K., Féger, J., & Tremblay, L. (2009). Behavioral and Movement Disorders Induced by Local Inhibitory Dysfunction in Primate Striatum. *Cerebral Cortex*, *19*(8), 1844–1856. https://doi.org/10.1093/cercor/bhn214

Worbe, Y., Sgambato-Faure, V., Epinat, J., Chaigneau, M., Tandé, D., François, C., Féger, J., & Tremblay, L. (2013). Towards a primate model of Gilles de la

Tourette syndrome: Anatomo-behavioural correlation of disorders induced by striatal dysfunction. *Cortex*, *49*(4), 1126–1140. https://doi.org/10.1016/j.cortex.2012.08.020

Worsley, K. J. (2001). Statistical analysis of activation images. In *Functional Magnetic Resonance Imaging* (pp. 251–270). Oxford University PressOxford. https://doi.org/10.1093/acprof:oso/9780192630711.003.0014

Worsley, K. J., Marrett, S., Neelin, P., Vandal, A. C., Friston, K. J., & Evans, A. C. (1996). A unified statistical approach for determining significant signals in images of cerebral activation. *Human Brain Mapping*, *4*(1), 58–73. https://doi.org/10.1002/(SICI)1097-0193(1996)4:1<58::AID-HBM4>3.0.CO;2-O

Wu, T., Sommer, M., Tergau, F., & Paulus, W. (2000). Lasting influence of repetitive transcranial magnetic stimulation on intracortical excitability in human subjects. *Neuroscience Letters*, *287*(1), 37–40. https://doi.org/10.1016/S0304-3940(00)01132-0

Yang, S. N., Tang, Y. G., & Zucker, R. S. (1999). Selective induction of LTP and LTD by postsynaptic [Ca2+](i) elevation. *Journal of Neurophysiology*, *81*(2), 781–787. https://doi.org/10.1152/jn.1999.81.2.781

Yeşilyurt, B., Uğurbil, K., & Uludağ, K. (2008). Dynamics and nonlinearities of the BOLD response at very short stimulus durations. *Magnetic Resonance Imaging*, *26*(7), 853–862. https://doi.org/10.1016/j.mri.2008.01.008

Yousry, T. A., Schmid, U. D., Alkadhi, H., Schmidt, D., Peraud, A., Buettner, A., & Winkler, P. (1997). Localization of the motor hand area to a knob on the precentral gyrus. A new landmark. *Brain*, *120*(1), 141–157. https://doi.org/10.1093/brain/120.1.141

Zanette, G., Manganotti, P., Fiaschi, A., & Tamburin, S. (2004). Modulation of motor cortex excitability after upper limb immobilization. *Clinical Neurophysiology*, *115*(6), 1264–1275. https://doi.org/10.1016/j.clinph.2003.12.033

Zhong, M., Cywiak, C., Metto, A. C., Liu, X., Qian, C., & Pelled, G. (2021). Multi-session delivery of synchronous rTMS and sensory stimulation induces long-term plasticity. *Brain Stimulation*, *14*(4), 884–894. https://doi.org/10.1016/j.brs.2021.05.005

Zhu, S., Noviello, C. M., Teng, J., Walsh, R. M., Kim, J. J., & Hibbs, R. E. (2018). Structure of a human synaptic GABAA receptor. *Nature*, *559*(7712), 67–72. https://doi.org/10.1038/s41586-018-0255-3

Ziemann, U. (2004). Cortico-motoneuronal excitation of three hand muscles determined by a novel penta-stimulation technique. *Brain*, *127*(8), 1887–1898. https://doi.org/10.1093/brain/awh212

Ziemann, U. (2013). Chapter 32 - Pharmaco-transcranial magnetic stimulation studies of motor excitability. In A. M. Lozano & M. Hallett (Eds.), *Handbook of Clinical Neurology* (Vol. 116, pp. 387–397). Elsevier. https://doi.org/10.1016/B978-0-444-53497-2.00032-2

Ziemann, U., Paulus, W., & Rothenberg, A. (1997). Decreased motor inhibition in Tourette's disorder: Evidence from transcranial magnetic stimulation. *American Journal of Psychiatry*, *154*, 1277–1284.

Appendices

Appendix A

Appendix A.1

Diagnoses, medication and clinical scores of TS participants in Chapter 3 (Study 1)

						YGTSS			
ID	**Age**	**Sex**	**Diagnoses (incl. self-diagnoses)**	**Medication**	**PUTS-R**	**Motor**	**Phonic**	**Impairment**	**Global**
TS01	23	2	TS, CTD	None	44	10	10	5	25
TS02	36	2	TS, ADHD	Clonidine HCl 150 mcg	26	19	13	10	42
TS03	33	2	TS, ADHD, ASD	None	36	18	12	20	50
TS04	51	1	TS, OCD	Clonidine 25 mcg, Mirtazapine 30 mg, muscle relaxants	62	22	10	35	67
TS05	23	1	TS, GAD	Sertraline	61	14	8	25	25
TS06	54	2	CTD	None	39	12	0	20	32
TS07	19	1	CTD	None	46	16	0	15	31
TS08	19	1	TS, ADHD	Concerta XI 45 mg	72	21	20	44	81
TS09	54	2	TS, OCD	None	5				
TS10	50	2	TS	None	36	14	13	10	37
TS11	29	2	TS	None	11	18	10	10	38
TS12	18	1	TS	None	20	13	12	20	45
TS13	32	2	TS, ADHD	None	70	20	13	40	73
TS14	38	1	TS	None	45	18	13	10	41
TS15	30	2	TS, ADHD	Clonidine 300 mcg, Escitalopram 10 mg	44	21	18	35	74
TS16	31	2	TS	None	54	22	5	20	47
TS17	38	1	TS, GAD, OCD, Trichotillomania	None	50	19	0	30	49
TS18	37	1	TS	None	55	20	8	30	58
TS19	33	2	TS, ADHD	Clonidine 1 mg	42	11	12	20	43
TS20	34	2	TS, ADHD, ASD	None	19	10	0	4	14
TS21	29	1	TS, GAD, Depression, Fibromyalgia	None	38	15	14	25	54
TS22	21	1	TS	None	60	18	17	40	75
TS23	21	1	TS, GAD, ADHD, dyslexia	Sertraline 75 mg	47	11	12	10	33
TS24	19	1	TS	None	59	20	18	38	30
TS25	32	1	TS, GAD, ASD	None	45	15	20	43	78
TS26	22	1	TS, ADHD, Borderline PD	Elvanse 50 mg, Propranolol 80 mg, Lamotrigine 25 mg	64	23	17	35	75
TS27	19	1	CTD	None	42	16	13	25	54
TS28	22	1	TS, ASD	None		11	15	10	36
TS29	17	1	TS, OCD, ASD	None	31	11	13	15	39

Appendix A.2

Diagnoses, medication and clinical scores of TS participants in Chapter 3 (Study 2)

						YGTSS			
ID	**Age**	**Sex**	**Diagnoses (incl. self-diagnoses)**	**Medication**	**PUTS-R**	**Motor**	**Phonic**	**Impairment**	**Global**
TS01	23	2	TS, CTD	None	44	10	10	5	25
TS02	37	2	TS, ADHD	Clonidine HCl 225 mcg	29	16	24	30	70
TS04	52	1	TS, OCD	Gabapentin 100 mg, Baclofen 10 mg, Clonidine 25 mcg, Mirtazapine 30 mg	50	16	11	10	37
TS05	23	1	TS, GAD	Sertraline 100 mg	61	14	8	25	47
TS07	19	1	CTD	None	51	16	0	15	32
TS12	18	1	TS	None	20	13	12	20	45
TS13	32	2	TS, ADHD	None	48	18	15	30	45
TS14	39	1	TS	None	41	10	0	11	21
TS21	29	1	TS, GAD, Depression, Fibromyalgia	Amitriptyline 10 mg	38	15	14	25	54
TS22	21	1	TS	None	60	18	17	40	75
TS23	21	1	TS, GAD, ADHD, dyslexia	Sertraline 75 mg	47	11	12	10	33
TS24	19	1	TS	None	59	20	18	38	30
TS26	22	1	TS, ADHD, Borderline PD	Elvanse 50 mg, Propranolol 80 mg, Lamotrigine 25 mg	64	23	17	35	75
TS27	20	1	CTD	None	42	16	13	25	54
TS28	22	1	TS, ASD	None		11	15	10	36
TS29	17	1	TS, OCD, ASD	None	31	11	13	15	39

Appendix A.3

Interoceptive Accuracy Scale (IAS), from Murphy et al. (2020)

Below are several statements regarding how accurately you can perceive specific bodily sensations. Please rate on the scale how well you believe you can perceive each specific signal. For example, if you often feel you need to urinate and then realise you do not need to when you go to the toilet you would rate your accuracy perceiving this bodily signal as low.

Please only rate how well you can perceive these signals without using external cues, for example, if you can only perceive how fast your heart is beating when you measure it by taking your pulse this would not count as accurate internal perception.

Scale: 5 = strongly agree, 4 = agree, 3 = neither agree nor disagree, 2 = disagree, 1 = disagree strongly

1. I can always accurately perceive when my heart is beating fast
2. I can always accurately perceive when I am hungry
3. I can always accurately perceive when I am breathing fast
4. I can always accurately perceive when I am thirsty
5. I can always accurately perceive when I need to urinate
6. I can always accurately perceive when I need to defecate
7. I can always accurately perceive when I encounter different tastes
8. I can always accurately perceive when I am going to vomit
9. I can always accurately perceive when I am going to sneeze
10. I can always accurately perceive when I am going to cough
11. I can always accurately perceive when I am hot/cold
12. I can always accurately perceive when I am sexually aroused
13. I can always accurately perceive when I am going to pass wind
14. I can always accurately perceive when I am going to burp

15. I can always accurately perceive when my muscles are tired/sore
16. I can always accurately perceive when I am going to get a bruise
17. I can always accurately perceive when I am in pain
18. I can always accurately perceive when my blood sugar is low
19. I can always accurately perceive when someone is touching me affectionately rather than nonaffectionatel
20. I can always accurately perceive when something is going to be ticklish
21. I can always accurately perceive when something is going to be itchy

Appendix A.4

Sensory Processing Sensitivity Questionnaire (SPSQ), Sensory Sensitivity subscale (items 1-8) from Malinakova et al. (2021)

Please indicate to what extent you think that compared to other people you are sensitive to the following stimuli, conditions or experiences.

Scale:
0 = compared to others, I am not sensitive to them at all
5 = about the same as the people around me
10 = much more sensitive than the people around me

1. Light
2. Sound
3. Smells
4. Taste
5. Tactile stimuli – touch, clothing, etc.
6. Hunger
7. Heat
8. Cold

Appendix A.5

Correlation analyses in Chapter 3 (Study 2).

	TD						TS					
	MRS-GABA			MRS-Glu			MRS-GABA			MRS-Glu		
Task	df	r	p	df	r	p	df	r	p	df	r	p
seqAD (µm)	9	-0.05	0.882	10	0.05	0.873	11	0.22	0.464	12	0.08	0.785
simAD (µm)	11	-0.11	0.720	12	0.14	0.626	10	-0.24	0.451	11	-0.49	0.091
SSA (µm)	11	0.27	0.367	12	**-0.58**	**0.031***	9	-0.17	0.620	10	-0.05	0.877
Adaptation effect (%)	11	0.07	0.835	12	-0.48	0.085	10	0.25	0.443	11	**0.59**	**0.032***
TOJ (ms)	11	-0.13	0.678	12	-0.17	0.567	10	0.17	0.608	11	0.26	0.390
cTOJ (ms)	9	-0.26	0.451	10	-0.24	0.463	8	0.15	0.680	9	0.06	0.872
Carrier effect (%)	9	0.06	0.881	10	-0.13	0.683	10	0.45	0.147	11	0.047	0.879
SPSQ	8	-0.40	0.255	8	0.12	0.752	8	**0.75**	**0.013***	9	-0.12	0.723
IAS	9	0.26	0.451	9	0.004	0.991	9	-0.24	0.485	10	0.205	0.523
PUTS-R							10	0.15	0.649	10	**-0.60**	**0.041***
YGTSS (motor)							11	0.27	0.369	11	-0.14	0.648
YGTSS (phonic)							11	-0.32	0.288	11	-0.35	0.246
YGTSS (impairment)							11	0.05	0.867	11	-0.12	0.705
YGTSS (total)							11	-0.25	0.418	11	-0.11	0.721

Note. In the TD group, all MRS-GABA correlations and MRS-Glu correlations for SSA, cTOJ and Carrier effect (%) did not pass normality checks and are reported with Spearman's *rho*

Appendix B

Appendix B.1

Diagnoses, medication and clinical scores of TS participants in Chapter 4

						YGTSS			
ID	**Age**	**Sex**	**Diagnoses (incl. self-diagnoses)**	**Medication**	**PUTS-R**	**Motor**	**Phonic**	**Impairment**	**Global**
TS01	23	M	TS, CTD	None	44	10	10	5	25
TS05	23	F	TS, GAD	Sertraline 100 mg	61	14	8	25	47
TS07	19	F	CTD	None	51	16	0	15	32
TS14	39	F	TS	None	41	10	0	11	21
TS21	29	F	TS, GAD, Depression, Fibromyalgia	Amitriptyline 10 mg	38	15	14	25	54
TS22	21	F	TS	None	60	18	17	40	75
TS24	19	F	TS	None	59	20	18	38	30
TS28	22	F	TS, ASD	None		11	15	10	36
TS29	17	F	TS, OCD, ASD	None	31	11	13	15	39

Appendix C

Appendix C.1

Diagnoses, medication and clinical scores of TS participants in Chapter 5 (Study 1)

						YGTSS			
ID	**Age**	**Sex**	**Diagnoses (incl. self-diagnoses)**	**Medication**	**PUTS-R**	**Motor**	**Phonic**	**Impairment**	**Global**
TS04	51	F	TS, OCD	Clonidine 25 mcg, Mirtazapine 30 mg, muscle relaxants	62	22	10	35	67
TS05	23	F	TS, GAD	Sertraline 100 mg	61	14	8	25	47
TS06	54	M	CTD	None	39	12	0	20	32
TS07	19	F	CTD	None	46	16	0	15	31
TS08	19	F	TS, ADHD	Concerta XI 45 mg	72	21	20	44	81
TS09	54	M	TS, OCD	None	5				
TS10	50	M	TS	no change	36	14	13	10	37
TS12	18	F	TS	None	20	13	12	20	45
TS13	32	M	TS, ADHD	None	70	20	13	40	73
TS14	38	F	TS	None	45	18	13	10	41
TS15	30	M	TS, ADHD	Clonidine 300 mcg, Escitalopram 10 mg	44	21	18	35	74
TS16	31	M	TS	None	54	22	5	20	47
TS17	38	F	TS, OCD, GAD, Trichotillomania	None	50	19	0	30	49
TS18	37	F	TS	None	55	20	8	30	58
TS19	33	M	TS, ADHD	Clonidine 1 mg	42	11	12	20	43
TS20	34	M	TS, ADHD, ASD	None	19	10	0	4	14

Appendix C.2

Significant cluster activations in Chapter 5 (Study 1) for (a) blink, (b) grimace, and (c) jaw clench blocks

a.

Blink

Group	Cluster	Cluster size (voxels)	Z-score	MNI coordinates x	y	z	Location
TD	3	2815	5.34	-48	-6	58	Pre-central gyrus
	2	2605	7.08	48	4	38	Pre-central gyrus
	1	1440	6.01	0	4	62	Supplementary motor area
TS	3	2410	6.89	60	16	16	Inferior Frontal Gyrus
	2	1930	7.66	-58	0	42	Pre-central gyrus
	1	839	8.31	-4	2	62	Supplementary motor area

b.

Grimace

Group	Cluster	Cluster size (voxels)	Z-score	MNI coordinates x	y	z	Location
TD	3	6320	6.49	-4	2	56	Supplementary motor area
	2	4300	5.67	-58	4	32	Pre-central gyrus
	1	257	4.18	14	-34	48	Pre-central gyrus
TS	3	1623	9.3	50	-8	56	Pre-central gyrus
	2	948	6.37	-46	-12	44	Pre-central gyrus

c.

Jaw clench

Group	Cluster	Cluster size (voxels)	Z-score	MNI coordinates x	y	z	Location
TD	3	4099	6.28	-62	8	18	Pre-central gyrus
	2	4051	11.7	68	-6	16	Post-central gyrus
	1	2022	7.02	4	12	56	Superior Frontal Gyrus
TS	3	2752	8.07	-60	-14	18	Post-central gyrus
	2	2722	6.8	64	0	6	Planum Polare
	1	762	5.21	-6	4	62	Supplementary motor area

Appendix C.3

Diagnoses, medication and clinical scores of TS participants in Chapter 5 (Study 2)

						YGTSS			
ID	**Age**	**Sex**	**Diagnoses (incl. self-diagnosis)**	**Medication**	**PUTS-R**	**Motor**	**Phonic**	**Impairment**	**Global**
TS05	23	F	TS, GAD	Sertraline 100 mg	61	14	8	25	47
TS12	18	F	TS	None	20	13	12	20	45
TS13	32	M	TS, ADHD	None	48	18	15	30	45
TS14	39	F	TS	None	41	10	0	11	21
TS21	29	F	TS, GAD, Depression, Fibromyalgia	Amitriptyline 10 mg	38	15	14	25	54
TS23	21	F	TS, GAD, ADHD and dyslexia	Sertraline 75 mg	47	11	12	10	33

Appendix C.4

Graphs and tables showing average and standard deviations of (a) temperature across scans, and (b) change in temperature across scans

(a)

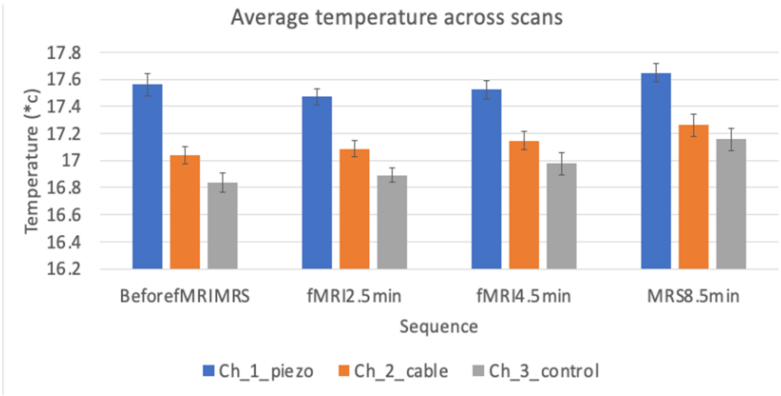

Average Temp across scans			
	Ch_1_piezo	Ch_2_cable	Ch_3_control
BeforefMRIMRS	17.5618985	17.03795113	16.83774436
fMRI2.5min	17.47066667	17.08624242	16.89121212
fMRI4.5min	17.52219355	17.14535484	16.97658065
MRS8.5min	17.64867521	17.26051282	17.15602564
SD of average temp across scans			
	Ch_1_SD	Ch_2_SD	Ch_3_SD
BeforefMRIMRS	0.08189128	0.064706592	0.068805975
fMRI2.5min	0.058769219	0.059973078	0.053962361
fMRI4.5min	0.067409496	0.068419772	0.0844126
MRS8.5min	0.070491979	0.083032422	0.084706417

(b)

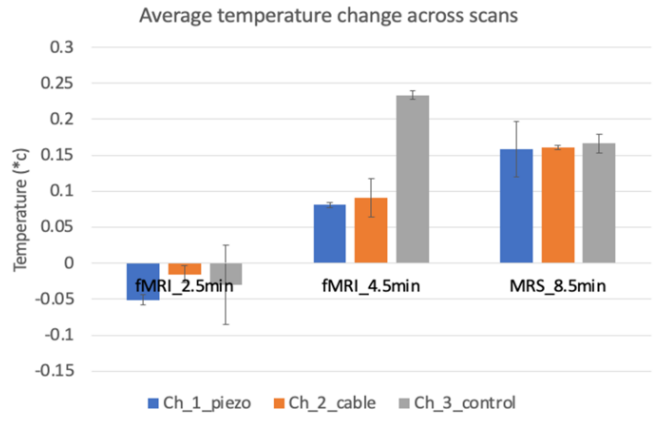

Average temperature change across scans			
	Ch_1_piezo	Ch_2_cable	Ch_3_control
fMRI_2.5min	-0.050897	-0.01533	-0.03003663
fMRI_4.5min	0.081	0.091	0.2335
MRS_8.5min	0.158095	0.160952	0.166190476
SD of temperature change across scans			
	Ch_1_SD	Ch_2_SD	Ch_3_SD
fMRI_2.5min	0.007372	-0.011972	-0.055104127
fMRI_4.5min	0.003661	-0.02678	-0.006016161
MRS_8.5min	0.038471	0.003047	0.013371329

Appendix C.5

Raw temperature across time for: (a) baseline (9 minutes), (b) fMRI (2.5 minutes), (c) fMRI (4.5 minutes) and (d) MRS (8.5 minutes)

a.

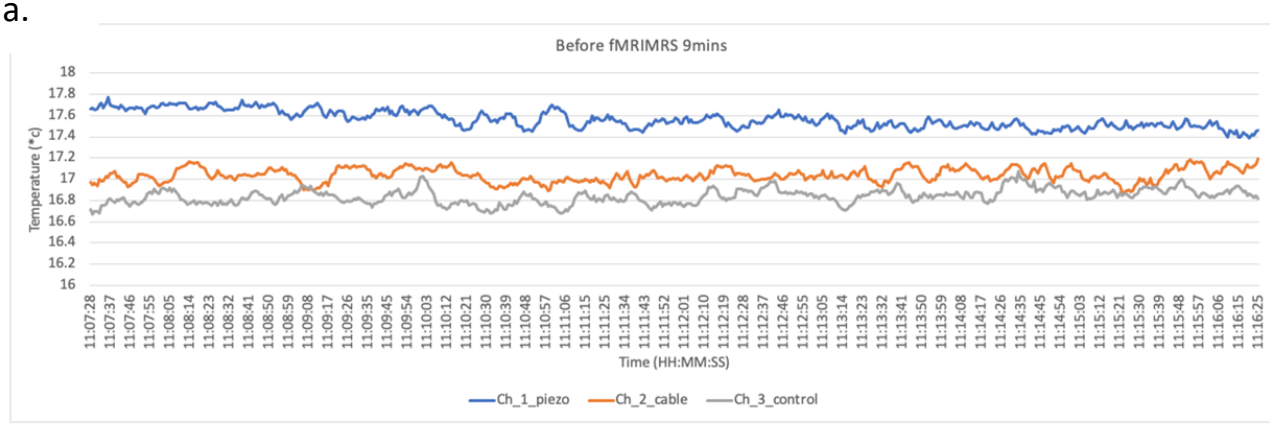

Before fMRI/MRS - 9 min			
Temp	Ch_1_piezo	Ch_2_cable	Ch_3_control
Min	17.39	16.87	16.67
Max	17.77	17.19	17.07
Average	17.561898	17.037951	16.83774436
SD	0.0818913	0.0647066	0.068805975

b.

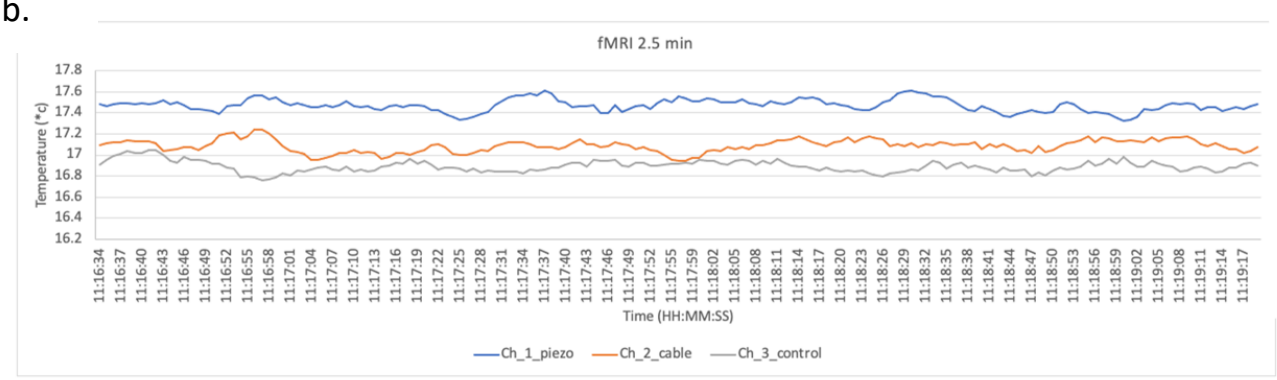

fMRI 2.5 mins			
Temp	Ch_1_piezo	Ch_2_cable	Ch_3_control
Min	17.32	16.94	16.76
Max	17.61	17.24	17.05
Average	17.470667	17.086242	16.89121212
SD	0.0587692	0.0599731	0.053962361

c.

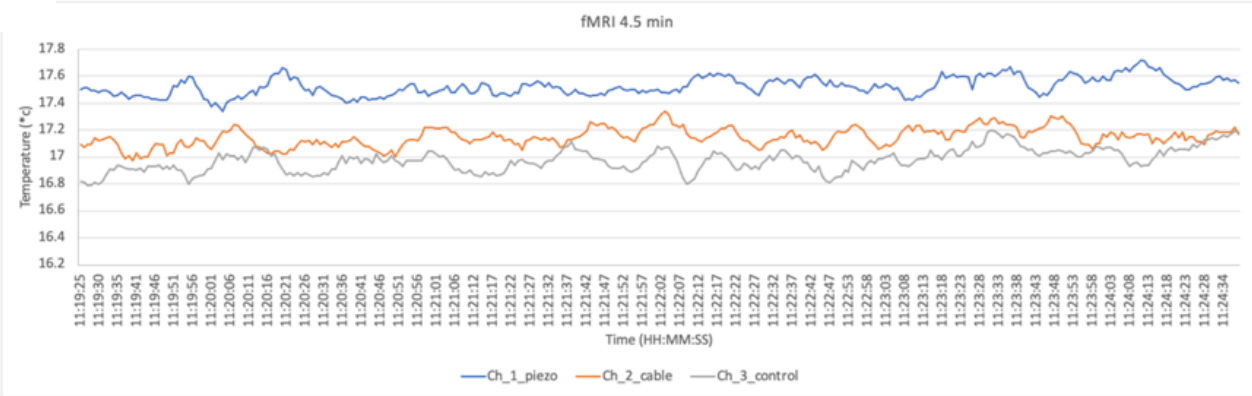

fMRI 4.5 mins			
Temp	Ch_1_piezo	Ch_2_cable	Ch_3_control
Min	17.34	16.97	16.79
Max	17.72	17.34	17.2
Average	17.522194	17.145355	16.97658065
SD	0.0674095	0.0684198	0.0844126

d.

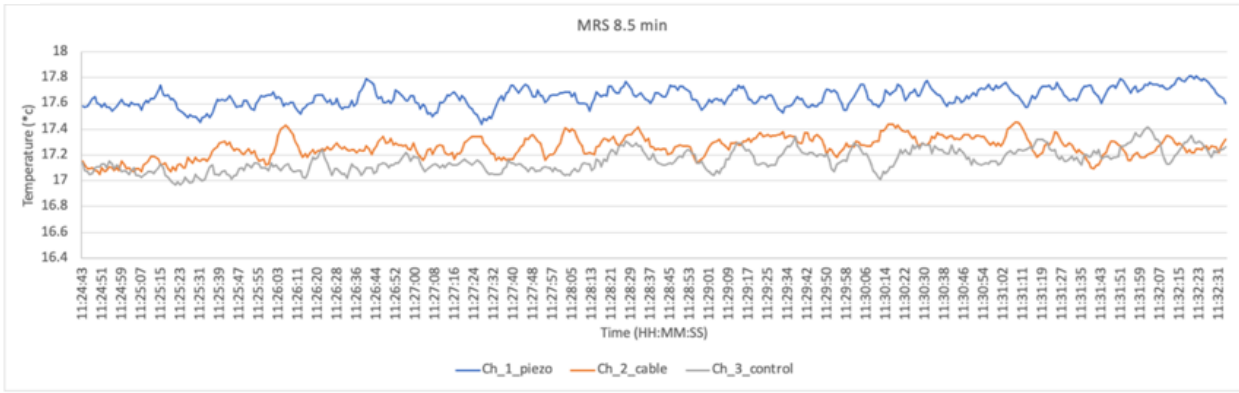

MRS 8.5 mins			
Temp	Ch_1_piezo	Ch_2_cable	Ch_3_control
Min	17.44	17.05	16.97
Max	17.81	17.45	17.42
Average	17.648675	17.260513	17.15602564
SD	0.070492	0.0830324	0.084706417

Appendix C.6

Significant cluster activations in Chapter 5 (Study 2)

				MNI coordinates			
Group	**Cluster**	**Cluster size (voxels)**	**Z-score**	**x**	**y**	**z**	**Location**
O. oculi	**1**	122	3.7	2	10	54	Paracingulate gyrus
Masseter	**3**	378	4.46	44	8	34	Pre-central gyrus
	2	91	3.57	8	6	62	Supplementary motor area
	1	79	4.18	58	-18	28	Post-central gyrus
O. oris	**2**	348	4.18	48	4	46	Pre-central gyrus
	1	111	3.53	4	-4	60	Supplementary motor area

Appendix D

Appendix D.1.

Outlier removals from TMS mapping in Chapter 6.

3D COG coordinate measures for FDI maps in the active group, two L-R COG, one P-A COG datapoints were removed from the before iTBS timepoint and one L-R COG, one P-A COG datapoints were removed from the after iTBS timepoint. In the control group, two P-A COG datapoints were removed from the after iTBS timepoint. In Euclidean distances for FDI maps one datapoint in the active group and one datapoint in the control group were removed from the before iTBS timepoint. In absolute change in L-R COG 3D coordinates, one datapoint was removed from the active group. For absolute change in Euclidean distances, one datapoint was removed from the active group. For absolute percentage change in area of FDI maps, two datapoints were removed from the active group.

For ADM maps in the active group, two L-R COG datapoints were removed from the before iTBS datapoint, with two L-R COG and one P-A COG datapoints removed from the after iTBS timepoint. For the control group, two P-A COG datapoints were removed from the after iTBS timepoint. For Euclidean distances, one datapoint was removed from the before iTBS timepoint in the control group. For the ADM map areas, one datapoint was removed from the before iTBS timepoint in the active group. For absolute change in COG coordinates, one datapoint was removed from the L-R COG coordinates in the control group. one datapoint was also removed from the control group in the absolute change in Euclidean distances. For absolute percentage change in ADM area, two datapoints were removed from the active group and one datapoint was removed from the control group.

For APB maps in the active group, one L-R COG, one P-A COG datapoints were removed from the before iTBS timepoint and one P-A COG was removed from the after iTBS timepoint. In the control group, one P-A COG datapoint was removed from

the after iTBS timepoint. For Euclidean distances, one datapoint from the before iTBS timepoint and one datapoint from the after iTBS timepoint were removed from the control group. For APB map areas, one datapoint was removed from the after iTBS timepoint in the control group. For absolute change in COG coordinates, one datapoint was removed from L-R COG coordinates in the active group and one datapoint was removed from P-A COG coordinates in the control group. For absolute change in Euclidean distances, one datapoint was removed from the active group, and one was removed from the control group.

Appendix D.2

Outlier removal for fMRI digit maps – Chapter 6

For digit ratios in the active group in the before iTBS timepoint, this resulted in the removal of two D2, two D3 and one D1 digit ratio datapoints. For the control group, one D1 digit ratio datapoint was removed. In the after iTBS timepoint in the active group, this resulted in the removal of one D1 and one D5 datapoints. For the control group, this resulted in the removal of one D2 and two D3 datapoints.

For Euclidean distances between before and after iTBS D1 3D COG coordinates in the active group, one D3, one D5 datapoints were removed. In the control group, one D1, one D4 and three D5 datapoints were removed.